Sapienza – University of Rome
Faculty of Civil and Industrial Engineering
Department of Structural and Geotechnical Engineering

Budapest University of Technology and Economics
Faculty of Mechanical Engineering
Department of Applied Mechanics

Stability and bifurcation analysis of mechanical systems subject to digital position control

Supervisors:

Prof. Giuseppe Rega
Prof. Gábor Sépán

PhD Dissertation

by

Giuseppe Habib

July 2013, Rome

Stability and bifurcation analysis of mechanical systems subject to digital position control

ABSTRACT

Precision and stability in position control of robots are critical parameters in many industrial applications where high accuracy is needed. It is well known that digitization is affecting the stability and most of the industrial robotic systems are equipped with digital controllers. Still, their dynamic analysis is often treated using continuous-time (analog) approaches and models; indeed, the sampling frequency can be so high that from an engineering point of view it can be considered continuous. However, these approaches do not provide always conservative estimates for stability.

In this work, the stability of the position control of simple robotic arms is investigated. The analyses aim at showing the limits of a continuous-time approach and the main effects of the digitization. The investigation goes through different configurations, namely a one- and a two- degree-of-freedom mechanical system, which highlights occurrences when it is more or less critical taking into account the digitization into the model.

Large part of the work is devoted to the analysis of the bifurcations occurring at the loss of stability of the control systems. In particular, a single and a double Neimark-Sacker bifurcation are analytically investigated. These analyses show the transition of the system to multi-frequency quasiperiodic and chaotic motions.

The application of the so-called act-and-wait controller is then implemented into the control system. Advantages and drawbacks of this periodic controller are analyzed with respect to stability, speed of convergence and bifurcation behavior of the system.

The last part of the work is dedicated to the presentation of experimental results, regarding the stability analysis of the so-called aeropendulum. The obtained results validate the adopted methodology for the stability analysis and evidence the need of modeling the digitization of the control system in the case of low sampling frequencies.

Acknowledgments

In first place, I would like to express my gratitude to my supervisors, Prof. Giuseppe Rega and Prof. Gábor Stépán, for their precious guidance and encouragement throughout the full period of my studies for my PhD. Besides their unquestionably valuable help in all the technical matters, I especially appreciated their patient and help with the numerous bureaucratic issues that characterized the collaboration between the two institutes.

I would like to acknowledge Prof. Oded Gottlieb for truly motivating me in continuing my studies after I completed my Master thesis under his supervision.

I wish to thank the reviewers of the first draft version of this dissertation, Prof. Achille Paolone, Prof. Danilo Capecchi e Dr. Zoltán Dombóvári, for their careful and fruitful reading of the manuscript.

I am pleased to acknowledge my colleagues at the Department of Applied Mechanics of the Budapest University of Technology and Economics, who helped me with any kind of issues and allowed me to spend a great time in a pleasant working atmosphere.

I am sincerely thankful to my parents and family for supporting and encouraging me throughout my whole studies.

Finally and foremost, I am infinitely grateful to Nelli for supporting and motivating me in my work, and letting me have a wonderful life experience during my stay in Budapest.

In Memory of
My Grandmother, Emilia
and My Aunt, Irene

Contents

List of Figures

Chapter 1

Introduction

1.1 Generalities about position control

Position control consists in the ability to move a mechanical system to a defined configuration with certain accuracy and within certain time. This task is generally achieved with a feedback loop, i.e. the control system receives an input information about the kinematic state of the system to control and elaborates a signal that affects the motion, in order to reach the desired configuration. If no feedback information is available, the control system needs to calculate and plan the whole motion starting from the available initial conditions. Generally, this second case decreases accuracy and requires more precise information.

Examples of the two cases are experienced by everyone in everyday life. Walking in a room, in order to avoid obstacles as chairs or tables, our brain controls our motion elaborating real time information about our position and velocity in the room. If we think about doing the same operation in a dark room, although we suppose that we know the exact configuration of the environment, the operation is much harder to be performed and the probability that we will hit an object is much higher, because of the removed feedback information provided by the sight.

Between the two extreme cases (full and clear information and no information at all) there are several possibilities. It can occur that the information is corrupted, if for example the person walking in the room is myopic or the room is in semi-darkness. Other than that, the feedback information might be elaborated with certain delay. Then, the information may not be continuous, as in the case of a stroboscopic light, as experienced by many people for example in discos or rock concerts. All the phenomena that compromise clearness, correct timing and continuity of the feedback information have effect on the stability and accuracy of the control system.

Acknowledging the difference between the two, analogous phenomena occur in robotic systems, as well. In this work, we will present the problem of loss of stability due to the digitization in time of the control system, applied to simple models of robotic arms subject to proportional-differential (PD) position control.

1.2 Literature review

Position and trajectory control of robots are very important tasks in many industrial applications. The positioning must be fast, precise, reliable and stable in order to guarantee high standards of production. This topic has been a subject of intensive studies for decades, but it is still an interesting one, in virtue of the increasing demands from any field using robots and of the increasing number of their applications. Robotic systems are usually equipped with digital controllers, while their dynamic analysis is often treated using continuous-time (analog) approaches and models [21, 48, 57]; indeed, the sampling frequency can be so high, that from an engineering point of view it can be considered continuous. However, these approaches do not provide always conservative estimates for stability.

In the last decades several authors studied the stability of digital control systems [37,58,59,61], finding surprising results about stability domains, which are strongly influenced by the sampling frequency. Industrial

robots often present instabilities that cause the arm to oscillate around the desired position. The stability is then reached through several tests aimed at "calibrating" the control system, which generally imply a reduction of the control gains. This approach, although works in many cases, neither allows to predict the stability properties of the system, nor to have optimal values of the control gains with respect to fast speed of convergence and precision of positioning.

Today's digital processors have very high sampling frequencies, several orders of magnitude higher than the natural frequencies of the mechanical structures they are controlling or interacting with. However, the sampling frequency of industrial robots is not as high as that of available processor. This is due to the increased complexity of the applied control algorithms which are computationally heavy and decrease the overall sampling frequency. This occurs especially in multi-DoF (Degrees of Freedom) applications.

The finite stiffness of connecting joints is another element, often underestimated, that can compromise the stability of robotic systems. Although their stiffness may be very high, in some cases it should be taken into account in the mechanical model. In the case of harmonic drives, the teflon teeth introduce a small angular displacement (called hysteresis backlash) between the motor and the driven link. Similarly, belts or long shafts introduce a non negligible elasticity [13, 62]. In service robots for close human cooperation, in order to reduce stiffness and apparent inertia for safety reasons, elastic actuation should be used, relocating actuators close to the robots base and transmitting the motion through steel cables and pulleys [28]. Usually, the elasticity introduced by these elements, can be considered concentrated at the joint with an elastic or a visco-elastic term.

The introduction of an elastic term in the joint doubles the number of independent variables needed to describe the state of the system. A set of sensors able to measure the full state of such systems is hardly available [14]. Typically, sensors measure only the state of the rotor of the motor, while only recently, sensors for directly (or indirectly) measuring the position of the arm at the end effector have been proposed, as for example in [6].

Several authors [33, 34, 51, 64] proposed different state observers, which simulate the state of the link, based on the known magnitudes, and allow to control the full motion of the robot. In order to control the system, one approach is based on the idea of feedback linearization; this approach is robust to parameter uncertainty only if the acceleration and jerk of the link are known [19]. Another approach is based on the concept of integral manifolds. In this case, the robot dynamics is restricted to an integral manifold in the state space, which allows reducing the order of the model. This method overcomes the need of knowledge of acceleration and jerk, but it is not robust with respect to parametric uncertainty [19].

Although the problem of the control of robotic arms with elastic joints is well known and widely investigated, as we already mentioned, very few authors take into account the effect of digitization of the control force due to the presence of digital processors. Besides the delay introduced by the digital controller, which can be often neglected in modern processors due to the high value of the sampling frequency, this can still generate "resonances" with the natural frequency of the system, as shown for example in [68], where the digital control of a rotating elastic arm and the resonances occurring between the sampling frequency and the modes of vibration are analyzed. Other works [9, 12, 20, 37, 52, 56, 58], regarding the control of robots, consider the digital effect. Nicosia et al. [52] derive the equation of motion of a two-link flexible manipulator, including the discrete time effect. In [58], the stability domain of a simple single DoF system, subject to digital force control, is obtained, highlighting the need of taking into account the finite sampling frequency of the processor. Out of the context of robotics, the effects of the finite sampling frequency of controllers is analyzed also by Krutova [38], regarding the control of a flexible spacecraft, and by Konishi et al. [36], regarding coupled oscillators.

In the case of force control, if the contact surface is very stiff, the coupled system robot-environment can have very high natural frequency, reducing the ratio between the sampling and the natural frequency of the system. In such cases, the digital effect becomes significant and cannot be neglected. Examples for this situation are in [1,12,60]. Turbine blade polishing is a typical example for the case where digital effects and the variable effective stiffness along the blade cause unexpected vibrations in the system under digital force control [60].

Besides stability, another aspect that will be investigated in this research is the bifurcation behavior of the system at the loss of stability. Although most of the industrial systems of any kind are designed to work in stable conditions, it is important to study the effects of instabilities in order to know the damages caused by instabilities and estimate their danger, especially in cases of close human cooperation. In particular, subcritical bifurcations can compromise the robustness of the stability of the system, generating unexpected motions, in

conditions where stability has been previously experienced. In some cases such events can have catastrophic consequences.

The rich dynamics experienced in cases of instabilities is another aspect that motivated us to investigate the bifurcation behavior of digitally controlled system. Multi-frequency quasiperiodic and chaotic attractors can occur, which cannot be explained by a linear analysis and can be hardly understood from simple numerical investigations of nonlinear models.

Considerable work has been devoted to analyzing bifurcations of discrete-time systems [26, 66, 69], however these works refer to codim-1 bifurcations of these systems. Analytical methods to solve this kind of bifurcations are well known and presented in many textbooks [25, 40, 65]. On the other side, few works [41, 42, 43] are dedicated to the analysis of codim-2 bifurcations that are often occurring in multi-DoF systems. Up to our knowledge, one of the most common codim-2 bifurcations occurring in robotic system is the double Neimark-Sacker (NS) bifurcation. Analysis of case studies of this kind of bifurcation are almost nonexistent, this makes the analytical and detailed study of a double NS bifurcation, performed in this work, more interesting, even out of the context of position control.

1.3 Aims of the work

In this work we perform the stability and bifurcation analyses of a robotic arm subject to digital position control. The model of the robotic arm is intentionally very simple, this allows performing analytical investigations and understanding the basic mechanisms leading to instabilities in digitally controlled systems. The stability analysis aims at identifying in which circumstances the digitalization is relevant and should be taken into account. This will be done analyzing two different models: a one- and a two- DoF system. Being the former a purely inertial system (no restoring forces), it is qualitatively different from the latter, where two inertial components are connected by a spring. The aim of the stability investigation is to characterize the two cases with respect to digitization.

Large part of the work is dedicated to several bifurcation analyses, which aims at characterizing the bifurcations occurring at the loss of stability of digitally controlled systems. In particular, it will be defined under which circumstances the bifurcations are supercritical and when they are subcritical. This analysis is of great practical importance, since subcriticalities generally compromise the robustness of the stability of the desired solution. In other words, if a system loses stability through a subcritical bifurcation, most likely it can experience unexpected vibrations also in the region of linear stability of the system.

Another section of this work is dedicated to the act-and-wait controller. This controller, recently developed by Insperger and Stepan [30,31] for delayed systems, periodically switches on (act) and off (wait) the actuator. The main practical effect of this intermittent actuation is the reduction of the number of poles in the system. Previous studies [30,31,32] show that this controller sensibly enlarges the stable region in the space of the control gains and even allows deadbeat control (achievement of the desired position in a finite number of time steps). The aim of this section is to apply the act-and-wait controller to the single DoF system under study and compare its features with a regular digital controller. In particular, we will analyze the nonlinear behavior of the act-and-wait in order to define a clearer picture of advantages and drawbacks of this periodic controller.

In order to strengthen the results obtained from the numerical and analytical investigation, results of experimental analysis are shown. The experiment consists in studying the stability properties of the so-called aeropendulum, developed by Enikov [15]. The aeropendulum consists of a single DoF rigid pendulum, digitally controlled by a propeller attached at its free end. The propeller moves according to a signal received in a feedback loop sent by the processor. The aim of the experiment is to show proofs that the digitization is indeed modifying the stability properties of controlled systems as predicted by the theory.

1.4 Thesis outline

This thesis work is divided in 9 different chapters, describing different features of the same mechanical models. After this introduction, the second chapter is dedicated to the stability analysis. Two mechanical models are analyzed: a purely inertial single DoF system and a two-DoF system, the former modeling a single link rigid

robotic arm and the latter modeling the same robotic arm with an elastic joint. The differences between a continuous time approach (neglecting the digitization in time of the controller) and a discrete time approach are analyzed. Then, the differences between the two models (with rigid and with elastic joint) are investigated. Finally, two different configurations of the two-DoF system are considered, namely a collocated and a non-collocated case. The different features of the two systems will be shown, highlighting the particular effects that the digitization has in the two cases.

In the third chapter, a detailed procedure to analytically investigate single and double NS bifurcations and period-doubling bifurcations is presented. The procedure uses the methods of the center manifold reduction and near identity normal form transformation. Most of the steps of the procedure are already presented in textbooks [40,49,65], however, the aim of this chapter is to outline a method easy to follow that will be adopted in the following analysis.

In the fourth chapter, the single NS bifurcation and the double NS bifurcation occurring in the one- and in the two-DoF systems, respectively, are analyzed. In order to have bounded solutions at the loss of stability, the saturation of the control force is included in the model. The investigation goes through the passages outlined in the previous chapter, showing which parameters influence the features of the bifurcations and defining critical values for transitions between qualitatively different behaviors of the system.

In the fifth chapter effects of asymmetry of the saturation of the control force are investigated. Starting from the results obtained in the previous chapter, the analysis is extended for an asymmetric system. The obtained results are combinations of analytical and numerical investigations.

The sixth chapter analyzes the transition to chaos of the system, mainly due to an increased asymmetry of the saturation. Regarding the two-DoF system, it will be shown that the chaos is generated through torus breakdown. The main features of this route to chaos are experienced and shown for the system under study. The analysis of the chaotic motion is performed using the Lyapunov exponents, the fractal dimension and a visual analysis of several "sections" of the fractal attractors.

In the seventh chapter, the act-and-wait controller is introduced and applied to the single DoF system under study. The advantages in terms of enlarged stability chart and possibility of deadbeat control are presented. Then, it is shown how the system can lose stability through a period-doubling bifurcation and a NS bifurcation, the latter presenting a degenerate form that can be solved by adding a damping term. Also, drawbacks of the act-and-wait method, related to multiple solutions existing in the stable region, are shown.

The eighth chapter shows the results obtained through an experimental investigation of the aeropendulum. The first part of the chapter is dedicated to parameter identification, which is not a trivial task in the case of nonlinear systems. Then, a comparison between analytical/numerical and experimental results validates the method used to estimate stability. The obtained results strengthen the importance of considering the digital effect in the analysis of stability of robotic systems.

The concluding chapter summarizes all the results obtained throughout the dissertation, in order to give a short overview of the main achievement of this work.

Chapter 2

Stability analysis of positioning mechanical systems

In this chapter we present a simple and straightforward technique to analyze the stability of the digital PD position control applied to linear systems. We will show the different features of both a single and a two-DoF system, highlighting the existing criticality of a system with a proper natural frequency, combined with a digital controller. The analysis will focus on the differences between a continuous and a discrete time approach.

The system under study wants to model a single link robotic arm. In the single DoF system the link is considered rigidly connected to the rotor of the DC motor. In this case, besides the inertia, the only force acting on the link is the force imposed by the magnetic field of the motor. In the two-DoF system, the link is considered to be connected to the rotor of the DC motor through a visco-elastic joint, as for example a belt. In this case the control force is acting on the first inertial component, while the motion of the other inertial component is controlled by the spring and damper connecting the two masses with each other. The two-DoF mechanical system can be considered to model also a single elastic robotic arm. In this case the spring and the damper should be related to the first mode of vibration of the arm.

2.1 Single DoF mechanical system

Figure 2.1 presents an ideal one-DoF mechanical model of the position control, where m stands for the mass modeling the inertia of the robot and Q is the control force. The desired position x_d is set to zero in order to simplify the equations without losing generality of the problem. The digital processor reads the input, the position x and the velocity $\dot{x}$ of the mass, and elaborates a current signal that is sent to the DC motor.

The characteristic curve of the force of the DC motor is considered linearly proportional to the input current,

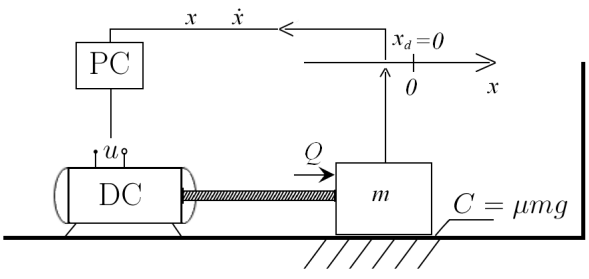

Figure 2.1: Mechanical model of a single DoF system

so we can express the control force as

$$Q = -Px - D\dot{x} \tag{2.1}$$

where P and D are the proportional and the differential gains, respectively. The mass is considered to be rigidly connected to the motor. The equation of motion of the system is then

$$m\ddot{x} = -Px - D\dot{x} - C\left(\dot{x}\right), \tag{2.2}$$

where $C(\dot{x})$ is the dry friction. It can be easily verified that, although $x = 0$ is the desired position, all the positions such that $|x| < C/P$ satisfy Eq. (2.2). Thus, the maximal positioning error is equal to $\epsilon_{\max} = C/P$. In this respect, it is clear that a large proportional gain is required in order to achieve accurate positioning. As we will show in the next sections, too large proportional gains can, at the same time, destabilize the system.

Since dry friction decreases the total mechanical energy during motion, the stability properties of a stable frictionless system should not be better than in the presence of friction. In other words, an analysis of the system, with neglected the dry friction, is conservative with respect to stability. Thus, the forthcoming stability analysis will be carried out with $C = 0$.

2.1.1 Continuous time approach

We first consider a continuous time approach, i.e. we neglect the effects of the digitization of the processor, that will be introduced and explained in the next section.

Neglecting the dry friction C, the equation of motion is the same of an ideal mass-spring-damper system. The only solution is the trivial one, that is stable if the proportional and the differential gains P and D are larger than zero. The fastest convergence can be obtained choosing properly the control gains, such that the damping factor is equal to 1, i.e.

$$\frac{D}{2\sqrt{Pm}} = 1. \tag{2.3}$$

Detailed analysis of a mass-spring-damper system can be found in any basic textbook of mechanics, so we will not investigate further this simple case.

2.1.2 Discrete time approach

As we already mentioned, in most of real applications in robotics, the control force is calculated by a digital processor, which, due to its digital nature, does not work continuously neither in time nor in space. The discretization in space is due to the finite number of digits dedicated to each physical quantity processed by the controller, thus all sampled physical quantities have a finite resolution which cause a rounding error (for an introduction on the topic see [54]). However, this error is usually so small that can be neglected, as we will also do in this work. The discretization in time is instead due to the finite sampling frequency of the processor, which for physical limitation cannot continuously sample the input quantities, but it needs a finite time between following samples, called sampling time.

There exist several methods to model the time discretization of the processor. The most typical approach is the zero-order hold, which consists in considering piecewise constant the output of the controller, that in our case is the force Q. Furthermore, in order to consider the time the processor and the motor need to calculated and impose the force to the system, the control force is calculated from the position and the velocity sampled at the beginning of the previous sampling interval (see Fig. 2.2). Calling the discrete sampling instants $t_j = j\tau$, $j = 0, 1, 2, ...$, where τ stands for the sampling time, $f_s = 1/\tau$ is the sampling frequency, the control force can be defined as

$$Q\left(t\right) = -Px\left(t_{j-1}\right) - D\dot{x}\left(t_{j-1}\right), \quad t \in [t_j, t_{j+1}). \tag{2.4}$$

Neglecting the dry friction again, the equation of motion is

$$m\ddot{x}\left(t\right) = -Px\left(t_j - \tau\right) - D\dot{x}\left(t_j - \tau\right), \quad t \in [t_j, t_{j+1}). \tag{2.5}$$

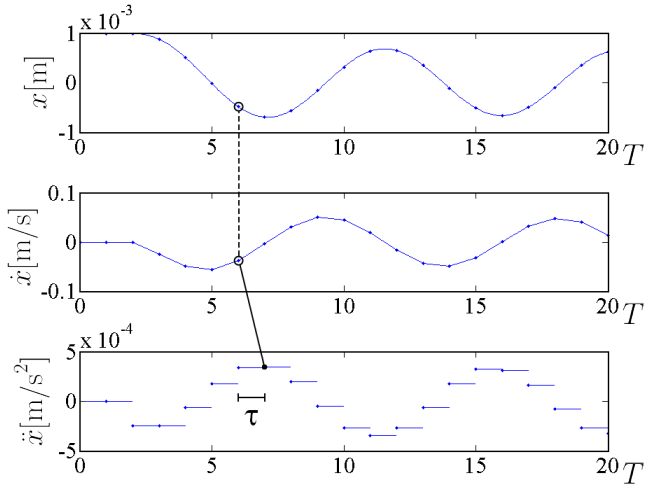

Figure 2.2: Time characteristics of the digital control

The system in Eq. (2.5) is piecewise linear with constant time intervals. A typical approach to analyze such systems, consists in solving the linear equation of motion within a single general time step, considering the final state of a time step as the initial conditions of the following one. The continuous time system can be then transformed into a discrete map, which describes the state of the system at the beginning of each time interval [39]. The stability properties of this map are the same of the original continuous time system.

In order to simplify the system, we introduce the dimensionless time T as

$$T = \frac{t}{\tau}, \qquad \frac{\mathrm{d}}{\mathrm{d}t} = \frac{1}{\tau}\frac{\mathrm{d}}{\mathrm{d}T}, \qquad \frac{\mathrm{d}\square}{\mathrm{d}t} = \dot{\square}, \qquad \frac{\mathrm{d}\square}{\mathrm{d}T} = \square'$$

so the equation of motion becomes

$$x''(T) = -\frac{P\tau^2}{m}x(j-1) - \frac{D\tau}{m}x'(j-1), \quad T \in [j, j+1) \tag{2.6}$$

where prime stands for the dimensionless time derivative. Calling $p = P\tau^2/m$ and $d = D\tau/m$ we can rewrite Eq. (2.6) in the simpler form

$$x''(T) = -px(j-1) - dx'(j-1), \quad T \in [j, j+1) \tag{2.7}$$

where the only parameters controlling the dynamics of the system are p and d. Thus, $x''(T)$ is piecewise constant and we call $x''_j = x''(T = j)$.

After integration of Eq. (2.7) we can define the acceleration, the velocity and the position in the following way:

$$x''_{j+1} = -px(j) - dx'(j) \tag{2.8}$$
$$x'(T) = x'(j) + x''_j(T-j) \tag{2.9}$$
$$x(T) = x(j) + x'(j)(T-j) + \frac{1}{2}x''_j(T-j)^2 \tag{2.10}$$
$$T \in [j, j+1)$$

where $T - j$, calculated in j+1, is equal to 1. So in matrix form we have

$$\begin{pmatrix} x_{j+1} \\ x'_{j+1} \\ x''_{j+1} \end{pmatrix} = \begin{pmatrix} 1 & 1 & \frac{1}{2} \\ 0 & 1 & 1 \\ -p & -d & 0 \end{pmatrix} \begin{pmatrix} x_j \\ x'_j \\ x''_j \end{pmatrix} \tag{2.11}$$

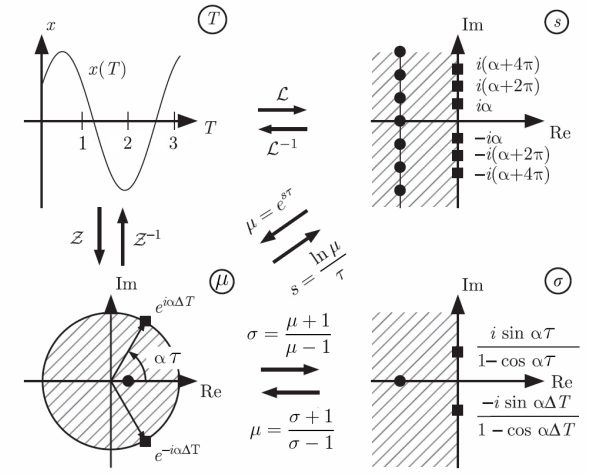

Figure 2.3: Transformation for stability analysis

or in compact form

$$\mathbf{x}_{j+1} = \mathbf{A}\mathbf{x}_j \tag{2.12}$$

with obvious meaning of the terms.

Note that the dependence of the control force (and acceleration x'') on the position and velocity sampled at the beginning of the previous sampling interval has allowed to reduce the system dimension from four (x_{j+1}, x'_{j+1}, x_j and x'_j) to three (x_{j+1}, x'_{j+1} and x''_{j+1}). Should there be no delay in the system (Q_j depending on $\mathbf{x}_j$), it would be possible to reduce the dimension to two; but this is not the case for most of actual applications.

Equation (2.11) is a discrete map that describes the dynamics of the system; as we already mentioned, the convergence of the 3-D geometrical series in Eq. (2.11) is equivalent to the asymptotic stability of the zero solution of Eq. (2.5).

As explained in basic textbooks, the trivial solution of the linear mapping (2.11) is asymptotically stable if and only if all the eigenvalues of $\mathbf{A}$, i.e. the eigenvalues $|\mu_{1,2,3}| < 1$ are located within the unit circle of the complex plane. However, the study of the possible bifurcations and vibration frequencies along the stability limits also requires the use of the characteristic exponents s. Their relations are represented in Fig. 2.3 in accordance with the following standard calculation [37].

The substitution of the exponential trial solution $\boldsymbol{x}(T) = \boldsymbol{K}e^{sT}$ ($s \in \mathbb{C}, \boldsymbol{K} \in \mathbb{R}^3$) into (2.11) yields the characteristic equation $\det(e^{s\tau}\mathbf{I} - \mathbf{A}) = 0$. This has an infinite number of roots s_k, $k = 1, 2, ...$ called characteristic exponents, which are situated along a finite number of vertical lines in the complex plane as shown in Fig. 2.3. Clearly, there is only a finite number of characteristic multipliers defined by $\mu = e^{s\tau}$. These are actually the three eigenvalues of the transition matrix $\mathbf{A}$. The criterion for the exponential stability of the position control can be written as

$$\det(\mu\mathbf{I} - \mathbf{A}) = 0, \qquad |\mu_{1,2,3}| < 1 \Leftrightarrow \Re(s_k) < 0. \tag{2.13}$$

The same stability condition can be derived using the Laplace transformation $\mathcal{L}$, which is illustrated in Fig. 2.3.

For the stability analysis, we follow the calculation of the eigenvalues μ from the characteristic equation (2.13)

$$\det(\mu\mathbf{I} - \mathbf{A}) = \sum_{k=0}^{3} b_k \mu^k = 0, \tag{2.14}$$

where

$$\begin{pmatrix} b_3 \\ b_2 \\ b_1 \\ b_0 \end{pmatrix} = \begin{pmatrix} 1 \\ -2 \\ 1+d+p/2 \\ -d+p/2 \end{pmatrix}.$$

In order to avoid the tedious algebraic work during the solution of the above third degree equation, the so-called Moebius transformation can be used for the new variable σ [53].

$$\mu = \frac{\sigma+1}{\sigma-1} \Rightarrow \{|\mu| < 1 \Leftrightarrow \Re(\sigma < 0\}. \tag{2.15}$$

The transformation is also shown in Fig. 2.3; the open unit circle is mapped back to the left half of the complex plane. After the application of the transformation in Eq. (2.15), the equation again becomes a third degree polynomial

$$p_3(\sigma) = \sum_{k=0}^{3} a_k \sigma^k = 0, \tag{2.16}$$

$$\begin{pmatrix} a_3 \\ a_2 \\ a_1 \\ a_0 \end{pmatrix} = \begin{pmatrix} 1 & 1 & 1 & 1 \\ 3 & 1 & -1 & -3 \\ 3 & -1 & -1 & 3 \\ 1 & -1 & 1 & -1 \end{pmatrix} \begin{pmatrix} b_3 \\ b_2 \\ b_1 \\ b_0 \end{pmatrix} = \begin{pmatrix} p \\ 2(d-p) \\ 4-4d+p \\ 2(2+d) \end{pmatrix}, \tag{2.17}$$

the kth column of the transformation matrix contains the binomial coefficients of $(\sigma+1)^{4-k} \times (\sigma-1)^{k-1}$, $k = 1, 2, 3, 4$.

In order to verify when the roots of p_3 are located on the left half of the complex plane, the Routh-Hurwitz criterion can be applied to the coefficients in Eq. (2.17). It gives the following conditions to be satisfied in order to have stability:

$$\begin{aligned} &a_3 > 0 \Leftrightarrow p > 0 \\ &a_2 > 0 \Leftrightarrow d - p > 0 \\ &a_1 > 0 \Leftrightarrow d < \frac{4+p}{4} \\ &a_0 > 0 \Leftrightarrow d > -2 \\ &H_2 = a_2 a_1 - a_3 a_0 > 0 \Leftrightarrow p^2 - 4pd + 4d^2 + 6p - 4d < 0 \end{aligned}$$

In Fig. 2.4(a) the stability chart is shown. The maximal allowed value of p, in order to have stability, is $p = 1/4$ when $d = 5/8$, i.e. $P\tau^2/m = 1/4$ and $D\tau/m = 5/8$. From the stability chart we immediately notice that the stability domain is bounded due to the digital effect.

Within the stable region, the speed of convergence of the system to the zero position depends on the absolute value of the maximal eigenvalue $\mu_{\max}$ of $\mathbf{A}$. At each time step, it will converge to zero with the factor $M = |\mu_{\max}| < 1$. It can be verified that the maximal speed of convergence is at $p = 1/27$ and $d = 17/54$, where $M_{\min} = 2/3$, as shown in Fig. 2.4(a).

Dynamic behavior

The most interesting stability limit in Fig. 2.4 is the one where $H_2 = 0$, since the other ($p = 0$) is a simple static loss of stability. It is easy to find that when the coefficient p is increased up to the stability limit, two complex conjugate eigenvalues of $\mathbf{A}$ go out from the unit circle of the complex plane with the value $\mu_{1,2} = e^{\pm i\alpha}$. According to Floquet theory in this circumstance there is a Neimark-Sacker (NS) bifurcation [25].

A detailed analysis of the occurring NS bifurcation will be presented in Ch. 4, but still, considering this linear system, the lowest angular frequencies of the oscillation at the loss of stability can be calculated in closed form. To do so we substitute the generic value $i\omega$ to σ in Eq. (2.16), then we separate the real and the imaginary

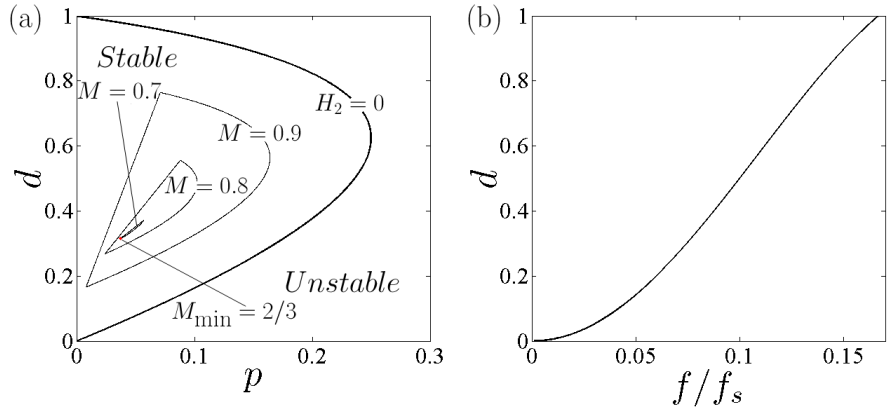

Figure 2.4: (a): stability chart in the p, d space. (b): vibration frequencies at the stability border.

parts. Imposing the real part to be equal to zero, we can find the value of ω on the curve $H_2 = 0$ (at the loss of stability σ is purely imaginary). When σ_1 has a pure imaginary value, considering that $\mu = (\sigma + 1)/(\sigma - 1)$ (see Eq. (2.15)), we can easily find that

$$\mu_1 = \frac{\omega^2 - 1}{\omega^2 + 1} + i\frac{2\omega}{\omega^2 + 1}. \tag{2.18}$$

Since $|\mu_1| = 1$ and $\mu_1 = |\mu_1|e^{i\alpha} = e^{i\alpha} = \cos\alpha + i\sin\alpha$, so

$$\alpha = \tan^{-1}\left(\frac{2\omega}{\omega^2 - 1}\right). \tag{2.19}$$

The vibration frequency is then

$$f = \frac{\alpha}{2\pi\tau}, \qquad f_s = \frac{1}{\tau} \quad \Rightarrow \quad \frac{f}{f_s} = \frac{\alpha}{2\pi}. \tag{2.20}$$

Applying this procedure we obtain for the vibration frequency

$$\frac{f}{f_s} = \text{atan}\left(\frac{2\sqrt{\frac{2+d}{3-\sqrt{9-8d}-d}}}{-1 + \frac{2+d}{3-\sqrt{9-8d}-d}}\right)\frac{1}{2\pi} \tag{2.21}$$

that is plotted in Fig. 2.4(b).

2.2 Two-DoF mechanical system

The idea in the background of the work presented in this section is to model a robot that was designed as an n DoF rigid body system with a higher number of degrees-of-freedom, in order to account for the elasticity of some of its parts (like joints or links). For the sake of simplicity and as a natural extension of the previous section, we consider a single DoF rigid body system that is modeled as a two-DoF system because of the elasticity of one of its elements.

In the case of a robotic arm with an elastic joint (Fig. 2.5 (a)) the system has two inertial components, one is related to the inertia I_1 of the rotor and the other one I_2 pertains to the arm itself. The two elements are connected through an elastic joint (represented by a belt in the figure) which can be modeled as a purely viscoelastic component (with parameters k and c). A single elastic link robotic arm (in Fig. 2.5 with (b) prismatic or (c) revolute joints) can also be modeled as a two-lumped mass system with a viscoelastic element modeling the first mode of vibration of the arm.

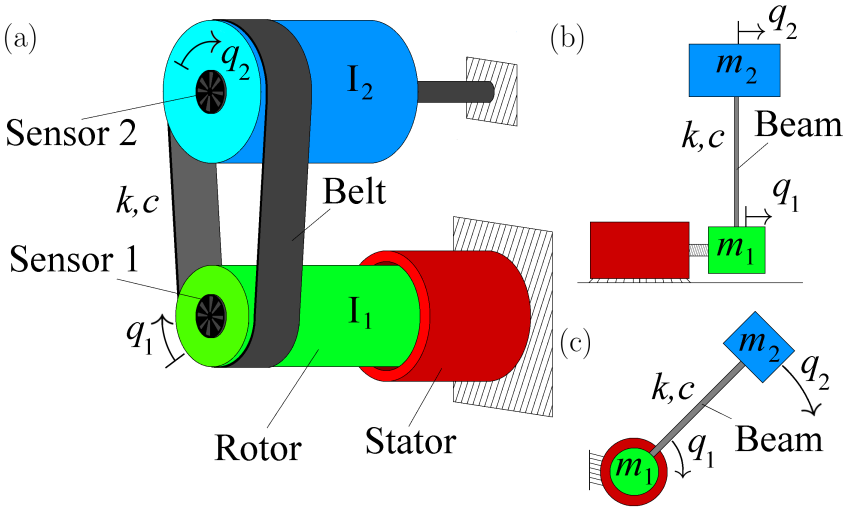

Figure 2.5: Examples of possible elastic parts of robotic arms. (a): transmission provided by an elastic belt. (b), (c): elastic robotic arms prismatic (b) or revolute (c) joints.

The system under study in Fig. 2.6 consists of two lumped masses, m_1 and m_2, connected to each other through a spring of stiffness k and a damper of damping factor c. In the system, the control force is directly applied to the mass m_1. The aim of the controller is to stabilize the position of m_2. In applications, the sensors detecting the position and the velocity of the system usually measure the position and the velocity of one component only, typically those of the motor, i.e. they measure the state of m_1. However, in some high precision applications [50], the sensors are placed at the end-effector, i.e. they measure the state of m_2. In this section, we compare these two cases: when the sensors are placed on the motor (m_1) (*configuration A*, Figure 2.6(a)) and when the sensors are placed on the arm (m_2) (*configuration B*, Figure 2.6(b)). In the case of configuration A we have a so-called collocated system, while in the case of configuration B we have a non-collocated system. Since the system has two degrees of freedom and only one actuator, it is underactuated, in some sense. In order to keep the analysis as general as possible, the kind of sensors used is not specified. Of course some kinds of sensors may require specific modifications to the model, especially regarding the time modeling in the discrete time approach.

2.2.1 Continuous time approach

Collocated case (Configuration A)

Considering configuration A, the processor reads the position and the velocity, q_1 and $\dot{q}_1$, in input and elaborates an electric signal, that is converted into the force Q_A by the motor. In the model the dry friction is neglected and the desired position q_d is again set to zero.

The characteristic curve of the force of the DC motor is considered linearly proportional with the electric signal in input, so we can express the control force as

$$Q_A = -P_A q_1 - D_A \dot{q}_1 \tag{2.22}$$

where P_A and D_A are the proportional and the differential gain, respectively. The system has two degrees of freedom and the system of equations governing the motion is

$$\begin{pmatrix} m_1 & 0 \\ 0 & m_2 \end{pmatrix} \begin{pmatrix} \ddot{q}_1 \\ \ddot{q}_2 \end{pmatrix} + \begin{pmatrix} c + D_A & -c \\ -c & c \end{pmatrix} \begin{pmatrix} \dot{q}_1 \\ \dot{q}_2 \end{pmatrix} + \begin{pmatrix} k + P_A & -k \\ -k & k \end{pmatrix} \begin{pmatrix} q_1 \\ q_2 \end{pmatrix} = \begin{pmatrix} 0 \\ 0 \end{pmatrix} \tag{2.23}$$

that can be rewritten as

$$\mathbf{I}\ddot{\mathbf{q}} + \mathbf{C_A}\dot{\mathbf{q}} + \mathbf{K_A}\mathbf{q} = \mathbf{0} \tag{2.24}$$

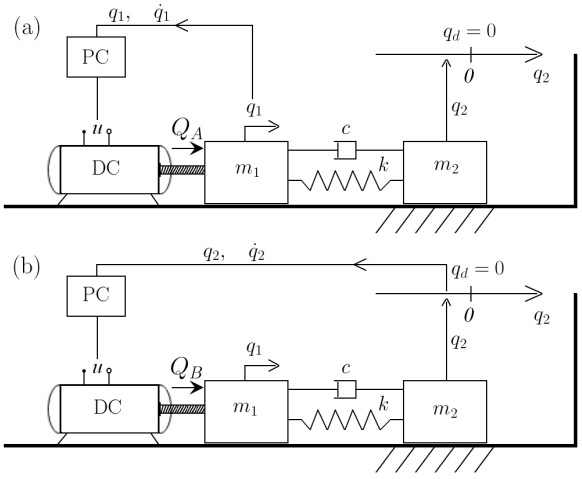

Figure 2.6: Mechanical model of the two-DoF system. (a): configuration A (sensor 1 on, 2 off), collocated system. (b): configuration B (sensor 1 off, 2 on), non-collocated system.

where

$$\mathbf{q} = \begin{pmatrix} q_1 \\ q_2 \end{pmatrix}, \quad \mathbf{C_A} = \begin{pmatrix} 2r\delta_0\omega_0 + \tilde{d}_A(1+r) & -2r\delta_0\omega_0 \\ -2\delta_0\omega_0 & 2\delta_0\omega_0 \end{pmatrix}, \quad \mathbf{K_A} = \begin{pmatrix} \omega_0^2 r + \tilde{p}_A(1+r) & -\omega_0^2 r \\ -\omega_0^2 & \omega_0^2 \end{pmatrix},$$

$\mathbf{I}$ is the identity matrix, $\omega_0 = \sqrt{k/m_2}$, $\delta_0 = c/\left(2\sqrt{km_2}\right)$, $r = m_2/m_1$, $\tilde{p}_A = P_A/\left(m_1+m_2\right)$ and $\tilde{d}_A = D_A/\left(m_1+m_2\right)$. Clearly the trivial solution $(q_1, q_2) = (0, 0)$ satisfies Eq. (2.24).

In order to study the stability of the trivial solution, we calculate the characteristic polynomial of the system, i.e.

$$a_4\lambda^4 + a_3\lambda^3 + a_2\lambda^2 + a_1\lambda + a_0 = 0 \tag{2.25}$$

where

$$\begin{aligned} a_4 &= 1 \\ a_3 &= \left(\tilde{d}_A + 2\delta_0\omega_0\right)(1+r) \\ a_2 &= \left(\tilde{p}_A + 2\delta_0\omega_0\tilde{d}_A + \omega_0^2\right)(1+r) \\ a_1 &= \left(2\delta_0\omega_0\tilde{p}_A + \omega_0^2\tilde{d}_A\right)(1+r) \\ a_0 &= \omega_0^2\tilde{p}_A(1+r). \end{aligned} \tag{2.26}$$

The trivial position is a stable solution of the system, if all roots of (2.25) have real part smaller than zero. As we already did previously, applying the Routh-Hurwitz criterion we obtain the following conditions to be satisfied in order to have stability:

$$\begin{aligned} &a_4 > 0 \\ &a_3 > 0 \iff \tilde{d}_A > -2\delta_0\omega_0 \\ &a_2 > 0 \iff \tilde{p}_A > -2\delta_0\omega_0\tilde{d}_A - \omega_0^2 \\ &a_1 > 0 \iff \tilde{d}_A > -\tfrac{2\delta_0\tilde{p}_A}{\omega_0} \\ &a_0 > 0 \iff \tilde{p}_A > 0 \\ &c_2 = \tfrac{a_3a_2 - a_4a_1}{a_3} > 0 \\ &c_3 = c_2a_1 - a_3a_0 > 0. \end{aligned} \tag{2.27}$$

Figure 2.7 shows the stability chart in the space of the control gains, for a specific set of parameter values. As

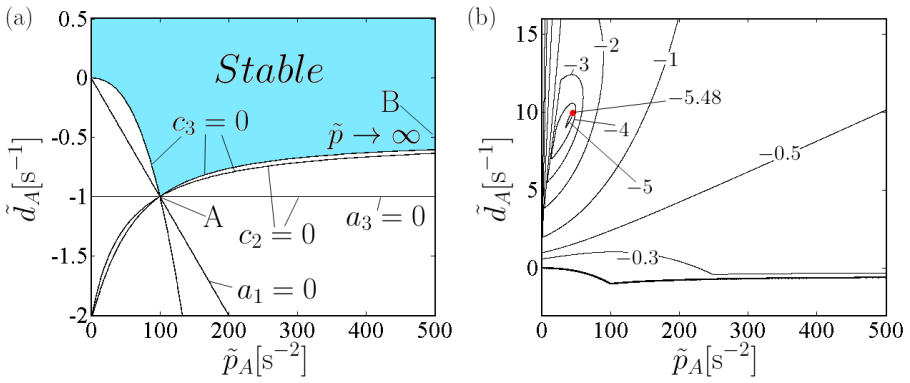

Figure 2.7: Stability chart for the parameter values $\omega_0 = 10\ \mathrm{s}^{-1}$, $r = 1$ and $\delta_0 = 0.05$ of configuration A. (b): the numbers mark loci with the same speed of convergence and correspond to the maximal real part of the roots of Eq. (2.25).

shown, the stability domain is unbounded. It includes all the region where $\tilde{p}_A > 0$ and $\tilde{d}_A > 0$, plus a small region for negative values of $\tilde{d}_A$. The position of point A can be determined in closed form, it is the intersection of the straight lines $a_1 = 0$ and $a_3 = 0$ and it corresponds to the values $\tilde{p}_A = \omega_0^2$ and $\tilde{d}_A = -2\delta_0\omega_0$. Also the position of point B can be determined, it corresponds to the coordinate values $\tilde{p}_A \to \infty$ and $\tilde{d}_A = -2\delta_0\omega_0 r/(r+1)$.

Figure 2.7(b) also shows loci of points in the space of the control gains with the same speed of convergence. The numbers marking the lines indicate the real part of the root of Eq. (2.25) with the biggest real part, that is directly related to the speed of convergence. The red dot in the figure marks the point with the fastest convergence. The maximal speed of convergence is growing linearly with increasing values of ω_0, while it depends also on r in a nonlinear way that we did not define precisely. On the contrary, its dependence on δ is very small and almost negligible, unless δ is very big.

Figure 2.8 shows the influence of parameter values on the stability. An increase in the damping δ_0 would pull down points A and B, while if $\delta_0 = 0$ the stability region would be the same as for the rigid case. An increase in ω_0 would pull down A and B as well and would move A to the right, while an increase in r would enlarge the stable region towards negative values of $\tilde{d}_A$, without moving point A. It should be noted that, if the mass ratio r is very small ($r < 4\delta_0^2(1-\delta_0^2)/(2\delta_0^2-1)^2$), the curve $c_3 = 0$ (see Fig. 2.7(a)) will change its shape, reducing the stable region for negative values of $\tilde{d}_A$ and letting point A out of it (Fig. 2.8(c), $r = 0.001$).

In the case of a single DoF, subject to a continuous time control (see Eq. 2.2), the system was stable only for positive values of the proportional and differential gains. In this respect, we notice that the finite stiffness of the joint increases the stability region, thanks to the damping, which is dissipating energy and can compensate a negative value of the differential gain.

Non-collocated case (configuration B)

We now consider the model in Fig. 2.6(b). Also in this configuration, the aim of the control system is to stabilize the trivial solution, but in this case, the control system reads in input the position and the velocity of the mass m_2. The control force is then

$$Q_B = -P_B q_2 - D_B \dot{q}_2 \tag{2.28}$$

and the equation of motion can be written as

$$\begin{pmatrix} m_1 & 0 \\ 0 & m_2 \end{pmatrix} \begin{pmatrix} \ddot{q}_1 \\ \ddot{q}_2 \end{pmatrix} + \begin{pmatrix} c & D_B - c \\ -c & c \end{pmatrix} \begin{pmatrix} \dot{q}_1 \\ \dot{q}_2 \end{pmatrix} + \begin{pmatrix} k & P_B - k \\ -k & k \end{pmatrix} \begin{pmatrix} q_1 \\ q_2 \end{pmatrix} = \begin{pmatrix} 0 \\ 0 \end{pmatrix} \tag{2.29}$$

or in compact form

$$\mathbf{I}\ddot{\mathbf{q}} + \mathbf{C_B}\dot{\mathbf{q}} + \mathbf{K_B}\mathbf{q} = \mathbf{0} \tag{2.30}$$

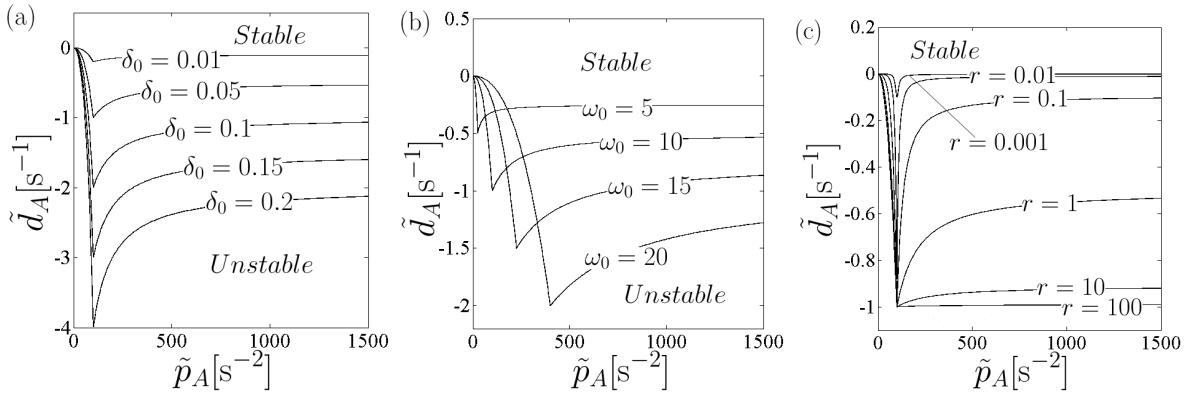

Figure 2.8: Stability chart in the parameter space of the control gains for different coefficient values. Relative to the continuous time approach of configuration A. (a): $\omega_0 = 10\,\mathrm{s}^{-1}$, $r = 1$. (b): $r = 1$, $\delta_0 = 0.05$. (c): $\omega_0 = 10\,\mathrm{s}^{-1}$, $\delta_0 = 0.05$.

where

$$\mathbf{q} = \begin{pmatrix} q_1 \\ q_2 \end{pmatrix}, \quad \mathbf{C_B} = \begin{pmatrix} 2r\delta_0\omega_0 & \tilde{d}_B(1+r) - 2r\delta_0\omega_0 \\ -2\delta_0\omega_0 & 2\delta_0\omega_0 \end{pmatrix}, \quad \mathbf{K_B} = \begin{pmatrix} \omega_0^2 r & \tilde{p}_B(1+r) - \omega_0^2 r \\ -\omega_0^2 & \omega_0^2 \end{pmatrix}.$$

As in the case of configuration A, we calculate the characteristic polynomial, that is

$$a_4\lambda^4 + a_3\lambda^3 + a_2\lambda^2 + a_1\lambda + a_0 = 0. \tag{2.31}$$

where

$$\begin{aligned} a_4 &= 1 \\ a_3 &= 2\delta_0\omega_0\,(1+r) \\ a_2 &= \omega_0\left(2\tilde{d}_B\delta_0 + \omega_0\right)(1+r) \\ a_1 &= \omega_0\left(2\tilde{p}_B\delta_0 + \tilde{d}_B\omega_0\right)(1+r) \\ a_0 &= \omega_0^2\tilde{p}_B(1+r). \end{aligned} \tag{2.32}$$

Applying the Routh-Hurwitz criterion, we obtain the following conditions, to be satisfied in order to have stability

$$\begin{aligned} &a_4 > 0 \\ &a_3 > 0 \\ &a_2 > 0 \iff \tilde{d}_B > -\tfrac{\omega_0}{2\delta_0} \\ &a_1 > 0 \iff \tilde{p}_B > -\tfrac{\tilde{d}_B\omega_0}{2\delta_0} \\ &a_0 > 0 \iff \tilde{p}_B > 0 \\ &c_2 = \tfrac{a_3a_2 - a_4a_1}{a_3} > 0 \\ &c_3 = c_2a_1 - a_3a_0 > 0. \end{aligned} \tag{2.33}$$

Figure 2.9 shows the stability chart in the parameter space of the control gains. A comparison between the two stability domains in Figs. 2.7 and 2.9, immediately shows that in the case of configuration B the stable region is bounded, in contrast to the unbounded stable region of configuration A. In this configuration, if $\delta_0 = 0$ there is no stable region. It is possible to determine in closed form the intersections of the border of the stable region with the axes that are the origin and point N, which has coordinates

$$\mathrm{N} = \left(0, \frac{2\delta_0(1+r)\omega_0}{1 - 4\delta_0^2(1+r)}\right), \tag{2.34}$$

while the stable point with the maximal proportional gain is point M, that has coordinates

$$\mathrm{M} = \left(\frac{\left[1 - 2\delta_0^2(1+r) - \sqrt{1 - 4\delta_0^2(1+r)}\right]\omega_0^2}{8\delta_0^4(1+r)}, \left[\frac{1 - 2\delta_0^2(1+r)}{\sqrt{1 - 4\delta_0^2(1+r)}} - 1 \right] \frac{\omega_0}{4\delta_0^3(1+r)} \right). \tag{2.35}$$

Figure 2.10 shows the influence of parameter values on the stability. Also for configuration B, an increase in δ_0, ω_0 or r enlarges the stable region, although the parameters have different effects with respect to stability.

Increasing the values of r and δ_0, as $1 - 4\delta_0^2(1+r)$ tends to zero, the stable area increases its extent. For $1 - 4\delta_0^2(1+r) \leq 0$, the stable region becomes unbounded. As shown in Fig. 2.11, the stability border follows a line which starts from zero and develops along the straight asymptote with inclination $2\delta_0 / \left[(4\delta_0^2(1+r) - 1)\omega_0\right]$.

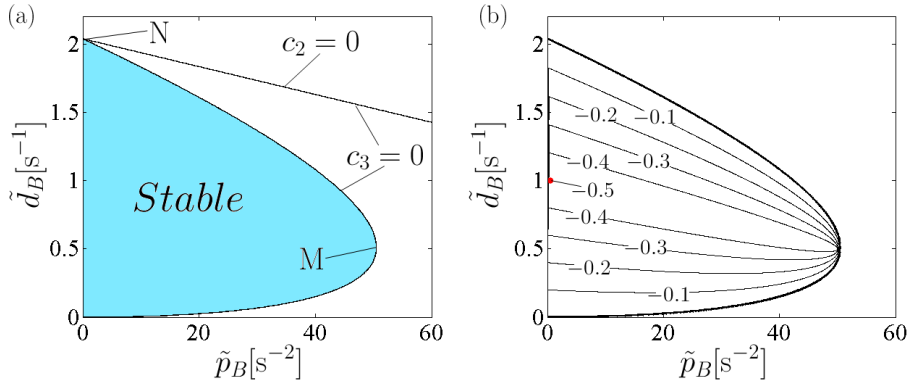

Figure 2.9: Stability chart for the parameter values $\omega_0 = 10\ \mathrm{s}^{-1}$, $r = 1$ and $\delta_0 = 0.05$ of configuration B. (b): the numbers mark loci with the same speed of convergence and correspond to the maximal real part of the roots of Eq. (2.31).

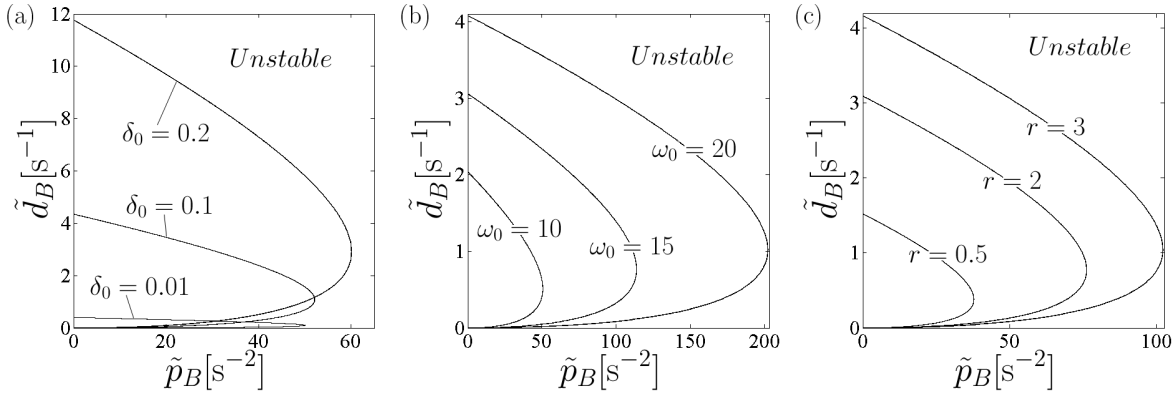

Figure 2.10: Stability charts in the parameter space of the control gains for different coefficient values. Relative to the continuous time approach of configuration B. (a): $\omega_0 = 10\,\mathrm{s}^{-1}$, $r = 1$. (b): $r = 1$, $\delta_0 = 0.05$. (c): $\omega_0 = 10\,\mathrm{s}^{-1}$, $\delta_0 = 0.05$.

Figures 2.9(b) and 2.11 show loci of points in the space of the control gains with the same speed of convergence. The red dot marks the point with the fastest convergence. In that point, the maximal real part of the roots of Eq. (2.31) is equal to $\omega_0\delta_0(r+1)/2$. This result has been found from interpolation of results obtained numerically, but it appears to be valid also in the case of $1 - 4\delta_0^2(1+r) < 0$ (figure 2.11) without any approximation.

The smaller stable region in the case of configuration B, can be explained considering that, in configuration A, the control system is collocated, i.e. the control force is acting on the sensed mass. The control force is trying to stabilize m_1 and it acts depending on its position and velocity, while m_2 is a kind of appendage of m_1 that is dissipating energy, so if m_2 is very small ($r \to 0$) or there is no internal damping ($\delta_0 \to 0$) the stable region is the same as in the case of a rigid arm. On the other hand, in the case of configuration B, the system is non-collocated, i.e. the force is acting on the non-sensed mass. In this case the system is trying to stabilize the position of m_2, but the force is acting on m_1. Since the control system does not consider the dynamical coupling between the two masses, and it acts according to the position and the velocity of m_2 only, it may give a positive force while a negative one would be required to stabilize the system or vice versa, so it may have a negative effect on the stability. These kinds of stability problems, related to non-collocated systems, are widely discussed in literature [10, 67]. With respect to the speed of convergence, in the shown cases configuration A has a faster convergence, but high values of r and δ_0 can both enlarge the stable region (up to make it unbounded) and increase the speed of convergence in configuration B. In this respect, if $m_2 \gg m_1$, the non-collocated configuration may be more efficient.

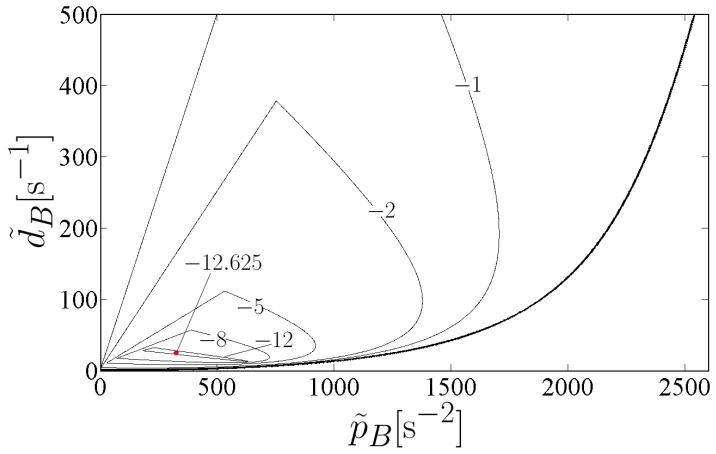

Figure 2.11: Stability chart for the parameter values $\omega_0 = 5\ \mathrm{s}^{-1}$, $r = 100$ and $\delta_0 = 0.05$ of configuration B.

2.2.2 Discrete time approach

Similarly to how we did for the single DoF case, we now consider finite the sampling time τ of the processor and we call f_s the sampling frequency. The control force is again piecewise constant and the system is piecewise linear.

Collocated case (configuration A)

In the case of configuration A, the control force can be written as

$$Q_A(t) = -P_A q_1(t_{j-1}) - D_A \dot{q}_1(t_{j-1}), \qquad t \in [t_j, t_{j+1}). \tag{2.36}$$

Introducing again the dimensionless time $T = t/\tau$, the equations of motion can be written as

$$\begin{aligned} &\frac{m_1}{\tau^2} q_1''(T) + k\left[q_1(T) - q_2(T)\right] + \frac{c}{\tau}\left[q_1'(T) - q_2'(T)\right] + P_A q_1(j-1) + D_A q_1'(j-1) = 0 \\ &\frac{m_2}{\tau^2} q_2''(T) + k\left[q_2(T) - q_1(T)\right] + \frac{c}{\tau}\left[q_2'(T) - q_1'(T)\right] = 0 \\ &T \in [j, j+1) \end{aligned} \tag{2.37}$$

Proceeding as for the single DoF system, we transform the system into a map, solving the equation of motion for each time step in closed form. In a single time step the equation of motion can be written as

$$\mathbf{M}\mathbf{q}'' + \mathbf{C}\mathbf{q}' + \mathbf{K}\mathbf{q} = \mathbf{f}_A \tag{2.38}$$

where

$$\mathbf{M} = \begin{pmatrix} \frac{m_1}{\tau^2} & 0 \\ 0 & \frac{m_2}{\tau^2} \end{pmatrix}, \mathbf{C} = \begin{pmatrix} \frac{c}{\tau} & -\frac{c}{\tau} \\ -\frac{c}{\tau} & \frac{c}{\tau} \end{pmatrix}, \mathbf{K} = \begin{pmatrix} k & -k \\ -k & k \end{pmatrix}, \mathbf{q} = \begin{pmatrix} q_1(T) \\ q_2(T) \end{pmatrix}, \mathbf{f}_A = \begin{pmatrix} Q_A \\ 0 \end{pmatrix}.$$

The system in (2.38) is coupled, in order to decouple it, we use the modal analysis. We look for the eigenvectors of the matrix $\mathbf{M}^{-1}\mathbf{K}$ that are

$$\mathbf{u}_1 = \begin{pmatrix} 1 \\ 1 \end{pmatrix} \text{ and } \mathbf{u}_2 = \begin{pmatrix} -\frac{m_2}{m_1} \\ 1 \end{pmatrix}, \tag{2.39}$$

then we define the transformation matrix

$$\mathbf{U} = \begin{pmatrix} \mathbf{u}_1 & \mathbf{u}_2 \end{pmatrix} = \begin{pmatrix} 1 & -\frac{m_2}{m_1} \\ 1 & 1 \end{pmatrix} \tag{2.40}$$

and we change the coordinate system according to the transformation $\mathbf{q} = \mathbf{U}\mathbf{x}$, so we can rewrite Eq. (2.38) as

$$\mathbf{U}^T\mathbf{M}\mathbf{U}\mathbf{x}'' + \mathbf{U}^T\mathbf{C}\mathbf{U}\mathbf{x}' + \mathbf{U}^T\mathbf{K}\mathbf{U}\mathbf{x} = \mathbf{U}^T\mathbf{f}_A \tag{2.41}$$

i.e.

$$\begin{pmatrix} \frac{m_1+m_2}{\tau^2} & 0 \\ 0 & \frac{m_2(m_1+m_2)}{m_1\tau^2} \end{pmatrix} \begin{pmatrix} x_1''(T) \\ x_2''(T) \end{pmatrix} + \begin{pmatrix} 0 & 0 \\ 0 & \frac{c(m_1+m_2)^2}{m_1^2} \end{pmatrix} \begin{pmatrix} x_1'(T) \\ x_2'(T) \end{pmatrix} + \begin{pmatrix} 0 & 0 \\ 0 & \frac{k(m_1+m_2)^2}{m_1^2} \end{pmatrix} \begin{pmatrix} x_1(T) \\ x_2(T) \end{pmatrix} = \begin{pmatrix} Q_A \\ -\frac{m_2}{m_1}Q_A \end{pmatrix} \tag{2.42}$$

The system in (2.42) is decoupled, so we can solve the two equations separately. Considering that

$$\begin{array}{ll} q_1 = x_1 - \frac{m_2}{m_1}x_2 & \longrightarrow \quad x_1 = \frac{m_1q_1+m_2q_2}{m_1+m_2} \\ q_2 = x_1 + x_2 & \quad\;\; x_2 = \frac{m_1(q_2-q_1)}{m_1+m_2}, \end{array} \tag{2.43}$$

and the equations in (2.42), it is clear that the variable x_1 is related to the rigid movement of the system, while x_2 is related to the relative movement between the two masses.

The first of the two equations of (2.42) is

$$x_1''(T) = \frac{\tau^2}{m_1+m_2}Q_{A,j} \qquad T \in [j, j+1) \tag{2.44}$$

where $Q_{A,j}$ is constant, since we are considering a single time step. Integrating (2.44), we have

$$x_1'(T) = x_{1,j}''(T-j) + x_{1,j}' = \frac{\tau^2}{m_1+m_2}Q_{A,j}(T-j) + x_{1,j}' \tag{2.45}$$

$$x_1(T) = \frac{1}{2}x_{1,j}''(T-j)^2 + x_{1,j}'(T-j) + x_{1,j} = \frac{1}{2}\frac{\tau^2}{m_1+m_2}Q_{A,j}(T-j)^2 + x_{1,j}'(T-j) + x_{1,j} \tag{2.46}$$

$T \in [j, j+1)$.

where $x_{1,j} = x_1(T = j)$, $x'_{1,j} = x'_1(T = j)$ and similary for the other variables. Since $T = j + 1$ at the end of the time step, we can write

$$x'_{1,j+1} = \frac{\tau^2}{m_1 + m_2} Q_{A,j} + x'_{1,j} \tag{2.47}$$

$$x_{1,j+1} = \frac{1}{2}\frac{\tau^2}{m_1 + m_2} Q_{A,j} + x'_{1,j} + x_{1,j}. \tag{2.48}$$

The second equation of (2.42) is

$$\frac{r\,(m_1 + m_2)}{\tau^2} x''_2\,(T) + \frac{c\,(m_1 + m_2)^2}{\tau m_1^2} x'_2\,(T) + \frac{k\,(m_1 + m_2)^2}{m_1^2} x_2\,(T) = -rQ_{A,j} \qquad T \in [j, j + 1), \tag{2.49}$$

calling

$$\omega_n = \sqrt{\frac{k\,(m_1 + m_2)}{m_1 m_2}} = \omega_0\sqrt{1 + r}, \qquad \Omega = \omega_n \tau \tag{2.50}$$

$$\delta = \frac{c}{2\sqrt{k}}\sqrt{\frac{m_1 + m_2}{m_1 m_2}} = \delta_0\sqrt{1 + r} \tag{2.51}$$

$$\hat{Q}_{A,j} = \frac{\tau^2}{(m_1 + m_2)} Q_{A,j} \tag{2.52}$$

we can rewrite (2.49) as

$$x''_2\,(T) + 2\delta\Omega x'_2\,(T) + \Omega^2 x_2\,(T) = -\hat{Q}_{A,j} \qquad T \in [j, j + 1). \tag{2.53}$$

Equation (2.53) can be solved in closed form, and its general solution is

$$x_2\,(T) = -\frac{\hat{Q}_{A,j}}{\Omega^2} + (A\cos(\Omega T) + B\sin(\Omega T))\, e^{-\delta\Omega T} \qquad T \in [j, j + 1). \tag{2.54}$$

Considering the initial conditions $x_2\,(j) = x_{2,j}$ and $x'_2\,(j) = x'_{2,j}$, we have

$$\begin{aligned} x_2\,(T) = & -\frac{\hat{Q}_{A,j}}{\Omega^2} + e^{-\delta\Omega(T-j)}\left[\left(x_{2,j} + \frac{\hat{Q}_{A,j}}{\Omega^2}\right)\cos(\Omega(T - j))\right. \\ & \left. + \left(\frac{x'_{2,j}}{\Omega} + \delta x_{2,j} + \frac{\delta\hat{Q}_{A,j}}{\Omega^2}\right)\sin(\Omega(T - j))\right] \end{aligned} \tag{2.55}$$

$$\begin{aligned} x'_2\,(T) = & \; e^{-\delta\Omega(T-j)}\left[x'_{2,j}\cos(\Omega(T - j))\right. \\ & \left. + \left(x_{2,j}\left(-\delta^2\Omega - \Omega\right) - x'_{2,j}\delta - \hat{Q}_{A,j}\left(\frac{\delta^2}{\Omega} + \frac{1}{\Omega}\right)\right)\sin(\Omega(T - j))\right] \end{aligned} \tag{2.56}$$

$T \in [j, j + 1)$.

At the end of the time step, for $T = j + 1$, we have

$$x_{2,j+1} = x_{2,j}\,(\cos\Omega + \delta\sin\Omega)\, e^{-\delta\Omega} + x'_{2,j}\frac{e^{-\delta\Omega}}{\Omega}\sin\Omega + \frac{\hat{Q}_{A,j}}{\Omega^2}\left[1 + e^{-\delta\Omega}\,(-\cos\Omega - \delta\sin\Omega)\right] \tag{2.57}$$

$$x'_{2,j+1} = x_{2,j}e^{-\delta\Omega}\left(-\delta^2 - 1\right)\Omega\sin\Omega + x'_{2,j}e^{-\delta\Omega}\,(\cos\Omega - \delta\sin\Omega) + \hat{Q}_{A,j}e^{-\delta\Omega}\left(\delta^2 + 1\right)\frac{\sin\Omega}{\Omega}. \tag{2.58}$$

We then consider the control force $Q_{A,j}$, that is

$$Q_{A,j+1} = -P_A q_{1,j} - \frac{D_A}{\tau} q'_{1,j},$$

but considering equations (2.43), we have

$$Q_{A,j+1} = -P_A x_{1,j} + \frac{m_2}{m_1} P_A x_{2,j} - \frac{D_A}{\tau} x'_{1,j} + \frac{m_2}{m_1} \frac{D_A}{\tau} x'_{2,j}. \tag{2.59}$$

Considering equations (2.47), (2.48), (2.57), (2.58) and (2.59) and calling $p_A = P_A \tau^2 / (m_1 + m_2)$ and $d_A = D_A \tau / (m_1 + m_2)$, we can write the following map

$$\begin{pmatrix} x_{1,j+1} \\ x'_{1,j+1} \\ x_{2,j+1} \\ x'_{2,j+1} \\ \hat{Q}_{A,j+1} \end{pmatrix} = \begin{pmatrix} 1 & 1 & 0 & 0 & \frac{1}{2} \\ 0 & 1 & 0 & 0 & 1 \\ 0 & 0 & e^{-\delta\Omega}(c_\Omega + \delta s_\Omega) & \frac{e^{-\delta\Omega}}{\Omega} s_\Omega & -\frac{1}{\Omega^2} + \frac{e^{-\delta\Omega}}{\Omega^2}(c_\Omega + \delta s_\Omega) \\ 0 & 0 & e^{-\delta\Omega}\left(-\delta^2 - 1\right)\Omega s_\Omega & e^{-\delta\Omega}(c_\Omega - \delta s_\Omega) & -e^{-\delta\Omega}\left(1 + \delta^2\right)\frac{s_\Omega}{\Omega} \\ -p_A & -d_A & r p_A & r d_A & 0 \end{pmatrix} \begin{pmatrix} x_{1,j} \\ x'_{1,j} \\ x_{2,j} \\ x'_{2,j} \\ \hat{Q}_{A,j} \end{pmatrix} \tag{2.60}$$

or in compact form

$$\mathbf{x}_{j+1} = \mathbf{B_A} \mathbf{x}_j \tag{2.61}$$

where $c_\Omega = \cos(\Omega)$ and $s_\Omega = \sin(\Omega)$.

Note that the dependence of the control force on the position and velocity sampled at the beginning of the previous sampling interval has allowed to reduce the system dimension from eight ($\mathbf{x}_{j+1}$ and $\mathbf{x}_j$) to five ($\mathbf{x}_{j+1}$ and $\hat{Q}_{\mathbf{A}j+1}$). Should there be no delay in the system ($\hat{Q}_{\mathbf{A},j}$ depending on $\mathbf{x}_j$), it would be possible to reduce the dimension to four; as we mentioned in for the single DoF case, this is not the case for most of actual applications.

Non-collocated case (configuration B)

In the case of configuration B, the control force in (2.36) is redefined as

$$Q_B(t) = -P_B q_2(t_{j-1}) - D_B \dot{q}_2(t_{j-1}), \qquad t \in [t_j, t_{j+1}), \tag{2.62}$$

where P_B and D_B are analogous to P_A and D_A, but referred to m_2. Then the whole procedure, as in the case of configuration A, can be carried out. The only difference is in the control force, so Eq. (2.59) becomes

$$Q_{B,j+1} = -P_B x_{1,j} - P_B x_{2,j} - \frac{D_B}{\tau} x'_{1,j} - \frac{D_B}{\tau} x'_{2,j} \tag{2.63}$$

and matrix $\mathbf{B_B}$ is

$$\mathbf{B_B} = \begin{pmatrix} 1 & 1 & 0 & 0 & \frac{1}{2} \\ 0 & 1 & 0 & 0 & 1 \\ 0 & 0 & e^{-\delta\Omega}(c_\Omega + \delta s_\Omega) & \frac{e^{-\delta\Omega}}{\Omega} s_\Omega & -\frac{1}{\Omega^2} + \frac{e^{-\delta\Omega}}{\Omega^2}(c_\Omega + \delta s_\Omega) \\ 0 & 0 & e^{-\delta\Omega}\left(-\delta^2 - 1\right)\Omega s_\Omega & e^{-\delta\Omega}(c_\Omega - \delta s_\Omega) & -e^{-\delta\Omega}\left(1 + \delta^2\right)\frac{s_\Omega}{\Omega} \\ -p_B & -d_B & -p_B & -d_B & 0 \end{pmatrix}.$$

It should be noted that r is not explicitly appearing in $\mathbf{B_B}$.

In order to compare this two-DoF case with the single DoF one, we should limit our analysis to the variable x_1, that is related to the rigid movement of the arm, and neglect the variable x_2, related to the relative movements between the two masses. So, if we eliminate the third and the fourth rows and the third and the fourth columns of matrix $\mathbf{B_A}$ and $\mathbf{B_B}$, we obtain in both cases the matrix

$$\begin{pmatrix} 1 & 1 & \frac{1}{2} \\ 0 & 1 & 1 \\ -p_{A(B)} & -d_{A(B)} & 0 \end{pmatrix} \tag{2.64}$$

that is exactly as matrix $\mathbf{A}$ of Eq. (2.11).

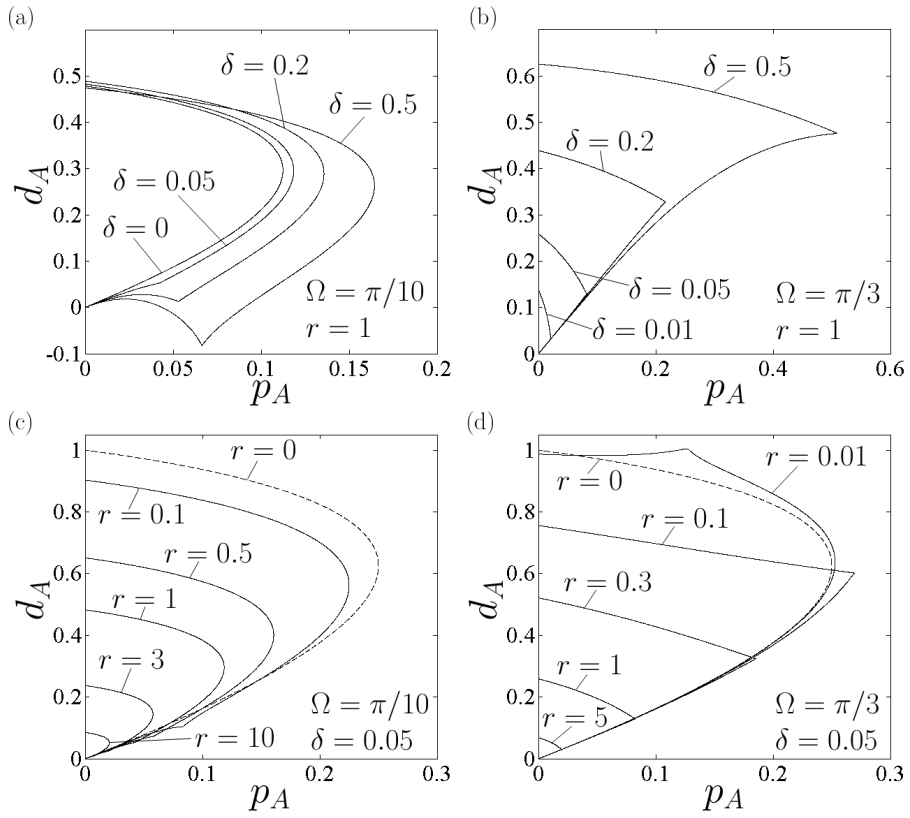

Figure 2.12: Stability charts, referred to the configuration A, in the parameter space of the proportional and differential gains. (a), (b): variation of δ, (c), (d): variation of r.

Stability analysis

The analysis of the stability of the geometric series in Eq. (2.60) is analogous to the one already performed regarding the single DoF case. Thus, also in this case we apply the Moebius transformation and the Routh-Hurwitz criterion. As a result we obtain the following conditions to be satisfied

$$
\begin{array}{ll}
a_5 > 0 & \\
a_4 > 0 & c_4 = \frac{a_4 a_3 - a_5 a_2}{a_4} > 0 \\
a_3 > 0 & c_3 = \frac{a_4 a_1 - a_5 a_0}{a_4} > 0 \\
a_2 > 0 & d_3 = \frac{c_4 a_2 - a_4 c_3}{c_4} > 0 \\
a_1 > 0 & e_2 = d_3 c_3 - c_4 a_0 > 0 \\
a_0 > 0 &
\end{array}
$$

where the coefficients are explicitly written in Appendix A. Of course, in the two cases A and B the coefficients are different.

Referring to the configuration A, the coefficients $a_{5\ldots0}$, $c_{4,3}$, d_3 and e_2 depend on the parameters r, δ, Ω, p_A and d_A. Figs. 2.12-2.14 show the effect of the parameters δ, r and Ω on the stability. From the figures it is clear that reducing the value of r (i.e. reducing m_2) or increasing the rigidity of the connection (i.e. increasing the value of Ω) the stability domain tends to the one relative to the single DoF case, i.e. with a rigid connection between the two masses (Fig. 2.4(a) and Figs. 2.12(c) and (d) dashed line). The damping has always a stabilizing effect, but the sensibility of the system to variations of the damping depends on Ω, i.e. the ratio between the natural frequency of the system and the sampling frequency; in this respect, comparing Figs. 2.12(a) and (b), we can notice that for $\Omega = \pi/10$ and $\delta = 0$ (Fig. 2.12(a)) there exists a stable region and large

variations of δ change the stability domain only slightly, while for $\Omega = \pi/3$ and $\delta = 0$ (Fig. 2.12(b)) there is no stable region at all, but large variations of δ can sensibly enlarge the stable region.

Figures 2.12(c) and (d) show the effect of variations of r on the stability. In this case the effect is very different from what we saw in the case of a continuous time approach: using a continuous time approach, an increase in r enlarges the stable region for negative values of the differential gain $\tilde{d}_A$ (Fig. 2.8), thanks to the dissipating effect of m_2. In the case of a discrete time approach, increases in the value of r sensibly reduce the stable region (Figs. 2.12(c) and (d)). In the case of $\Omega = \pi/3$ (Fig. 2.12(d)), very small values of r enlarge the stable region, but larger values of r make the stable region smaller and smaller. While analyzing Figs. 2.12(c) and (d), it should be noted that variations of the mass ratio r implicitly affect the values of δ and Ω proportionally to $\sqrt{1+r}$, if the physical quantities are not varied (see Eqs. (2.50) and (2.51)). Furthermore $p_A = P_A\tau^2/(m_1+m_2)$ and $d_A = D_A\tau/(m_1+m_2)$, so a small stable region in the $p_A d_A$ space does not necessarily imply a small stable region in the space of the physical control gains $P_A D_A$. In the figures only the dimensionless parameters are considered, and not the physical quantities.

Figure 2.13 shows the effect of variations of Ω on the stability for a fixed value of the differential gain. From the figure it is visible that the most dangerous interval is for $\Omega \in (0.3\pi, \pi)$: in this interval the stable region is extremely small. In the Ω direction, the stable region creates a periodic pattern with period equal to 2π. Increasing the damping the stable region enlarges breaking up the periodic pattern. However, for $\Omega \approx \pi/2$, very high damping is required in order to have stability. We remind that $\Omega = \omega_n\tau$, $\tau = 1/f_s$, so $\Omega = 2\pi f_n/f_s$ and $\Omega = \pi/2$ corresponds to $f_n/f_s = 1/4$.

In Fig. 2.13, the numbers in the circles indicate how many eigenvalues are out of the unit circle in the complex plane. 2 corresponds to two complex conjugate eigenvalues, so to the occurrence of a NS bifurcation [25], while 1 corresponds to one eigenvalue leaving the unit circle through -1, so to a flip or period-doubling bifurcation. In most of the cases, the system is losing stability through a NS bifurcation, while there is a flip bifurcation for $\Omega \approx (1+2n)\pi$ (i.e. $f_n/f_s = 0.5 + n$).

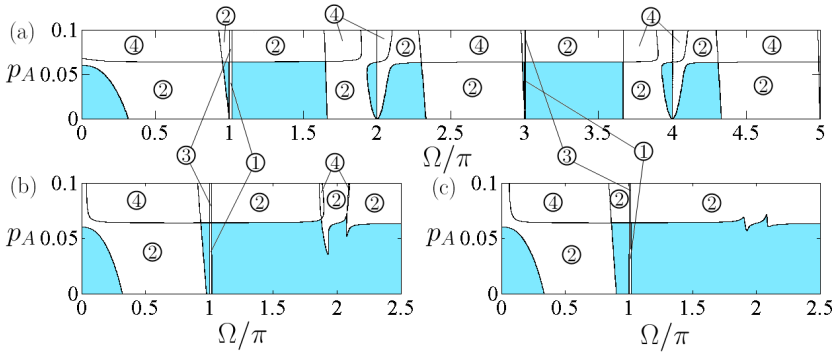

Figure 2.13: Stability charts, referred to the configuration A, in the parameter space of the proportional gain and the dimensionless natural frequency. In all diagrams $r = 1$ and $d = 0.1$, while δ is varying in the following way: (a): $\delta = 0$, (b): $\delta = 0.001$, (c): $\delta = 0.005$. Shaded area: stable, clear area: unstable.

Although Fig. 2.13 shows the stability chart for a large range of values of Ω, in real applications, the sampling time is usually extremely small, making Ω very small as well ($\Omega = \omega_n\tau$). Fig. 2.14 shows the stability chart for $\Omega = \pi/1000$. The stable region is simply connected and can be defined through the coordinates of points Q and R, that are respectively the point with the maximal value of d_A and with the maximal value of p_A. The coordinates of Q in the p_A, d_A space are

$$\mathrm{Q} = \left(0, \frac{\Omega\left(3e^{2\delta\Omega} + 2e^{\delta\Omega}\cos\Omega - 1\right)}{2\Omega + 2e^{\delta\Omega}\left(\Omega\cos\Omega + 2r\sin\Omega(1+\delta^2)\right)}\right) \tag{2.65}$$

while the coordinates of R are given by an implicit formula ($e_2 = 0$) which cannot be solved analytically with

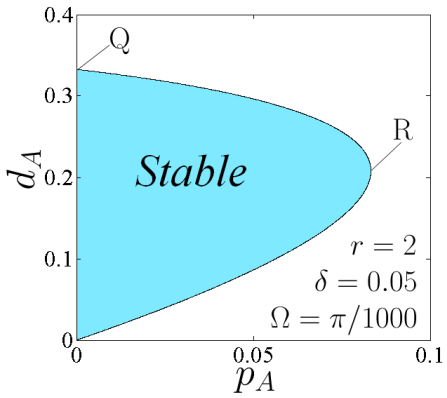

Figure 2.14: Stability charts, referred to the configuration A, in the parameter space of the proportional and differential gains, for a very small value of Ω.

standard techniques. Considering the limit for $\Omega \to 0$, in the $p_A d_A$ space we have

$$\mathrm{Q} = \left(0, \frac{1}{1 + r(1+\delta^2)}\right), \qquad \mathrm{R} = \left(\frac{1}{4\,(1 + r(1+\delta^2))}, \frac{5}{8\,(1 + r(1+\delta^2))}\right). \tag{2.66}$$

This means that variations of r and δ modify the extent of the stable region, but not its shape, for sufficiently small values of Ω. In particular, increases in r or δ reduce the stable region, which exists also for $\delta = 0$. Furthermore, it should be noted that the shape of the stable region is the same as the one in Fig. 2.4(a), referred to a rigid connection, i.e. for $\Omega \to \infty$. As we already mentioned, in Fig. 2.4(a) the stable points with the maximal values of d_A and p_A have coordinates respectively $(0, 1)$ and $(1/4, 5/8)$.

Besides stability, another aspect to be considered in real applications is the speed of convergence, which depends on the maximal absolute value of the eigenvalues of $\mathbf{B_A}$. Calling M the maximal absolute value of the eigenvalues for a specific point in the parameter space, the amplitude of oscillation is reducing proportionally to the factor M (convergence radius) at each time step.

Considering Fig. 2.12, the minimal values of M are summed up in Tab. 2.1. The values in the table show that the response of the system to variations of δ is very different with respect to the speed of convergence, for different values of Ω. For $\Omega = \pi/10$, increases in δ decrease the speed of convergence (enlarging only slightly the stable region), while for $\Omega = \pi/3$, increases in δ increase the speed of convergence (with substantial enlargement of the stable region as well). The effect of variations of r on the speed of convergence is harder to be studied since it does not have a monotonous trend (for $\Omega = \pi/10$ or $\Omega = \pi/1000$) or it has a very small effect (for $\Omega = \pi/3$). Differently from the case $\Omega = \pi/10$, for $\Omega = \pi/1000$ increases in δ increase the speed of convergence. The bigger values of M for smaller values of Ω do not imply a slower convergence of the physical system, since small values of Ω correspond to small values of the sampling time and the reduction given by M refers to each single time step. For comparison, we remind that in the single DoF case, the minimal value of M is $2/3$.

Referring to the configuration B, the coefficients $a_{5,..,0}$, $c_{4,3}$ and d_3 are functions of the parameters δ, Ω, p and d only, so they do not explicitly depend on r.

Figure 2.15 shows the stability chart in the parameter space of the proportional gain and the dimensionless natural frequency. Again, in the figure it is clearly visible that the stability is strongly influenced by Ω. Fig. 2.16 shows that the effect of the damping is very different for different values of Ω. For $\Omega = \pi/10$, the damping is basically controlling the stability, while for $\Omega = \pi/3$, large variations in the damping have much slighter effects (the opposite than in the collocated case). It should be noted that, while in the continuous time approach, zero damping would make the system unstable (Fig. 2.10), in the discrete time approach stability depends on Ω, and for most of the cases there exists a stable region (Fig. 2.15(a)).

Figure 2.17(a) shows the stability chart in the case of $\Omega = \pi/1000$, that is closer to a typical real case in

$\Omega = \pi/10$, $r = 1$		$\Omega = \pi/3$, $r = 1$	
δ	M	δ	M
0	0.793	0.01	0.9897
0.05	0.805	0.05	0.952
0.2	0.847	0.2	0.856
0.5	0.8846	0.5	0.7639
$\Omega = \pi/10$, $\delta = 0.05$		$\Omega = \pi/3$, $\delta = 0.05$	
r	M	r	M
0	0.984	0	0.949
0.1	0.928	0.01	0.949
0.5	0.849	0.1	0.949
1	0.804	0.3	0.9492
3	0.907	1	0.952
10	0.948	5	0.974
$\Omega = \pi/1000$, $r = 1$		$\Omega = \pi/1000$, $\delta = 0.05$	
δ	$1 - M$	r	$1 - M$
0	2.63×10^{-6}	0	1.57×10^{-4}
0.01	1.83×10^{-5}	0.1	1.44×10^{-5}
0.05	8.25×10^{-5}	1	8.25×10^{-5}
0.5	6.99×10^{-4}	5	2.62×10^{-5}

Table 2.1: Radius of convergence referred to the stability charts in Figs. 2.12 and 2.14

virtue of the high sampling frequency of digital systems. The stable region appears to be sensibly reduced (see the scale of the figure), but its shape is the same as the one in Fig. 2.9, referred to a continuous time system. Transforming the equations of the coordinates of points N and M in the $\tilde{p}_B, \tilde{d}_B$ space (equations (2.34) and (2.35)) to the p_B, d_B space and considering that $p_B = \tilde{p}_B \tau^2$, $d_B = \tilde{d}_B \tau$, $\Omega = \omega_0 \tau \sqrt{1+r}$ and $\delta = \delta_0 \sqrt{1+r}$, we obtain

$$\mathrm{N} \quad \rightarrow \quad \left(0, \frac{2\delta\Omega}{1-4\delta^2} \right) \tag{2.67}$$

$$\mathrm{M} \quad \rightarrow \quad \left(\frac{\left(1 - 2\delta^2 - \sqrt{1-4\delta^2}\right)\Omega^2}{8\delta^4}, \left[\frac{(1-2\delta^2)}{\sqrt{1-4\delta^2}} - 1 \right] \frac{\Omega}{4\delta^3} \right) \tag{2.68}$$

which gives an excellent approximation of the coordinates of points T and S in Fig. 2.17(a). This means that, if we would consider the stability of the system in the space of the dimensional control gains $P_B D_B$, we would obtain approximately the same results for the continuous time and for the discrete time case (for high sampling time). Figs. 2.17(b) and (c) show that the approximation becomes worst for increasing values of Ω. Furthermore, considering that for $\delta = 0$ the discrete time system gives stable solutions in a large range of Ω values, while the continuous time system does not give stable solutions at all, the digital system is intrinsically more stable.

Regarding the speed of convergence, the loci of the points with the same speed of convergence have the same shape of the one obtained in the continuous time case (compare Fig. 2.17(a) and Fig. 2.9(b)). Furthermore, regarding the continuous time system, we found out that, in correspondence to the point with the maximal speed of convergence, the matrix governing the system has maximal real part of the eigenvalues equal to $\Re(\lambda) = -\omega_0 \delta_0 (r+1)/2$. In the continuous time system, the reduction of the amplitude of oscillation in time is equal to $e^{\Re(\lambda)t}$. In order to transfer this value to the discrete time system, we consider a single sampling time, so we have

$$e^{\Re(\lambda)\tau} = e^{-\frac{\omega_0 \delta_0 (r+1)}{2}\tau} = e^{-\frac{\Omega\delta}{2}} \approx M. \tag{2.69}$$

This value gives an excellent approximation of the minimum radius of convergence (called M) in the case of the discrete time system, for small values of Ω. In the case relative to Fig. 2.17(a) the error is less than 0.1%

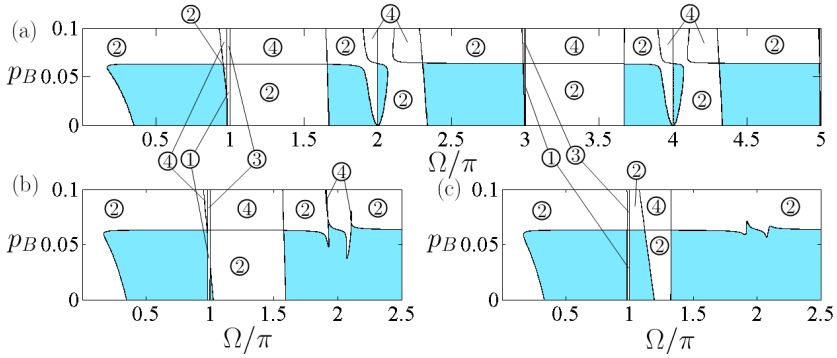

Figure 2.15: Stability charts, referred to the configuration B, in the parameter space of the proportional gain and the dimensionless natural frequency. In all diagrams $d = 0.1$, while δ is varying in the following way: (a): $\delta = 0$, (b): $\delta = 0.001$, (c): $\delta = 0.005$. Shaded area: stable, clear area: unstable.

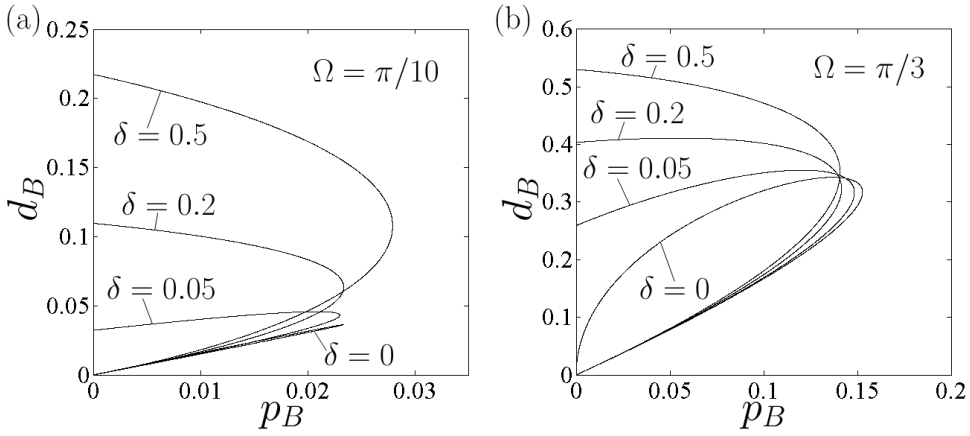

Figure 2.16: Stability charts, referred to the configuration B, in the parameter space of the proportional and differential gains, for different values of δ.

$(1 - e^{-\Omega\delta/2} = 7.854 \times 10^{-5}$ and $1 - M = 7.848 \times 10^{-5})$, for $\Omega = \pi/100$ (Fig. 2.17(b)) the error is 0.17%, while for different values of Ω and δ the error is larger as shown in Tab. 2.2, referring to the cases analyzed in Fig. 2.16.

Comparing the minimum values of the radius of convergence for the two configurations, it results that, although for small values of Ω the configuration A is much more stable (of several orders of magnitude), the speed of convergence has the same order of magnitude. Considering higher values of Ω ($\Omega = \pi/3$), when the stable region have a similar surface, the speed of convergence is still similar.

A comparison between Fig. 2.13 and Fig. 2.15, shows a complementary pattern of the two stability domains in the Ω direction, which is especially visible in the case of no damping (Fig. 2.13(a) and Fig. 2.15(a)). This effect is due to the modes of vibration, which are related to the transformation of coordinates in Eq. (2.43), i.e. $x_1 = (m_1 q_1 + m_2 q_2)/(m_1 + m_1)$ and $x_2 = m_1(q_2 - q_1)/(m_1 + m_2)$. If $r = 1$, as in Fig. 2.13, we have $x_1 = (q_1 + q_2)/2$ and $x_2 = (q_2 - q_1)/2$. So, in the second mode of vibration (x_2), the two masses are moving in opposite direction. Different values of r will enlarge or reduce the stable region related to configuration A, compromising the complementarity of the pattern. Thus, the position of the sensors, combined with the time delay, can make the system stable or unstable, creating this complementary shape. Of course, the damping changes the phase of the motion breaking the pattern.

Considering Fig. 2.15, we can say that the destabilization effect due to the non-collocation can be compensated by a proper delay, which can put the mode of vibrations in phase with the sampling time. It should be

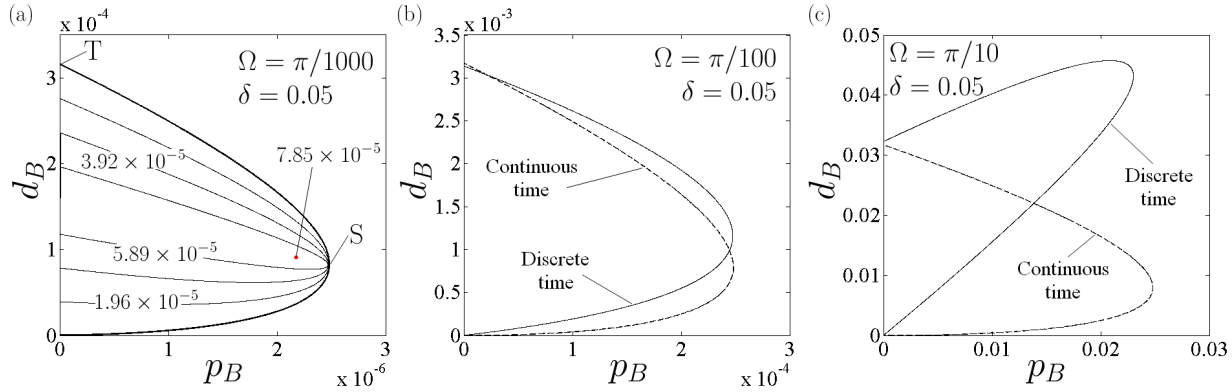

Figure 2.17: Stability charts, referred to the configuration B, in the parameter space of the proportional and differential gains. (a): the numbers mark loci with the same speed of convergence and correspond to $1 - M$. (b), (c): comparison between the continuous time (dashed line) and the discrete time (solid line) cases. For the transformation from continuous to discrete time, we considered $\delta_0 = \delta/\sqrt{1+r}$ and $\omega_0 = \Omega/(\tau\sqrt{1+r})$ with $r = 1$ and $\tau = 10^{-3}$ s.

$\Omega = \pi/10$			$\Omega = \pi/3$		
δ	M	$e^{-\frac{\Omega\delta}{2}}$	δ	M	$e^{-\frac{\Omega\delta}{2}}$
0	0.9993	1	0	0.9255	1
0.05	0.9916	0.9922	0.05	0.9023	0.9742
0.2	0.970	0.969	0.2	0.8483	0.9006
0.5	0.9357	0.9245	0.5	0.7931	0.7697

Table 2.2: Radius of convergence referred to the stability charts in Fig. 2.16

noted that Ω is not a fixed value, but it depends on m_2 for fixed values of r, so an increase in the payload would decrease Ω and it may destabilize the system.

Chapter 3

Bifurcation analysis: general procedure

In this chapter we will present a technique to analyze bifurcations of maps, in particular we will focus on single and double NS bifurcations, extending the results to the analysis of flip bifurcations. The analysis is based on the passages outlined by Kuznetsov and Meijer in [40, 41, 42] and other authors [65]. The analysis will go through the following passages: transformation to Jordan normal form, center manifold reduction, elimination of non-internally resonant terms, reduction to an amplitude map and analysis of the normal form. The different characteristics of a single and a double NS bifurcation will be presented in detail. Considering the differences of the normal form of a flip bifurcation with a NS bifurcation, an independent section will be dedicated to it.

3.1 Notes on bifurcations of maps

Considering the map

$$\mathbf{x}_{j+1} = \mathbf{f}(\mathbf{x}_j; \mathbf{p}) \tag{3.1}$$

$\mathbf{x}_0$ is a fixed point of Eq. (3.1) if it satisfies the condition

$$\mathbf{x}_0 = \mathbf{f}^m(\mathbf{x}_0; \mathbf{p}_0) \,\forall\, m \in \mathbb{Z} \tag{3.2}$$

where $\mathbf{p}$ is a vector of control parameters and $\mathbf{p}_0$ is a specific set of it. It can be easily proven (e.g. [49]) that this fixed point is asymptotically stable if the eigenvalues of $D_x\mathbf{f}|_{\mathbf{x}=\mathbf{x}_0,\mathbf{p}=\mathbf{p}_0}$ are inside the unit circle of the complex plane. Where $D_x\mathbf{f}$ is the matrix of the first partial derivatives of $\mathbf{f}$. This result has been already used in Ch. 2 for the stability analysis.

If all the eigenvalues μ_i of $D_x\mathbf{f}$ are either inside or outside the unit circle (but not on it, i.e. $|\mu_i| \neq 1$), the corresponding fixed point is called hyperbolic fixed point. If some of them are inside and others outside the unit circle, the hyperbolic fixed point is called a saddle point, if they are all inside the unit circle it is called a sink, if they are all outside it is called a source. If at least one eigenvalue lies on the unit circle, the fixed point is called a nonhyperbolic fixed point.

As a single control parameter is varied, a fixed point of a map can lose stability and experience a bifurcation if it is nonhyperbolic. There are three possible conditions at the loss of stability:

1. $D_x\mathbf{f}|_{\mathbf{x}=\mathbf{x}_0,\mathbf{p}=\mathbf{p}_0}$ has one eigenvalue equal to 1, with the remaining eigenvalues within the unit circle,
2. $D_x\mathbf{f}|_{\mathbf{x}=\mathbf{x}_0,\mathbf{p}=\mathbf{p}_0}$ has one eigenvalue equal to -1, with the remaining eigenvalues within the unit circle,
3. $D_x\mathbf{f}|_{\mathbf{x}=\mathbf{x}_0,\mathbf{p}=\mathbf{p}_0}$ has a pair of complex conjugate eigenvalues on the unit circle, with the remaining eigenvalues within it.

These three cases correspond to the three possible codimension-one bifurcations of maps. In this research we will encounter only the second and the third type of nonhyperbolic fixed point, so for the first type we address the interested reader to textbooks as [25, 40, 49 or 65].

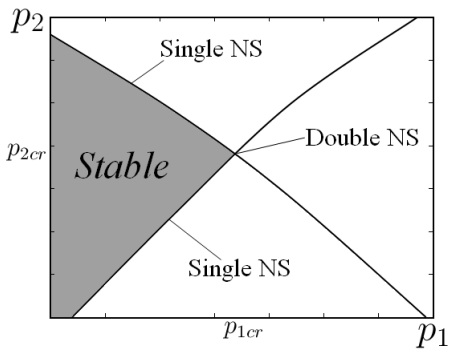

Figure 3.1: Typical stability diagram in correspondence to a double Neimark-Sacker bifurcation.

In the second case, i.e. one eigenvalue leaves the unit circle through -1, with the remaining eigenvalues within the unit circle, the system experiences a period-doubling or flip bifurcation. As a consequence, two branches of period-two solutions emerge from the bifurcation point. Of course the bifurcation point changes the stability properties of the fixed point.

In the third case, i.e. a couple of complex conjugate eigenvalues leave the unit circle, with the remaining eigenvalues within the unit circle, the system experience a NS bifurcation. As a consequence a stable or unstable limit circle is generated around the fixed point.

Differently from attractors of continuous time systems, regarding attractors of maps, dimension zero attractors (finite number of points) correspond to periodic solutions, dimension one attractors (closed lines) to 2-torus quasiperiodic solutions, dimension two attractors (surfaces) to 3-torus quasiperiodic solutions and so on. Thus, the nontrivial solution generated by a period doubling bifurcation is generally represented by two points in the phase plane, which correspond to a periodic solution. While the nontrivial solution generated by a NS bifurcation is represented by a closed line in the phase plane and corresponds to a 2-torus quasiperiodic solution. In the spacial case that the frequency introduced by the NS bifurcation is a rational number, the attractor is reduced to a finite number of points and corresponds to a periodic motion.

As already mentioned, at the occurrence of period doubling or NS bifurcations the trivial solution loses its stability. The bifurcation is generally said to be supercritical (subcritical) if the nontrivial solution is stable (unstable) and exists in the region of instability (stability) of the trivial solution.

A double NS bifurcation occurs at the intersection of two loci of single NS bifurcations, as shown in Fig. 3.1. In the neighborhood of the double NS bifurcation, the two single NS bifurcation interact with each other. Thus, in order to study the dynamics of the system in that region, it is necessary to consider both the bifurcations. Such a bifurcation can occur only in an n-dimensional space, where $n \geq 4$.

In this chapter, a procedure to analyze these three kinds of bifurcations will be presented.

3.2 Mathematical model

Single NS bifurcation
We consider a generic map

$$\mathbf{x}_{j+1,s} = \mathbf{f}_s(\mathbf{x}_{j,s}; p) \tag{3.3}$$

where $\mathbf{f}_s = [f_{1,s}(\mathbf{x}; p) \dots f_{n,s}(\mathbf{x}; p)]^T$, $\mathbf{x}_s = [x_1 \dots x_n]^T$, p is a scalar real number and $n \geq 2$. The trivial solution $\mathbf{x}_{0,s} = [0 \dots 0]^T$ satisfies the equation

$$\mathbf{x}_{0,s} = \mathbf{f}_s(\mathbf{x}_{0,s}; p). \tag{3.4}$$

We consider the case for which the trivial solution $\mathbf{x}_{0,s}$ of (3.3) is stable for $p < p_{cr}$, while it is unstable for $p > p_{cr}$. We call p the control parameter of the bifurcation occurring at $p = p_{cr}$.

Assuming that $f_{1,s}, ..., f_{n,s}$ are sufficiently smooth, we expand them in their Taylor series around 0, with respect to $x_1, ..., x_n$ up to the third order, so we can rewrite Eq. (3.3) as

$$\mathbf{x}_{j+1,s} = \mathbf{A}_s(p)\mathbf{x}_{j,s} + \mathbf{b}_s(\mathbf{x}_{j,s}) \tag{3.5}$$

where the vector $\mathbf{b}_s(\mathbf{x}_s)$ contains all the nonlinear terms. The stability of the trivial solution depends on the eigenvalues of $\mathbf{A}_s(p)$: the solution is asymptotically stable if and only if all the eigenvalues of $\mathbf{A}_s$ are inside the unite circle of the complex plane, i.e. $|\mu_{i,s}| < 1 \,\text{for}\, i = 1, ..., n$. We consider that

$$\begin{array}{lll} \text{for} & p < p_{cr} & |\mu_{i,s}| < 1 \quad \forall\, i = 1, ..., n \\ \text{for} & p = p_{cr} & |\mu_{1,s}| = |\mu_{2,s}| = 1 \quad \mu_{1,s} = \bar{\mu}_{2,s} \neq \pm 1 \\ & & \frac{\mathrm{d}|\mu_{(1,2),s}|}{\mathrm{d}p}|_{p=p_{cr}} > 0 \\ & & |\mu_{i,s}| < 1 \quad \forall\, i = 3, ..., n. \end{array} \tag{3.6}$$

If the conditions in Eq. (3.6) are satisfied, a NS bifurcation is occurring for $p = p_{cr}$ [25].

Double NS bifurcation
We now consider the generic map

$$\mathbf{x}_{j+1,d} = \mathbf{f}_d(\mathbf{x}_{j,d}; p_1, p_2) \tag{3.7}$$

where $\mathbf{f}_d = [f_{1,d}(\mathbf{x}_d; p_1, p_2) \, ... \, f_{m,d}(\mathbf{x}_d; p_1, p_2)]^T$, $\mathbf{x}_d = [x_1 \, ... \, x_m]^T$, p_1 and p_2 are scalar real numbers and $m \geq 4$. The trivial solution $\mathbf{x}_{0,d} = [0 \, ... \, 0]^T$ satisfies the equation

$$\mathbf{x}_{0,d} = \mathbf{f}_d(\mathbf{x}_{0,d}; p_1, p_2). \tag{3.8}$$

We consider that the stability properties of the trivial solution of the system are analogous to those shown in Fig. 3.1. p_1 and p_2 are the control parameters of the bifurcation under study.

Assuming that $f_{1,d}, ..., f_{m,d}$ are sufficiently smooth, we expand them in their Taylor series around 0, with respect to $x_1, ..., x_m$ up to the third order, so we can rewrite Eq. (3.7) as

$$\mathbf{x}_{j+1,d} = \mathbf{A}_d(p_1, p_2)\mathbf{x}_{j,d} + \mathbf{b}_d(\mathbf{x}_{j,d}) \tag{3.9}$$

where the vector $\mathbf{b}_d(\mathbf{x}_d)$ contains all the nonlinear terms. In some cases, it may be needed to expand the Taylor series up to the fifth order and keep, during all the procedure, terms up to the fifth order, as explained in [42]. We will come back later to this point, during the analysis of the normal form.

The stability of the trivial solution depends on the eigenvalues of $\mathbf{A}_d(p_1, p_2)$: the solution is stable and hyperbolic if and only if all the eigenvalues of $\mathbf{A}_d$ are inside the unite circle of the complex plane, i.e. $|\mu_{i,d}| < 1 \,\text{for}\, i = 1, ..., m$, otherwise it is unstable or nonhyperbolic. We consider that

$$\text{for} \quad \begin{array}{l} p_1 = p_{1cr} \\ p_2 = p_{2cr} \end{array} \quad \left\{ \begin{array}{l} |\mu_{1,d}| = |\mu_{2,d}| = 1 \quad \mu_{1,d} = \bar{\mu}_{2,d} \neq \pm 1 \\ \frac{\mathrm{d}|\mu_{(1,2),d}|}{\mathrm{d}p_1}|_{(p_1,p_2)=(p_{1cr},p_{2cr})} \neq 0 \\ |\mu_{3,d}| = |\mu_{4,d}| = 1 \quad \mu_{3,d} = \bar{\mu}_{4,d} \neq \pm 1 \\ \frac{\mathrm{d}|\mu_{(3,4),d}|}{\mathrm{d}p_1}|_{(p_1,p_2)=(p_{1cr},p_{2cr})} \neq 0 \\ |\mu_{i,d}| < 1 \quad \forall\, i = 5, ..., m. \end{array} \right. \tag{3.10}$$

If the conditions in (3.10) are satisfied, a double NS bifurcation is occurring for $(p_1, p_2) = (p_{1cr}, p_{2cr})$ [40].

3.3 Jordan normal form

It is possible to reduce the system to its Jordan normal form, i.e. to reorganize the linear part of the system, in order to linearly decouple the variable related to the bifurcation from the others.

We call $\mathbf{H}_s = \mathbf{A}_s|_{p=p_{cr}}$ (for the single NS bifurcation) and $\mathbf{H}_d = \mathbf{A}_d|_{(p_1,p_2)=(p_{1cr},p_{2cr})}$ (for the double NS bifurcation). $\mathbf{s}_{i,s}$, $i = 1, ..., n$ are the eigenvectors related to the eigenvalues $\mu_{i,s}$ of $\mathbf{H}_s$ and $\mathbf{s}_{i,d}$, $i = 1, ..., m$ are the eigenvectors related to the eigenvalues $\mu_{i,d}$ of $\mathbf{H}_d$.

Regarding the single NS bifurcation, if the eigenvalues $\mu_{3...n,s}$ are real and have algebraic multiplicity equal to 1, we can define the transformation matrix

$$\mathbf{T}_s = \begin{pmatrix} \Re(\mathbf{s}_{1,s}) & \Im(\mathbf{s}_{1,s}) & \mathbf{s}_{3,s} & \cdots & \mathbf{s}_{n,s} \end{pmatrix}. \tag{3.11}$$

In the case of the double NS bifurcation the transformation matrix is

$$\mathbf{T}_d = \begin{pmatrix} \Re(\mathbf{s}_{1,d}) & \Im(\mathbf{s}_{1,d}) & \Re(\mathbf{s}_{3,d}) & \Im(\mathbf{s}_{3,d}) & \mathbf{s}_{5,d} & \cdots & \mathbf{s}_{m,d} \end{pmatrix}. \tag{3.12}$$

It can be easily verified that

$$\mathbf{T}_s^{-1}\mathbf{H}_s\mathbf{T}_s = \begin{pmatrix} \Re(\mu_{1,s}) & \Im(\mu_{1,s}) & 0 & \cdots & 0 \\ \Im(\mu_{2,s}) & \Re(\mu_{2,s}) & 0 & \cdots & 0 \\ 0 & 0 & \mu_{3,s} & \cdots & \vdots \\ \vdots & \vdots & & \ddots & 0 \\ 0 & 0 & \cdots & 0 & \mu_{n,s} \end{pmatrix}. \tag{3.13}$$

and

$$\mathbf{T}_d^{-1}\mathbf{H}_d\mathbf{T}_d = \begin{pmatrix} \mathbf{J}_1 & \mathbf{0} & \mathbf{0} & \cdots & \mathbf{0} \\ \mathbf{0} & \mathbf{J}_2 & \mathbf{0} & \cdots & \mathbf{0} \\ \mathbf{0} & \mathbf{0} & \mu_{5,d} & \cdots & \vdots \\ \vdots & \vdots & & \ddots & 0 \\ \mathbf{0} & \mathbf{0} & \cdots & 0 & \mu_{n,d} \end{pmatrix} \tag{3.14}$$

where

$$\mathbf{J}_1 = \begin{pmatrix} \Re(\mu_{1,d}) & \Im(\mu_{1,d}) \\ \Im(\mu_{2,d}) & \Re(\mu_{2,d}) \end{pmatrix} \text{ and } \mathbf{J}_2 = \begin{pmatrix} \Re(\mu_{3,d}) & \Im(\mu_{3,d}) \\ \Im(\mu_{4,d}) & \Re(\mu_{4,d}) \end{pmatrix}. \tag{3.15}$$

Applying the transformation

$$\mathbf{x}_s = \mathbf{T}_s\mathbf{y}_s, \quad \mathbf{y}_s = [y_1 \, ... \, y_n]_s^T = \mathbf{T}_s^{-1}\mathbf{x} \tag{3.16}$$

and

$$\mathbf{x}_d = \mathbf{T}_d\mathbf{y}_d, \quad \mathbf{y}_d = [y_1 \, ... \, y_m]_d^T = \mathbf{T}_d^{-1}\mathbf{x} \tag{3.17}$$

we can rewrite the maps in Eq. (3.5) and Eq. (3.9) in Jordan normal form, that respectively are

$$\mathbf{y}_{j+1,s} = \mathbf{T}_s^{-1}\mathbf{H}_s\mathbf{T}_s\mathbf{y}_{j,s} + \mathbf{T}_s^{-1}\mathbf{b}_s(\mathbf{y}_{j,s}) \tag{3.18}$$

and

$$\mathbf{y}_{j+1,d} = \mathbf{T}_d^{-1}\mathbf{H}_d\mathbf{T}_d\mathbf{y}_{j,d} + \mathbf{T}_d^{-1}\mathbf{b}_d(\mathbf{y}_{j,d}). \tag{3.19}$$

If the eigenvalues $\mu_{3...n,s}$ and $\mu_{3...n,d}$ are not real or have algebraic multiplicity larger than 1, the procedure to obtain the Jordan normal form is slightly different (see [46]), but the matrices $\mathbf{T}_s^{-1}\mathbf{H}_s\mathbf{T}_s$ and $\mathbf{T}_d^{-1}\mathbf{H}_d\mathbf{T}_d$, controlling the linear part of the two systems, will still be block diagonal matrices.

In Eqs. (3.18) and (3.19), the variables related to the bifurcations are $(y_{1,s}, y_{2,s})$ for the single NS bifurcation and $(y_{1,d}, y_{2,d}, y_{3,d}, y_{4,d})$ for the double NS bifurcation. In both cases they are linearly decoupled from the other variables.

3.4 Center manifold reduction

At each fixed point, undergoing a local bifurcation, there is a center manifold associated. This manifold is a curved k-dimensional surface that is tangent at the bifurcation point to the subspace spanned by the k critical eigenvectors $\mathbf{s}_1$, $\mathbf{s}_2$, ..., $\mathbf{s}_k$, corresponding to the k critical eigenvalues with absolute value equal to 1. For a flip bifurcation, $k = 1$, for a single NS bifurcation $k = 2$ and for a double NS bifurcation $k = 4$. The dimension k of the manifold is necessarily less or equal than the the dimension of the full system. The center manifold reduction consist in reducing the dynamics of the full system to the k-dimensional manifold, which still contains all the information related to the local dynamics of the system, in correspondence to the bifurcation [49].

Following the procedure outlined in [25] and [65], we want to reduce the dynamics of the system to its center manifold, i.e. to the variables related to the bifurcation, $y_{1,s}$ and $y_{2,s}$ for the single NS bifurcation and $y_{1,d}$, $y_{2,d}$, $y_{3,d}$ and $y_{4,d}$ for the double NS bifurcation. Of course, if the system is respectively already two and four dimensional, this procedure can be skipped, since the system is already naturally limited to its center manifold.

The first step consists in defining the variables not related to the bifurcation, as nonlinear functions of the variables related to the bifurcation, i.e. the local center manifold. Generally, it is enough to consider up to third order terms, here we consider up to second order terms, but the procedure can be easily extended to higher order terms.

For the single NS bifurcation we define the local center manifold in the form

$$\begin{pmatrix} y_{3,j} \\ \vdots \\ y_{n,j} \end{pmatrix}_s = \mathbf{t}_s(y_{1,j}, y_{2,j})_s = \begin{pmatrix} g_{320}y_{1,j}^2 + g_{311}y_{1,j}y_{2,j} + g_{302}y_{2,j}^2 \\ \vdots \\ g_{n20}y_{1,j}^2 + g_{n11}y_{1,j}y_{2,j} + g_{n02}y_{2,j}^2 \end{pmatrix}_s, \tag{3.20}$$

where $\mathbf{t}_s$ satisfies Eq. (3.18) only for small values of $y_{1,s}$ and $y_{2,s}$. The cubic terms are neglected, since, after the transformation, they would produce terms higher than the third order.

For the double NS bifurcation, we define the local center manifold in the form

$$\begin{pmatrix} y_{5,j} \\ \vdots \\ y_{n,j} \end{pmatrix}_d = \mathbf{t}_d(y_{1,j}, y_{2,j}, y_{3,j}, y_{4,j})_d = \begin{pmatrix} g_{52000}y_{1,j}^2 + g_{50200}y_{2,j}^2 + g_{50020}y_{3,j}^2 + g_{50002}y_{4,j}^2 \\ \quad + g_{51100}y_{1,j}y_{2,j} + g_{51010}y_{1,j}y_{3,j} + g_{51001}y_{1,j}y_{4,j} \\ \quad + g_{50110}y_{2,j}y_{3,j} + g_{50101}y_{2,j}y_{4,j} + g_{50011}y_{3,j}y_{4,j} \\ \vdots \\ g_{m2000}y_{1,j}^2 + g_{m0200}y_{2,j}^2 + g_{m0020}y_{3,j}^2 + g_{m0002}y_{4,j}^2 \\ \quad + g_{m1100}y_{1,j}y_{2,j} + g_{m1010}y_{1,j}y_{3,j} + g_{m1001}y_{1,j}y_{4,j} \\ \quad + g_{m0110}y_{2,j}y_{3,j} + g_{m0101}y_{2,j}y_{4,j} + g_{m0011}y_{3,j}y_{4,j} \end{pmatrix}_d. \tag{3.21}$$

The coefficients g_{ihk} are $3(n-2)$ unknowns, while g_{ihklm} are $10(m-4)$ unknowns. In order to find them, in the case of the single NS bifurcation, we substitute the $n-2$ equations of (3.20) into the first two equations of (3.18). Then, we substitute these two new equations and the equations in (3.20) into the remaining $n-2$ equations of (3.18). Collecting terms with the same power order, we obtain $3(n-2)$ equations in the $3(n-2)$ unknowns g_{ihk}. These equations are organized in a linear system that can be solved in closed form. If now we substitute again the equations in (3.20) (where g_{ihk} are now known) into the first two equations of (3.18), we obtain

$$\begin{pmatrix} y_{1,j+1} \\ y_{2,j+1} \end{pmatrix}_s = \begin{pmatrix} \Re(\mu_{1,d}) & \Im(\mu_{1,d}) \\ \Im(\mu_{2,d}) & \Re(\mu_{2,d}) \end{pmatrix} \begin{pmatrix} y_{1,j} \\ y_{2,j} \end{pmatrix}_s + \begin{pmatrix} \sum_{h+k=2,3} a_{hk}y_{1,j}^h y_{2,j}^k \\ \sum_{h+k=2,3} b_{hk}y_{1,j}^h y_{2,j}^k \end{pmatrix}_s + \text{h.o.t.} \tag{3.22}$$

that is the system in Eq. (3.18), limited to its center manifold, i.e. a two dimensional surface in the n dimensional space. Terms higher than the third order, are generated during the transformation and can be neglected. The dynamics of the system in Eq. (3.22), for small values of $y_{1,s}$ and $y_{2,s}$, is the same of the system in Eq. (3.18).

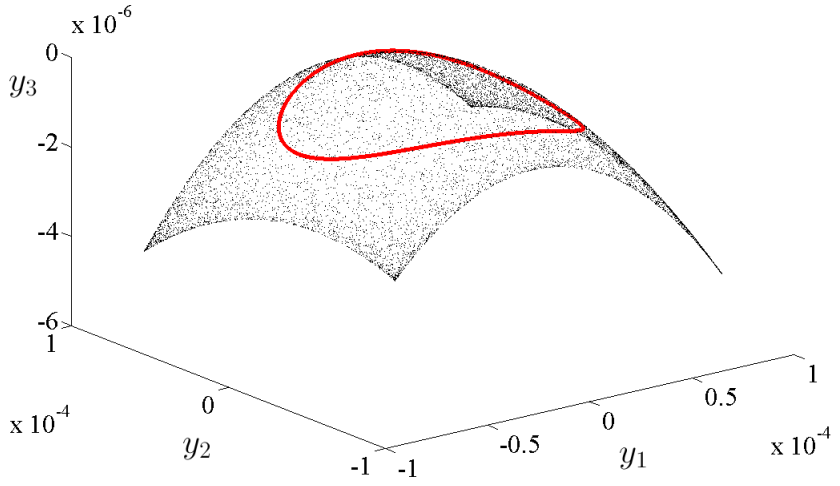

Figure 3.2: Example of a center manifold reduction for a NS bifurcation.

In the case of the double NS bifurcation, the procedure is the same, but lengthier because of the increased number of unknown. In detail, repeating the same procedure, we substitute the $m-4$ equations of (3.21) into the first four equations of (3.19). Then, we substitute these four new equations and the equations in (3.21) into the remaining $m-4$ equations of (3.19). Collecting terms with the same power order, we obtain $10(n-4)$ equations in the $10(n-4)$ unknowns g_{ihklm}. These equations are organized in a linear system that can be solved in closed form. Substituting again the equations in (3.21) into the first four equations of (3.19), we obtain

$$\begin{pmatrix} y_{1,j+1} \\ y_{2,j+1} \\ y_{3,j+1} \\ y_{4,j+1} \end{pmatrix}_d = \begin{pmatrix} \Re(\mu_{1,d}) & \Im(\mu_{1,d}) & 0 & 0 \\ \Im(\mu_{2,d}) & \Re(\mu_{2,d}) & 0 & 0 \\ 0 & 0 & \Re(\mu_{3,d}) & \Im(\mu_{3,d}) \\ 0 & 0 & \Im(\mu_{4,d}) & \Re(\mu_{4,d}) \end{pmatrix} \begin{pmatrix} y_{1,j} \\ y_{2,j} \\ y_{3,j} \\ y_{4,j} \end{pmatrix}_d + \begin{pmatrix} \sum_{h+k+l+m=2,3} a_{hklm} y_{1,j}^h y_{2,j}^k y_{3,j}^l y_{4,j}^m \\ \sum_{h+k+l+m=2,3} b_{hklm} y_{1,j}^h y_{2,j}^k y_{3,j}^l y_{4,j}^m \\ \sum_{h+k+l+m=2,3} c_{hklm} y_{1,j}^h y_{2,j}^k y_{3,j}^l y_{4,j}^m \\ \sum_{h+k+l+m=2,3} d_{hklm} y_{1,j}^h y_{2,j}^k y_{3,j}^l y_{4,j}^m \end{pmatrix}_d + \text{h.o.t.} \tag{3.23}$$

that is the system under study, limited to its center manifold. The dynamics of the system in Eq. (3.23) is the same of the system in Eq. (3.7), for small values of $(y_1, y_2, y_3, y_4)_d$.

Fig. 3.2 shows an example of a center manifold reduction, in the case of a single NS bifurcation, reduced from a three to a two dimensional system. In the figure, the red solid line is the limit cycle obtained from a direct numerical simulation of the original system, while the dotted surface is the local center manifold at the bifurcation of the fixed point $[0;0;0]$. The local center manifold has been obtained with the technique just shown, and it is clearly visible how the limit circle lays on the local center manifold, with very good accuracy.

3.5 Elimination of non-internally resonant nonlinear terms

Bifurcations are generally related to simple normal forms, which include few nonlinear terms. Eqs. (3.22) and (3.23) present all the possible nonlinear terms up to the third order, for a general two and four dimensional system respectively. It is possible to transform out most of the nonlinear terms in the system, reducing it to the normal form of the bifurcation under study, which allows to investigate the main features of the bifurcation from few coefficients.

In our analysis, we follow the steps outlined in [40] and [65]. First of all, we rewrite Eqs. (3.22) and (3.23) in complex form, i.e.

$$z_{j+1} = \mu_{2,s} z_j + \alpha_{20} z_j^2 + \alpha_{11} z_j \bar{z}_j + \alpha_{02} \bar{z}_j^2 + \alpha_{30} z_j^3 + \alpha_{21} z_j^2 \bar{z}_j + \alpha_{12} z_j \bar{z}_j^2 + \alpha_{03} \bar{z}_j^3 \tag{3.24}$$

for the single NS bifurcation, and

$$\begin{pmatrix} z_{1,j+1} \\ z_{2,j+1} \end{pmatrix} \mapsto \begin{pmatrix} \mu_{2,d} z_{1,j} + \sum_{h+k+l+m=2,3} \alpha_{hklm} z_{1,j}^h \bar{z}_{1,j}^k z_{2,j}^l \bar{z}_{2,j}^m \\ \mu_{4,d} z_{2,j} + \sum_{h+k+l+m=2,3} \beta_{hklm} z_{1,j}^h \bar{z}_{1,j}^k z_{2,j}^l \bar{z}_{2,j}^m \end{pmatrix} \tag{3.25}$$

for the double NS bifurcation, where

$$\begin{array}{lll} z = y_{1,s} + i y_{2,s} & \rightarrow & y_{1,s} = \frac{z+\bar{z}}{2} \\ \bar{z} = y_{1,s} - i y_{2,s} & & y_{2,s} = \frac{z-\bar{z}}{2i} \end{array} \tag{3.26}$$

$$\begin{array}{lll} z_1 = y_{1,d} + i y_{2,d} & \rightarrow & y_{1,d} = \frac{z_1+\bar{z}_1}{2} \\ \bar{z_1} = y_{1,d} - i y_{2,d} & & y_{2,d} = \frac{z_1-\bar{z}_1}{2i} \\ z_2 = y_{3,d} + i y_{4,d} & \rightarrow & y_{3,d} = \frac{z_2+\bar{z}_2}{2} \\ \bar{z_2} = y_{3,d} - i y_{4,d} & & y_{4,d} = \frac{z_2-\bar{z}_2}{2i} \end{array} \tag{3.27}$$

and $\alpha_{hk}, \alpha_{hklm}, \beta_{hklm} \in \mathbb{C}$.

Substituting the variables $y_{1,s}$ and $y_{2,s}$, as expressed in Eq. (3.26), into Eq. (3.22), the coefficients α_{ij} can be easily defined as linear combinations of the coefficients a_{hk} and b_{hk}. Similarly, substituting the variables $(y_1, y_2, y_3, y_4)_d$, as expressed in Eq. (3.27), into Eq. (3.23) we can define the values of the coefficients α_{hklm} and β_{hklm}. Their explicit values are given in Appendix B.

The next step consists in eliminating all the nonlinear terms not related to internal resonances. This can be done through the near identity transformation. For the sake of clarity, we first consider the single NS bifurcation, and then we will extend the result to the double NS bifurcation. In order to eliminate the second order terms, we apply the transformation

$$z_j = v_j + h_{1,s}(v_j, \bar{v}_j) \tag{3.28}$$

to Eq. (3.24), where

$$h_{1,s}(v_j, \bar{v}_j) = c_{20} v_j^2 + c_{11} v_j \bar{v}_j + c_{02} \bar{v}_j^2, \tag{3.29}$$

hence we obtain

$$\begin{aligned} & v_{j+1} + c_{20} v_{j+1}^2 + c_{11} v_{j+1} \bar{v}_{j+1} + c_{02} \bar{v}_{j+1}^2 = \mu_{2,s}(v_j + c_{20} v_j^2 + c_{11} v_j \bar{v}_j + c_{02} \bar{v}_j^2) \\ & \quad + \alpha_{20}(v_j + c_{20} v_j^2 + c_{11} v_j \bar{v}_j + c_{02} \bar{v}_j^2)^2 + \alpha_{11}(v_j + c_{20} v_j^2 + c_{11} v_j \bar{v}_j + c_{02} \bar{v}_j^2) \\ & \quad (\bar{v}_j + \bar{c}_{20} \bar{v}_j^2 + \bar{c}_{11} v_j \bar{v}_j + \bar{c}_{02} v_j^2) + \alpha_{02}(\bar{v}_j + \bar{c}_{20} \bar{v}_j^2 + \bar{c}_{11} v_j \bar{v}_j + \bar{c}_{02} v_j^2)^2 \\ & \quad + \alpha_{30} v_j^3 + \alpha_{21} v_j^2 \bar{v}_j^2 + \alpha_{12} v_j \bar{v}_j^2 + \alpha_{03} \bar{v}_j^3 + \text{h.o.t.} \end{aligned} \tag{3.30}$$

where h.o.t. indicates terms higher than the third order. Since we want to eliminate the second order terms, we impose that

$$v_{j+1} = \mu_{2,s} v_j + \hat{\alpha}_{30} v_j^3 + \hat{\alpha}_{21} v_j^2 \bar{v}_j^2 + \hat{\alpha}_{12} v_j \bar{v}_j^2 + \hat{\alpha}_{03} \bar{v}_j^3 \tag{3.31}$$

where the $\hat{\alpha}_{ij}$ are the coefficient of the third order terms, after the effect of the transformation in Eq. (3.28). So we obtain

$$\begin{aligned} & v_{j+1} + c_{20} \mu_{2,s}^2 v_j^2 + c_{11} \mu_{2,s} \bar{\mu}_{2,s} v_j \bar{v}_j + c_{02} \bar{\mu}_{2,s}^2 \bar{v}_j^2 = \mu_{2,s}(v_j + c_{20} v_j^2 + c_{11} v_j \bar{v}_j + c_{02} \bar{v}_j^2) \\ & \quad + \alpha_{20}(v_j + c_{20} v_j^2 + c_{11} v_j \bar{v}_j + c_{02} \bar{v}_j^2)^2 + \alpha_{11}(v_j + c_{20} v_j^2 + c_{11} v_j \bar{v}_j + c_{02} \bar{v}_j^2) \\ & \quad (\bar{v}_j + \bar{c}_{20} \bar{v}_j^2 + \bar{c}_{11} v_j \bar{v}_j + \bar{c}_{02} v_j^2) + \alpha_{02}(\bar{v}_j + \bar{c}_{20} \bar{v}_j^2 + \bar{c}_{11} v_j \bar{v}_j + \bar{c}_{02} v_j^2)^2 \\ & \quad + \alpha_{30} v_j^3 + \alpha_{21} v_j^2 \bar{v}_j^2 + \alpha_{12} v_j \bar{v}_j^2 + \alpha_{03} \bar{v}_j^3 + \text{h.o.t.} \end{aligned} \tag{3.32}$$

Collecting terms with the same power order, we obtain

$$\begin{aligned} v_j^2 &\rightarrow c_{20}\mu_{2,s}^2 = c_{20}\mu_{2,s} + \alpha_{20} \\ v_j\bar{v}_j &\rightarrow c_{11}\mu_{2,s}\bar{\mu}_{2,s} = c_{11}\mu_{2,s}v_j\bar{v}_j + \alpha_{11} \\ \bar{v}_j^2 &\rightarrow c_{02}\bar{\mu}_{2,s}^2 = c_{02}\mu_{2,s}\bar{v}_j^2 + \alpha_{02} \end{aligned}$$

so, in order to eliminate the second order terms, we must impose

$$c_{20} = -\frac{\alpha_{20}}{\mu_{2,s} - \mu_{2,s}^2}, \quad c_{11} = -\frac{\alpha_{11}}{\mu_{2,s} - \mu_{2,s}\bar{\mu}_{2,s}}, \quad c_{02} = -\frac{\alpha_{02}}{\mu_{2,s} - \bar{\mu}_{2,s}^2}. \tag{3.33}$$

Then, collecting the coefficients of the third order terms, we obtain

$$v_j^3 \rightarrow \hat{\alpha}_{30} = \alpha_{30} - \frac{\bar{\alpha}_{20}\alpha_{11}}{\bar{\mu}_{2,s} - \mu_{2,s}^2} - \frac{2\alpha_{20}^2}{\mu_{2,s} - \mu_{2,s}^2} \tag{3.34}$$

$$v_j^2\bar{v}_j \rightarrow \hat{\alpha}_{21} = \alpha_{21} + \frac{\alpha_{20}\alpha_{11}(1 - 2\mu_{2,s})}{\mu_{2,s}^2 - \mu_{2,s}} + \frac{|\alpha_{11}|^2}{1 - \bar{\mu}_2} + \frac{2\,|\alpha_{02}|^2}{\mu_{2,s}^2 - \bar{\mu}_2} \tag{3.35}$$

$$v_j\bar{v}_j^2 \rightarrow \hat{\alpha}_{12} = \alpha_{12} - \frac{2\alpha_{02}\bar{\alpha}_{11}}{\bar{\mu}_{2,s} - 1} - \frac{\alpha_{11}\bar{\alpha}_{20}}{\bar{\mu}_{2,s} - \bar{\mu}_{2,s}^2} - \frac{\alpha_{11}^2}{\mu_{2,s} - 1} - \frac{2\alpha_{20}\alpha_{02}}{\mu_{2,s} - \bar{\mu}_{2,s}^2} \tag{3.36}$$

$$\bar{v}_j^3 \rightarrow \hat{\alpha}_{03} = \alpha_{03} - \frac{2\bar{\alpha}_{20}\alpha_{02}}{\bar{\mu}_{2,s} - \bar{\mu}_{2,s}^2} - \frac{\alpha_{11}\alpha_{02}}{\mu_{2,s} - \bar{\mu}_{2,s}^2} \tag{3.37}$$

we remind that $\bar{\mu}_{2,s} = \mu_{1,s}$ and $\mu_{2,s}\mu_{1,s} = 1$, so the previous equations can be slightly simplified. The transformation in Eq. (3.28) modifies also the higher order terms, that can be neglected in this procedure. After the transformation, Eq. (3.24) will become

$$v_{j+1} = \mu_{2,s}v_j + \hat{\alpha}_{30}v_j^3 + \hat{\alpha}_{21}v_j^2\bar{v}_j^2 + \hat{\alpha}_{12}v_j\bar{v}_j^2 + \hat{\alpha}_{03}\bar{v}_j^3. \tag{3.38}$$

With a similar procedure, we can eliminate most of the third order terms. We apply the transformation

$$v_j = w_j + h_{2,s}(w_j, \bar{w}_j) \tag{3.39}$$

to Eq. (3.38), where

$$h_{2,s}(w_j, \bar{w}_j) = c_{30}w_j^3 + c_{21}w_j^2\bar{w}_j + c_{12}w_j\bar{w}_j^2 + c_{03}\bar{w}_j^3. \tag{3.40}$$

Neglecting terms higher than the third order, we obtain

$$\begin{aligned} w_{j+1} + c_{30}\mu_{2,s}^3 w_j^3 + c_{21}\mu_{2,s}^2\bar{\mu}_{2,s}w_j^2\bar{w}_j + c_{12}\mu_{2,s}\bar{\mu}_{2,s}^2 w_j\bar{w}_j^2 + c_{03}\bar{\mu}_{2,s}^3\bar{w}_j^3 = \mu_{2,s}(w_j + c_{30}w_j^3 \\ + c_{21}w_j^2\bar{w}_j + c_{12}w_j\bar{w}_j^2 + c_{03}\bar{w}_j^3) + \hat{\alpha}_{30}w_j^3 + \hat{\alpha}_{21}w_j^2\bar{w}_j + \hat{\alpha}_{12}w_j\bar{w}_j^2 + \hat{\alpha}_{03}\bar{w}_j^3 + \text{h.o.t.} \end{aligned} \tag{3.41}$$

Collecting terms with the same power order, we have

$$\begin{aligned} w_j^3 &\rightarrow c_{30}\mu_{2,s}^3 = \mu_{2,s}c_{30} + \hat{\alpha}_{30} \\ w_j^2\bar{w}_j &\rightarrow c_{21}\mu_{2,s}^2\bar{\mu}_{2,s} = \mu_{2,s}c_{21} + \hat{\alpha}_{21} \\ w_j\bar{w}_j^2 &\rightarrow c_{12}\mu_{2,s}\bar{\mu}_{2,s}^2 = \mu_{2,s}c_{12} + \hat{\alpha}_{12} \\ \bar{w}_j^3 &\rightarrow c_{03}\bar{\mu}_{2,s}^3 = \mu_{2,s}c_{03} + \hat{\alpha}_{03}. \end{aligned}$$

In order to eliminate the third order terms, we must impose

$$c_{30} = -\frac{\hat{\alpha}_{30}}{\mu_{2,s} - \mu_{2,s}^3}, \quad c_{12} = -\frac{\hat{\alpha}_{12}}{\mu_{2,s} - \mu_{2,s}\bar{\mu}_{2,s}^2}, \quad c_{03} = -\frac{\hat{\alpha}_{03}}{\mu_{2,s} - \bar{\mu}_{2,s}^3} \tag{3.42}$$

while, to eliminate the term related to $w_j^2\bar{w}_j$, we should have $c_{21} = -\hat{\alpha}_{21}/(\mu_{2,s} - \mu_{2,s}^2\bar{\mu}_{2,s})$ that has no mathematical sense, since $\mu_{2,s} - \mu_{2,s}^2\bar{\mu}_{2,s} = \mu_{2,s} - \mu_{2,s} = 0$, so $c_{21} \rightarrow \infty$. This is due to the internal resonance between the terms $\mu_{2,s}w_j$ and $\hat{\alpha}_{21}w_j^2\bar{w}_j$. So we let $c_{21} = 0$.

It is possible to generalize the value of the coefficients used for the near identity transformation. While eliminating the second order terms, we had

$$c_{hk} = -\frac{\alpha_{hk}}{\mu_{2,s} - \mu_{2,s}^h \bar{\mu}_{2,s}^k} \tag{3.43}$$

where in case of the third order terms, α_{hk} is substituted by $\hat{\alpha}_{hk}$.

After the transformation in Eq. (3.39), Eq. (3.38) becomes

$$w_{j+1} = \mu_{2,s} w_j + \hat{\alpha}_{21} w_j^2 \bar{w}_j. \tag{3.44}$$

We now repeat the same procedure for the case of the double NS bifurcation. As we will show, the larger dimension of the system, will not affect the general procedure.

We apply the near identity transformation

$$\begin{aligned} z_1 &= v_1 + h_{1,d}(v_1, \bar{v}_1, v_2, \bar{v}_2) \\ z_2 &= v_2 + h_{2,d}(v_1, \bar{v}_1, v_2, \bar{v}_2) \end{aligned} \tag{3.45}$$

to Eq. (3.25), where

$$\begin{aligned} h_{1,d} &= \sum_{h+k+l+m=2} e_{hklm} v_1^h \bar{v}_1^k v_2^l \bar{v}_2^m \\ h_{2,d} &= \sum_{h+k+l+m=2} f_{hklm} v_1^h \bar{v}_1^k v_2^l \bar{v}_2^m. \end{aligned} \tag{3.46}$$

As in the case of a single NS bifurcation, choosing properly the values of the coefficients e_{hklm} and f_{hklm}, all the second order terms can be eliminated. Of course, this procedure will modify the terms higher than the second order. The procedure is analogous to the one just shown, but in this case it is much more lengthy due to the higher dimension of the system. For this reason, we skip this passage and we write directly the values of the coefficients, which follow the same rule of Eq. (3.43), i.e.

$$e_{hklm} = -\frac{\alpha_{hklm}}{\mu_{2,d} - \mu_{2,d}^h \bar{\mu}_{2,d}^k \mu_{4,d}^l \bar{\mu}_{4,d}^m} \tag{3.47}$$

$$f_{hklm} = -\frac{\beta_{hklm}}{\mu_{4,d} - \mu_{2,d}^h \bar{\mu}_{2,d}^k \mu_{4,d}^l \bar{\mu}_{4,d}^m}. \tag{3.48}$$

As a result of this transformation we will obtain the system

$$\begin{pmatrix} v_{1,j+1} \\ v_{2,j+1} \end{pmatrix} = \begin{pmatrix} \mu_{2,d} v_{1,j} + \sum_{h+k+l+m=3} \hat{\alpha}_{hklm} v_{1,j}^h \bar{v}_{1,j}^k v_{2,j}^l \bar{v}_{2,j}^m \\ \mu_{4,d} v_{2,j} + \sum_{h+k+l+m=3} \hat{\beta}_{hklm} v_{1,j}^h \bar{v}_{1,j}^k v_{2,j}^l \bar{v}_{2,j}^m \end{pmatrix} + \text{h.o.t.} \tag{3.49}$$

where $\hat{\alpha}_{hklm}$ and $\hat{\beta}_{hklm}$ are the coefficients of the third order terms, modified by the transformation in Eq. (3.46). The explicit formulas of these new coefficients as a function of α_{hklm} and β_{hklm} can be found in Appendix B.

With an analogous transformation, we eliminate the third order terms not related to internal resonances, i.e. we apply the transformation

$$\begin{aligned} v_1 &= w_1 + h_{3,d}(w_1, \bar{w}_1, w_2, \bar{w}_2) \\ v_2 &= w_2 + h_{4,d}(w_1, \bar{w}_1, w_2, \bar{w}_2) \end{aligned} \tag{3.50}$$

to Eq. (3.49), where

$$\begin{aligned} h_{3,d} &= \sum_{h+k+l+m=3} e_{hklm} w_1^h \bar{w}_1^k w_2^l \bar{w}_2^m \\ h_{4,d} &= \sum_{h+k+l+m=3} f_{hklm} w_1^h \bar{w}_1^k w_2^l \bar{w}_2^m. \end{aligned} \tag{3.51}$$

The values of the coefficients in the transformation are

$$e_{hklm} = -\frac{\hat{\alpha}_{hklm}}{\mu_2 - \mu_2^h \bar{\mu}_2^k \mu_4^l \bar{\mu}_4^m} \tag{3.52}$$

$$f_{hklm} = -\frac{\hat{\beta}_{hklm}}{\mu_4 - \mu_2^h \bar{\mu}_2^k \mu_4^l \bar{\mu}_4^m}. \tag{3.53}$$

This procedure allows us to eliminate all third order terms, except the ones related to $w_1^2\bar{w}_1$ and $w_1 w_2 \bar{w}_2$ in the first equation of (3.49), and related to $w_2^2\bar{w}_2$ and $w_1\bar{w}_1 w_2$ in the second equation of (3.49). These terms are related to internal resonances and cannot be eliminated. From Eqs. (3.52)-(3.53) we can easily identify the terms related with internal resonances, in fact, to eliminate those terms, the coefficient e_{hklm} should tend to infinit. For example, to eliminate the term related to $w_1 w_2 \bar{w}_2$, we should have

$$e_{1011} = -\frac{\hat{\alpha}_{1011}}{\mu_2 - \mu_2\mu_4\bar{\mu}_4} = -\frac{\hat{\alpha}_{1011}}{\mu_2 - \mu_2} \to \infty. \tag{3.54}$$

After this lengthy procedure, and considering that $w\bar{w} = |w|^2$, we obtain the following system

$$\begin{pmatrix} w_1 \\ w_2 \end{pmatrix} \mapsto \begin{pmatrix} w_1\left(\mu_2 + \hat{\alpha}_{2100}|w_1|^2 + \hat{\alpha}_{1011}|w_2|^2\right) \\ w_2\left(\mu_4 + \hat{\beta}_{1110}|w_1|^2 + \hat{\beta}_{0021}|w_2|^2\right) \end{pmatrix} + \text{h.o.t.} \tag{3.55}$$

For the sake of simplicity, from now on we substitute the notation $\square_{j+1} = f(\square_j)$ with $\square \mapsto f(\square)$.

3.6 Reduction to an amplitude map

A NS bifurcation consists in the generation of a limit circle around a fixed point. In the previous section, respectively for the single and the double NS bifurcation, we obtained the forms in Eqs. (3.44) and (3.55), that are expressed in complex variables and contain only the nonlinear terms strictly related to the bifurcation. In this form the limit circle generated by the bifurcation is reduced to a circle of the complex plane, in the nearby of the bifurcation itself. Thus, it can be defined by an amplitude and a phase. In order to do so, we transform Eqs. (3.44) and (3.55) into amplitude and phase maps.

First, we introduce the parameter k, k_1 and k_2 where

$$k = |\mu_{2,s}| - 1 \tag{3.56}$$

and

$$k_1 = |\mu_{2,d}| - 1, \qquad k_2 = |\mu_{4,d}| - 1 \tag{3.57}$$

so, in the vicinity of the bifurcation, Eq. (3.44) can be approximated with the map

$$w \mapsto w(1+k)e^{i\phi} + \hat{\alpha}_{21} w|w|^2 \tag{3.58}$$

and Eq. (3.55) can be approximated with

$$\begin{pmatrix} w_1 \\ w_2 \end{pmatrix} \mapsto \begin{pmatrix} w_1(1+k_1)e^{i\phi_2} \\ w_2(1+k_2)e^{i\phi_4} \end{pmatrix} + \begin{pmatrix} w_1\left(\hat{\alpha}_{2100}|w_1|^2 + \hat{\alpha}_{1011}|w_2|^2\right) \\ w_2\left(\hat{\beta}_{1110}|w_1|^2 + \hat{\beta}_{0021}|w_2|^2\right) \end{pmatrix} + \text{h.o.t.} \tag{3.59}$$

where $e^{i\phi} = \mu_{2,s}$, $e^{i\phi_2} = \mu_{2,d}$ and $e^{i\phi_4} = \mu_{4,d}$. In order to simplify the calculation, k, k_1 and k_2 can be linearized in the following way

$$k = \frac{\mathrm{d}|\mu_2|}{\mathrm{d}p}(p - p_{cr}) \tag{3.60}$$

$$k_1 = \frac{\mathrm{d}|\mu_2|}{\mathrm{d}p_1}(p_1 - p_{1cr}) + \frac{\mathrm{d}|\mu_2|}{\mathrm{d}p_2}(p_2 - p_{2cr}) \tag{3.61}$$

$$k_2 = \frac{\mathrm{d}|\mu_4|}{\mathrm{d}p_1}(p_1 - p_{1cr}) + \frac{\mathrm{d}|\mu_4|}{\mathrm{d}p_2}(p_2 - p_{2cr}). \tag{3.62}$$

The next step consists in reducing Eq. (3.58) and (3.59) to amplitude maps. To do so, we introduce the polar coordinates $(r, \psi) \in \mathbb{R}$ for the single NS bifurcation, and $(r_1, r_2, \psi_1, \psi_2) \in \mathbb{R}$ for the double NS bifurcation, where

$$w = re^{i\psi} \tag{3.63}$$

and

$$w_1 = r_1 e^{i\psi_1}, \qquad w_2 = r_2 e^{i\psi_2}. \tag{3.64}$$

Applying the transformation in Eqs. (3.63) and (3.64) to Eqs. (3.58) and (3.59), we have

$$re^{i\psi} \mapsto r(1+k)e^{i(\psi+\phi)} + \hat{\alpha}_{21} r^3 e^{i\psi} \tag{3.65}$$

or

$$re^{i(\psi-\phi)} \mapsto re^{i\psi}\left[(1+k) + \hat{\alpha}_{21} e^{-i\phi} r^2\right] \tag{3.66}$$

for the single NS bifurcation, and

$$\begin{pmatrix} r_1 e^{i(\psi_1-\phi_2)} \\ r_2 e^{i(\psi_2-\phi_4)} \end{pmatrix} \mapsto \begin{pmatrix} r_1 e^{i\psi_1}\left[(1+k_1) + \hat{\alpha}_{2100} e^{-i\phi_2} r_1^2 + \hat{\alpha}_{1011} e^{-i\phi_2} r_2^2\right] \\ r_2 e^{i\psi_2}\left[(1+k_2) + \hat{\beta}_{1110} e^{-i\phi_4} r_1^2 + \hat{\beta}_{0021} e^{-i\phi_4} r_2^2\right] \end{pmatrix} \tag{3.67}$$

for the double NS bifurcation. Separating the absolute value from the phase, considering that $r, r_1, r_2 \geq 0$, we have from Eq. (3.66)

$$r \mapsto r\sqrt{\left[(1+k) + r^2 \Re(\hat{\alpha}_{21} e^{-i\phi})\right]^2 + \left[r^2 \Im(\hat{\alpha}_{21} e^{-i\phi})\right]^2} \tag{3.68}$$

then, expanding in Taylor series the square root, we have

$$r \mapsto (1+k)r + \rho r^3 + \text{h.o.t.} \tag{3.69}$$

where

$$\rho = \Re(\hat{\alpha}_{21} e^{-i\phi}). \tag{3.70}$$

Instead, selecting the phase of Eq. (3.66), we have

$$\psi - \phi \mapsto \psi + \arctan\left(\frac{r^2 \Im(\hat{\alpha}_{21} e^{-i\phi})}{(1+k) + r^2 \Re(\hat{\alpha}_{21} e^{-i\phi})}\right) \tag{3.71}$$

and expanding the arctangent in its Taylor series we have

$$\psi \mapsto \phi + \psi + \left(\frac{\Im(\hat{\alpha}_{21} e^{-i\phi})}{1+k} r^2\right) + \text{h.o.t.} \tag{3.72}$$

Eq. (3.69) is the normal form of the NS bifurcation.

Taking the absolute value of Eq. (3.67) we have

$$\begin{pmatrix} r_1 \\ r_2 \end{pmatrix} \mapsto \begin{pmatrix} r_1\Big[\left((1+k_1) + \Re\left(\hat{\alpha}_{2100} e^{-i\phi_2}\right) r_1^2 + \Re\left(\hat{\alpha}_{1011} e^{-i\phi_2}\right) r_2^2\right)^2 \\ \quad + \left(\Im\left(\hat{\alpha}_{2100} e^{-i\phi_2}\right) r_1^2 + \Im\left(\hat{\alpha}_{1011} e^{-i\phi_2}\right) r_2^2\right)^2\Big]^{1/2} \\ r_2\Big[\left((1+k_2) + \Re\left(\hat{\beta}_{1110} e^{-i\phi_4}\right) r_1^2 + \Re\left(\hat{\beta}_{0021} e^{-i\phi_4}\right) r_2^2\right)^2 \\ \quad + \left(\Im\left(\hat{\beta}_{1110} e^{-i\phi_4}\right) r_1^2 + \Im\left(\hat{\beta}_{0021} e^{-i\phi_4}\right) r_2^2\right)^2\Big]^{1/2} \end{pmatrix}, \tag{3.73}$$

expanding the square roots in Taylor series we obtain

$$\begin{pmatrix} r_1 \\ r_2 \end{pmatrix} \mapsto \begin{pmatrix} r_1\left(1+k_1+a_{11}r_1^2+a_{12}r_2^2\right) \\ r_2\left(1+k_2+a_{21}r_1^2+a_{22}r_2^2\right) \end{pmatrix} + \text{h.o.t.} \tag{3.74}$$

where

$$a_{11} = \Re(e^{-i\phi_2}\alpha_{2100}), \qquad a_{12} = \Re(e^{-i\phi_2}\alpha_{1011}) \tag{3.75}$$
$$a_{21} = \Re(e^{-i\phi_4}\beta_{1110}), \qquad a_{22} = \Re(e^{-i\phi_4}\beta_{0021}). \tag{3.76}$$

Instead, considering the phase of the map in Eq. (3.67), we have

$$\begin{pmatrix} \psi_1-\phi_2 \\ \psi_2-\phi_4 \end{pmatrix} \mapsto \begin{pmatrix} \psi_1+\arctan\left(\frac{\Im(\hat{\alpha}_{2100}e^{-i\phi_2})r_1^2+\Im(\hat{\alpha}_{1011}e^{-i\phi_2})r_2^2}{1+k_1+\Re(\hat{\alpha}_{2100}e^{-i\phi_2})r_1^2+\Re(\hat{\alpha}_{1011}e^{-i\phi_2})r_2^2}\right) \\ \psi_2+\arctan\left(\frac{\Im(\hat{\beta}_{1110}e^{-i\phi_4})r_1^2+\Im(\hat{\beta}_{0021}e^{-i\phi_4})r_2^2}{1+k_2+\Re(\hat{\beta}_{1110}e^{-i\phi_4})r_1^2+\Re(\hat{\beta}_{0021}e^{-i\phi_4})r_2^2}\right) \end{pmatrix}, \tag{3.77}$$

expanding the arctangent in its Taylor series we obtain

$$\begin{pmatrix} \psi_1 \\ \psi_2 \end{pmatrix} \mapsto \begin{pmatrix} \phi_2+\psi_1+\left(b_{11}r_1^2+b_{12}r_2^2\right) \\ \phi_4+\psi_2+\left(b_{21}r_1^2+b_{22}r_2^2\right) \end{pmatrix} + \text{h.o.t.} \tag{3.78}$$

where

$$b_{11} = \frac{\Im(e^{-i\phi_2}\hat{\alpha}_{2100})}{1+k_1} \qquad b_{12} = \frac{\Im(e^{-i\phi_2}\hat{\alpha}_{1011})}{1+k_1} \tag{3.79}$$
$$b_{21} = \frac{\Im(e^{-i\phi_4}\hat{\beta}_{1110})}{1+k_2} \qquad b_{22} = \frac{\Im(e^{-i\phi_4}\hat{\beta}_{0021})}{1+k_2}. \tag{3.80}$$

3.7 Analysis of the normal form

3.7.1 Single NS bifurcation

The analysis of the single NS bifurcation, is reduced to the analysis of the amplitude map in Eq. (3.69). The trivial solution of Eq. (3.69), corresponds to the trivial solution of Eq. (3.3), while nontrivial solutions of Eq. (3.69), correspond to 2-torus quasiperiodic solutions of Eq. (3.3). We remind that $k > 0$ for $p > p_{cr}$, while $k < 0$ for $p < p_{cr}$.

Analyzing Eq. (3.69), it is clear that the trivial solution exists for each value of k and ρ, while it is stable only for $k < 0$, i.e. for $p < p_{cr}$. At the same time, to have nontrivial solutions, we must have

$$\hat{r} = (1+k)\hat{r} + \rho\hat{r}^3 \quad \Longrightarrow \quad \hat{r} = \sqrt{-\frac{k}{\rho}}. \tag{3.81}$$

Nontrivial solutions of Eq. (3.69) exist, if and only if $k/\rho < 0$. So there are two different possibilities:

$$\begin{aligned} \rho < 0 \;&\Rightarrow\; \hat{r}\ \exists \text{ for } k > 0 \;\rightarrow\; \text{supercritical bifurcation} \\ \rho > 0 \;&\Rightarrow\; \hat{r}\ \exists \text{ for } k < 0 \;\rightarrow\; \text{subcritical bifurcation} \end{aligned}$$

The stability of the nontrivial solution can be analyzed considering the first derivate of Eq. (3.69) for $r = \hat{r}$

$$J|_{r=\hat{r}} < 1 \iff (1+k) + 3\rho\hat{r}^2 = 1 - 2k < 1 \iff k > 0 \tag{3.82}$$

so, the solution is stable for $k > 0$ and unstable for $k < 0$, as expected according to standard bifurcation theory (see Fig. 3.3). As a practical consequence, we would like to point out that subcritical bifurcations limit the basin of attraction of the trivial solution in the stable region, compromising its robustness and causing unexpected motions, if not properly analyzed.

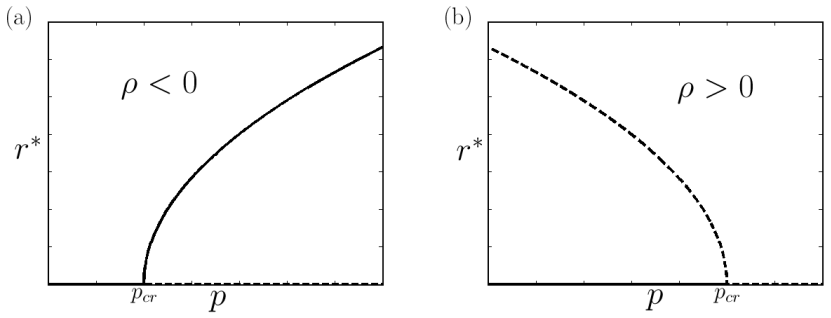

Figure 3.3: Typical bifurcation diagrams of a supercritical (a) and a subcritical (b) NS bifurcation.

3.7.2 Double Neimark-Sacker bifurcation

It is possible to investigate the dynamics in the vicinity of a double NS bifurcation, analyzing the fixed points of Eq. (3.74). If there are fixed points different from the trivial solution, the map in Eq. (3.7) admits quasiperiodic solutions. If the fixed point is semitrivial, i.e. it lays on one axis, the map in Eq. (3.7) will show a 2-torus quasiperiodic motion, while, if the fixed point is nontrivial, the map in Eq. (3.7) will show a 3-torus quasiperiodic motion. According to the scheme:

fixed point $(\tilde{r}_1, 0)$	$\rightarrow$	2-torus quasiperiodic motion with amplitude $\tilde{r}_1$ and frequency depending on Eq. (3.78_1)
fixed point $(0, \tilde{r}_2)$	$\rightarrow$	2-torus quasiperiodic motion with amplitude $\tilde{r}_2$ and frequency depending on Eq. (3.78_2)
fixed point (r_1^*, r_2^*)	$\rightarrow$	3-torus quasiperiodic motion given by two motions with amplitudes r_1^* and r_2^* and frequencies depending on Eq. (3.78)

The stability properties of these motions are analogous to the stability properties of the fixed points of Eq. (3.74).

There exists a fixed point on the r_1 axis $(\tilde{r}_1, 0)$ for

$$\tilde{r}_1 = \tilde{r}_1 + k_1\tilde{r}_1 + a_{11}\tilde{r}_1^3 \Leftrightarrow \tilde{r}_1 = \sqrt{-\frac{k_1}{a_{11}}}, \tag{3.83}$$

so, in order to have a fixed point on the r_1 axis, we must have $k_1/a_{11} < 0$.

The semitrivial fixed point is stable if and only if the eigenvalues of the Jacobian matrix have absolute value less than 1, i.e.

$$J|_{\tilde{r}_1} = \begin{pmatrix} 1 + k_1 + 3a_{11}\tilde{r}_1^2 & 0 \\ 0 & 1 + k_2 + a_{21}\tilde{r}_1^2 \end{pmatrix} = \begin{pmatrix} 1 - 2k_1 & 0 \\ 0 & 1 + k_2 - \frac{a_{21}}{a_{11}}k_1 \end{pmatrix}. \tag{3.84}$$

$$(\tilde{r}_1, 0) \text{ is stable } \iff \begin{cases} k_1 > 0 \\ k_2 - \frac{a_{21}}{a_{11}}k_1 < 0 \end{cases}. \tag{3.85}$$

If only one of the two inequalities is verified, the fixed point is a saddle, if both are not verified it is totally unstable. Considering that $\tilde{r}_1 = \sqrt{-k_1/a_{11}}$ and the conditions for stability in Eq. (3.85), if $a_{11} > 0$, this semitrivial fixed point is necessarily unstable, otherwise its stability depends also on a_{21} and k_2.

We now verify the existence of semitrivial fixed points on the r_2 axis $(0, \tilde{r}_2)$. There exists a semitrivial fixed point on the r_2 axis for

$$\tilde{r}_2 = \tilde{r}_2 + k_2\tilde{r}_2 + a_{22}\tilde{r}_2^3 \Leftrightarrow \tilde{r}_2 = \sqrt{-\frac{k_2}{a_{22}}}, \tag{3.86}$$

similarly to the previous case, in order to have the semitrivial fixed point, we must have $k_2/a_{22} < 0$.

The Jacobian matrix in correspondence of $(0, \tilde{r}_2)$ is

$$J|_{\tilde{r}_2} = \begin{pmatrix} 1 + k_2 + a_{12}\tilde{r}_2^2 & 0 \\ 0 & 1 + k_2 + 3a_{22}\tilde{r}_2^2 \end{pmatrix} = \begin{pmatrix} 1 + k_1 - \frac{a_{12}}{a_{22}}k_2 & 0 \\ 0 & 1 - 2k_2 \end{pmatrix}, \tag{3.87}$$

so

$$(0, \tilde{r}_2) \text{ is stable } \iff \begin{cases} k_2 > 0 \\ k_1 - \frac{a_{12}}{a_{22}}k_2 < 0 \end{cases} . \tag{3.88}$$

If only one of the two inequalities is verified, the fixed point is a saddle, if both are not verified it is totally unstable. As in the previous case, considering that $\tilde{r}_2 = \sqrt{-k_2/a_{22}}$ and the condition for stability in Eq. (3.88), if $a_{22} > 0$, this semitrivial fixed point is necessarily unstable, otherwise its stability depends also on a_{12} and k_2.

There exists a general fixed point (r_1^*, r_2^*) for

$$\begin{cases} r_1^* = r_1^* + k_1 r_1^* + a_{11} r_1^{*3} + a_{12} r_1^* r_2^{*2} \\ r_2^* = r_2^* + k_2 r_2^* + a_{21} r_1^{*2} r_2^* + a_{22} r_2^{*3} \end{cases} \rightarrow \begin{cases} a_{11} r_1^{*2} + a_{12} r_2^{*2} = -k_1 \\ a_{21} r_1^{*2} + a_{22} r_2^{*2} = -k_2 \end{cases} , \tag{3.89}$$

whose solution is

$$\begin{aligned} r_1^{*2} &= \frac{k_1 a_{22} - k_2 a_{12}}{a_{21} a_{12} - a_{11} a_{22}} \\ r_2^{*2} &= \frac{k_2 a_{11} - k_1 a_{21}}{a_{21} a_{12} - a_{11} a_{22}}. \end{aligned} \tag{3.90}$$

In order to have real solutions we must have $r_1^{*2} > 0$ and $r_2^{*2} > 0$. To investigate the stability of this fixed point, we have to study the eigenvalues of the Jacobian matrix

$$\begin{aligned} \mathbf{J}|_{r_1^* r_2^*} &= \begin{pmatrix} 1 + k_1 + 3a_{11} r_1^{*2} + a_{12} r_2^{*2} & 2a_{12} r_1^* r_2^* \\ 2a_{21} r_1^* r_2^* & 1 + k_2 + a_{21} r_1^{*2} + 3a_{22} r_2^{*2} \end{pmatrix} = \\ &\begin{pmatrix} 1 + k_1 + \frac{k_1(3a_{11}a_{22} - a_{21}a_{12}) - 2a_{11}a_{12}k_2}{a_{21}a_{12} - a_{11}a_{22}} & 2a_{12}\sqrt{\frac{(k_1 a_{22} - k_2 a_{12})(k_2 a_{11} - k_1 a_{21})}{a_{21}a_{12} - a_{11}a_{22}}} \\ 2a_{21}\sqrt{\frac{(k_1 a_{22} - k_2 a_{12})(k_2 a_{11} - k_1 a_{21})}{a_{21}a_{12} - a_{11}a_{22}}} & 1 + k_2 + \frac{k_2(3a_{11}a_{22} - a_{21}a_{12}) - 2a_{21}a_{22}k_1}{a_{21}a_{12} - a_{11}a_{22}} \end{pmatrix}. \end{aligned} \tag{3.91}$$

If both the eigenvalues are inside the unit circle of the complex plane, the nontrivial fixed point is stable, and it corresponds to a stable 3-torus quasiperiodic motion of the map in Eq. (3.7). If only one eigenvalue is out of the unit circle, the nontrivial fixed point is a saddle, so the corresponding 3-torus quasiperiodic motion of the map in Eq. (3.7) is unstable. If both the eigenvalues are out of the unit circle, the fixed point is a repellor. As better explained in [42], the nontrivial solution (r_1^*, r_2^*) arises from a pitchfork bifurcation of one of the two semitrivial solutions $(\tilde{r}_1, 0)$ or $(0, \tilde{r}_2)$.

In Fig. 3.4, we show an example of a possible bifurcation structure in the vicinity of a double NS bifurcation. In the figure, the two single NS bifurcations are both supercritical. In regions B and F there is no interaction between the two bifurcations. In regions C and E there are two coexisting 2-torus quasiperiodic solutions, one stable and one unstable, while in region D, the interaction between the two bifurcations generates an unstable 3-torus quasiperiodic solution ((r_1^*, r_2^*) is a saddle in this case), which coexists with two stable 2-torus quasiperiodic solutions. Similar bifurcation structures have been obtained in [44, 18] in correspondence to double Hopf bifurcations (of a continuous time system). The possible bifurcation structures are several and in another section a case study will show some typical features. For more details we address the readers to [42] and [43].

In case of instability of the nontrivial fixed point (r_1^*, r_2^*), it is important to analyze the values of the eigenvalues. If they are complex conjugate, the fixed point undergoes a NS bifurcation, adding one more frequency of vibration to the quasiperiodic motion of the map in Eq. (3.7), which will have four main frequencies of vibration and will move on a 4-torus. In order to analyze this 4-torus quasiperiodic motion, it is necessary to include in the analysis terms up to the fifth order, starting from the Taylor expansion in Eq. (3.9). The procedure, in this case, is extremely lengthy. More details, about this very special case, are given in [42] and [43], however, in the system analyzed in detail in the Ch. 4, this event is not occurring, thus the analysis will be still limited to third order terms.

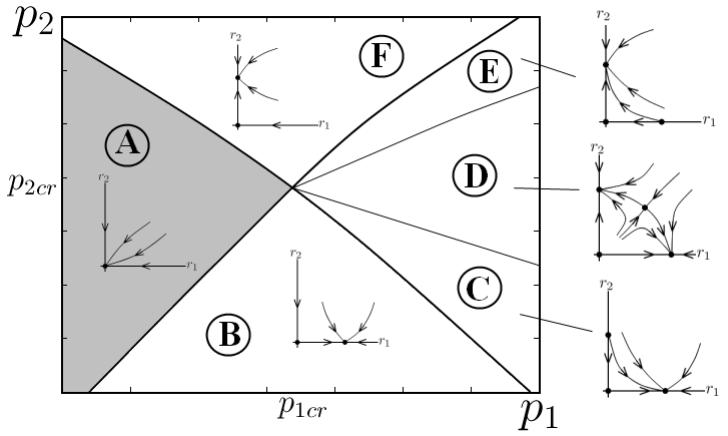

Figure 3.4: One possible bifurcation diagram of a double NS bifurcation, in the case of supercritical bifurcations. The letters from A to F indicate regions with different behaviors. The shaded area indicates stability of the trivial solution.

3.8 Flip bifurcation

As we already mentioned, the flip (or period-doubling) bifurcation, is occurring when at the loss of stability of a fixed point of a map, an eigenvalues of $D_x\mathbf{f}$ is leaving the unit circle of the complex plane through -1. It causes the birth of two branches of period-two solutions.

We consider the generic map

$$\mathbf{x}_f \mapsto \mathbf{f}_f(\mathbf{x}_f; p) \tag{3.92}$$

where $\mathbf{f}_f = [f_{1,f}(\mathbf{x}; p) \dots f_{n,f}(\mathbf{x}; p)]^T$, $\mathbf{x}_f = [x_1 \dots x_n]^T$ and p is a scalar real number. The map is analogous to the one in Eq. 3.3, with the exception that n can be also equal to 1. Again the trivial solution $\mathbf{x}_{0,f} = [0 \dots 0]^T$ satisfies Eq. (3.92), and it is stable for $p < p_{cr}$ and unstable for $p > p_{cr}$

Assuming that $f_{1,f} \dots, f_{n,f}$ are sufficiently smooth, we expand them in their Taylor series around 0, with respect to $x_1, \dots, x_n$ up to the third order, so we can rewrite Eq. (3.92) as

$$\mathbf{x}_f \mapsto \mathbf{A}_f(p)\mathbf{x}_f + \mathbf{b}_f(\mathbf{x}_f) \tag{3.93}$$

where the vector $\mathbf{b}_f(\mathbf{x}_f)$ contains all the nonlinear terms. Considering that

$$\begin{array}{lll} \text{for} & p < p_{cr} & |\mu_{i.f}| < 1 \quad \forall\, i = 1, \dots, n \\ \text{for} & p = p_{cr} & \mu_{1,f} = -1 \\ & & \frac{\mathrm{d}|\mu_{1,f}|}{\mathrm{d}p}|_{p=p_{cr}} > 0 \\ & & |\mu_i| < 1 \quad \forall\, i = 2, \dots, n, \end{array} \tag{3.94}$$

for $p = p_{cr}$ the system under study undergoes a flip bifurcation.

Jordan normal form

Similarly to the analysis of a NS bifurcation, we transform the system into its Jordan normal form. Calling $\mathbf{H}_f = \mathbf{A}_f|_{p=p_{cr}}$ and $\mathbf{s}_{i,f}$, $i = 1, \dots, n$ the eigenvectors related to the eigenvalues $\mu_{i,f}$ of $\mathbf{H}_f$, we define the transformation matrix

$$\mathbf{T} = \begin{pmatrix} \mathbf{s}_{1,f} & \cdots & \mathbf{s}_{n,f} \end{pmatrix}. \tag{3.95}$$

Such that

$$\mathbf{T}^{-1}\mathbf{H}\mathbf{T} = \begin{pmatrix} \mu_{1,f} & \cdots & 0 \\ \vdots & \ddots & \vdots \\ 0 & \cdots & \mu_{n,f} \end{pmatrix}, \tag{3.96}$$

where $\mu_{1,f} = -1$.

Applying the transformation

$$\mathbf{x}_f = \mathbf{T}_f \mathbf{y}_f, \quad \mathbf{y}_f = [y_1 \dots y_n]_f^T = \mathbf{T}_f^{-1}\mathbf{x} \tag{3.97}$$

we rewrite the maps in Eq. (3.93) in Jordan normal form, i.e.

$$\mathbf{y}_f \mapsto \mathbf{T}_f^{-1}\mathbf{H}_f\mathbf{T}_f\mathbf{y}_f + \mathbf{T}_f^{-1}\mathbf{b}_f(\mathbf{y}_f). \tag{3.98}$$

Center manifold reduction

Also the center manifold reduction can be performed analogously to the case of a NS bifurcation. In this case, the system will be reduced to a mono-dimensional one.

The local center manifold is defined in the form

$$\begin{pmatrix} y_2 \\ \vdots \\ y_n \end{pmatrix}_f = \mathbf{t}_f(y_1)_f = \begin{pmatrix} g_{22}y_1^2 + g_{23}y_1^3 \\ \vdots \\ g_{n2}y_{1,j}^2 + g_{n3}y_{1,j}^3 \end{pmatrix}_f, \tag{3.99}$$

where $g_{23} \dots g_{n3}$ can be neglected in most of the cases, limiting it to second order terms.

In order to find the $n-1$ coefficients g_{j2}, we substitute the $n-1$ equations of (3.99) into the first equation of (3.98). Then, we substitute this new equation and the equations in (3.99) into the remaining $n-1$ equations of (3.98). Collecting terms with the same power order, we obtain $n-1$ equations in the $n-1$ unknowns g_{i2} (if third order terms are not neglected the procedure is the same, with more unknowns). If now we substitute again the equations in (3.99) into the first equation of (3.98), we obtain

$$y_{1,f} \mapsto \mu_{1,f}y_{1,f} + \alpha_2 y_{1,f}^2 + \alpha_3 y_{1,f}^3 + \text{h.o.t.} \tag{3.100}$$

that is the system in Eq. (3.98), limited to its center manifold.

Elimination of the quadratic term

It is possible to transform out the quadratic term [40] applying the near identity transformation

$$y_{1,f} = z_f + c_2 z_f^2 \tag{3.101}$$

to Eq. (3.100) and imposing $c_2 = \alpha_2/2$. In this way we obtain the map

$$z_f \mapsto \mu_{1,f}z_f + \hat{\alpha}_3 z_f^3 + \text{h.o.t.} \tag{3.102}$$

where $\hat{\alpha}_3 = \alpha_3 + \alpha_2^2$.

Normal form

Rescaling the map according to $z_f = v_f/\sqrt{\hat{\alpha}_3}$ and calling

$$k_f = -(1+\mu_{1,f}) \approx -\frac{\mathrm{d}|\mu_{1,f}|}{\mathrm{d}p}\bigg|_{p=p_{cr}} (p - p_{cr}) \tag{3.103}$$

we obtain the map

$$v_f \mapsto -(1-k_f)v_f + \text{sgn}(\hat{\alpha}_3)v_f^3 + \text{h.o.t.} \tag{3.104}$$

that is the normal form of a flip bifurcation.

It can be easily verified that the trivial solution is stable for $k < 1$ and unstable for $k > 1$, while there exist a solution for the second iterate of the map in Eq. (3.104), i.e.

$$v_{1,2,f} = \pm \left(\sqrt{\frac{k}{\mathrm{sgn}(\hat{\alpha}_3)}} + O(k) \right). \tag{3.105}$$

If $\hat{\alpha}_3 > 0$, period-two stable solutions will exist for $k > 0$ and the bifurcation will be supercritical, otherwise, if $\hat{\alpha}_3 < 0$, period-two unstable solutions will exist for $k < 0$ and the bifurcation will be subcritical. For the detailed analysis of the stability of these solutions see [40] or [65].

Chapter 4

Bifurcation analysis in digital position control

In this chapter we will investigate in detail both a single and a double NS bifurcation, occurring in the digital position control of respectively a one and a two-DoF system, similar to the ones analyzed in Ch. 2. The systems analyzed in Ch. 2 are modeled by linear maps, thus at the loss of stability their motion would simply grow unboundedly. In order to study the bifurcations occurring at these losses of stability, we considered in the system the nonlinearity related to the saturation of the control force. This will limit the response of the system in the unstable regions. The analytical investigation will follow the procedures explained in Ch. 3, while numerical simulations will validate the results obtained analytically.

4.1 Single Neimark-Sacker bifurcation

4.1.1 Mechanical model

We consider the same system as in Fig. 2.1, reported in Fig. 4.1, still subject to PD digital control. The only difference with the system studied in Ch. 2 consists in the control force (now called Q_s). We now approximate it to an artangent function of the current (Fig. 4.2), while the current is a linear function of the displacement and the velocity of the mass m, i.e.

$$Q_s(t) = -\frac{Q_{\max}}{\pi/2}\left[\arctan(u-u_0)+q_0\right], \quad u = Px(t_j-\tau)+D\dot{x}(t_j-\tau) \tag{4.1}$$

where $Q_{\max}>0$ is the maximal output force of the motor, the parameter q_0, assumed positive without loss of generality, indicates that the saturation of the control force is not symmetric, while the parameter $u_0=\tan q_0$ is introduced in order to have zero force for $u=0$.

We apply the transformation $T=t/\tau$ and we call $Q_0=2Q_{\max}/(m\pi)$, so we can rewrite Eq. (4.1) as

$$x''_{j+1} = -\tau^2 Q_0\left[\arctan\left(Px_j+\frac{D}{\tau}x'_j-u_0\right)+q_0\right]. \tag{4.2}$$

Proceeding similarly to Ch. 2, we obtain the map

$$\begin{aligned} x &\mapsto x+x'+\frac{1}{2}x'' \\ x' &\mapsto x'+x'' \\ x'' &\mapsto -\tau^2 Q_0\left[\arctan\left(Px_j+\frac{D}{\tau}x'_j-u_0\right)+q_0\right]. \end{aligned} \tag{4.3}$$

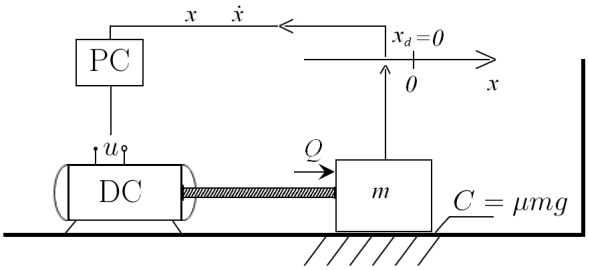

Figure 4.1: Mechanical model of a single DoF system

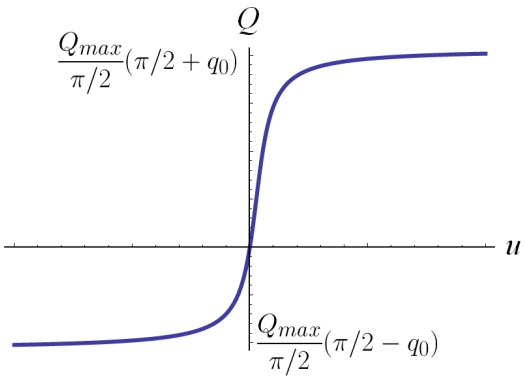

Figure 4.2: Asymmetric control force

Transforming the arctangent in its Taylor series we have

$$x'' \mapsto -\tau^2 Q_0 \left[-\arctan(u_0) + \frac{Px + \frac{D}{\tau}x'}{1+u_0^2} + \frac{u_0\left(Px+\frac{D}{\tau}x'\right)^2}{\left(1+u_0^2\right)^2} + \frac{\left(-1+3u_0^2\right)\left(Px+\frac{D}{\tau}x'\right)^3}{3\left(1+u_0^2\right)^3} + q_0 + \text{h.o.t.} \right] \quad (4.4)$$

and collecting terms with the same power order

$$\begin{aligned} x'' \quad \mapsto \quad & -\tau^2 Q_0 \left[\frac{P}{1+u_0^2}x + \frac{D}{\tau\left(1+u_0^2\right)}x' + \frac{u_0}{\left(1+u_0^2\right)^2}\left(P^2x^2 + \frac{2PD}{\tau}xx'_j + \frac{D^2}{\tau^2}x'^2\right) \right. \\ & \left. + \frac{\left(-1+3u_0^2\right)}{3\left(1+u_0^2\right)^3}\left(P^3x^3 + 3\frac{P^2D}{\tau}x^2x' + 3\frac{PD^2}{\tau^2}x_jx'^2 + \frac{D^3}{\tau^3}x'^3\right)\right]. \end{aligned} \quad (4.5)$$

Thus, we obtain the map

$$\begin{pmatrix} x \\ x' \\ x'' \end{pmatrix} \mapsto \begin{pmatrix} 1 & 1 & \frac{1}{2} \\ 0 & 1 & 1 \\ -p & -d & 0 \end{pmatrix} \begin{pmatrix} x \\ x' \\ x'' \end{pmatrix} + \begin{pmatrix} 0 \\ 0 \\ \sum_{h+k=2,3} b_{hk}x^h x'^k \end{pmatrix}, \quad (4.6)$$

where we redefined $p = \tau^2 PQ_0/\left(1+u_0^2\right)$ and $d = \tau DQ_0/\left(1+u_0^2\right)$, while the coefficients of the quadratic terms are

$$b_{hk} = -\gamma_2 \frac{u_0 Q_0 \tau^2}{\left(1+u_0^2\right)^2} P^h \left(\frac{D}{\tau}\right)^k = -\gamma_2 \frac{u_0 p^h d^k}{\tau^2 Q_0}, \quad \gamma_2 = \begin{cases} 1 \text{ if } \max(h,k) = 2 \\ 2 \text{ if } \max(h,k) = 1 \end{cases} \quad (4.7)$$

and the coefficients of the third order terms are

$$b_{hk} = \gamma_3 \frac{\left(1-3u_0^2\right)Q_0\tau^2}{3\left(1+u_0^2\right)^3} P^h \left(\frac{D}{\tau}\right)^k = -\gamma_3 \frac{\left(1-3u_0^2\right)p^h d^k}{\tau^4 Q_0^2}, \quad \gamma_3 = \begin{cases} 1 \text{ if } \max(h,k) = 3 \\ 3 \text{ if } \max(h,k) = 2. \end{cases} \quad (4.8)$$

The maps in Eqs. (4.3) and (4.6) have the same stability properties of Eq. (2.11) (see Fig. 2.4). As we already mentioned, on the right stability border the system undergoes a NS bifurcation and it satisfies the same conditions of Eq. (3.3) in Eq. (3.6). Thus, it is possible to analyze the occurring NS bifurcation according to the procedure shown in Ch. 3. In the following section we will first analyze the bifurcation locally, fixing the value of d such that p_{cr} is the maximal possible ($p_{cr} = 0.25$), then we will generalize the procedure along the whole stability border.

4.1.2 Analytical investigation

The system in Eq. (4.6) is already expanded in Taylor series. The next step consists in transforming the system in Jordan normal form, in order to decouple the linear part of the system. Before that, we fix $d = 5/8$, such that p is the bifurcation parameter and $p_{cr} = 0.25$. The values of the coefficients can be calculated according to Eqs. (4.7) and (4.8).

Applying the transformation into Jordan normal form, as explained in Ch. 3, we obtain the following

$$\begin{pmatrix} y_1 \\ y_2 \\ y_3 \end{pmatrix} \mapsto \begin{pmatrix} \frac{3}{4} & \frac{\sqrt{7}}{4} & 0 \\ -\frac{\sqrt{7}}{4} & \frac{3}{4} & 0 \\ 0 & 0 & \frac{1}{2} \end{pmatrix} \begin{pmatrix} y_1 \\ y_2 \\ y_3 \end{pmatrix} + \begin{pmatrix} \sum_{h+k+l=2,3} s_{1hkl} y_1^h y_2^k y_3^l \\ \sum_{h+k+l=2,3} s_{2hkl} y_1^h y_2^k y_3^l \\ \sum_{h+k+l=2,3} s_{3hkl} y_1^h y_2^k y_3^l \end{pmatrix}. \tag{4.9}$$

From the matrix it is possible to identify the eigenvalues at the bifurcation, i.e. $\mu_1 = 3/4 + i\sqrt{7}/4$, $\mu_2 = 3/4 - i\sqrt{7}/4$ and $\mu_3 = 1/2$, clearly $\mu_1 = \bar{\mu}_2$ and $|\mu_{1,2}| = 1$. The values of the coefficients s_{ihkl} can be found in Appendix C.

Since the system in Eq. (4.9) has dimension three, it should be reduced to its local center manifold. Applying the procedure explained in Ch. 3, we obtain the following equation for the center manifold

$$\gamma = -\frac{17u_0}{24Q_0\tau^2} y_1^2 + \frac{\sqrt{7}u_0}{12Q_0\tau^2} y_1 y_2 - \frac{7u_0}{24Q_0\tau^2} y_2^2 \tag{4.10}$$

that is the surface, in the three dimensional space, on which the system is evolving, in the vicinity of the bifurcation. Substituting the surface γ to the variable y_3, we reduce the system to a two dimensional one, i.e.

$$\begin{pmatrix} y_1 \\ y_2 \end{pmatrix} \mapsto \begin{pmatrix} \frac{3}{4} & \frac{\sqrt{7}}{4} \\ -\frac{\sqrt{7}}{4} & \frac{3}{4} \end{pmatrix} \begin{pmatrix} y_1 \\ y_2 \end{pmatrix} + \begin{pmatrix} \sum_{h+k=2,3} a_{hk} y_1^h y_2^k \\ \sum_{h+k=2,3} b_{hk} y_1^h y_2^k \end{pmatrix}. \tag{4.11}$$

The second order coefficients are not modified by the transformation. So, for example, $s_{1200} = a_{20}$ and $s_{220} = b_{20}$. Anyway, all the coefficients are explicitly given in Appendix C.

The next step consists in transforming the system in complex form, applying the transformation

$$\begin{array}{lcl} z = y_1 + iy_2 & \rightarrow & y_1 = \frac{z+\bar{z}}{2} \\ \bar{z} = y_1 - iy_2 & & y_2 = \frac{z-\bar{z}}{2i} \end{array} \tag{4.12}$$

that will give the system

$$z \mapsto \mu_2 z + \alpha_{20} z^2 + \alpha_{11} z\bar{z} + \alpha_{02} \bar{z}^2 + \alpha_{30} z^3 + \alpha_{21} z^2 \bar{z} + \alpha_{12} z\bar{z}^2 + \alpha_{03} \bar{z}^3 \tag{4.13}$$

The complex coefficients α_{hk} can be obtained using the a_{hk} and b_{hk} coefficients, given in Appendix C, and applying Eqs. from (B.1) to (B.7). The explicit values of α_{hk} are given in Appendix C.

Applying the near identity transformation $z = v + h_1(v, \bar{v})$, where $h_1(v, \bar{v}) = c_{20} v^2 + c_{11} v\bar{v} + c_{02} \bar{v}^2$ and

$$c_{hk} = -\frac{\alpha_{hk}}{\mu_2 - \mu_2^h \mu_1^k}, \tag{4.14}$$

the second order terms can be transformed out, modifying the coefficients of the third order terms according to Eqs. from (3.34) to (3.37), as explained in Ch. 3. Similarly, applying the transformation $v = w + h_2(w, \bar{w})$, where $h_2(w, \bar{w}) = c_{30} w^3 + c_{12} w\bar{w}^2 + c_{03} \bar{w}^3$ and

$$c_{hk} = -\frac{\hat{\alpha}_{hk}}{\mu_2 - \mu_2^h \mu_1^k}, \tag{4.15}$$

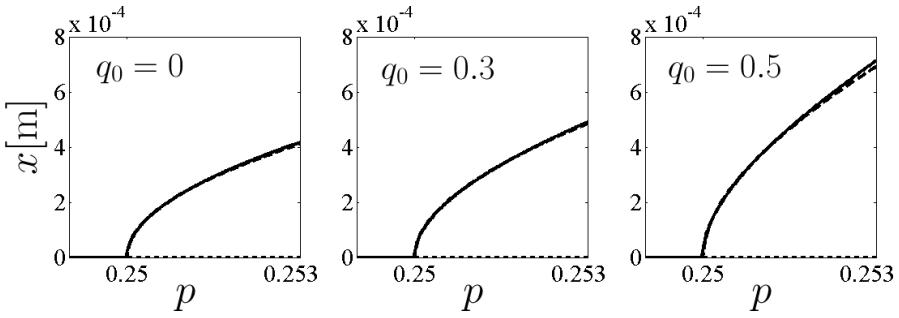

Figure 4.3: Bifurcation diagram. Solid lines: analytical results; dashed lines: numerical results. The diagrams have been obtained fixing $\tau = 0.01$ s and $Q_0 = 10$ m/s^2. Numerical results are obtained from Eq. (4.3).

all the non-internally resonant third order terms can be transformed out. The resulting map is

$$w \mapsto \mu_2 w + \hat{\alpha}_{21} w^2 \bar{w} \tag{4.16}$$

where

$$\hat{\alpha}_{21} = \left[\frac{1}{32} + i\frac{11}{32\sqrt{7}} + u_0^2 \left(\frac{29}{160} + i\frac{61}{480\sqrt{7}} \right) \right] \frac{1}{Q_0^2 \tau^4}. \tag{4.17}$$

Proceeding as explained in Ch. 3, we introduce the parameter $k = |\mu_2| - 1 \approx \frac{\mathrm{d}|\mu_2|}{\mathrm{d}p}(p - p_{cr})$ and we rewrite Eq. (4.16) as

$$w \mapsto w(1+k)e^{i\phi} + \hat{\alpha}_{21} w |w|^2, \tag{4.18}$$

where $e^{i\phi} = \mu_2$. For $d = 5/8$, along the stability border $\mathrm{d}|\mu_2|/\mathrm{d}p = 1$. Introducing the polar coordinates (r, ψ), such that $w = re^{i\psi}$, separating the absolute value from the phase and expanding it in Taylor series, we obtain the map

$$r \mapsto (1+k)r + \rho r^3 \tag{4.19}$$

$$\psi \mapsto \phi + \psi + \arctan\left(\frac{r^2 \Im(\hat{\alpha}_{21} e^{-i\phi})}{(1+k) + r^2 \Re(\alpha_{21} e^{-i\phi})} \right) \tag{4.20}$$

where

$$\rho = \Re\left(\alpha_{21} e^{-i\phi}\right) = \frac{-3 + 5u_0^2}{48 Q_0^2 \tau^4}. \tag{4.21}$$

Eq. (4.19) is the normal form of a NS bifurcation.

As already explained, the bifurcation is supercritical if $\rho < 0$ and subcritical if $\rho > 0$. The limit circle generated by the NS bifurcation has radius $r^* = \sqrt{-k/\rho}$, from which value its original shape can be obtained, transforming back the system from Eq. (4.19) to Eq. (4.6). From Eq. (4.21), we can see that $\rho < 0$ for $u_0 < \sqrt{3/5}$, i.e. $q_0 < 0.659$. So, if the saturation of the control force is symmetric, the bifurcation is supercritical, while if it is enough asymmetric, it becomes subcritical.

In Fig. 4.3 the comparison between the analytical and the numerical bifurcation diagram is represented. The matching around the critical value $p_{cr} = 0.25$ is excellent. Due to the asymmetry, the quasiperiodic attractor is asymmetric itself; the bifurcation curves in Fig. 4.3 refer to the maximum absolute value of the mass displacement during its motion.

Throughout this research work, numerical results of maps are plotted only for stable solutions and for unstable solutions of saddle type (see later). Numerical stable solutions have been obtained with a simple evolution of the map under study, while unstable solutions of saddle type have been plotted finding, with good

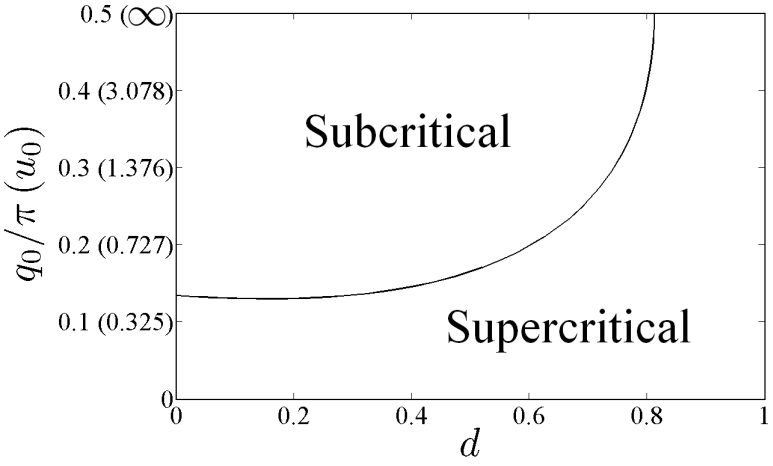

Figure 4.4: Regions in the d, q_0 space, along the stability border, where the NS bifurcation is either supercritical or subcritical.

accuracy, a point of the attractive branch from the saddle-cycle. Starting a simulation from that point the system is first approaching the unstable solution, giving an approximate idea of its shape, and then leaving it. This techniques allowed us to plot most of the unstable solutions of saddle type.

Repeating this procedure of analysis of the bifurcation along the whole stability boundary, we found that for a symmetric saturation the bifurcation is always supercritical, while the asymmetry can make it subcritical. According to the diagram in Fig. 4.4, the bifurcation can become subcritical up to $d = 0.812737$, for greater values of d, the bifurcation is supercritical even for extremely asymmetric saturations.

Numerical simulations for different values of the control gains p and d allow to identify regions with different amplitudes of oscillation of the quasiperiodic attractor. Fig. 4.5 shows lines of isoamplitude of oscillations of the system in the case of instability, for a symmetric saturation of the control force. It is remarkable the existence of unbounded motions (marked with UB), in spite of the limit of the control force. The line delimiting the area of unbounded motions appears to correspond to the line $2d = 3p$.

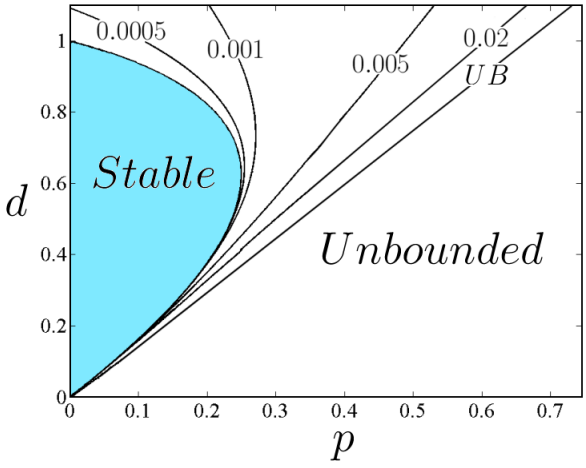

Figure 4.5: Amplitude of the 2-torus quasiperiodic oscillations (in meter) in the case of instability ($\tau = 0.01$ s, $Q_0 = 10$ m/s^2).

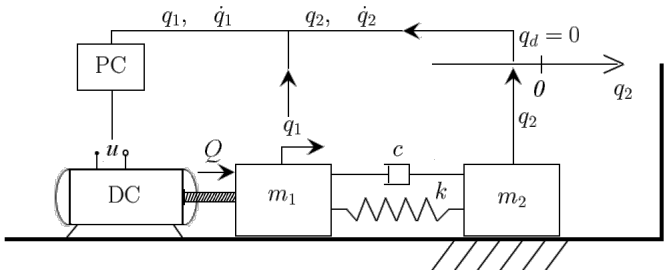

Figure 4.6: Mechanical model for analysis of a double NS bifurcation.

4.2 Double Neimark-Sacker bifurcation

4.2.1 Mechanical model

We now consider a two-Dof mechanical system, similar to those in Fig. 2.6, which stability has been analyzed in Ch. 2. The only difference consists in the data read in input by the controller, which now reads the position and the velocity of both the masses (Fig. 4.6).

The controller is considered to be digital, similarly to the system already analyzed, furthermore we consider the saturation of the control force in the same way we did regarding the single DoF system just analyzed in this chapter. The control force is then

$$Q_D(t) = -\frac{Q_{\max}}{\pi/2}\left[\arctan(u - u_0) + q_0\right] \tag{4.22}$$

where

$$u\left(t\right) = P_A q_1\left(t_j - \tau\right) + D_A \dot{q}_1\left(t_j - \tau\right) + P_B q_2\left(t_j - \tau\right) + D_B \dot{q}_2\left(t_j - \tau\right) \tag{4.23}$$

$$t \in [t_j, t_{j+1}).$$

P_A and D_A (P_B and D_B) are the proportional and differential gains related to the position and the velocity of m_1 (m_2), using the same notation of Ch. 2.

The linear part of the system (neglecting the saturation) is analogous to the one of the system in Fig. 2.6, thus it can be treated applying the same modal analysis. The result consists in the linear map

$$\left(\begin{array}{ccccc} x_1 & x_1' & x_2 & x_2' & \hat{Q}_D \end{array}\right)^{\mathrm{T}} \mapsto \mathbf{B}\left(\begin{array}{ccccc} x_1 & x_1' & x_2 & x_2' & \hat{Q}_D \end{array}\right)^{\mathrm{T}} \tag{4.24}$$

where

$$\mathbf{B} = \begin{pmatrix} 1 & 1 & 0 & 0 & \frac{1}{2} \\ 0 & 1 & 0 & 0 & 1 \\ 0 & 0 & e^{-\delta\Omega}\left(c_\Omega + \delta s_\Omega\right) & \frac{e^{-\delta\Omega}}{\Omega} s_\Omega & -\frac{1}{\Omega^2} + \frac{e^{-\delta\Omega}}{\Omega^2}\left(c_\Omega + \delta s_\Omega\right) \\ 0 & 0 & e^{-\delta\Omega}\left(-\delta^2 - 1\right)\Omega s_\Omega & e^{-\delta\Omega}\left(c_\Omega - \delta s_\Omega\right) & -e^{-\delta\Omega}\left(1 + \delta^2\right)\frac{s_\Omega}{\Omega} \\ -p_1 & -d_1 & p_2 & d_2 & 0 \end{pmatrix}$$

$c_\Omega = \cos\Omega$, $s_\Omega = \sin\Omega$ and $x_{1,j} = x_1(j)$. δ and Ω have the same meaning as in Ch. 2, $\hat{Q}_D = \tau^2 Q_D/(m_1 + m_2)$, $p_1 = P_1\tau^2/(m_1 + m_2)$, $p_2 = P_2\tau^2/(m_1 + m_2)$, $d_1 = D_1\tau/(m_1 + m_2)$ and $d_2 = D_2\tau/(m_1 + m_2)$. P_1, P_2, D_1 and D_2 are obtained as a consequence of the coordinate transformation in Eq. (2.43) and are: $P_1 = P_A + P_B$, $D_1 = D_A + D_B$, $P_2 = P_A m_2/m_1 - P_B$ and $D_2 = D_A m_2/m_1 - D_B$. As a consequence, P_1 and D_1 are directly related to the variable x_1 (rigid movement of the system), while P_2 and D_2 are related to the variable x_2 (relative movement between the two masses).

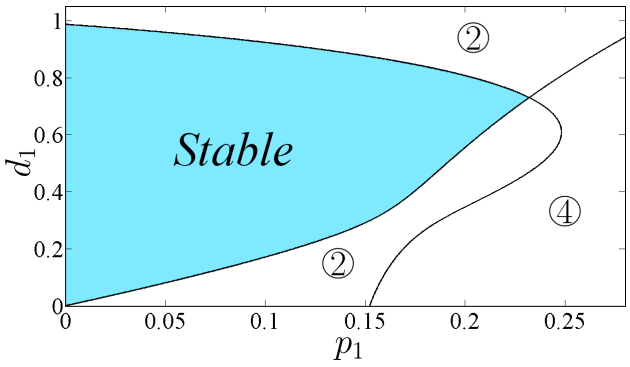

Figure 4.7: Stability chart for the parameter values $\Omega = 0.15\pi$, $\delta = 0.001$, $p_2 = 0.001$ and $d_2 = 0.01$, with two loci of Neimark-Sacker bifurcation.

Considering the full nonlinear system, the equations of motion of the system become

$$\begin{aligned}
x_1 &\mapsto x_1 + x_1' + \frac{\hat{Q}_D}{2} \\
x_1' &\mapsto x_1' + \hat{Q}_D \\
x_2 &\mapsto e^{-\delta\Omega}\left(c_\Omega + \delta s_\Omega\right) x_2 + \frac{e^{-\delta\Omega}}{\Omega} s_\Omega x_2' - \left(\frac{1}{\Omega^2} - \frac{e^{-\delta\Omega}}{\Omega^2}\left(c_\Omega + \delta s_\Omega\right)\right)\hat{Q}_D \\
x_2' &\mapsto e^{-\delta\Omega}\left(-\delta^2 - 1\right)\Omega s_\Omega x_2 + e^{-\delta\Omega}\left(c_\Omega - \delta s_\Omega\right) x_2' - e^{-\delta\Omega}\left(1 + \delta^2\right)\frac{s_\Omega}{\Omega}\hat{Q}_D \\
\hat{Q}_D &\mapsto -Q_0\tau^2\left[\arctan\left(P_1 x_1 + \frac{D_1}{\tau}x_1' - P_2 x_2 - \frac{D_2}{\tau}x_2' - u_0\right) + q_0\right]
\end{aligned} \tag{4.25}$$

where $Q_0 = 2Q_{\max}/\left(\pi(m_1 + m_2)\right)$.

For large ranges of the parameter values, the system shows to lose stability through NS bifurcations. In particular, we fixed the values of $\Omega = 0.15\pi$, $\delta = 0.001$, $p_2 = 0.001$, $d_2 = 0.01$ and, analyzing the eigenvalues of $\mathbf{B}$, we obtained the stability chart in Fig. 4.7. In the figure the two loci of NS bifurcations are clearly visible, at the intersection of the two loci the system undergoes a double NS bifurcation.

4.2.2 Analytical investigation

Following the procedure explained in Ch. 3, we analyze the double NS bifurcation occurring for $\Omega = 0.15\pi$, $\delta = 0.001$, $p_2 = 0.001$, $d_2 = 0.01$ in the p_1, d_1 space, at $p_1 = 0.232083$ and $d_1 = 0.730225$.

Expanding the arctangent in its Taylor series up to the third order with respect to x_1 and x_2 we have

$$\hat{Q}_D \mapsto -p_1 x_1 - d_1 x_1' + p_2 x_2 + d_2 x_2' + \sum_{h+k+l+m=2,3} b_{hklm} x_1^h x_1'^k x_2^l x_2'^m + Q_0\tau^2\left[\arctan(u_0) - q_0\right] \tag{4.26}$$

where we redefine $p_1 = Q_0\tau^2 P_1/(1+u_0^2)$, $d_1 = Q_0\tau D_1/(1+u_0^2)$, $p_2 = Q_0\tau^2 P_2/(1+u_0^2)$, $d_2 = Q_0\tau D_2/(1+u_0^2)$, while the coefficients of the second order terms are

$$b_{hklm} = -\alpha_2 \frac{p_1^h d_1^k (-p_2)^l (-d_2)^m u_0}{Q_0\tau^2}, \quad \alpha_2 = \begin{cases} 1 \text{ if } \max(h,k,l,m) = 2 \\ 2 \text{ if } \max(h,k,l,m) = 1 \end{cases}, \tag{4.27}$$

and the coefficients of the third order terms are

$$b_{hklm} = \alpha_3 \frac{1}{3} \frac{p_1^h d_1^k (-p_2)^l (-d_2)^m (1 - 3u_0^2)}{Q_0^2\tau^4}, \quad \alpha_3 = \begin{cases} 1 \text{ if } \max(h,k,l,m) = 3 \\ 3 \text{ if } \max(h,k,l,m) = 2 \\ 6 \text{ if } \max(h,k,l,m) = 1 \end{cases}. \tag{4.28}$$

The linear part of Eq. (4.26) has the same expression of $\hat{Q}$ in Eq. (4.24), so the equation of motion of the nonlinear system can be written in the following way:

$$\mathbf{x} \mapsto \mathbf{B}\mathbf{x} + \mathbf{b}(\mathbf{x}) \tag{4.29}$$

where

$$\mathbf{b}(\mathbf{x}) = \begin{pmatrix} 0 \\ 0 \\ 0 \\ 0 \\ \sum_{h+k+l+m=2,3} b_{hklm} x_1^h x_1'^k x_2^l x_2'^m \end{pmatrix}. \tag{4.30}$$

Jordan Normal Form

We call $p_{1cr} = 0.232083$ and $d_{1cr} = 0.730225$, i.e. the point in the p_1, d_1 space of the intersection of the two bifurcation loci, and we let p_1 and d_1, the bifurcation parameters, vary around these values. We define $\mathbf{H} = \mathbf{B}|_{p_1=p_{1cr}, d_1=d_{1cr}}$. The eigenvalues of $\mathbf{H}$ are

$$\mu_1 = 0.893314 + i0.449432 \rightarrow |\mu_1| = 1 \tag{4.31}$$
$$\mu_2 = 0.893314 - i0.449432 \rightarrow |\mu_2| = 1 \tag{4.32}$$
$$\mu_3 = 0.685901 + i0.727695 \rightarrow |\mu_3| = 1 \tag{4.33}$$
$$\mu_4 = 0.685901 - i0.727695 \rightarrow |\mu_4| = 1 \tag{4.34}$$
$$\mu_5 = 0.622744. \tag{4.35}$$

Applying the transformation into Jordan normal form, as explained in Ch. 3, we obtain the following

$$\begin{pmatrix} y_1 \\ y_2 \\ y_3 \\ y_4 \\ y_5 \end{pmatrix} \mapsto \begin{pmatrix} \Re(\mu_1) & \Im(\mu_1) & 0 & 0 & 0 \\ \Im(\mu_2) & \Re(\mu_2) & 0 & 0 & 0 \\ 0 & 0 & \Re(\mu_3) & \Im(\mu_3) & 0 \\ 0 & 0 & \Im(\mu_4) & \Re(\mu_4) & 0 \\ 0 & 0 & 0 & 0 & \mu_5 \end{pmatrix} \begin{pmatrix} y_1 \\ y_2 \\ y_3 \\ y_4 \\ y_5 \end{pmatrix} + \begin{pmatrix} \sum_{h+k+l+m+n=2,3} s_{1hklmn} y_1^h y_2^k y_3^l y_4^m y_5^n \\ \sum_{h+k+l+m+n=2,3} s_{2hklmn} y_1^h y_2^k y_3^l y_4^m y_5^n \\ \sum_{h+k+l+m+n=2,3} s_{3hklmn} y_1^h y_2^k y_3^l y_4^m y_5^n \\ \sum_{h+k+l+m+n=2,3} s_{4hklmn} y_1^h y_2^k y_3^l y_4^m y_5^n \\ \sum_{h+k+l+m+n=2,3} s_{5hklmn} y_1^h y_2^k y_3^l y_4^m y_5^n \end{pmatrix}. \tag{4.36}$$

The values of the coefficients s_{ihklmn} can be found in Appendix D.

In Eq. (4.36) the five equations are linearly coupled in pairs, considering the absolute values of the eigenvalues, it is possible to identify the four equations related to the bifurcation ($y_{1,\ldots,4}$) and the equation not related to the bifurcation (y_5).

Center Manifold Reduction

It is possible to reduce the dimension of the system eliminating the variable y_5. To do so, we have to reduce the dynamics of y_5 to its local center manifold [25]. Applying the procedure explained in Ch. 3, we obtain the following center manifold:

$$y_5 = \gamma(y_1, y_2, y_3, y_4) = \sum_{h+k+l+m=2} \tilde{b}_{hklm} y_1^h y_2^k y_3^l y_4^m \tag{4.37}$$

where

$$\begin{aligned} &\tilde{b}_{2000} = \tfrac{7.20153\times10^{-5}u_0}{Q_0\tau^2}, && \tilde{b}_{0200} = \tfrac{2.60017\times10^{-5}u_0}{Q_0\tau^2}, \\ &\tilde{b}_{0020} = \tfrac{0.253123u_0}{Q_0\tau^2}, && \tilde{b}_{0002} = \tfrac{0.136102u_0}{Q_0\tau^2}, \\ &\tilde{b}_{1100} = -\tfrac{1.04591\times10^{-6}u_0}{Q_0\tau^2}, && \tilde{b}_{1010} = -\tfrac{6.89914\times10^{-3}u_0}{Q_0\tau^2}, \\ &\tilde{b}_{1001} = \tfrac{1.67954\times10^{-3}u_0}{Q_0\tau^2}, && \tilde{b}_{0110} = -\tfrac{2.14827\times10^{-3}u_0}{Q_0\tau^2}, \\ &\tilde{b}_{0101} = -\tfrac{233564\times10^{-3}u_0}{Q_0\tau^2}, && \tilde{b}_{0011} = \tfrac{0.0325571u_0}{Q_0\tau^2} \end{aligned} \tag{4.38}$$

In the vicinity of the bifurcation, for small amplitude of oscillations, the system consists of the first four equations of (3.18), where y_5 is substituted by γ, i.e.

$$\begin{pmatrix} y_1 \\ y_2 \\ y_3 \\ y_4 \end{pmatrix} \mapsto \begin{pmatrix} \Re(\mu_1) & \Im(\mu_1) & 0 & 0 \\ \Im(\mu_2) & \Re(\mu_2) & 0 & 0 \\ 0 & 0 & \Re(\mu_3) & \Im(\mu_3) \\ 0 & 0 & \Im(\mu_4) & \Re(\mu_4) \end{pmatrix} \begin{pmatrix} y_1 \\ y_2 \\ y_3 \\ y_4 \end{pmatrix} + \begin{pmatrix} \sum_{h+k+l+m=2,3} a_{hklm} y_1^h y_2^k y_3^l y_4^m \\ \sum_{h+k+l+m=2,3} b_{hklm} y_1^h y_2^k y_3^l y_4^m \\ \sum_{h+k+l+m=2,3} c_{hklm} y_1^h y_2^k y_3^l y_4^m \\ \sum_{h+k+l+m=2,3} d_{hklm} y_1^h y_2^k y_3^l y_4^m \end{pmatrix}. \quad (4.39)$$

The coefficients a_{hklm}, b_{hklm}, c_{hklm} and d_{hklm} can be found in Appendix E.

Transformation to Normal Form

In order to study the bifurcation after the center manifold reduction, we follow the steps outlined in Ch. 3. Rewriting the system in complex form we have

$$\begin{pmatrix} z_1 \\ z_2 \end{pmatrix} \mapsto \begin{pmatrix} \mu_2 z_1 + \sum_{h+k+l+m=2,3} \alpha_{hklm} z_1^h \bar{z}_1^k z_2^l \bar{z}_2^m \\ \mu_4 z_2 + \sum_{h+k+l+m=2,3} \beta_{hklm} z_1^h \bar{z}_1^k z_2^l \bar{z}_2^m \end{pmatrix} \quad (4.40)$$

where $z_1 = y_1 + iy_2$, $z_2 = y_3 + iy_4$, α_{hklm} and $\beta_{hklm} \in \mathbb{C}$. α_{hklm} and β_{hklm} are linear combinations of a_{hklm}, b_{hklm}, c_{hklm} and d_{hklm}. Their values can be found according to the linear relations in Eqs. From (B.8) to (B.67) of Appendix B.

Applying the near identity transformation, as explained in Ch. 3, we can eliminate all the non-internally resonant terms. The only third order nonlinear terms left are related to the coefficients α_{2100}, α_{1011}, β_{0021} and β_{1110}; these terms cannot be eliminated because they are related to internal resonances so are dominant in the bifurcation.

After this transformation and considering that $w\bar{w} = |w|^2$, we obtain the system

$$\begin{pmatrix} w_1 \\ w_2 \end{pmatrix} \mapsto \begin{pmatrix} w_1 \left(\mu_2 + \hat{\alpha}_{2100}|w_1|^2 + \hat{\alpha}_{1011}|w_2|^2\right) \\ w_2 \left(\mu_4 + \hat{\beta}_{1110}|w_1|^2 + \hat{\beta}_{0021}|w_2|^2\right) \end{pmatrix} + \text{h.o.t.} \quad (4.41)$$

where $\hat{\alpha}_{2100}$, $\hat{\alpha}_{1011}$, $\hat{\beta}_{1110}$ and $\hat{\beta}_{0021}$ correspond to the respective α and β, modified by the near identity transformation. Their final values can be found in Appendix E.

Operating as explained in Ch. 3, we now introduce the two parameters

$$k_1 = |\mu_2| - 1, \qquad k_2 = |\mu_4| - 1$$

that can be linearized as

$$\begin{aligned} k_1 &= \tfrac{\mathrm{d}|\mu_2|}{\mathrm{d}p_1}\big|_{p_{1cr},d_{1cr}}(p_1 - p_{1cr}) + \tfrac{\mathrm{d}|\mu_2|}{\mathrm{d}d_1}\big|_{p_{1cr},d_{1cr}}(d_1 - d_{1cr}) \\ k_2 &= \tfrac{\mathrm{d}|\mu_4|}{\mathrm{d}p_1}\big|_{p_{1cr},d_{1cr}}(p_1 - p_{1cr}) + \tfrac{\mathrm{d}|\mu_4|}{\mathrm{d}d_1}\big|_{p_{1cr},d_{1cr}}(d_1 - d_{1cr}) \end{aligned} \quad (4.42)$$

and in numerical values are

$$\begin{aligned} k_1 &= 0.0212225(p_1 - p_{1cr}) - 0.0042641(d_1 - d_{1cr}) \\ k_2 &= 0.809618(p_1 - p_{1cr}) + 0.233615(d_1 - d_{1cr}). \end{aligned} \quad (4.43)$$

Calling $e^{i\phi_2} = \mu_2$ and $e^{i\phi_4} = \mu_4$ and introducing the polar coordinates $(r_1, r_2, \psi_1, \psi_2) \in \mathbb{R}$, where

$$w_1 = r_1 e^{i\psi_1}, \qquad w_2 = r_2 e^{i\psi_2}, \quad (4.44)$$

following once again the procedure of Ch. 3, we can transform the system in Eq. 4.41 into the amplitude and phase map

$$\begin{pmatrix} r_1 \\ r_2 \end{pmatrix} \mapsto \begin{pmatrix} r_1 \left(1 + k_1 + a_{11} r_1^2 + a_{12} r_2^2\right) \\ r_2 \left(1 + k_2 + a_{21} r_1^2 + a_{22} r_2^2\right) \end{pmatrix} + \text{h.o.t.} \quad (4.45)$$

$$\begin{pmatrix} \psi_1 \\ \psi_2 \end{pmatrix} \mapsto \begin{pmatrix} \phi_2 + \psi_1 + b_{11} r_1^2 + b_{12} r_2^2 \\ \phi_4 + \psi_2 + b_{21} r_1^2 + b_{22} r_2^2 \end{pmatrix} + \text{h.o.t.} \quad (4.46)$$

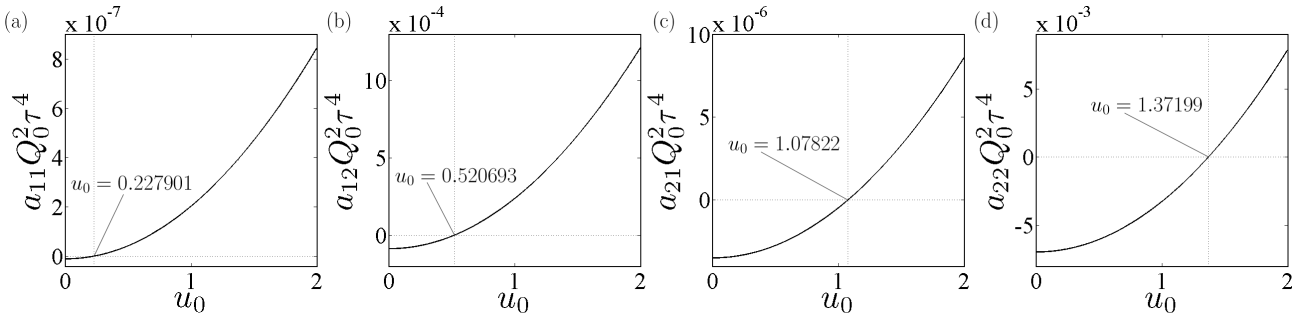

Figure 4.8: Variation of the coefficients a_{11}, a_{12}, a_{21} and a_{22} as functions of u_0.

where

$$a_{11} = \Re(e^{-i\phi_2}\hat{\alpha}_{2100}), \qquad a_{12} = \Re(e^{-i\phi_2}\hat{\alpha}_{1011}), \tag{4.47}$$

$$a_{21} = \Re(e^{-i\phi_4}\hat{\beta}_{1110}), \qquad a_{22} = \Re(e^{-i\phi_4}\hat{\beta}_{0021}), \tag{4.48}$$

$$b_{11} = \frac{\Im(e^{-i\phi_2}\hat{\alpha}_{2100})}{1+k_1}, \qquad b_{12} = \frac{\Im(e^{-i\phi_2}\hat{\alpha}_{1011})}{1+k_1}, \tag{4.49}$$

$$b_{21} = \frac{\Im(e^{-i\phi_4}\hat{\beta}_{1110})}{1+k_2}, \qquad b_{22} = \frac{\Im(e^{-i\phi_4}\hat{\beta}_{0021})}{1+k_2}. \tag{4.50}$$

whose values at the bifurcation point are reported in Appendix E.

As already explained, the dynamics of the system in the vicinity of the bifurcation strongly depends on the values and on the sign of the coefficients a_{hk}. For a symmetric saturation of the control force, i.e. $u_0 = 0$, they are all negative, but for increasing values of u_0, they monotonically increase and become positive, as shown in Fig. 4.8.

Analysis of the Normal Form

In Ch. 3, the conditions of existence and stability of fixed points of the map in Eq. (4.45) have already been shown. Summing them up we have:

$$(0,0)\,\exists\,\forall\,(k_1,k_2),\ \text{stable} \iff \begin{cases} k_1 < 0 \\ k_2 < 0 \end{cases} \tag{4.51}$$

$$(\tilde{r}_1, 0)\,\exists \iff \frac{k_1}{a_{11}} < 0,\ \text{stable} \iff \begin{cases} k_1 > 0 \\ k_2 - \frac{a_{21}}{a_{11}}k_1 < 0 \end{cases} \quad \left(\tilde{r}_1 = \sqrt{-\frac{k_1}{a_{11}}}\right) \tag{4.52}$$

$$(0, \tilde{r}_2)\,\exists \iff \frac{k_2}{a_{22}} < 0,\ \text{stable} \iff \begin{cases} k_2 > 0 \\ k_1 - \frac{a_{12}}{a_{22}}k_2 < 0 \end{cases} \quad \left(\tilde{r}_2 = \sqrt{-\frac{k_2}{a_{22}}}\right) \tag{4.53}$$

$$(r_1^*, r_2^*)\,\exists \iff \begin{cases} \frac{k_1a_{22}-k_2a_{12}}{a_{21}a_{12}-a_{11}a_{22}} > 0 \\ \frac{k_2a_{11}-k_1a_{21}}{a_{21}a_{12}-a_{11}a_{22}} > 0 \end{cases} \text{ and } (r_1^*, r_2^*) = \left(\sqrt{\frac{k_1a_{22}-k_2a_{12}}{a_{21}a_{12}-a_{11}a_{22}}}, \sqrt{\frac{k_2a_{11}-k_1a_{21}}{a_{21}a_{12}-a_{11}a_{22}}}\right) \tag{4.54}$$

(r_1^*, r_2^*) is stable if and only if the eigenvalues of $\mathbf{J}$ are inside the unit circle of the complex plane, where

$$\mathbf{J} = \begin{pmatrix} 1 + k_1 + \frac{k_1(3a_{11}a_{22}-a_{21}a_{12})-2a_{11}a_{12}k_2}{a_{21}a_{12}-a_{11}a_{22}} & 2a_{12}\sqrt{\frac{(k_1a_{22}-k_2a_{12})(k_2a_{11}-k_1a_{21})}{a_{21}a_{12}-a_{11}a_{22}}} \\ 2a_{21}\sqrt{\frac{(k_1a_{22}-k_2a_{12})(k_2a_{11}-k_1a_{21})}{a_{21}a_{12}-a_{11}a_{22}}} & 1 + k_2 + \frac{k_2(3a_{11}a_{22}-a_{21}a_{12})-2a_{21}a_{22}k_1}{a_{21}a_{12}-a_{11}a_{22}} \end{pmatrix}.$$

If the eigenvalues of $\mathbf{J}$ are complex conjugate and have absolute value equal to 1, the fixed point (r_1^*, r_2^*) undergoes a NS bifurcation in the r_1, r_2 space. In order to analyze this case it would be necessary to consider

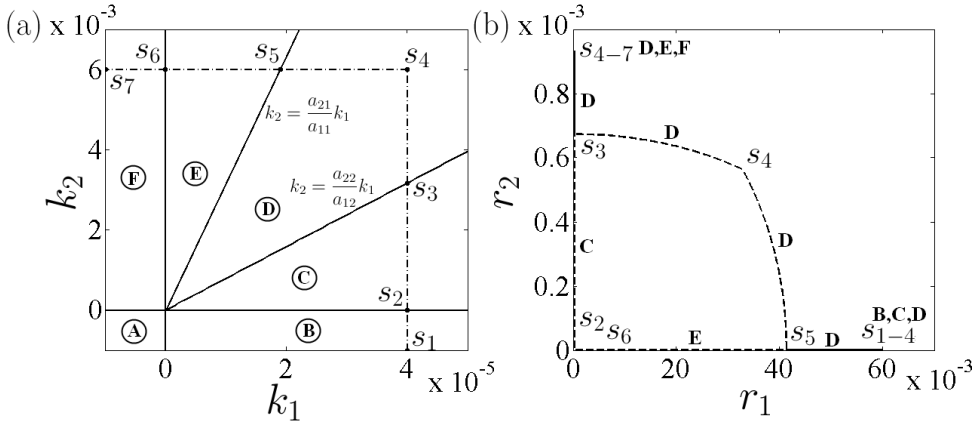

Figure 4.9: Response chart referred to the system in Eq. (4.45) with $u_0 = 0$. (a): existing regions in the space of the bifurcation parameters k_1, k_2. The letters from A to F indicate regions with different existing fixed points, while the dot-dash line indicates the bifurcation path we have followed. (b): existing attractors corresponding to the followed bifurcation path; solid lines: stable solutions, dashed lines: unstable solutions. The letters $s_1, ..., s_7$ indicates the correspondence between the two diagrams.

up to fifth order terms, as explained in [42]. Since this case is not occurring in this system, we consider up to third order terms, which are enough to describe the local dynamics of the system, related to small amplitude solutions.

4.2.3 Response charts and bifurcation diagrams

The performed analytical investigation transforms the system into its normal form, which allows to analyze the dynamic behavior in the vicinity of the bifurcation. Considering the values of the coefficients a_{hk}, it is possible to define regions in the k_1, k_2 (or p_1, d_1) space where the different solutions appear, namely the fixed points $(0,0)$, $(\tilde{r}_1, 0)$, $(0, \tilde{r}_2)$ and (r_1^*, r_2^*).

The coefficients a_{hk} are polynomial functions of u_0, as shown in Eqs. (E.85)-(E.89) and in Fig. 4.8. Considering the case of a symmetric saturation of the control force, i.e. assuming $u_0 = 0$, the values of the coefficients controlling the map in (4.45) are

$$\begin{aligned} a_{11} &= -\tfrac{1.10943\times10^{-8}}{Q_0^2\tau^4}, \quad a_{12} = -\tfrac{8.81111\times10^{-5}}{Q_0^2\tau^4}, \\ a_{21} &= -\tfrac{3.51185\times10^{-6}}{Q_0^2\tau^4}, \quad a_{22} = -\tfrac{6.97277\times10^{-3}}{Q_0^2\tau^4}. \end{aligned} \tag{4.55}$$

Since a_{11} and a_{22} are negative, the fixed point $(\tilde{r}_1, 0)$ exists for $k_1 > 0$ and the fixed point $(0, \tilde{r}_2)$ exists for $k_2 > 0$. While the nontrivial fixed point (r_1^*, r_2^*) exists for $k_2 > a_{22}k_1/a_{12}$ ($k_2 > 79.1361k_1$) and $k_2 < a_{21}k_1/a_{11}$ ($k_2 < 316.544k_1$) and it is a saddle.

The diagrams in Fig. 4.9 sum up all the existing bifurcations of the map in Eq. (4.45) for $u_0 = 0$. The letters from A to F in the figure indicate regions in the bifurcation parameter space with different fixed points. In region A we have $k_1 < 0$ and $k_2 < 0$, so the only existing solution is the trivial one. Passing from region A to region B, for $k_1 = 0$ the trivial solution undergoes a pitchfork bifurcation, so in region B the trivial solution becomes unstable and a new stable semitrivial fixed point is generated $(\tilde{r}_1)$. Passing from region B to region C, for $k_2 = 0$, the unstable trivial solution undergoes another pitchfork bifurcation, which generates an unstable semitrivial fixed point $(\tilde{r}_2)$, in Fig. 4.9(b) it corresponds to the point s_2 (see also Fig. 4.10(a)). The same pitchfork bifurcation would have been obtained passing from region A to region F, but in this case - starting from the stable trivial solution - it would have generated a stable semitrivial fixed point. In the passage from region C to region D (s_3) through the boundary $k_2 = 79.1361k_1$, the unstable semitrivial fixed point on the r_2 axis, undergoes a secondary pitchfork bifurcation: it becomes stable and generates an unstable fixed point

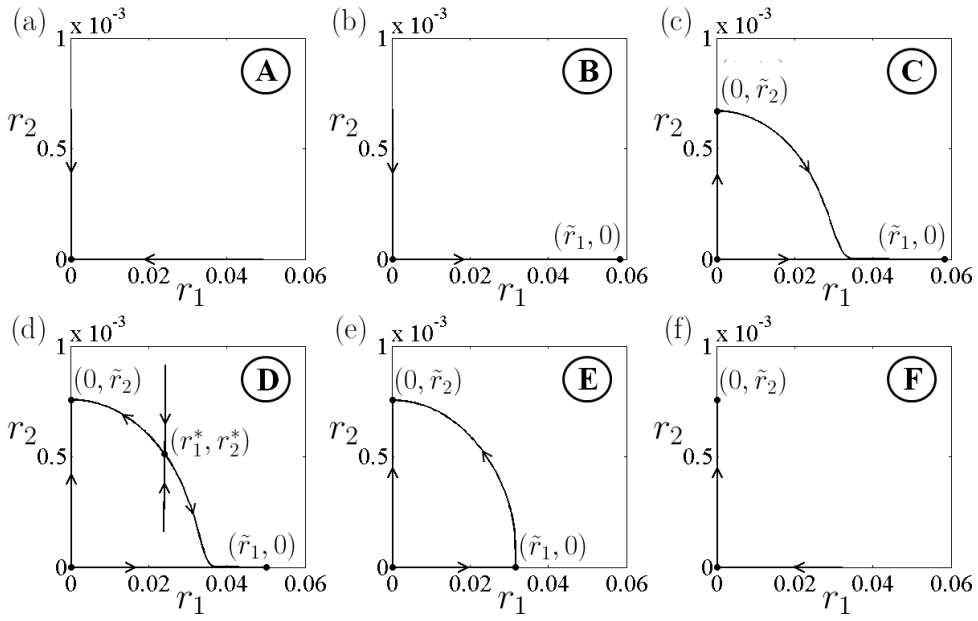

Figure 4.10: Phase portrait of the map in (4.45) for $u_0 = 0$ in the r_1, r_2 space. (a): $k_1 = -1 \times 10^{-5}$, $k_2 = -1 \times 10^{-3}$ (region A); (b): $k_1 = 4 \times 10^{-5}$, $k_2 = -1 \times 10^{-3}$ (region B); (c): $k_1 = 4 \times 10^{-5}$, $k_2 = 3.1 \times 10^{-3}$ (region C); (d): $k_1 = 3 \times 10^{-5}$, $k_2 = 4 \times 10^{-3}$ (region D); (e): $k_1 = 1.2 \times 10^{-5}$, $k_2 = 4 \times 10^{-3}$ (region E); (f): $k_1 = -1 \times 10^{-5}$, $k_2 = 4 \times 10^{-3}$ (region E).

(r_1^*, r_2^*), which in the figure is the branch $s_3 - s_4$. In region D there are two stable semitrivial fixed points ($\tilde{r}_1$ and $\tilde{r}_2$), the unstable trivial solution and another unstable fixed point (r_1^*, r_2^*) (Fig. 4.10(b)). In the passage from region D to region E (s_5) through the boundary $k_2 = 316.544k_1$, the unstable non trivial fixed point merges with the stable semitrivial fixed point ($\tilde{r}_1$) through a reverse secondary pitchfork bifurcation. So in region E the only stable solution is the semitrivial fixed point on the r_2 axis (Fig. 4.10(c)). Finally, in the passage between regions E and F, the unstable semitrivial fixed point ($\tilde{r}_1$) disappears through a reverse pitchfork bifurcation and it merges with the unstable trivial solution. Going back to region A again, also the stable semitrivial fixed point on the r_2 axis merges with the trivial solution, which becomes stable again.

The case of an asymmetric saturation of the control force, i.e. $u_0 \neq 0$, will be investigate in detail in Ch. 5. The bifurcation chart will be seen to change meaningfully according to the variations of the values of a_{hk}. The two bifurcation loci of secondary pitchfork bifurcation in Fig. 4.9(a), at $k_2 = a_{21}k_1/a_{11}$ and $k_2 = a_{22}k_1/a_{12}$, will rotate counterclockwise around the origin. Critical values of u_0, that qualitatively modify the response, correspond to changes of sign from negative to positive of the coefficients a_{hk}. From Fig. 4.8, we can see that these critical values are at $u_0 = 0.227901$ (a_{11} becomes positive), $u_0 = 0.520693$, $u_0 = 1.07822$ and $u_0 = 1.37199$ (a_{22} becomes positive).

Considering Eqs. (4.52) and (4.53), we can already state that the NS bifurcation related to the fixed point $(\tilde{r}_1, 0)$ will become subcritical for $a_{11} > 0$, i.e. $u_0 > 0.227901$. Similarly, the NS bifurcation related to the fixed point $(0, \tilde{r}_2)$ becomes subcritical for $a_{22} > 0$, i.e. $u_0 > 1.37199$.

Bifurcation diagram

In order to compare the analytical results with the numerical ones, we transform the response chart in Fig. 4.9(a) from the k_1, k_2 space to the p_1, d_1 space. The result is shown in Fig. 4.11(a). In the figure, the regions marked with the letters from A to F, correspond to the regions marked with the same letters in Fig. 4.9.

In Fig. 4.11(b), a comparison between the numerical and the analytical bifurcation diagrams is represented. The solid black lines are the (stable) numerical results, while the colored lines are the analytical results. The

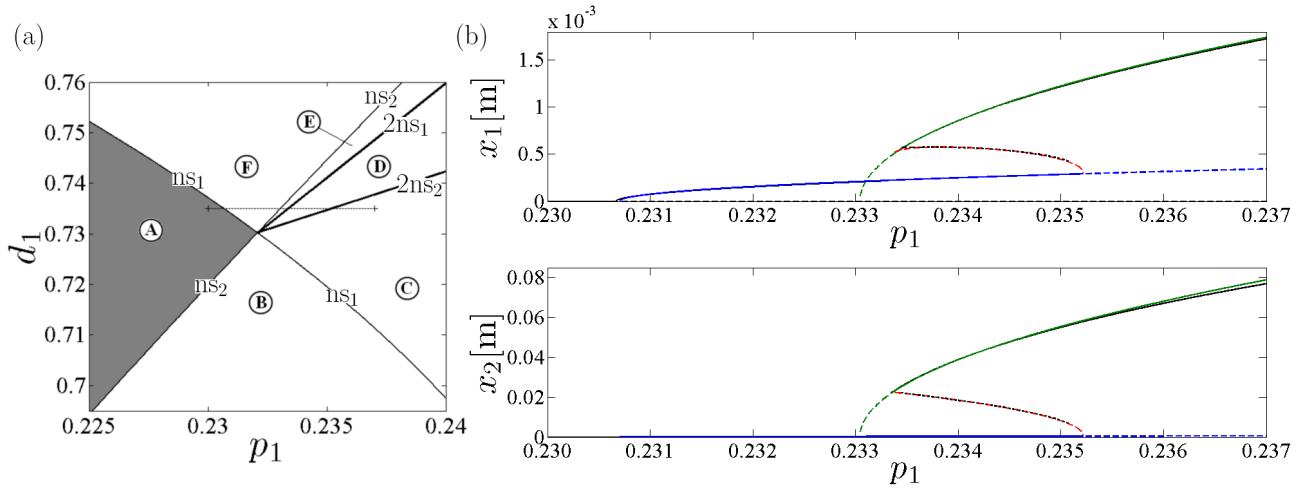

Figure 4.11: (a): stability chart in the parameter space of the control gains p_1, d_1 in the vicinity of the bifurcation for $u_0 = 0$. Uppercase letters in the circle indicate the correspondence between the regions in the p_1, d_1 space and in the k_1, k_2 space (Fig. 4.9). Lowercase letters indicate bifurcation loci: "ns_1" and "ns_2" NS bifurcations, "$2\mathrm{ns}_1$" and "$2\mathrm{ns}_2$" secondary NS bifurcations. (b): bifurcation diagram with respect to the bifurcation parameter p_1, for $d_1 = 0.735$ and $u_0 = 0$. Solid lines: stable solutions, dashed lines: unstable solutions. The black lines refer to the numerical results while the colored lines to the analytical results. During the simulation $Q_0 = 10\mathrm{m/s}^2$, $\tau = 0.01$ s.

numerical results have been obtained through a direct evolution of the map in Eq. (4.25), describing the dynamics of the system, without taking into account the expansion in Taylor series.

In the figure, the bifurcation parameter is the proportional gain p_1. The variation of p_1 moves the state of the system through regions A, F, E, D and C (horizontal dash-dot line in Fig. 4.11(a)). Going from left to right, at the beginning the system is in region A, so the only solution is the trivial one and it is stable. At $p_1 = 0.2307$ the system enters region F, the trivial solution undergoes a supercritical NS bifurcation (ns_1), generating a branch of 2-torus quasiperiodic solutions (blue line) of the map in (4.25), which corresponds to the semitrivial fixed point $(0, \tilde{r}_2)$ of Eq. (4.45). In Fig. 4.11, due to the scale of the axis, it is not possible to recognize the non-vanishing amplitude of x_2. At $p_1 \approx 0.233$, entering region E, from the unstable trivial solution, another branch of unstable 2-torus quasiperiodic solutions (green line) is generated, which corresponds to the semitrivial fixed point $(\tilde{r}_1, 0)$. At $p_1 \approx 0.2334$ the system goes into region D, the branch of unstable 2-torus quasiperiodic solutions undergoes a secondary NS bifurcation ($2\mathrm{ns}_1$): it becomes stable and generates a branch of unstable 3-torus quasiperiodic solutions (red line). The quasiperiodic solutions correspond to the fixed point (r_1^*, r_2^*) of Eq. (4.45). According to our analysis, for the considered symmetric saturation, this is the only region where there are two coexisting stable 2-torus quasiperiodic solutions. At $p_1 \approx 0.2352$, entering region C, the unstable 3-torus quasiperiodic branch merges with the other 2-torus quasiperiodic branch, which becomes unstable. If we compute the bifurcation diagram through a sweep up, the system will start in a rest position, then it will start oscillating for $p_1 > 0.2307$, increasing gradually the amplitude of oscillation, until it reaches $p_1 \approx 0.2352$, where the system will jump onto the other 2-torus quasiperiodic attractor with a much larger amplitude of oscillation. In case of a sweep down, the system will oscillate and decrease the amplitude of vibration for decreasing p_1, until $p_1 \approx 0.2334$, when it will suddenly reduce the amplitude of vibration, jumping onto the lower branch of 2-torus quasiperiodic solutions. For $p_1 < 0.2307$ the system will settle down to the origin.

Figure 4.11 shows a very good matching between the numerical and the analytical results, both regarding the amplitude of oscillation and the borders of the regions for the different behaviors. The main difference regards the 2-torus quasiperiodic solution with higher amplitude, and it is due to the increasing effect of the higher order terms.

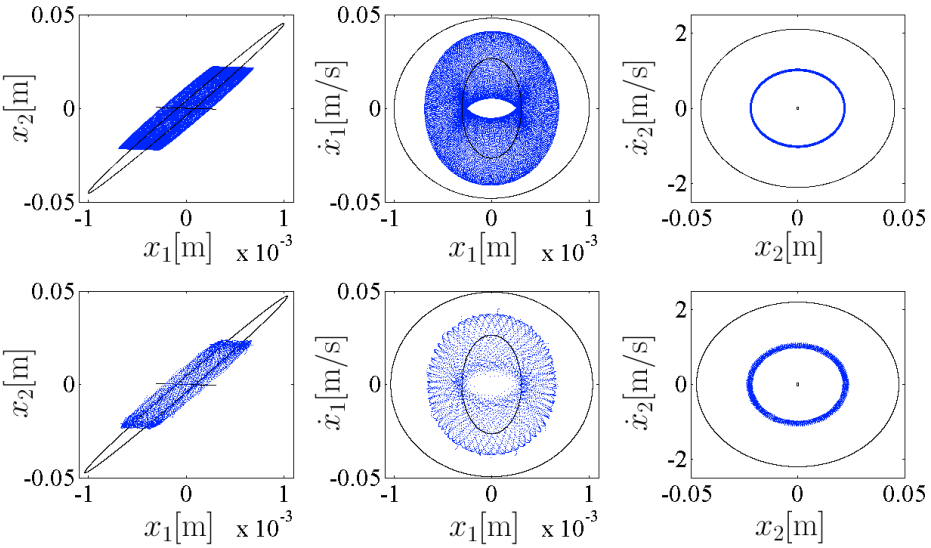

Figure 4.12: Existing periodic and quasiperiodic solutions for the parameter values $u_0 = 0$, $Q_0 = 10$ m/s^2, $\tau = 0.01$ s, $\Omega = 0.15\pi$, $\delta = 0.001$, $p_2 = 0.001$, $d_2 = 0.01$, $p_1 = 0.2349$, $d_1 = 0.7374$ ($k_1 = 3 \times 10^{-5}$, $k_2 = 4 \times 10^{-3}$), projected onto the x_1, x_2, $x_1, \dot{x}_1$ and $x_2, \dot{x}_2$ space. Larger closed line: attractor of the 2-torus quasiperiodic motion related to $(\tilde{r}_1, 0)$; smaller closed line: attractor of the 2-torus quasiperiodic motion related to $(0, \tilde{r}_2)$; blue fuzzy line: 3-torus quasiperiodic solution related to (r_1^*, r_2^*). *Top*: analytical results, *bottom*: numerical results.

Figure 4.12 shows the projections on different planes of the 2-torus and 3-torus quasiperiodic solutions of the map in Eq. (4.25). It shows a comparison of the numerical and the analytical results. In the figure, the displacement and the velocity are plotted for each time interval τ, so they can be considered as stroboscopic Poincaré maps of the underlying continuous time system. The blue fuzzy lines refer to the 3-torus quasiperiodic solution of the stroboscopic map. In the numerical simulation (Fig. 4.12*bottom*) the curve has been obtained plotting the first 1000 iterates of the system, before it diverges from the quasiperiodic repellor. The other curves (closed lines) refer to the coexisting 2-torus quasiperiodic attractors of the map. The matching between the numerical and the analytical results is very good, the main difference regards the amplitude of the largest attractor and it is due to the major role played by the higher order terms (the simulation refers to the system before the Taylor expansion). Considering Figs. 4.11 and 4.12, it can be recognized that the larger attractor corresponds to the fixed point $(\tilde{r}_1, 0)$, while the smaller attractor corresponds to $(0, \tilde{r}_2)$.

Although it is not visible because of the scale of the figures, the smaller attractor has the two coordinates x_1 and x_2 with the same order of magnitude ($x_{1,\max} \approx 3 \times 10^{-4}$, $x_{2,\max} \approx 5 \times 10^{-4}$), while the larger attractor has the coordinate x_2 fifty times larger than the coordinate x_1 ($x_{1,\max} \approx 0.001$, $x_{2,\max} \approx 0.05$), being mostly associated with a relative motion between the two masses (x_2) rather than an absolute motion of the system (x_1). This can be easily verified also analytically. If we neglect the near identity transformation and the center manifold reduction, which are acting only on the nonlinear terms and not affecting much the amplitudes, and we consider that $\mathbf{x} = \mathbf{T}\mathbf{y}$, $z_1 = y_1 + iy_2$, $z_2 = y_3 + iy_4$, $z_1 \approx w_1 = r_1 e^{i\psi_1}$ and $z_2 \approx w_2 = r_2 e^{i\psi_2}$ we have

$$\begin{aligned} x_1 &= t_{11}y_1 + t_{12}y_2 + t_{13}y_3 + t_{14}y_4 \\ &\approx t_{11}r_1\cos\psi_1 + t_{12}r_1\sin\psi_1 + t_{13}r_2\cos\psi_2 + t_{14}r_2\sin\psi_2 \end{aligned} \tag{4.56}$$

and similarly for the other coordinates, where t_{ij} are the elements of $\mathbf{T}$. Considering alternatively r_1 and r_2 equal to zero, we have that the maximal value of x_1 for $(\tilde{r}_1, 0)$ and $(0, \tilde{r}_2)$ are

$$\begin{aligned} x_{1,\max} &\approx \left(t_{11}\cos\left[\arctan\left(\tfrac{t_{12}}{t_{11}}\right)\right] + \left(t_{12}\sin\left[\arctan\left(\tfrac{t_{12}}{t_{11}}\right)\right]\right)\right)\tilde{r}_1 = 0.02005\tilde{r}_1 \\ x_{1,\max} &\approx \left(t_{13}\cos\left[\arctan\left(\tfrac{t_{14}}{t_{13}}\right)\right] + \left(t_{14}\sin\left[\arctan\left(\tfrac{t_{14}}{t_{13}}\right)\right]\right)\right)\tilde{r}_2 = -0.40504\tilde{r}_2 \end{aligned} \tag{4.57}$$

and similarly

$$\begin{aligned} x_{2,\max} &\approx \left(t_{31}\cos\left[\arctan\left(\tfrac{t_{32}}{t_{31}}\right)\right] + \left(t_{32}\sin\left[\arctan\left(\tfrac{t_{32}}{t_{31}}\right)\right]\right)\right)\tilde{r}_1 = 0.90620\tilde{r}_1 \\ x_{2,\max} &\approx \left(t_{33}\cos\left[\arctan\left(\tfrac{t_{34}}{t_{33}}\right)\right] + \left(t_{34}\sin\left[\arctan\left(\tfrac{t_{34}}{t_{33}}\right)\right]\right)\right)\tilde{r}_2 = 0.60889\tilde{r}_2 \end{aligned} \tag{4.58}$$

Considering the values in Eqs. (4.57) and (4.58) it is clear why the fixed point $(\tilde{r}_1, 0)$ is mostly associated with the variable x_2 ($x_{2,\max}/x_{1,\max} \approx 0.91/0.02$) and the fixed point $(0, \tilde{r}_2)$ is associated similarly with both the variables ($x_{2,\max}/x_{1,\max} \approx 0.61/0.41$).

Considering the different amplitudes of the two attractors, from an engineering point of view, region B is more dangerous than region F.

Chapter 5

Effects of asymmetry

In Ch. 4 a single and a double Neimark-Sacker bifurcation, occurring in the digital positioning of mechanical systems have been investigated. In both cases the nonlinearity of the system was related to the saturation of the control force. Although in the analytical investigation the saturation was considered asymmetric, only results related to symmetric saturations have been analyzed in detail and verified numerically.

Although generally DC motors work symmetrically and also saturate symmetrically, in several cases asymmetries can arise. For example, if gravity is involved, the control force can be shifted becoming asymmetric. Another typical case of asymmetry occurs if the control force is given by propellers, which generally have asymmetric airfoils.

In this chapter we will analyze in detail the cases of asymmetric saturation, related to the systems already studied in Ch. 4.

5.1 Single Neimark-Sacker bifurcation

Considering the mechanical system in Fig. 2.1 and the analytical results obtained in Ch. 4, we carry out numerical simulations of the map in Eq. (4.3). The aim of these simulations is to verify the effects of the asymmetry, comparing numerical results to those obtained from the analytical treatment. In addition, a systematic numerical investigation could show results overlooked by the analytical procedure.

From the analytical investigation we obtained that $\rho = \left(-3 + 5u_0^2\right) / \left(48 Q_0^2 \tau^4\right)$ (for $d = 5/8$ and $p = 1/4$). Considering that the NS bifurcation is supercritical for $\rho < 0$ and subcritical for $\rho > 0$, it will be supercritical for a symmetric system and subcritical for an asymmetric system such that $u_0 > \sqrt{3/5}$, i.e. $q_0 > 0.659$ ($u_0 = \tan q_0$). This result has been already pointed out in the previous chapter, and extended to the whole stability boundary (see Fig. 4.4). The point of transition of the bifurcation from supercritical to subcritical is also called Chenciner bifurcation [11,40].

Most of the numerical analysis in this section is made fixing the dimensionless differential gain $d = 5/8$ and varying the parameters p and q_0. Through continuation analysis and systematic numerical simulations, we obtain the response chart in Fig. 5.1, that shows the existing attractors of the map in Eq. (4.3) in the parameter space q_0 and p. Attention is focused on a neighborhood of the maximal stability value of p and to a range of q_0 where the NS bifurcation is subcritical. 2-torus quasiperiodic and chaotic attractors are seen to occur both below $p = 0.25$ and, mostly, above it. The region 5 can be extended down to $q_0 = 0$. The dashed line limiting the chaotic region indicates that within it also non chaotic attractors may exist and the chaotic attractor may disappear in some parts. Regions 2 and 5 present more than one periodic attractor in some subregions, we experienced up to three of them coexisting with each other.

In order to analyze the bifurcations outlined in Fig. 5.1, we plotted the bifurcation curves by varying one parameter per time, crossing all the boundaries in the diagram of Fig. 5.1.

The bifurcation occurring when crossing the line between regions 3 and 5 is represented by the diagrams in Fig. 5.2. According to the diagram in Fig. 5.1, the bifurcation under study is supercritical up to $q_0 \approx 0.65$, which is in good accordance with the analytical results.

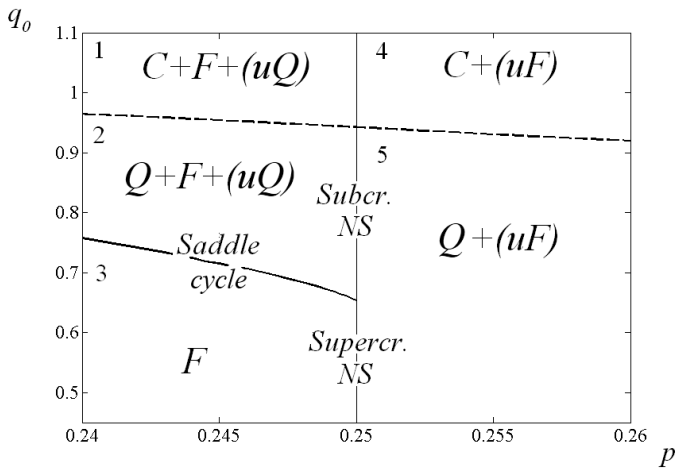

Figure 5.1: Existing attractors in the q_0 and p parameter space. F: stable focus, Q: stable quasiperiodic motion, C: chaotic motion. In brackets the unstable solutions. $Q_0 = 10$ m/s^2 and $\tau = 0.01$ s.

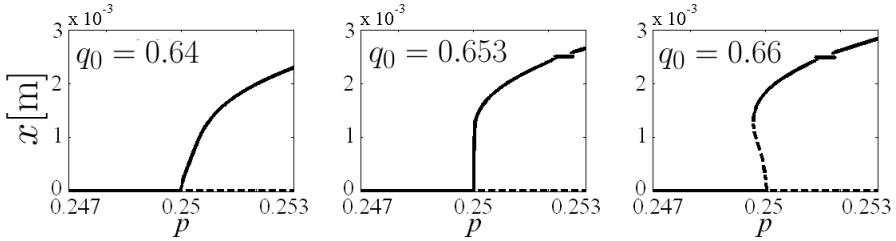

Figure 5.2: Bifurcation diagram for different values of q_0. $Q_0 = 10$ m/s^2 and $\tau = 0.01$ s. Solid lines: stable solutions, dashed lines: unstable solutions.

The typical bifurcation diagram ensuing from a subcritical NS (Fig. 5.3) marks the passage from region 2 to region 5. It can be divided into three regions: for $p < 0.2492$ we are in region 3 of Fig. 5.1, with the only attractor being the stable focus at the origin. For $0.2492 < p < 0.25$ we are in region 2, with three coexisting solutions, the stable focus in the origin, a stable quasiperiodic attractor and a quasiperiodic repellor in between. The quasiperiodic solutions arise from a saddle-cycle bifurcation. For $p > 0.25$ we are in region 5, where the unstable quasiperiodic solution disappears and the stable focus in the origin becomes unstable. This diagram has been obtained plotting for each value of p the maximal displacement (in absolute value) after the transient has faded away, by sweeping the control parameter up and down in order to find possibly coexisting attractors.

It is clear that, if we are in region 3 with $p < 0.249207$ and we increase p, the mass will stay at the origin until we reach $p = 0.25$, where it will start to oscillate and jump from point C to D; increasing the parameter p even more, the amplitude of vibration will progressively increase. If instead we start with a proportional gain $p > 0.25$, the mass will start oscillating, with a progressive reduction of the amplitude of vibration as we decrease p until reaching point B at $p = 0.2492$, then the mass will suddenly settle down onto the origin at point A.

Fig. 5.3 shows a good matching between the numerical and the analytical results, around $p = 0.25$. While the amplitude increases, the matching becomes poorer because of the influence of the terms higher than the third. In this respect, the saddle-cycle bifurcation, experienced in the numerical simulations, is totally overlooked by the analytical investigation limited to third order terms. The extension of the analytical procedure to higher order terms could allow to identify also this saddle-cycle bifurcation and the larger branch of stable periodic solutions. However, an attempt of the author of including fifth order terms did not give positive results.

The bifurcation occurring while crossing the border between regions 3 and 2, through a change in the

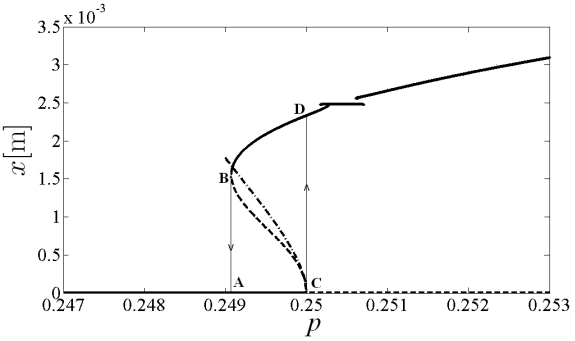

Figure 5.3: Bifurcation diagram for $q_0 = 0.67$, $Q_0 = 10$ m/s^2 and $\tau = 0.01$ s. Solid line: stable solutions, dashed line: unstable solutions, dash-dot line; analytical results.

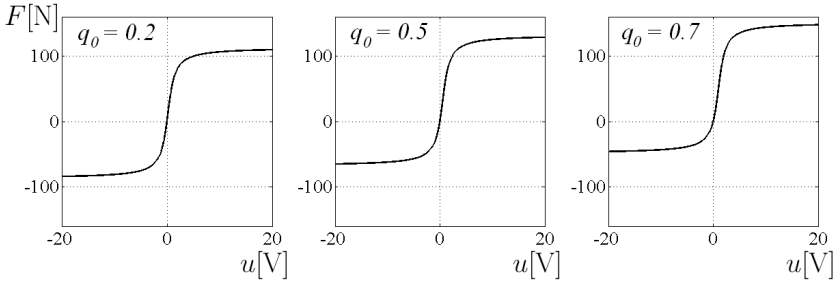

Figure 5.4: Diagram of the control force for different values of q_0 with increasing asymmetry.

parameter q_0 – which affects the asymmetry of the control force (see Fig. 5.4) –, is represented in Fig. 5.5. For $q_0 < 0.668$ we are in region 3 of the diagram in Fig. 5.1, as said before, where the only attractor is the stable focus in the origin. For $q_0 > 0.668$ we are in region 2, with three coexisting solutions, as already explained. For higher values of q_0 the motion becomes chaotic. The letters A and B of Fig. 5.5 correspond to those in Fig. 5.3. Also the bifurcation diagram in Fig. 5.5, shows an excellent agreement between the numerical and the analytical results, regarding the branch of unstable periodic solutions.

For high values of q_0, the unstable branch tends to go close to the origin, thus reducing the robustness of the stable focus; at the same time the amplitude of the quasiperiodic attractor strongly increases. The combination of these two factors makes this region very dangerous from an engineering point of view, since, even if the parameters p and d guarantee stability, small perturbations to the equilibrium position can cause large oscillations.

Some parts of the stable branch are broken by nearly horizontal plateaus corresponding to a phase locking of the torus, thus this plateaus are related to periodic solutions. Some of them are coexisting with the quasiperiodic solution and with each other, generating regions of multiple stable solutions. Increasing the value of q_0 the stable branch tends to be more and more rugged, highlighting a sequence of closer and closer bifurcations when approaching the chaotic region. This aspect will be investigated in more detail in Ch. 6.

5.2 Double Neimark-Sacker bifurcation

Considering the two-DoF mechanical system in Fig. 4.6, in Ch. 4 we already investigated analytically the occurring double NS bifurcation. Also, we verified the obtained results through comparison of bifurcation diagrams and attractors obtained both numerically and analytically. In this section we will analyze in detail the effects of an asymmetric saturation of the control force. As we already shown regarding a single DoF system, asymmetry can steer the system to much more complicated dynamics. Considering the higher dimension of the

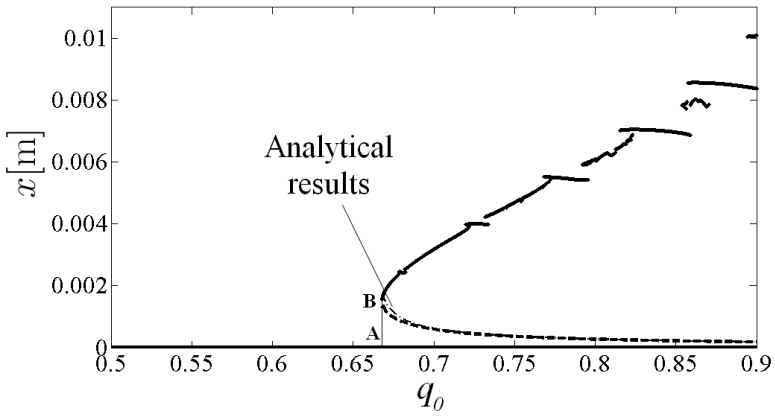

Figure 5.5: Bifurcation diagram for $p = 0.2492$, $Q_0 = 10$ m/s^2 and $\tau = 0.01$ s. Solid line: stable solutions, dashed line: unstable solutions, thin dash-dot line: analytical results.

two-DoF system and the several solutions already found by the analytical procedure, it will be necessary to combine an analytical and a numerical procedure to have a clear picture of the bifurcation scenario.

The amplitude map in Eq. (4.45) and the values of its coefficients a_{ij} in Eqs. (E.85)-(E.89) can already give an idea of the dynamics of the system for different values of u_0 (asymmetry), Q_0 (maximal control force) and τ (sampling time). The values of τ and Q_0 are not qualitatively affecting the solutions, but only their amplitude, since

$$a_{ij} = \frac{f_{ij}(u_0)}{Q_0^2 \tau^4}. \tag{5.1}$$

Thus, only the value of the asymmetry u_0 of the control force is important in order to qualitatively define the dynamics of the system (this omitting that the dimensionless control gains p_1, p_2, d_1 and d_2 are functions of both τ and Q_0). Thus, Q_0 and τ can be fixed (we choose $Q_0 = 10$ m/s^2 and $\tau = 0.01$ s), without loss of generality. In this respect, it has been already shown in Fig. 4.8 that the values of the four coefficients are negative for $u_0 = 0$, and monotonically increasing for increasing values of u_0. The main variations to the dynamics of the system may be expected to appear when the coefficients change their signs, i.e.

$$a_{11} < 0 \iff u_0 < 0.227901 \tag{5.2}$$
$$a_{12} < 0 \iff u_0 < 0.520693 \tag{5.3}$$
$$a_{21} < 0 \iff u_0 < 1.07822 \tag{5.4}$$
$$a_{22} < 0 \iff u_0 < 1.37199 \tag{5.5}$$

while it can be verified that $a_{21}a_{12} - a_{11}a_{22} > 0 \ \forall u_0 \in \mathbb{R}$.

As already mentioned, the map in Eq. (4.45) has two semitrivial solutions that are $(\tilde{r}_1, 0)$ and $(0, \tilde{r}_2)$. It has been shown that $\tilde{r}_1 = \sqrt{-k_1/a_{11}}$ and $\tilde{r}_2 = \sqrt{-k_2/a_{22}}$, thus changes of the sign of a_{11} and a_{22} make the bifurcations related to the two fixed points transit from supercritical to subcritical. On the other side, changes of the signs of a_{12} and a_{21} mainly affect the 3-torus quasiperiodic solution, related to the fixed point (r_1^*, r_2^*).

Considering Eqs. from (5.2) to (5.5), we can identify five different ranges of values of u_0. For $u_0 < 0.227901$ the behavior of the system is similar to the one presented in detail in Ch. 4, so we consider this case as symmetric or almost symmetric. The other four cases are organized and analyzed as follows

Case 1 $0.227901 < u_0 < 0.520693$

Case 2 $0.520693 < u_0 < 1.07822$

Case 3 $1.07822 < u_0 < 1.37199$

Case 4 $u_0 > 1.37199$

	$(0,0)$	$(\tilde{r}_1,0)$	$(0,\tilde{r}_2)$	(r_1^*,r_2^*)
Symmetric case (analyzed in Ch. 4)	A_{SN},B_{SD},F_{SD} C_{UN},D_{UN},E_{UN}	B_{SN},C_{SN} D_{SN},E_{SD}	C_{SD},D_{SN} E_{SN},F_{SN}	D_{SD}
Case 1	A_{SN},B_{SD},E_{SD} F_{SD},C_{UN},D_{UN}	A_{SD},F_{SD} E_{UN}	C_{SD},D_{SN} E_{SN},F_{SN}	D_{SD},E_{SD}
Case 2	A_{SN},B_{SD},D_{SD} E_{SD},F_{SD},C_{UN},	A_{SD},F_{SD} D_{UN},E_{UN}	C_{SD},D_{SD} E_{SN},F_{SN}	E_{SD}
Case 3	A_{SN},B_{SN},C_{SD} E_{SD},F_{SD},D_{UN}	A_{UN},E_{UN} F_{UN},B_{SD}	D_{SD},E_{SD} F_{SN}	A_{SD},F_{SD}
Case 4	A_{SN},B_{SN},C_{SN} D_{SD},F_{SD},E_{UN}	A_{UN},B_{UN} F_{UN},C_{SD}	A_{SD},B_{UN} C_{UN},D_{UN}	B_{SD}

Table 5.1: Existing solutions of Eq. (4.45) in the $k_1.k_2$ space for the different case. Uppercase letters refer to the different regions. Subscripts indicate: SN stable node, UN unstable node and SD saddle.

5.2.1 Response charts and bifurcation diagrams

Fig. 5.6 shows the response charts for the four asymmetric cases in the spaces of the bifurcation parameters k_1, k_2 and p_1, d_1. Comparing the different response charts in the space k_1, k_2, it is visible how the increasing asymmetry of the system makes the two lines $k_2 = a_{22}k_1/a_{12}$ and $k_2 = a_{21}k_1/a_{11}$ rotate counterclockwise. For u_0 equal to the values dividing the four cases, one of the two lines is vertical or horizontal, so it changes quadrant in the k_1, k_2 space, affecting the response scenario of the system. Accordingly, the position and the extent of all regions in the p_1, d_1 parameters space change remarkably, with some of them nearly vanishing. However, although they rotate, the relative position of the two loci of secondary NS bifurcation does not qualitatively change (which is due to the fact that $a_{21}a_{12} - a_{11}a_{22} > 0\ \forall u_0 \in \mathbb{R}$).

Figure 5.7 shows the phase portraits of the map in Eq. (4.45) in the r_1, r_2 space for the four different cases, from which the behavior of the system can be understood. Once again, we point out that the semitrivial fixed points $(\tilde{r}_1, 0)$ and $(0, \tilde{r}_2)$ correspond to 2-torus quasiperiodic solutions of the discrete map in Eq. (4.25), the nontrivial fixed point (r_1^*, r_2^*) corresponds to a 3-torus quasiperiodic solution, while the trivial solution corresponds to the equilibrium solution of the mechanical system. The stability of the fixed points in the r_1, r_2 space corresponds to the stability of the underlying motions.

We can sum up the possible solutions of Eq. (4.45) in the k_1, k_2 space for the different cases, as shown in Tab. 5.1. Note that, owing to the truncated analytical solution, the 3-torus quasiperiodic solution is unstable in all cases, a circumstance which is still confirmed by the numerical analysis.

All the phase portraits in Fig. 5.7 show the existence of an attractor for $r_1 \to \infty$. This attractor does not exist in the complete system (described by Eq. (4.25)) and it appears because of a degeneracy of the normal form, which is the result of a local analysis and cannot describe large attractors. If in the analysis higher order terms would had been considered, probably another attractor, with finite amplitude, would have appeared instead of this one with infinite amplitude. In fact, direct numerical simulations of Eq. (4.25) show the existence of a larger (but finite) attractor existing for each pair of values of k_1, k_2 (in the vicinity of the bifurcation).

Figure 5.8 shows the existing solutions in the region E of case 1 ($u_0 = 0.3$), projected onto the x_1, x_2, $x_1, \dot{x}_1$ and $x_2, \dot{x}_2$ space. In the figure it is possible to recognize the larger attractor that can be found numerically. Furthermore, the figure shows the excellent matching between the numerical and the analytical results. The figure shows the solutions of the map in Eq. (4.25), i.e. a stroboscopic Poincaré map of the underlying continuous time system. Thus, closed lines correspond to 2-torus quasiperiodic solutions of the underlying continuous time system, while the blue lines correspond to a 3-torus quasiperiodic solution of the continuous time system. The larger attractor in Fig. 5.8(g)-(i) is shown in separated diagrams from the other numerical solutions, because of its larger scale, for better visualization.

Figure 5.9 shows the bifurcation diagram with respect to the bifurcation parameter p_1, for $u_0 = 0.3$. In the figure the black lines are the numerical results, while the colored lines are the analytical results. The variation of the bifurcation parameter p_1 moves the state of the system through regions A, F, E, D and C of Fig. 5.6(b)

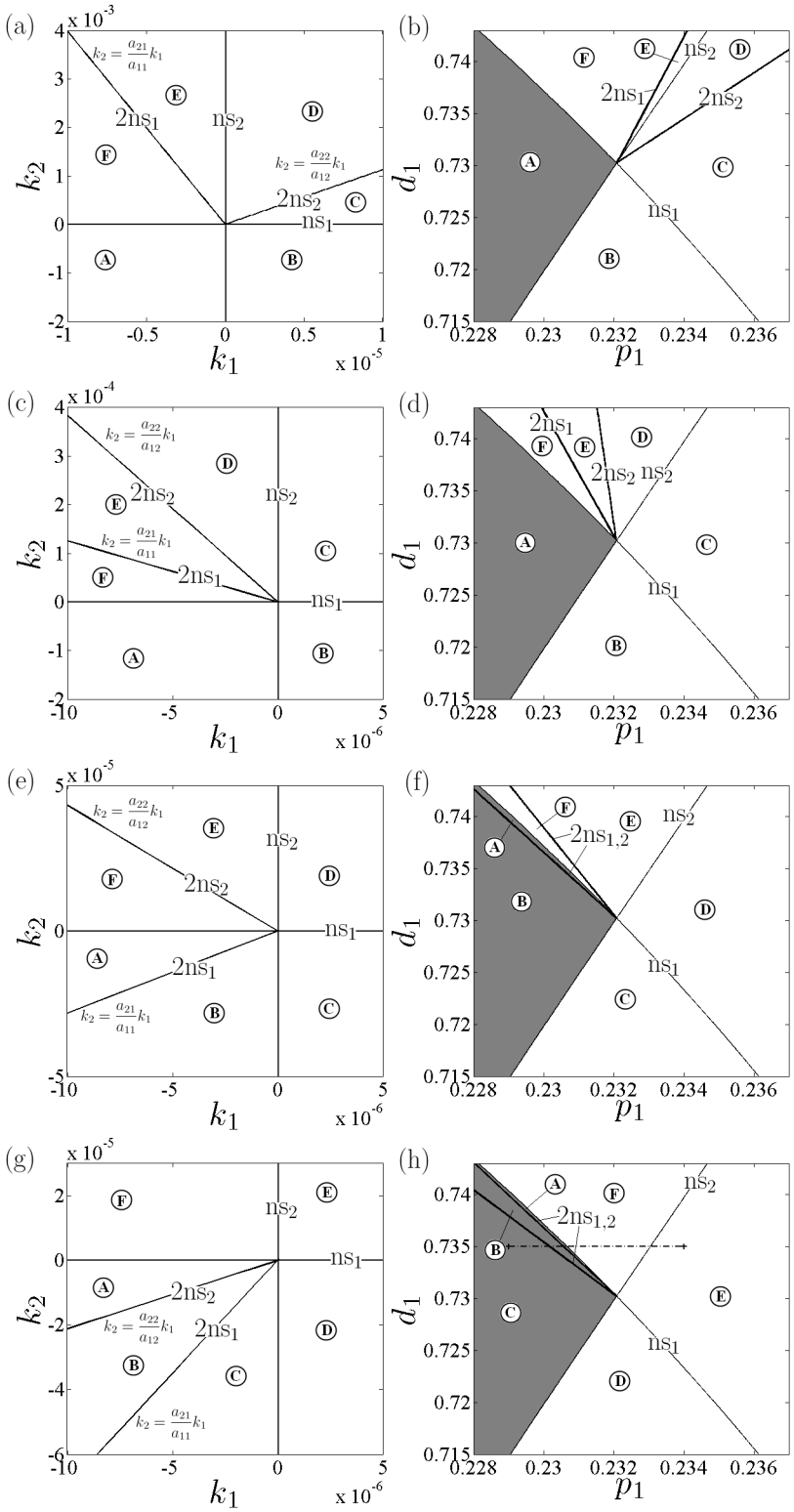

Figure 5.6: Response charts referred to the system in Eq. (4.45), in the space of the bifurcation parameters k_1, k_2 (*left*) and p_1, d_1 (*right*). (a), (b): $u_0 = 0.3$; (c), (d): $u_0 = 0.8$; (e), (f): $u_0 = 1.2$; (g), (h): $u_0 = 1.5$; the letters from A to F indicate regions with different existing fixed points.

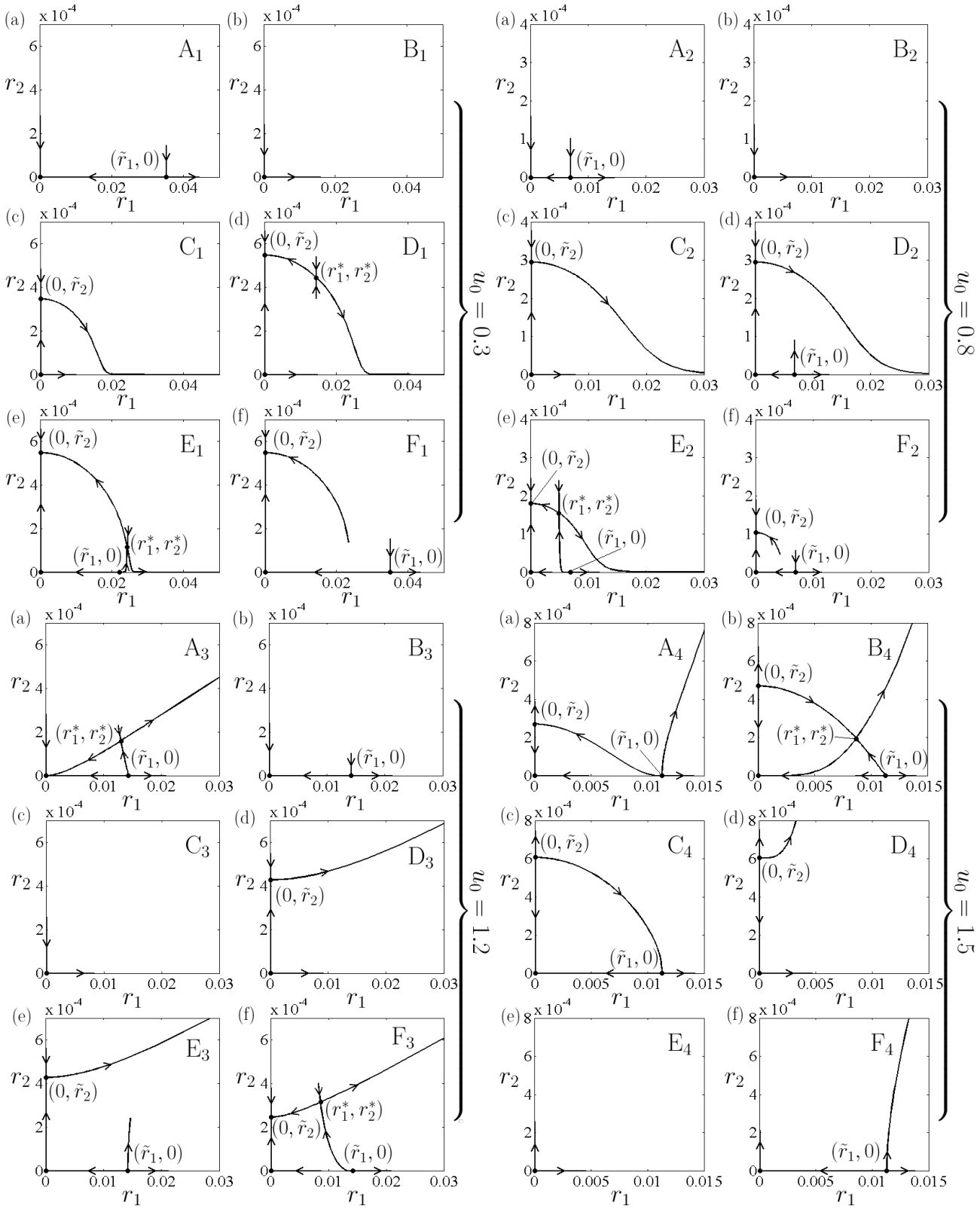

Figure 5.7: Phase portraits of the map in (4.45) in the r_1, r_2 space. The letters labeling the figures from A to F, correspond to the letters marking the regions in Fig. 5.6 for the corresponding value of u_0.

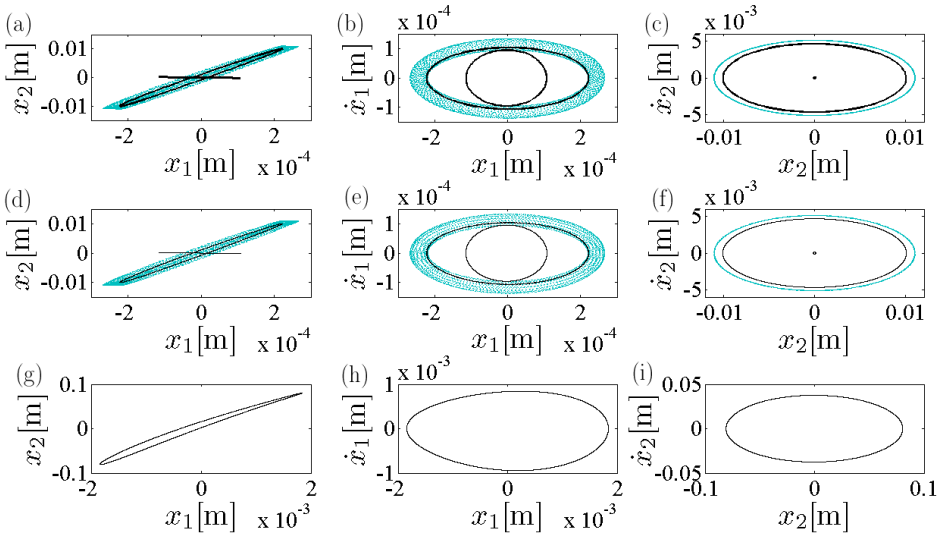

Figure 5.8: Existing 2-torus and 3-torus quasiperiodic solutions for the parameter values $u_0 = 0.3$, $p_1 = 0.232309$, $d_1 = 0.731583$ ($k_1 = -1 \times 10^{-6}$, $k_2 = 5 \times 10^{-4}$), projected onto the x_1, x_2, $x_1, \dot{x}_1$ and $x_2, \dot{x}_2$ space. (a)-(c): analytical results, (d)-(i): numerical results. The blue fuzzy line is the 3-torus quasiperiodic solution, the large closed lines is the 2-torus quasiperiodic solution related to $(\tilde{r}_1, 0)$, the smaller closed line is the 2-torus quasiperiodic solution related to $(0, \tilde{r}_2)$. (g)-(i) show the larger 2-torus quasiperiodic attractor, overlooked by the analytical investigation.

(see dash-dotted line). Compared with the case of symmetric saturation (Fig. 4.11), the various regions are trespassed through the same sequence, owing to the still minor degree of asymmetry, and indeed the passage from A to C shows similar general features. However, the finer transition scenario between the first and the last region is qualitatively different in the two cases, mainly because in the asymmetric case one of the two NS bifurcation is subcritical, furthermore because the second NS bifurcation marks the transition from F to E in the symmetric case against that from E to D in the slightly asymmetric case.

In fact, increasing the value of p_1 in Fig. 5.9, the system starts in region A, where, according to the analytical calculation, besides the stable trivial solution, there is an unstable 2-torus quasiperiodic solution $(\tilde{r}_1, 0)$ originated at $p_1 = 0.233$ (green line). For $p_1 = 0.23074$ the system enters region F and the trivial solution undergoes a supercritical NS bifurcation as in the symmetric case. The small nonvanishing amplitude of x_2 (not discernible in the figure) is due to the fact that this branch is mainly related to the rigid movement of the system. For $p_1 = 0.23294$ the system enters region E, the unstable 2-torus quasiperiodic branch (green line) undergoes a secondary NS bifurcation which generates a branch of unstable 3-torus quasiperiodic solutions (red line), related to the nontrivial fixed point (r_1^*, r_2^*). For $p_1 = 0.233$, entering region D, the branch of unstable 2-torus quasiperiodic solutions (green line) merges with the unstable trivial solution through a subcritical NS bifurcation. For $p_1 = 0.2342$ the system enters region C and the branch of unstable 3-torus quasiperiodic solutions (red line) merges with the branch of stable periodic solution (blue line), which becomes unstable. For higher values of p_1 the analytical investigation, limited to third order terms, shows no stable solutions, which instead exist according to the numerical simulations. From this point the only existing stable solution is the larger 2-torus quasiperiodic attractor, found numerically (solid black line).

The numerical (black lines) and the analytical (colored lines) results are in good agreement. The main difference is related to the backward unstable branch generated by the subcritical NS bifurcation, which, according to the numerical results, undergoes a saddle-cycle bifurcation, generating a branch of stable 2-torus quasiperiodic solutions. These quasiperiodic solutions are related to terms higher than the third, so cannot be found with the performed analytical procedure, which degenerates and shows instead a non-existing unbounded attractor (Fig. 5.7, $u_0 = 0.3$).

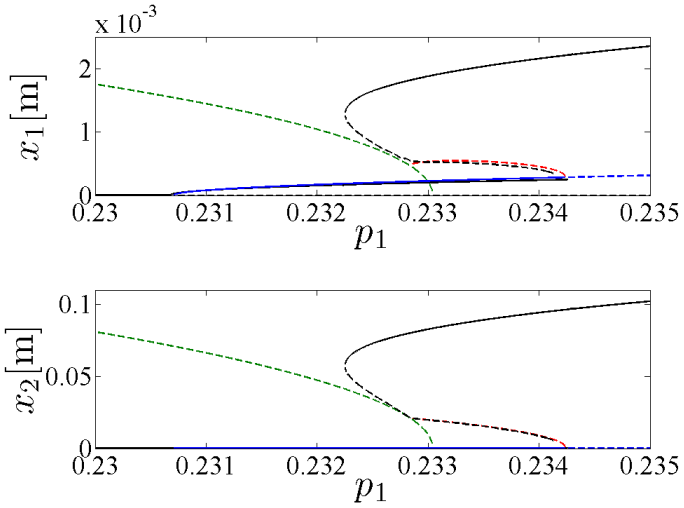

Figure 5.9: Bifurcation diagram with respect to the bifurcation parameter p_1, for $d_1 = 0.735$ and $u_0 = 0.3$. Solid line: stable solutions, dashed lines: unstable solutions. The black lines refer to the numerical results while the colored lines to the analytical results.

Considering this slightly asymmetric case, still analogies with the dynamics shown regarding the single DoF case can be found. Both Fig. 5.3 and Fig. 5.9 show a branch of unstable 2-torus quasiperiodic solutions generated by a subcritical NS bifurcation, which turns forward into a branch of stable periodic solutions in correspondence to a saddle-cycle bifurcation. However, in the single DoF case the transition from supercritical to subcritical of the NS bifurcation occurs for $u_0 = \sqrt{3/5} = 0.774597$, while in the two-DoF case it occurs for $u_0 = 0.227901$, so for a much less asymmetric system.

Figure 5.10 shows the bifurcation diagram with respect to the bifurcation parameter p_1, for $u_0 = 1.5$, so for a strongly asymmetric system. The variation of the parameter from $p_1 = 0.229$ to $p_1 = 0.234$, moves the state of the system through regions C, B, A, F and E of Fig. 5.6(h) (see dash-dotted line). The overall bifurcation diagram is very different from the one just outlined in Fig. 5.9. In this case both the NS bifurcations are subcritical, with the consequence that the analytical procedure does not show any stable solution besides the trivial one. Furthermore, the 3-torus quasiperiodic solutions now exist in the region of stability of the equilibrium solution.

Increasing the value of p_1 in Fig. 5.10, the system starts in region C. Here there exists, besides the stable trivial solution, two branches of unstable 2-torus quasiperiodic solutions, related to the subcritical NS bifurcations and originated respectively at $p_1 = 0.2307$ (blue line) and $p_1 = 0.233$ (green line) (as in the slightly asymmetric case). At $p_1 = 0.2302$ the system enters region B. One of the branches of unstable solutions (green line) undergoes a secondary NS bifurcation, generating a branch of unstable 3-torus quasiperiodic solutions (red line). At $p_1 = 0.2306$ the system enters region A and the branch of unstable 3-torus quasiperiodic solutions merges with the other branch of unstable 2-torus quasiperiodic solutions (blue line). At $p_1 = 0.2307$, entering region F, this latter branch of unstable 2-torus quasiperiodic solutions, merges with the trivial solution, which becomes unstable, through a subcritical NS bifurcation. At $p_1 = 0.233$, entering region E, also the other branch of unstable 2-torus quasiperiodic solutions merges with the unstable trivial solution through another subcritical NS bifurcation. In the figure, it is possible to recognize not even the non-vanishing amplitude x_1 of the unstable solutions, due to the larger scale of the attractor obtained numerically.

The numerical simulations showed the existence of a stable chaotic attractor along the whole investigated range of values of p_1. This attractor cannot be found with the performed analytical procedure. The chaotic nature of this attractor will be studied in more detail in the next chapter.

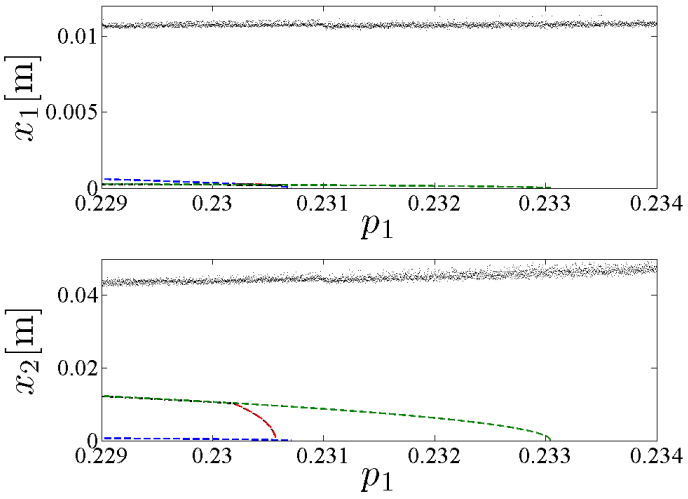

Figure 5.10: Bifurcation diagram with respect to the bifurcation parameter p_1, for $d_1 = 0.735$ and $u_0 = 1.5$. Solid line: stable solutions, dashed lines: unstable solutions. The black lines refer to the numerical results while the colored lines to the analytical results. During the simulation $Q_0 = 10$ m/s^2, $\tau = 0.01$ s.

5.2.2 A summary bifurcation chart for varying degree of asymmetry

Figure 5.11 shows a summary bifurcation chart in the space p_1, u_0 for a fixed value of d_1. The chart has been obtained both from analytical and numerical results. Uppercase letters refer to the corresponding regions in the diagram in Fig. 5.6, while the numbers from 0 to 4 indicate the symmetric (0) or the four asymmetric cases (1 to 4). The black thick lines are bifurcation loci, while the blue thin dashed lines divide the four asymmetric regions, according to the values found in Eqs. from (5.2) to (5.5). Lowercase letters indicate the type of bifurcation related to each bifurcation locus ("ns" NS bifurcation, "2ns" secondary NS bifurcation, "sc" saddle-cycle bifurcation). Finally, the red thin dash-dotted lines refer to bifurcation diagrams discussed later.

Let consider the bifurcation loci. The dash-dotted vertical line at $p_1 \approx 0.2307$ (indicated with ns_1 in the figure) marks the passage from the stable to unstable regions of the trivial solution (so from $k_2 < 0$ to $k_2 > 0$, while k_1 remains negative) and it can be found already by the linear analysis. It is the locus of the NS bifurcations related to the semitrivial fixed point $(0, \tilde{r}_2)$. For $u_0 < 1.37199$ (see the black dot) it is supercritical, while for $u_0 > 1.37199$ it is subcritical, according to the sign of a_{22} (see Eq. (5.5)). Fig. 5.12(a) shows regions where these NS bifurcations give stable or unstable results, according to the analytical investigation. From the figure it can be clearly understood that for $u_0 < 1.37199$ the bifurcations with varying p_1 are supercritical, generating stable solutions on the right side (that later become unstable because of the secondary NS bifurcations), while for $u_0 > 1.37199$ they are subcritical, generating unstable solutions on their left side. The black dot, dividing supercritical (below) and subcritical (above) NS bifurcations, corresponds to a Chenciner bifurcation [11,40].

The dash-dotted vertical line at $p_1 = 0.233$ (marked with ns_2 in the figure) is the locus of the NS bifurcations related to the other semitrivial fixed point $(\tilde{r}_1, 0)$. This bifurcation is supercritical for $u_0 < 0.227901$, while it is subcritical above this value, according to the sign of a_{11} (see Eq. (5.2)). Fig. 5.12(b) shows regions where these bifurcations generate stable and unstable 2-torus quasiperiodic solutions, according to the analytical investigation. The figure confirms that for $u_0 > 0.227901$ the bifurcations are subcritical, while for $u_0 < 0.227901$ they are supercritical, although they generate unstable solutions, that become stable only after the locus of secondary NS bifurcations (see also Fig. 4.11(b)). Again, the black dot, dividing supercritical and subcritical NS bifurcations, corresponds to a Chenciner bifurcation.

The two solid lines marked with 2ns_1 and 2ns_2 in the figure correspond to two loci of secondary NS bifurcations. They delimit a diagonal strip, going from the top left to the bottom right corners of Fig. 5.11, where the unstable 3-torus quasiperiodic solution exists (i.e. the red lines in Fig. 5.9 and 5.10). In the figure the two loci are obtained from the analytical calculation, however, they are confirmed by numerical simulations.

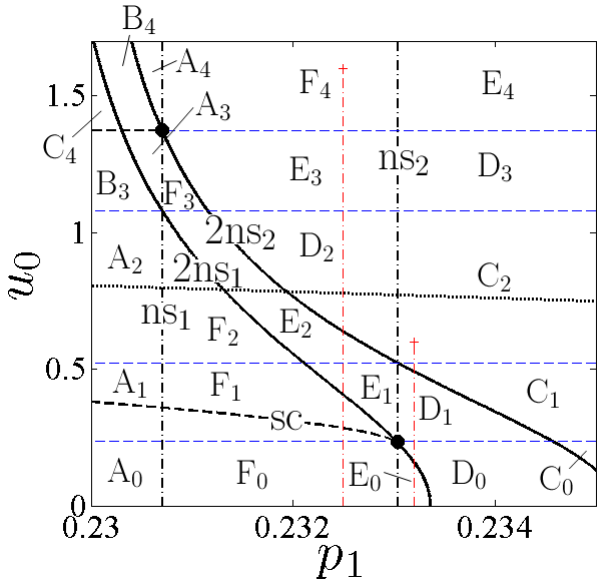

Figure 5.11: Bifurcation chart in the space of the parameters p_1, u_0. In the diagram $d_1 = 0.735$. Uppercase letters refer to the corresponding regions in the diagram in Fig. 5.6. 0 indicates the symmetric case, while the numbers from 1 to 4 indicates the different asymmetric cases. Lowercase letters mark the bifurcation loci: $2ns_1$ and $2ns_2$ (secondary NS bifurcations), ns_1 and ns_2 (NS bifurcations) and sc (saddle-cycle bifurcation).

Let us now consider also the numerical results. The dashed line passing through regions A_1 and F_1 (marked with sc in the figure), is the locus of the saddle-cycle bifurcations, as the one shown in Fig. 5.9, which bend the branch of unstable 2-torus quasiperiodic solutions forward to stable quasiperiodic solutions. These bifurcations are related to terms higher than the third order, thus the locus has been obtained numerically. Below this line, the system behaves as in the symmetric case, so there are no solutions related to the fixed point $(\tilde{r}_1, 0)$, while above this line there is a branch of stable and a branch of unstable solutions. This locus of saddle-cycle bifurcations arises from the point (lower black dot in the figure) marking the transition between supercritical and subcritical NS bifurcations, where a Chenciner bifurcation take place. The dynamics just described is typical in the event of a Chenciner bifurcation, however, the intersection of this point with the locus of secondary NS bifurcations complicates even further the local dynamics. A comparison of plotted bifurcation diagrams can clarify the behavior of the system in the vicinity of the Chenciner bifurcation. At this point the system undergoes a transition from the bifurcation diagram in Fig. 4.11(b) to the bifurcation diagram in Fig. 5.9 (or, see later, from the one in Fig. 5.13 to the one in Fig. 5.14). Increasing u_0 from the zero value in Fig. 4.11, the secondary NS bifurcation, already occurring at $p_1 = 0.2334$, will move to the left up to colliding with the supercritical NS bifurcation at $p_1 = 0.233$. In turn, decreasing u_0 from the 0.3 value in Fig. 5.9, the saddle-cycle bifurcation already at $p_1 = 0.2322$ and the secondary NS bifurcation at $p_1 = 0.23294$ will both move to the right, towards $p_1 = 0.233$, up to colliding with the subcritical NS bifurcation for $u_0 = 0.22790$. At this value, the degenerate NS bifurcation will generate a vertical branch of 2-torus quasiperiodic solutions, due to the vanishing of the coefficient of the third order term ($a_{11} = 0$), which will then bend to the right, thanks to the degenerated saddle-cycle bifurcation, and will immediately split in two branches due to the secondary NS bifurcation.

The upper black point, at $p_1 = 0.2307$ and $u_0 = 1.37199$, is the intersection of the other vertical locus of NS bifurcations (again at its transition from supercritical to subcritical) and of the upper locus of secondary NS bifurcation. As already mentioned, it also corresponds to the occurrence of a Chenciner bifurcation. Reasonably, we can conjecture the existence, in the vicinity of this bifurcation, of a dynamics similar to the one described for the other Chenciner bifurcation. In this respect, the dashed line dividing regions B_3 and C_4 probably corresponds to a locus of saddle-cycle bifurcations and most likely it is not horizontal as shown in the figure.

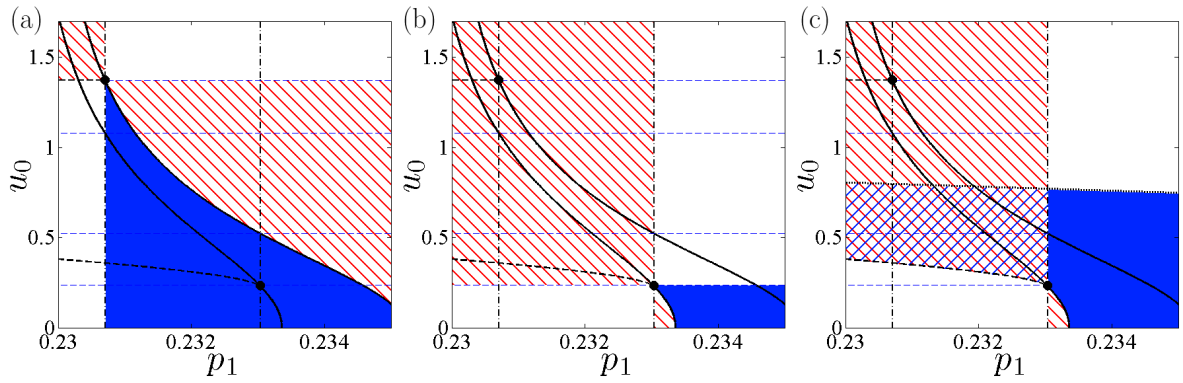

Figure 5.12: Bifurcation charts in the space of the parameters p_1, u_0. In the diagram $d_1 = 0.735$. Chart (a) refers to the NS bifurcation at $p_1 = 0.2307$ and the solution $(0, \tilde{r}_2)$. Charts (b) and (c) refer to the NS bifurcation at $p_1 = 0.233$ and the solution $(\tilde{r}_1, 0)$. The area dashed in red indicates the existence of unstable periodic solutions and the area shaded in blue indicates the existence of stable periodic solutions. Double dashed area indicates the coexistence of both stable and unstable solutions. White areas refer to regions where the relative solution does not exist. Charts (a) and (b) account for the sole effects of the two NS bifurcations, as also obtained analytically, chart (c) includes numerical results, too.

However, finding proofs of it is not trivial, since unstable solutions, hard to detect numerically or analytically, are involved.

The nearly horizontal dotted line at $u_0 \approx 0.75$ is another locus of secondary NS bifurcation, generating stable 3-torus quasiperiodic solutions. This locus has been obtained numerically and is discussed in more detail in Ch. 6, since it is the first step that will bring the system to chaotic motions.

The horizontal blue thin dashed lines at $u_0 = 0.227901$, $u_0 = 0.520693$, $u_0 = 1.07822$ and $u_0 = 1.37199$ mark the passages between the five symmetric/asymmetric cases previously defined. They do not correspond to a qualitative difference in the behavior. For example, analyzing Fig. 5.7 it can be seen that C_1, C_2, D_3 and E_4 have the same qualitative behavior. The absence of the unstable fixed point $(0, \tilde{r}_2)$ in E_4 is probably due to its dependence on terms higher than the third order, so it is overlooked by the analytical procedure, furthermore it is very hard to be found numerically.

Figure 5.12, although does not add any information not given by Fig. 5.11, allows to better understand the most important mechanisms of the bifurcations involved in the system. Charts (a) and (b) of Fig. 5.12 account for the sole effects of the two NS bifurcations, as also obtained analytically. Considering the loci of saddle-cycle bifurcations and secondary NS bifurcations obtained numerically, the diagram in Fig. 5.12(b), regarding the 2-torus quasiperiodic solutions generated by the NS bifurcations at $p_1 = 0.233$, should be adapted including these numerical results. This new diagram is shown in Fig. 5.12(c). From the figure, it is visible how stable 2-torus quasiperiodic solutions exist also on the left side of the bifurcations (for $p_1 < 0.233$), thanks to the saddle-cycle bifurcations, which bend forward the branches of unstable quasiperiodic solutions (see also Fig. 5.9). Then, it is visible how the nearly horizontal locus of secondary NS bifurcations (dotted line) limits the region of existence of stable 2-torus quasiperiodic solutions; passing this locus, the 2-torus quasiperiodic solutions become 3-torus quasiperiodic.

For the sake of completeness, it would be necessary to plot a similar chart, adapted from Fig. 5.12(a), including the numerical results referred to the fixed point $(0, \tilde{r}_2)$. Such a chart would be identical to Fig. 5.12(a) for $u_0 < 1.37199$, while for $u_0 > 1.37199$ and $p_1 > 0.2307$ it would probably be fully dashed in red, as we conjecture a scenario similar to one obtained regarding the other NS bifurcation (at $p_1 = 0.233$), this time involving unstable solution and not stable. In order to verify this conjectured scenario, it would be necessary to investigate about unstable solutions very hard to be found numerically. Thus, we did not perform this analysis.

Fig. 5.13(a) and (b) show the bifurcation diagram of the two coordinates with respect to the bifurcation parameter u_0. In the figure, the control gains are $p_1 = 0.2325$ and $d_1 = 0.735$, so the bifurcation diagram moves

along one of the vertical red dashed lines of Fig. 5.11. The variation of the parameter from $u_0 = 0$ to $u_0 = 1.6$ moves the system through regions F_0, F_1, E_1, E_2, D_2, E_3 and F_4 of Fig. 5.11. In the whole considered range of values of u_0 the trivial solution is unstable.

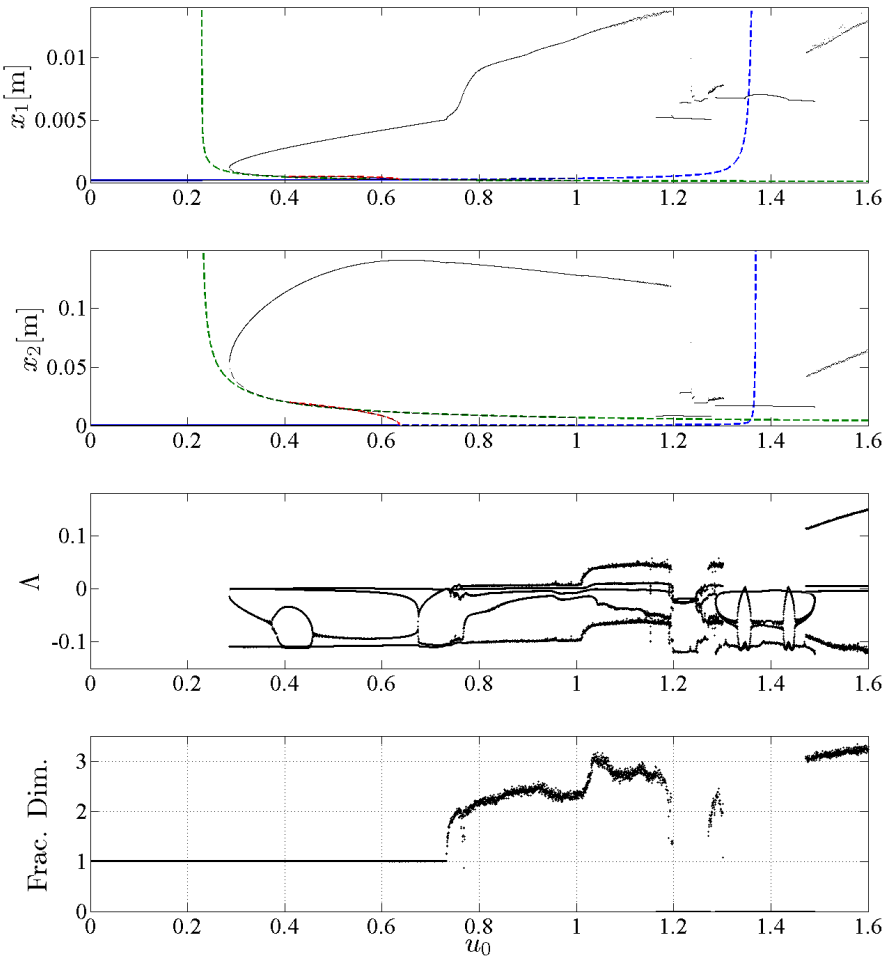

Figure 5.13: (a), (b): bifurcation diagram with respect to the bifurcation parameter u_0 (maximal absolute value x_1 and x_2 of the attractor), for $p_1 = 0.2325$ and $d_1 = 0.735$ ($k_1 = -1.15 \times 10^{-5}$, $k_2 = 1.45 \times 10^{-3}$). Solid lines: stable solutions, dashed lines: unstable solutions. Black lines: numerical results, colored lines: analytical results. (c): Lyapunov exponents of the stable solutions. (d): fractal dimension of the attractors..

Increasing the asymmetry of the system from $u_0 = 0$, the system starts in region F_0. In this region, besides the unstable trivial solution, there is a branch of stable 2-torus quasiperiodic solutions, not recognizable in the figure due to the larger scale of the other solutions. At $u_0 = 0.227901$ the system enters the first asymmetric case (passing the first dashed line of Fig. 5.11 and entering region F_1). The analytical investigation shows the appearance of a branch of unstable 2-torus quasiperiodic solutions (green line), associated with the subcritical NS bifurcation occurring at $p_1 = 0.233$ (which is not in the diagram, since p_1 is fixed at 0.2325). The infinite amplitude is due to a degeneracy of the analytical procedure, which is only local and cannot describe large solutions. Considering that $\tilde{r}_1 = \sqrt{-k_1/a_{11}}$ and for $u_0 = 0.227901$ $a_{11} = 0$, the normal form shows an unbounded solution, which does not exist. The numerical simulation, in accordance to what is shown in Figs. 5.11 and 5.12(c), shows that the branch of unstable 2-torus quasiperiodic solutions and a branch of stable 2-torus quasiperiodic solutions appear only at $u_0 = 0.285$, in correspondence to a saddle-cycle bifurcation, which is overlooked by the local analytical procedure. At $u_0 = 0.4$, the system enters region E_1. The branch of unstable

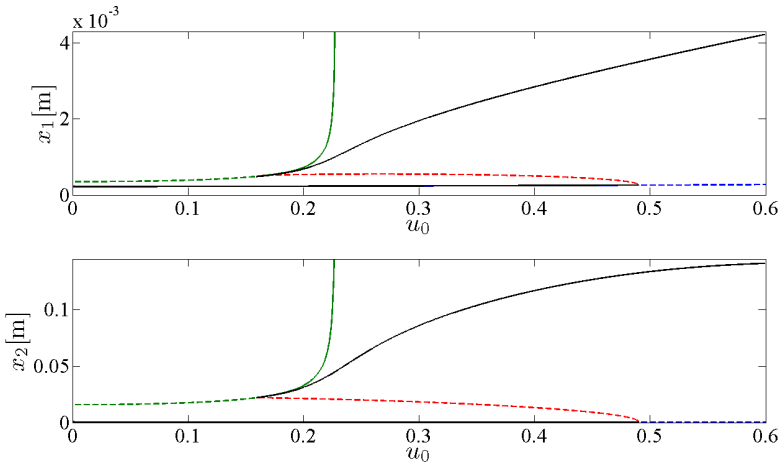

Figure 5.14: Bifurcation diagram with respect to the bifurcation parameter u_0, for $p_1 = 0.2332$ and $d_1 = 0.735$ ($k_1 = 3.34 \times 10^{-6}$, $k_2 = 2.02 \times 10^{-3}$). Solid lines: stable solutions, dashed lines: unstable solutions. Black lines: numerical results, colored lines: analytical results.

2-torus quasiperiodic solutions undergoes a secondary NS bifurcation, generating a branch of unstable 3-torus quasiperiodic solutions (red line). At $u_0 = 0.520693$ the system enters region E_2, without any qualitative change in the dynamics. At $u_0 = 0.636$ the system enters region D_2. The branch of unstable 3-torus quasiperiodic solutions merges with the branch of (low-amplitude) stable 2-torus quasiperiodic solution, which becomes also unstable (blue line). Above this value of u_0 the analytical investigation does not show any stable solution. At $u_0 = 1.07822$ the system enters region E_3. Also in this case there are no qualitative changes in the dynamics of the system. Increasing further the value of u_0, the amplitude of one of the branches of unstable 2-torus quasiperiodic solutions seems to increase up to becoming infinite for $u_0 = 1.37199$, because $a_{22} = 0$ so $\tilde{r}_2 = \sqrt{-k_2/a_{22}} \to \infty$. Of course, also in this case this is a degeneracy of the analytical solution, which describes only the local behavior of the system and fails if large solutions are involved.

The numerical results (black lines) are in good agreement with the non-degenerate analytical ones. They show the existence of a larger attractor, originated from a saddle-cycle bifurcation of the backward branch of unstable 2-torus quasiperiodic solutions, already introduced when discussing the previous bifurcation diagrams. This larger attractor increases in amplitude for increasing asymmetry, with a different trend with respect to the two coordinates x_1 and x_2. Remembering that x_1 is related to the rigid motion of the two masses and x_2 to their relative motion, the latter coordinate has a maximum for $u_0 \approx 0.65$, while the former has a sort of jump up starting at $u_0 = 0.73263$. As explained later in detail, this attractor is first 2-torus quasiperiodic, then 3-torus quasiperiodic and finally fractal and chaotic. For $u_0 > 1.2$ the branch of chaotic solutions fades away and generates smaller periodic attractors, related to a phase locking of the underlying continuous time system. This transition to chaos will be analyzed in Ch. 6, considering also the diagrams in Figs. 5.13 (c) and (d), indicating the Lyapunov exponents and the fractal dimension of the attractors.

Figure 5.14 shows a bifurcation diagram similar to the one just shown. The bifurcation parameter is still u_0, but the p_1 control gain is different, namely $p_1 = 0.2332$. Going from $u_0 = 0$ to $u_0 = 0.6$, the system moves through regions E_0, D_0, D_1, C_1 and C_2, along the red vertical line of Fig. 5.11, on the right of the locus of NS bifurcations.

For the symmetric system there are two branches of 2-torus quasiperiodic solutions, one stable (whose non-vanishing x_2 value is very small and cannot be distinguished in the figure) and the other one unstable (green line), besides the unstable trivial solution which exists along the whole range of values of u_0. At $u_0 = 0.159$, entering region D_0 of Fig. 5.11, the unstable branch undergoes a secondary NS bifurcation generating a (red) branch of unstable 3-torus quasiperiodic solutions and becoming stable. Increasing further the value of u_0, this branch of stable 2-torus quasiperiodic solutions grows up as a_{11} tends to zero, similarly to what can be seen in the previous bifurcation diagram, but this time the branch is stable. In the figure it is visible how the

numerical result (black line) leaves the analytical one (green line) as u_0 approaches the value 0.227901 because of the increasing relevance of the terms higher than the third order, which prevent this branch from going to infinity, but bend it to finite values. At $u_0 = 0.227901$ the system enters region D_1. The green branch of 2-torus quasiperiodic solutions is associated with the NS bifurcation occurring at $p_1 = 0.233$ (which is not in the diagram, since p is fixed at 0.2332). For $u_0 = 0.227901$, this NS bifurcation has a transition from supercritical to subcritical, thus, for $u_0 < 0.227901$ its associated branch of 2-torus quasiperiodic solutions exists for $p_1 > 0.233$ and it is stable (green line in Fig. 5.14), while for $u_0 > 0.227901$ it exists for $p_1 < 0.233$ (green line in Fig. 5.13) (see also Fig. 5.12(b)). For $u_0 = 0.227901$, according to the analytical results, it tends to infinity since $\tilde{r}_1 = \sqrt{-k_1/a_{11}}$ and for $u_0 = 0.227901$, $a_{11} = 0$. Of course this is again a degeneracy of the local analytical investigation and the numerical results show that it does not go to infinity for $u_0 = 0.227901$, but it bends to the right, letting a branch of 2-torus quasiperiodic solutions exists also for $u_0 > 0.227901$ and $p_1 > 0.233$ (continuous black line in Fig. 5.14) (see also Fig. 5.12(c)). At $u_0 = 0.49$, entering region C_1, the (red) branch of unstable 3-torus quasiperiodic solutions merges with the other branch of stable 2-torus quasiperiodic solutions, which become unstable. At $u_0 = 0.520693$ the system enters region C_2, without any qualitative change to its dynamics. For higher values of u_0, not shown in this figure, the system would behave similarly to what is shown in Fig. 5.13.

Chapter 6

Transition to chaos

6.1 Single Neimark-Sacker bifurcation

Considering the mechanical system in Fig. 2.1, it has already been shown in Fig. 5.1 that for very asymmetric saturation (high values of u_0 or q_0), the system experiences chaotic motions.

Figure 6.1 shows the variation of the attractors of the map in Eq. (4.3) for different values of q_0, i.e. for increasing asymmetry of the control force. In the figure, the displacement and the velocity are plotted for each time interval τ, so they can be considered as stroboscopic Poincaré maps of the underlying continuous time system. The figures on the top of Fig. 6.1 show a closed line, i.e. a 2-torus quasiperiodic motion of the system. For some specific parameter values, the continuous closed line is reduced to a finite number of points ($q_0 = 0.9$), this corresponds to a phase locking of the different frequencies of the quasiperiodic motion that becomes periodic. In the bifurcation diagrams of the map (Figs. 5.2, 5.3 and 5.5), the phase locking shows up as an almost horizontal line breaking the continuous one. Fig. 6.2 shows the regions, in the q_0 and p parameter space, where there is a phase locking. These regions assume the structure of tongues, indeed similar structures are usually called *Arnold tongues* [40].

In Fig. 6.1 it is also visible how the attractor moves to the left and becomes more and more asymmetric for larger values of q_0. Increasing the value of q_0 even more, the motion is not quasiperiodic anymore and the attractor looks like being a *strange attractor* with a fractal structure, so there is a likely chaotic motion.

In order to verify if the attractor of the map (Eq. (4.3)), for the fixed values $q_0 = 0.97$, $p = 0.2501$ $Q_0 = 10\,\mathrm{m/s^2}$ and $\tau = 0.01$ s (Fig. 6.3(a) and (b)) is actually chaotic, we calculated a positive Lyapunov

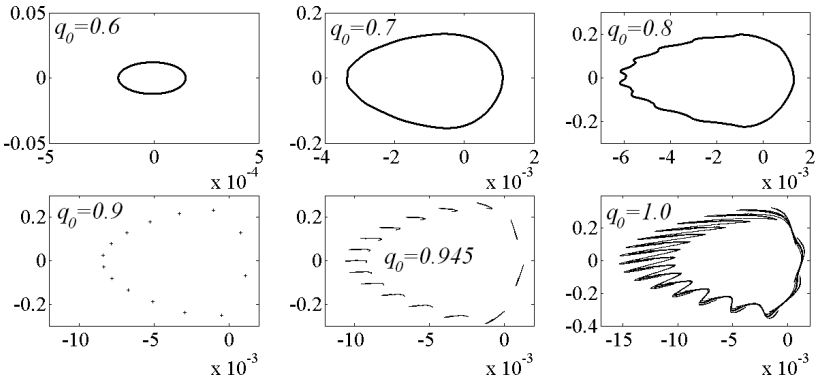

Figure 6.1: Attractors of the map (Eq. (4.3)) for increasing asymmetry of the control force. The diagram has been obtained fixing $p = 0.2501$, $\tau = 0.01$ s and $Q_0 = 10$ m/s^2. All figures have the displacement [m] in the x-axis and the velocity [m/s] in the y-axis.

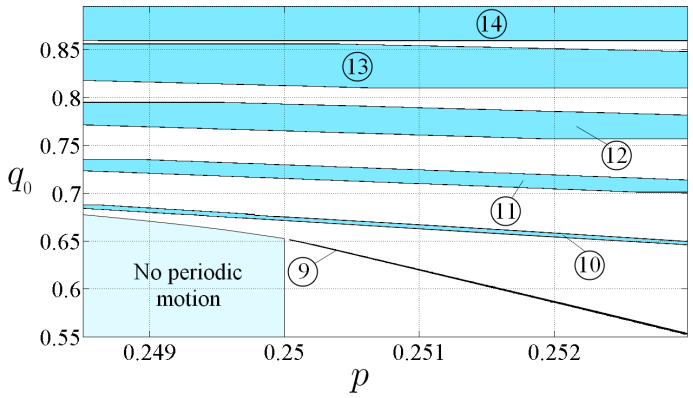

Figure 6.2: Zone with phase locking in the q_0 and p parameter space. The shaded area indicates the existence of an attractor with phase locking. The numbers in the circles indicate the ratio between the period of motion and τ.

exponent [16, 47], with the result being shown in Fig. 6.3(c). We also calculated its fractal dimension, using the Correlation Dimension [24, 27], the result for this particular case being 1.4, and we plotted the frequency spectrum (Fig. 6.3(d)), which shows a broad-band response.

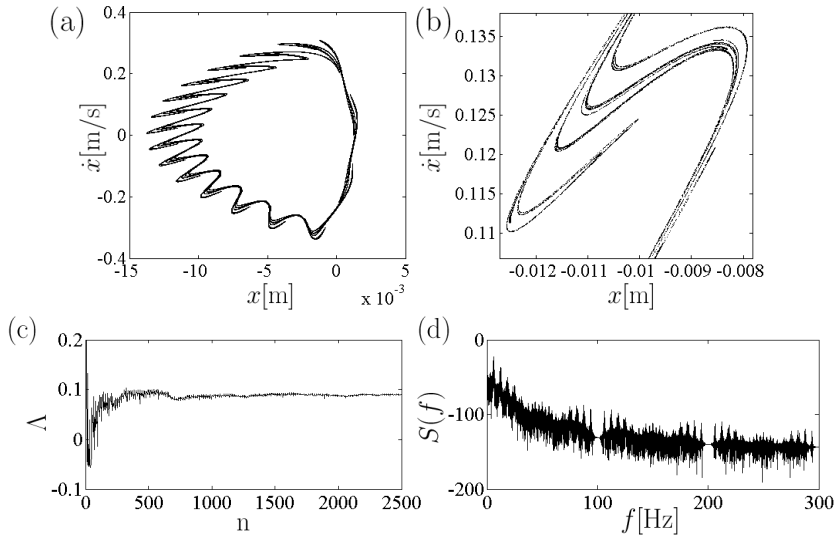

Figure 6.3: (a): chaotic attractor of the stroboscopic map (Eq. (4.3)), (b): detail of the attractor to show its fractal nature, (c): Lyapunov exponent and (d): FFT of the response. $q_0 = 0.97$, $p = 0.2501$ $Q_0 = 10$ m/s^2, $\tau = 0.01$ s.

6.2 Double Neimark-Sacker bifurcation

Considering now the two-DoF mechanical system in Fig. 4.6, we already mentioned the occurrence of chaotic motion for high values of u_0, in particular, an analysis of Fig. 5.13 shows the appearance of a strange behavior, that did not emerge in the analytical investigation, starting from $u_0 = 0.73263$ and for increasing values of u_0. Analyzing simultaneously the bifurcation diagram, the Lyapunov exponents Λ [16, 47], the fractal dimension (calculated with the Correlation Dimension [24, 27]) of the attractors and the attractors themselves, the complicated behavior of the system can be partially understood.

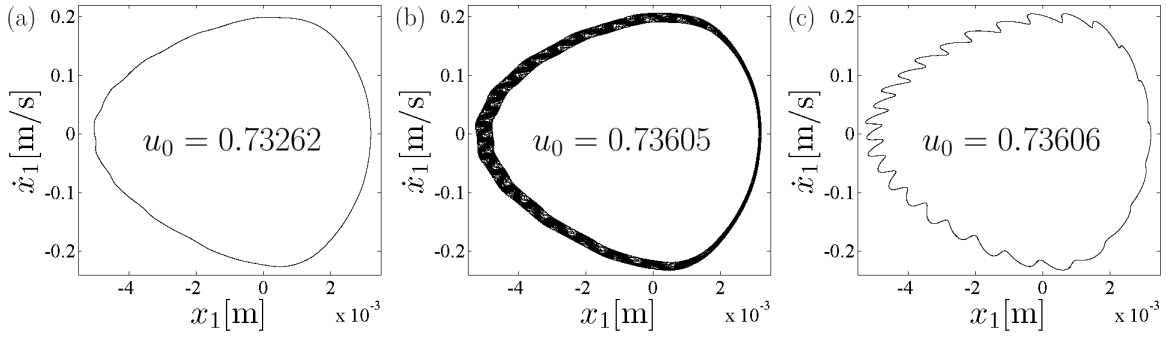

Figure 6.4: Attractors for different values of u_0, for $p_1 = 0.2325$ and $d_1 = 0.735$. (a): $u_0 = 0.73262$, (b): $u_0 = 0.73605$, (c): $u_0 = 0.73606$, projected onto the $x_1, \dot{x}_1$ space.

6.2.1 Generation and breakdown of a torus

For $u_0 < 0.73263$ the attractor is a closed line (its projection in the $x_1, \dot{x}_1$ space shown in Fig. 6.4(a)), so it corresponds to a 2-torus quasiperiodic solution of the map in Eq. (4.25). The maximal Lyapunov exponent is zero while the others are negative and the fractal dimension is equal to 1, since a closed line has only one dimension in the five dimensional space.

At $u_0 = 0.73263$, the 2-torus quasiperiodic solution undergoes a secondary NS bifurcation, this introduces another frequency of oscillation into the motion that becomes 3-torus quasiperiodic. The attractor, from being a closed line, degenerates into a stable torus, as shown in Fig. 6.4(b). Two more Lyapunov exponents goes to zero, but one of them immediately decreases again to negative values. The dimension of the attractor is now two.

The trends of the Lyapunov exponents and of the fractal dimension in Figs. 5.13 (c) and (d), show that for $u_0 > 0.77$ the maximal Lyapunov exponent is positive, while the attractor is fractal (with fractal dimension being between two and three). These are both evidences of chaoticity of the motion for $u_0 > 0.77$. Variations of the Lyapunov exponents and of the fractal dimension in correspondence of the appearance of chaos can be better recognized in Fig. 6.5.

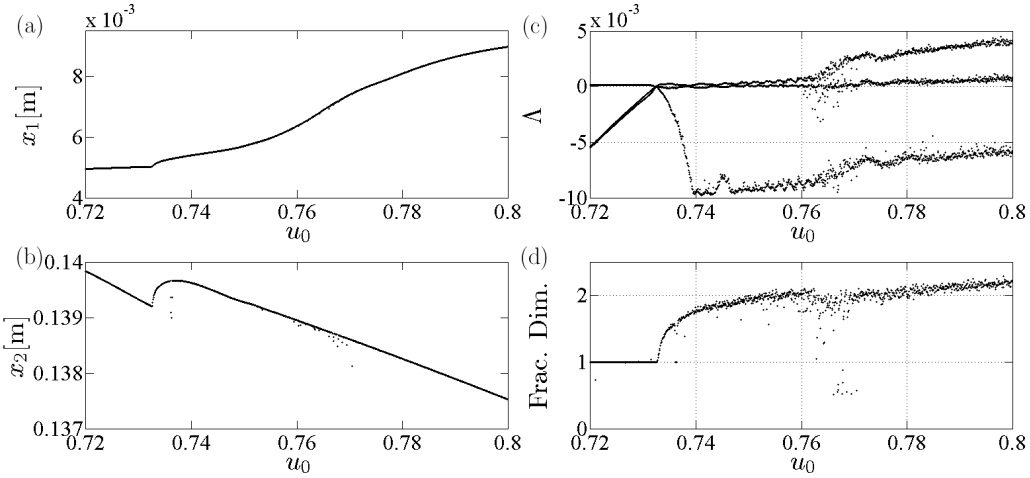

Figure 6.5: Enlargement of Fig. 5.13 in correspondence to the appearance of the stable torus and of the chaotic motion. (c): only the three largest Lyapunov exponents are represented.

It has been already shown, analytically, numerically and experimentally, that tori lose their smoothness

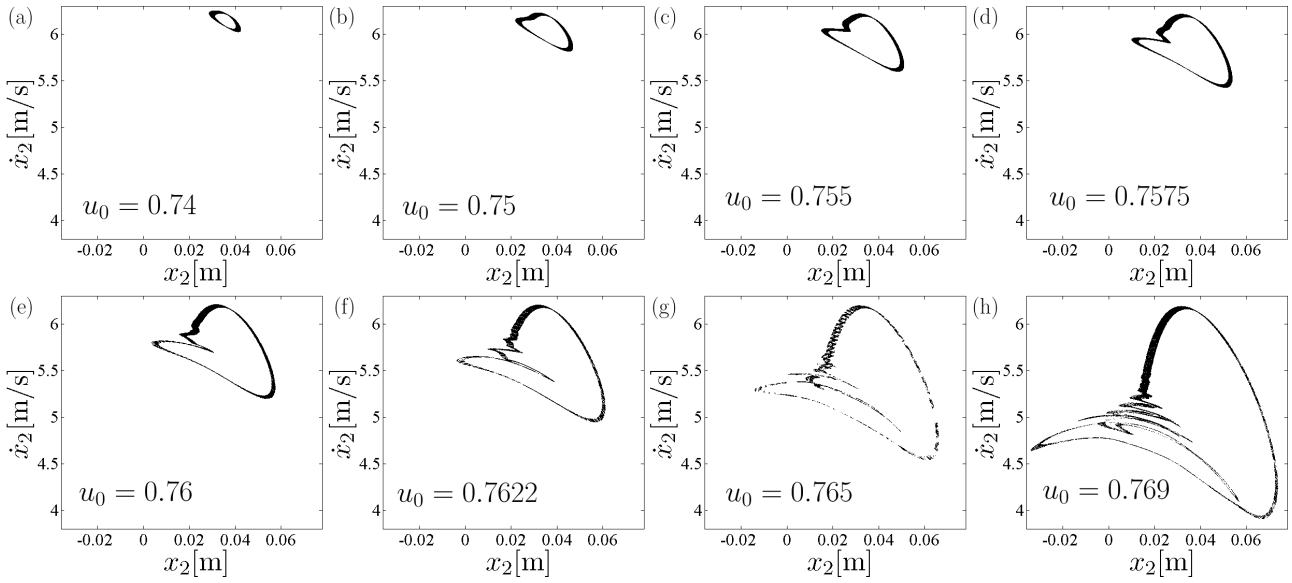

Figure 6.6: Semi-section of the torus for different values of u_0, for $p_1 = 0.2325$ and $d_1 = 0.735$. (a): $u_0 = 0.74$, (b): $u_0 = 0.75$, (c): $u_0 = 0.755$, (d): $u_0 = 0.7575$, (e): $u_0 = 0.76$, (f): $u_0 = 0.7622$, (g): $u_0 = 0.765$, (h): $u_0 = 0.769$ projected onto the $x_2, \dot{x}_2$ space. The section has been obtained selecting dots such that $|\hat{Q}_D| < 10^{-5}$. During the simulation $Q_0 = 10$ m/s^2, $\tau = 0.01$ s.

before breaking down into a fractal attractor (see for example [3, 7, 17, 45]). The quasiperiodic route to chaos via torus breakdown is one of the standard route to chaos, widely investigated in the literature; for a continuous experimental system in mechanics, see [4]. Still, it is interesting to visually analyze how this happens in this specific case, plotting sections of the attractors, as shown below. Most of the typical features described in the literature are clearly visible in this practical example.

Increasing the value of u_0 after the birth of the stable torus, the system undergoes several regions of phase locking, corresponding to the already mentioned Arnold tongues. This is clearly visible comparing Figs. 6.4 (b) and (c). For $u_0 \in (0.73606, 0.73636)$ there is one of these regions of phase locking that makes the motion lay on a continuous line that periodically evolves on the torus. The figure shows how the motion, from a torus, suddenly reduces to a solid line. Increasing further the value of u_0, the system meets more and more often regions of phase locking, that sometimes involve all the frequencies of motion of the system, reducing the attractor to a finite number of dots and not to a closed line.

In order to analyze the evolution of the torus, while approaching the chaotic region, we plotted artificial sections of the torus (Fig. 6.6), selecting the points of the attractor such that the control force $|\hat{Q}_D| < 10^{-5}$. We could not take real sections since the system is a discrete map and it jumps from one point to the other, without really crossing any section as a continuous time system would have done. The figures from (a) to (h) of Fig. 6.6 show how the section (only the semi-section in the figure), from being a smooth closed line, changes its shape until losing its smoothness for increasing values of u_0 (Fig. 6.6(e), $u_0 = 0.76$). Increasing further the value of u_0, more and more wrinkles appear, until the attractor becomes fractal breaking down the torus.

Fig. 6.7 shows the evolution of the section (this time the full section and not only one "slice" of the torus) from the first moments when it starts appearing fractal, with the two rings of the torus still recognizable, until the torus completely breaks down. A direct investigation of the attractor instead of its section, projected onto a two or a three dimensional space, would not give much information, because of the excessive density of the points. However, Fig. 6.8 shows the attractor of the system for different values of u_0, projected onto the $x_1, \dot{x}_1$ and the $x_2, \dot{x}_2$ spaces. Further evolutions of the strange attractor, shown in Fig. 6.8, are explained in the next section.

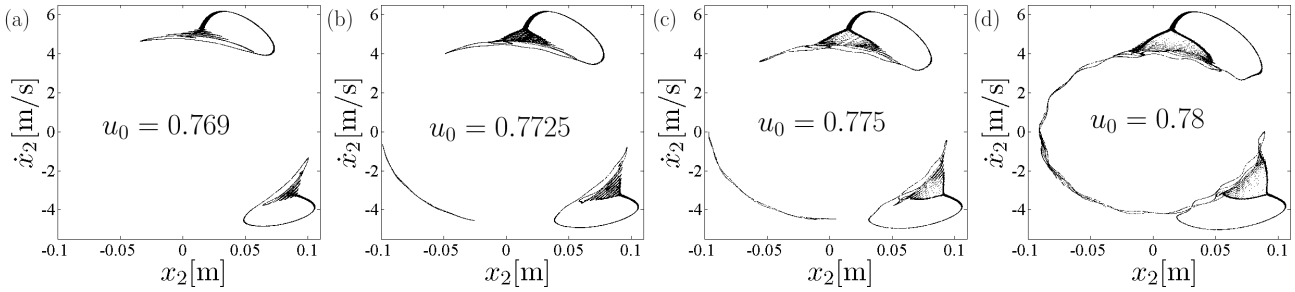

Figure 6.7: Section of the attractors for different values of u_0, for $p_1 = 0.2325$ and $d_1 = 0.735$. (a): $u_0 = 0.769$, (b): $u_0 = 0.7725$, (c): $u_0 = 0.775$, (d): $u_0 = 0.78$ projected onto the $x_2, \dot{x}_2$ space. The section has been obtained selecting dots such that $|\hat{Q}_D| < 10^{-5}$.

6.2.2 Evolution of the strange attractor

Increasing further the value of u_0, for $u_0 \in (1.02, 1.03)$, both the fractal dimension and the maximal Lyapunov exponent have a steep slope. The increase of the maximal Lyapunov exponent from $\Lambda \approx 0.004$ to $\Lambda \approx 0.04$ corresponds to an increase of unpredictability of the solution (faster divergence from nearby initial conditions), while the increase of the fractal dimension up to values larger than 3 corresponds to a dimensional enlargement of the attractor in the phase space.

Fig. 6.9 shows how the attractor (in the figure its section is shown) evolves from $u_0 = 1.00$ to $u_0 = 1.05$. It is visible how, for $u_0 \leq 1.02$, the fractal shape is still recognizable and has a well defined structure, while this structure is broken up and not recognizable anymore for $u_0 \geq 1.035$. In Fig. 6.9(g) the section of the attractor already consists of a cloud of dots which hide the previously existing structure. Considering that for $u_0 \geq 1.035$ the fractal dimension is closer to 3 than to 2, it is plausible that a single section of the attractor is not enough to recognize any structure. In this respect, Fig. 6.10 shows further sections of Figs. 6.9 (b) and (h), for $|x_1| < 10^{-5}$. From Fig. 6.10, it is clear how, for $u_0 = 1.01$, this further section reduces the attractor to few spots, this takes sense considering that we artificially removed two dimensions from an object of dimension ≈ 2.4. On the other side, for $u_0 = 1.05$, this further section shows a closed line, i.e. a nearly mono-dimensional object. This is the likely result of removing two dimensions from a nearly three-dimensional object (in the five dimensional space).

For $u_0 = 1.165$ the bifurcation diagram shows the appearance of much smaller attractors (shrinking especially visible regarding the x_2 coordinate) related to a phase locking. The phase locking involves all the frequencies of the motion, limiting the attractor to a finite number of points (Fig. 6.8(d)). In this case the system has a purely periodic motion. Of course, the fractal dimension of such an attractor is zero, while the maximal Lyapunov exponent is negative. The region of phase locking appears to exist from $u_0 = 1.165$ to $u_0 = 1.49$, but it is interrupted by a region with chaotic motion for $u_0 \approx 1.3$ and it is overlapped by the region with chaotic motion at both its borders. Furthermore, several attractors related to phase locking are coexisting. Figure 6.8(d) shows projections of two attractors coexisting for $u_0 = 1.25$: a smaller one with period equal to $11 \times \tau$ (red circles) and a larger one with much longer period (black dots). Figure 6.8(e) shows projections of the chaotic attractor existing for $u_0 = 1.3$, which appears to cover both the periodic attractors of Fig. 6.8(d).

Increasing the value of u_0 over 1.5, the phase locking disappears and the chaotic motion is again dominant over the dynamics of the system. In correspondence to this new chaotic motion, the maximal Lyapunov exponent has a big jump up to 0.1 and further, while also the fractal dimension appears to be permanently over 3. Figure 6.8(f) shows projections of the attractor for $u_0 = 1.5$, which, in spite of the larger value of Λ and of the fractal dimension, appears to be very similar to the one shown in Fig. 6.8(e), in the $x_1, \dot{x}_1$ plane; both of them show a fractal structure in that plane. It is interesting to notice the similarity of the chaotic attractor in Fig. 6.8(e) and the one in Fig. 6.3(a), related to the single DoF system. Bigger differences between the two attractors (for $u_0 = 1.3$ and $u_0 = 1.5$) can be recognized in the $x_2, \dot{x}_2$ space. Figure 6.11 shows the sections for $\hat{Q} \approx 0$ of the two attractors, projected onto the $x_2, \dot{x}_2$ space. From the figure it is visible how the attractor for $u_0 = 1.3$ (Fig. 6.11(a)) shows a fractal shape also in this plane, while the attractor for $u_0 = 1.5$ (Fig. 6.11(c)) does not show

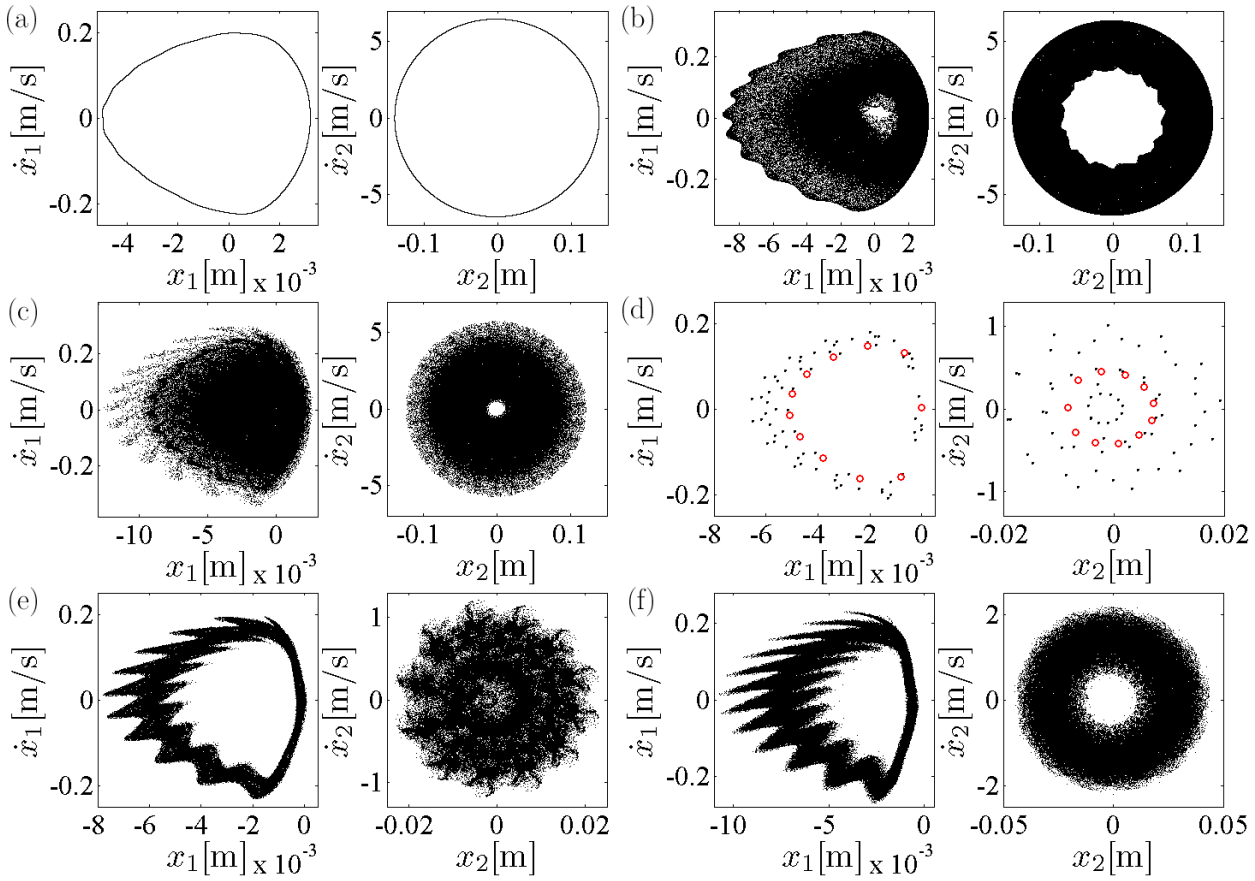

Figure 6.8: Attractors for different values of u_0, for $p_1 = 0.2325$ and $d_1 = 0.735$. (a): $u_0 = 0.725$, (b): $u_0 = 0.8$, (c): $u_0 = 1.1$, (d): $u_0 = 1.25$, (e): $u_0 = 1.3$, (f): $u_0 = 1.5$, projected onto the $x_1, \dot{x}_1$ and $x_2, \dot{x}_2$ space.

any recognizable structure. Furthermore, it appears to fill wider areas of the space than the other attractor, which is due to the increased fractal dimension. A further section of the attractor for a fixed value of x_1 (Figs. 6.11 (b) and (d)) does not clarify the differences between the two strange attractors.

Although the transition to chaos has been investigated in a region of instability of the trivial solution, chaotic motions exist also in the stable region. In general, the locus of secondary Neimark-Sacker bifurcations generating the quasiperiodic motion, first step on the route to chaos, is represented by the dotted line in Fig. 5.11. Figure 6.12, besides reproducing this locus of secondary NS bifurcations, shows the maximal Lyapunov exponent in the p_1, u_0 space. Shaded areas indicate a positive maximal Lyapunov exponent. The figure shows that the described dynamics occur in a large area around the double NS bifurcation and not only for specific values of p_1. Furthermore, since the chaotic attractor is related to global dynamics of the system, it is not affected by all the bifurcations described analytically, which are related to local dynamics. Similarly, the stability of the trivial solution, which is also a local characteristic of the system, does not affect the chaotic motion. In the figure it is clearly recognizable the increase of the maximal Lyapunov exponent for $u_0 \approx 1.05$ (darkening of the diagram, which corresponds to stronger chaos), the large region of phase locking for $u_0 > 1.3$ and the subsequent increase of the Lyapunov exponent for higher values of u_0. For $u_0 \approx 1.2$ the figure is white marked by gray vertical line. This is due to the coexistence of chaotic attractors and phase locked attractors: if during the simulations the system stays on the chaotic attractor the line is gray, if it jumps onto the phase locked attractor it will have negative Lyapunov exponents and it will show a white area.

In order to have a clearer picture of how the system is evolving in the different stages of chaotic motion, further investigation is needed, but this is out of the scope of this research.

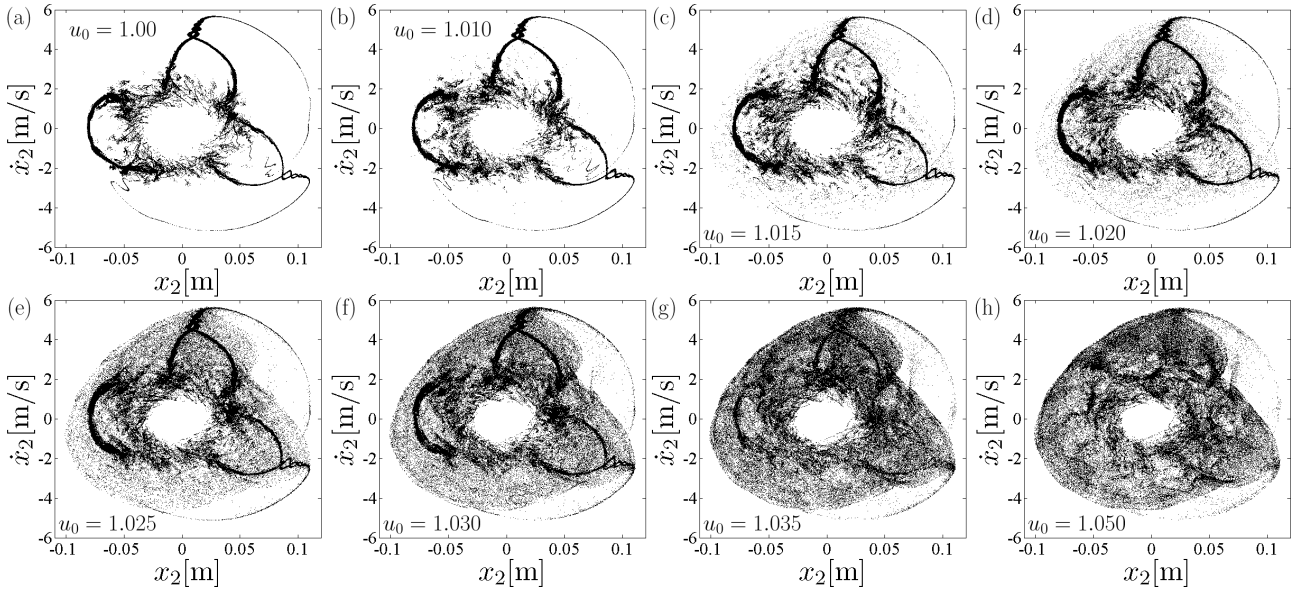

Figure 6.9: Sections of the fractal attractors for different values of u_0, for $p_1 = 0.2325$ and $d_1 = 0.735$. (a): $u_0 = 1.000$, (b): $u_0 = 1.010$, (c): $u_0 = 1.015$, (d): $u_0 = 1.020$, (e): $u_0 = 1.025$, (f): $u_0 = 1.030$, (g): $u_0 = 1.035$, (h): $u_0 = 1.050$ projected onto the $x_2, \dot{x}_2$ space. The section has been obtained selecting dots such that $|\hat{Q}_d| < 10^{-5}$.

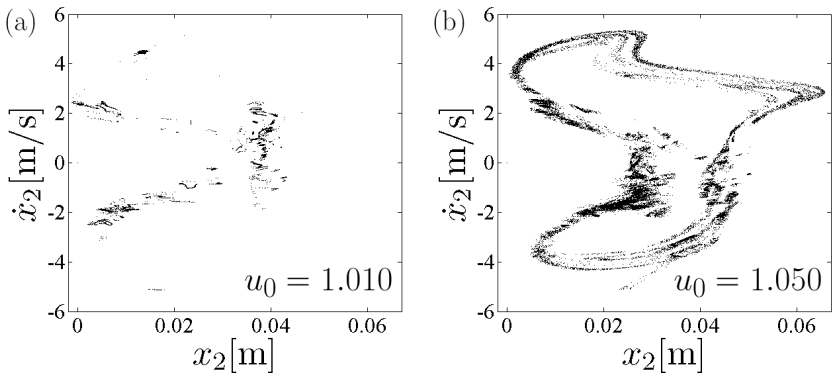

Figure 6.10: Double sections of the fractal attractors for different values of u_0, for $p_1 = 0.2325$ and $d_1 = 0.735$. (a): $u_0 = 1.01$, (b): $u_0 = 1.05$ projected onto the $x_2, \dot{x}_2$ space. The section has been obtained selecting dots such that $|\hat{Q}_D| < 10^{-5}$ and $|x_1| < 10^{-5}$.

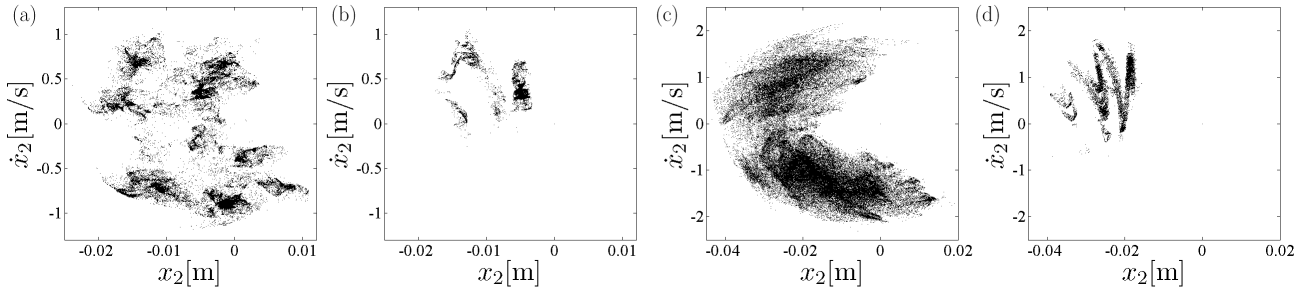

Figure 6.11: Sections of the fractal attractors for $p_1 = 0.2325$ and $d_1 = 0.735$. (a): $u_0 = 1.3$, (c): $u_0 = 1.5$ projected onto the $x_2, \dot{x}_2$ space. The sections has been obtained selecting dots such that $|\hat{Q}_D| < 10^{-5}$. (b) and (d): further sections of (a) and (c) for $-0.001003 < x_1 < -0.000397$ and $-0.001503 < x_1 < -0.001497$.

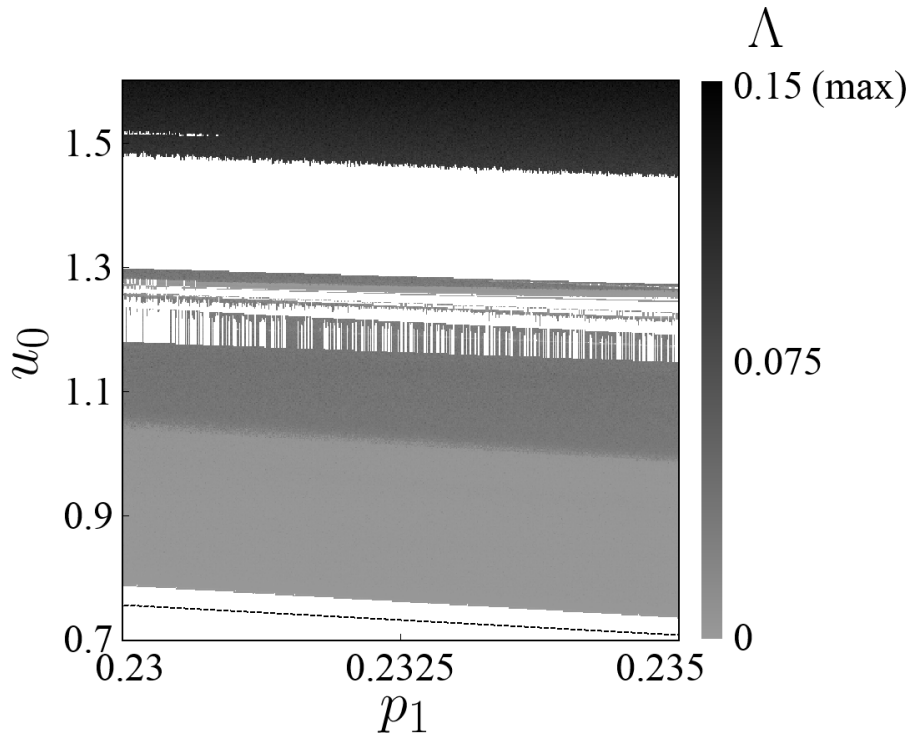

Figure 6.12: Contour plot of the maximal Lyapunov exponent in the space of the parameters p_1, u_0. The diagram has been obtained through sweeps down of u_0, starting from $u_0 = 1.6$ and for fixed values of p_1. The diagram has a resolution of 500x500. White area corresponds to zero or negative maximal Lyapunov exponent. The dashed line indicate the locus of secondary NS bifurcation, generating the stable 3-torus quasiperiodic motion.

Chapter 7

Application of the act-and-wait control concept

The act-and-wait controller is a periodic controller, introduced for control systems with feedback delay. Its concept consists in switching on and off the controller for specific time periods, where the off period is equal or larger than the delay of the system. This concept was first introduced by Insperger and Stepan in [29,31] for continuous time systems with feedback delay.

The main idea of this controller is to wait the effects of the control force before applying it again. In particular, for continuous time control system, feedback delays make systems have an infinite number of poles, making it very hard to stabilize the system through an appropriate pole placing. The act-and-wait controller reduces the pole of the system to a finite number, which allows to position them more easily and, furthermore, to obtain deadbeat control [29].

When applied to digital systems [30, 32], the controller should be on for one sampling interval and off for at least r sampling intervals, where r is the number of sampling intervals of delay the system has. In this chapter, we will apply the act-and-wait control concept to the single DoF system already analyzed regarding its stability in Ch. 2 and its bifurcation behavior in Ch. 4. Considering the act-and-wait controller, the stability and bifurcation behavior will be again investigated, highlighting the advantages of this approach.

7.1 Model

The model under study is exactly the same single DoF system previously studied in Ch. 2 and Ch. 4. For the convenience of the reader, it is reported in Fig. 7.1.

The time delay (at the beginning of each sampling interval) is exactly equal to one sampling interval, so the waiting time t_w of the controller should be $t_w \geq \tau$. Thus, the control force can be defined as

$$Q(t) = -P(t)x(t_{j-1}) - D(t)\dot{x}(t_{j-1}), \quad t \in [t_j, t_{j+1}), \tag{7.1}$$

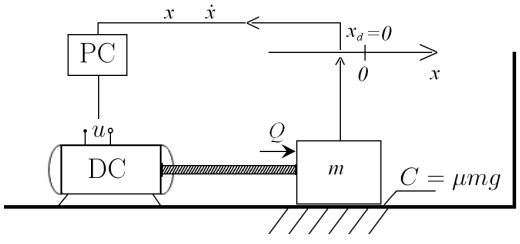

Figure 7.1: Mechanical model

where

$$P(t) = g(t)P \text{ and } D(t) = g(t)D \tag{7.2}$$

and

$$g(t) = \begin{cases} 1 & \text{for } t \in [2k\tau, (2k+1)\tau) \\ 0 & \text{for } t \in [(2k+1)\tau, 2k\tau) \end{cases} \qquad k = 0, 1, ... \tag{7.3}$$

Since the control force is periodic, with a full period equal to two time steps, the map describing the dynamics of the system must be modified accordingly, from the one defined in Ch. 2. At alternating intervals, the maps controlling the system are

$$\begin{array}{l} \mathbf{x}_{j+1} = \mathbf{A}_1 \mathbf{x}_j \\ \mathbf{x}_{j+2} = \mathbf{A}_2 \mathbf{x}_{j+1} \end{array} \quad \text{where} \quad \mathbf{A}_1 = \begin{pmatrix} 1 & 1 & \frac{1}{2} \\ 0 & 1 & 1 \\ -p & -d & 0 \end{pmatrix} \quad \text{and} \quad \mathbf{A}_2 = \begin{pmatrix} 1 & 1 & \frac{1}{2} \\ 0 & 1 & 1 \\ 0 & 0 & 0 \end{pmatrix}, \tag{7.4}$$

where $p = P\tau^2/m$ and $d = D\tau/m$ are the dimensionless control gains, τ is the sampling interval and m is the mass. Thus, it is possible to define the map

$$\mathbf{x}_{j+2} = \mathbf{A}_3 \mathbf{x}_j \quad \text{where} \quad \mathbf{A}_3 = \mathbf{A}_2 \mathbf{A}_1 = \begin{pmatrix} 1 - \frac{p}{2} & 2 - \frac{d}{2} & \frac{3}{2} \\ -p & 1 - d & 1 \\ 0 & 0 & 0 \end{pmatrix}. \tag{7.5}$$

As we see, the third line of matrix $\mathbf{A}_3$ is made of zeros. This makes one eigenvalue of $\mathbf{A}_3$ be zero and the coordinate x'' be zero every second sampling interval. Thus, the system can be considered two dimensional, i.e.

$$\mathbf{x}_{j+2} = \mathbf{A}\mathbf{x}_j \quad \text{where} \quad \mathbf{A} = \begin{pmatrix} 1 - \frac{p}{2} & 2 - \frac{d}{2} \\ -p & 1 - d \end{pmatrix}. \tag{7.6}$$

Considering that the system is simply inertial and the only active force is the control one, it is obvious that the acceleration x'' is zero during the "off-period" of the controller. The zeroing of one eigenvalue already shows the effect of reducing the number of poles of the act-and-wait controller.

7.2 Stability analysis

The stability depends on the eigenvalues of $\mathbf{A}$. These can be found in closed form and are

$$\mu_{1,2} = \frac{1}{4}\left(4 - 2d - p \pm 2\sqrt{d^2 + \frac{p^2}{4} + pd - 8p}\right), \tag{7.7}$$

while the characteristic polynomial of $\mathbf{A}$ is

$$\mu^2 + \left(d + \frac{p}{2} - 2\right)\mu + 1 - d + \frac{3}{2}p = 0. \tag{7.8}$$

Calling $a_1 = d + p/2 - 2$ and $a_0 = 1 - d + 3p/2$, the system is stable if $|a_1| < 1 + a_0$ and $|a_0| < 1$, which correspond to the inequalities

$$d > \frac{3}{2}p, \quad d < \frac{3}{2}p + 2, \quad d < \frac{p}{2} + 2, \quad p > 0. \tag{7.9}$$

Furthermore, considering the values of μ_1 and μ_2, it can be verified that one eigenvalue is zero for $d = 3p/2 + 1$, and both the eigenvalues are zero for $(p, d) = (1/2, 7/4)$, which corresponds to deadbeat control. The stability chart is represented in Fig. 7.2. It can be immediately noted the increased stable region, comparing to the stability chart in Fig. 2.4(a).

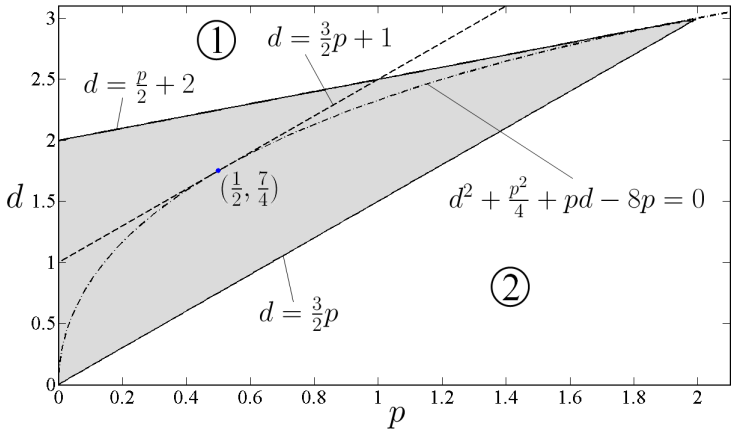

Figure 7.2: Stability chart using the act-and-wait control concept. Shaded area: stable, clear area: unstable. The numbers in the circle indicate the number of eigenvalues out of the unit circle of the complex plane.

Besides the stable region, analyzing the eigenvalues of $\mathbf{A}$ we can identify which kind of bifurcation occurs at the stability border. From the values of μ_1 and μ_2, it is obvious that the eigenvalues are complex conjugate if the radicand is negative, i.e. $d^2 + p^2/4 + pd - 8p < 0$. The curve corresponding to the radicand equal to zero is plotted in Fig. 7.2, the radicand is negative on the right side of the curve. Considering the result just obtained, we deduct that, if the system loses stability through the line $d = 3p/2$, there is a NS bifurcation, in virtue of the pair of complex conjugate eigenvalues out of the unit circle of the complex plane. On the other side, if the system loses stability through $d = p/2 + 2$, it undergoes a flip bifurcation since one eigenvalue leaves the unit circle through -1.

7.3 Bifurcation analysis

For an analysis of the effects of the use of the act-and-wait controller, it is interesting to investigate the bifurcation occurring at the stability border. As we did in Ch. 4, we consider the nonlinearity related to the saturation of the control force, which is modeled with the arctangent function

$$Q(t) = -\frac{2Q_{\max}}{\pi}\left[\arctan\big(Px(t_j - \tau) + D\dot{x}(t_j - \tau) - u_0\big) + q_0\right] g(t) \tag{7.10}$$

where $Q_{\max}$ is the maximal output force of the motor and the parameters q_0 and u_0 control the asymmetry of the saturation ($u_0 = \tan q_0$).

Considering Eq. (7.6), it can be easily verified that

$$\begin{pmatrix} x_{j+2} \\ x'_{j+2} \end{pmatrix} = \begin{pmatrix} 1 & 2 \\ 0 & 1 \end{pmatrix} \begin{pmatrix} x_j \\ x'_j \end{pmatrix} + \begin{pmatrix} -\left[\arctan\left(Px_j + Dx'_j - u_0\right) + q_0\right] \\ -2\left[\arctan\left(Px_j + Dx'_j - u_0\right) + q_0\right] \end{pmatrix} \frac{Q_{\max}}{m\pi}. \tag{7.11}$$

Redefining $Q_0 = 2Q_{\max}/(m\pi)$, $p = \tau^2 PQ_0/(1 + u_0^2)$ and $d = \tau DQ_0/(1 + u_0^2)$ and transforming the system in its Taylor series we obtain

$$\begin{pmatrix} x_{j+2} \\ x'_{j+2} \end{pmatrix} = \begin{pmatrix} 1 - \frac{1}{2}p & 2 - \frac{1}{2}d \\ -p & 1 - d \end{pmatrix} \begin{pmatrix} x_j \\ x'_j \end{pmatrix} + \begin{pmatrix} \frac{1}{2}\sum_{h+k=2,3} p_{hk} x_j^h x_j'^k \\ \sum_{h+k=2,3} p_{hk} x_j^h x_j'^k \end{pmatrix}, \tag{7.12}$$

or in compact form

$$\mathbf{x}_{j+2} = \mathbf{B}\mathbf{x}_j + \mathbf{b}, \tag{7.13}$$

where p_{hk} are the coefficients of the nonlinear terms. Regrading the second order terms

$$p_{hk} = -\alpha_2 \frac{p^h d^k u_0}{Q_0 \tau^2},\ \alpha_2 = \begin{cases} 1 \text{ if } \max(h,k) = 2 \\ 2 \text{ if } \max(h,k) = 1 \end{cases}, \tag{7.14}$$

while regarding the third order terms

$$p_{hk} = \alpha_3 \frac{p^h d^k \left(1 - 3u_0^2\right)}{3Q_0 \tau^2},\ \alpha_3 = \begin{cases} 1 \text{ if } \max(h,k) = 3 \\ 3 \text{ if } \max(h,k) = 2 \end{cases}. \tag{7.15}$$

The eigenvalues of $\mathbf{B}$ are $\mu_{1,2} = 1/4\left(4 - 2d - p \pm 2\sqrt{d^2 + p^2/4 + pd - 8p}\right)$. As we already pointed out, on the line $d = p/2 + 2$ one of the eigenvalues is equal to -1, so there is a flip bifurcation, while for $d = 3p/2$ the eigenvalues are complex conjugate with absolute value equal to 1, so there is a NS bifurcation.

7.3.1 Flip bifurcation

Moving along the line $p = 2d - 4$, we have

$$\mathbf{B} = \begin{pmatrix} 3 - d & 2 - \frac{d}{2} \\ 4 - 2d & 1 - d \end{pmatrix} \tag{7.16}$$

while the eigenvalues become $\mu_1 = -1$ and $\mu_2 = 5 - 2d$ for $2 < d < 3$. Applying the transformation $\mathbf{x} = \mathbf{T}\mathbf{y}$, where $\mathbf{T}$ is the matrix of the eigenvectors of $\mathbf{B}$, we can transform the system in its Jordan normal form, i.e. decouple the linear part of the system of equations, which becomes

$$\begin{pmatrix} y_1 \\ y_2 \end{pmatrix} \mapsto \begin{pmatrix} \mu_1 & 0 \\ 0 & 5 - 2d \end{pmatrix} \begin{pmatrix} y_1 \\ y_2 \end{pmatrix} + \begin{pmatrix} \sum_{h+k=2,3} a_{hk} y_1^h y_2^k \\ \sum_{h+k=2,3} b_{hk} y_1^h y_2^k \end{pmatrix} \tag{7.17}$$

where the coefficients a_{hk} and b_{hk} are explicitly given in Appendix F.

The system is two dimensional, but the flip bifurcation is related to a single eigenvalue and so to a single dimension. The system can be reduced to a single dimension, applying the center manifold reduction. The center manifold of y_2, limited to second order terms, is $y_2 = by_1^2$. Applying the procedure explained in Ch. 3, we can find that $b = b_{20}/(1 - \mu_2) = 2u_0/\left((3 - d)Q_0\tau^2\right)$, which will give the one dimensional map

$$y_1 \mapsto \mu_1 y_1 + \alpha_2 y_1^2 + \alpha_3 y_1^3 + \text{h.o.t.} \tag{7.18}$$

where

$$\alpha_2 = \frac{4u_0}{(d-3)Q_0\tau^2} \tag{7.19}$$

$$\alpha_3 = \frac{8\left(d + 3du_0^2 - 3(1 + u_0)^2\right)}{3(d-3)^2 Q_0^2 \tau^4} \tag{7.20}$$

We then applying the near identity transformation

$$y_1 = z + c_2 z^2 \tag{7.21}$$

to Eq. (7.18). If $c_2 = \alpha_2/2$, the second order term can be transformed out and we will obtain the map

$$z \mapsto \mu_1 z + \beta_3 z^3 + \text{h.o.t.} \tag{7.22}$$

where

$$\beta_3 = \alpha_3 + \alpha_2^2 = -\frac{8\left(1 + 3u_0^2\right)}{3(d-3)Q_0^2\tau^4}. \tag{7.23}$$

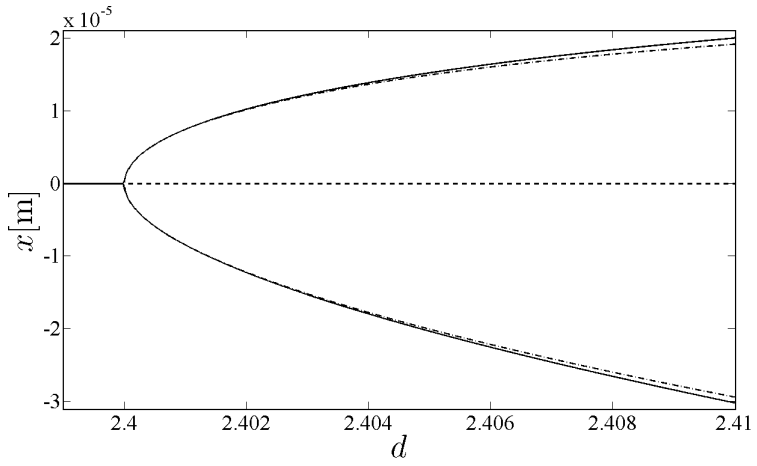

Figure 7.3: Flip bifurcation for $p = 0.8$, $u_0 = 0.4$, $Q_0 = 10$ m/s^2 and $\tau = 0.01$ s; solid lines: numerical results, dash-dot lines: analytical results.

In order to transform the obtained map to the normal form of a flip bifurcation, we rescale it according to $z = v/\sqrt{|\beta_3|}$ and we call

$$k = -(1 + \mu_1) \approx -\frac{\mathrm{d}|\mu_1|}{\mathrm{d}d}\bigg|_{p=2d_{cr}-4, d=d_{cr}} (d - d_{cr}), \tag{7.24}$$

where $d_{cr} \in (2, 3)$. This will give us the map

$$v \mapsto -(1 + k)\, v + \mathrm{sgn}(\beta_3) v^3 + \text{h.o.t.} \tag{7.25}$$

Considering the map in Eq. (7.25), its second iterate, beside the trivial solution (unstable for $k > 0 \iff d > d_{cr}$), has the solutions

$$v_{1,2} = \pm \left(\sqrt{\frac{k}{\mathrm{sgn}(\beta_3)}} + O(k) \right) \tag{7.26}$$

that exists if $k/\mathrm{sgn}(\beta_3) > 0$. If $\mathrm{sgn}(\beta_3) > 0$, it exists and is stable for $k > 0$, so it will be a supercritical flip bifurcation, while if $\mathrm{sgn}(\beta_3) < 0$, it exists and is unstable for $k < 0$, so it will be a subcritical flip bifurcation.

Considering the system under study, we found the values

$$\beta_3 = \frac{8(3u_0^2 + 1)}{3(3 - d_{cr}) Q_0^2 \tau^4}, \quad k \approx \left(\frac{1}{2} + \frac{d_{cr} - 1}{2(3 - d_{cr})} \right) (d - d_{cr}). \tag{7.27}$$

So we have that $\beta_3 > 0 \ \forall \ d_{cr} \in (2, 3)$, and for any real value of u_0, Q_0 and τ. While we see that k increases as $d_{cr} \to 3$, making the distance between the two branches of the bifurcation larger. Of course, for $d_{cr} \to 3$ the approximation in Eq. (7.24) is not valid anymore. Figure 7.3 shows a comparison between the numerical and the analytical results for $d_{cr} = 2.4$, $p = 0.8$ and $u_0 = 0.4$ (asymmetric saturation). The matching between the two results is excellent in the vicinity of the bifurcation.

7.3.2 Neimark-Sacker bifurcation

Moving along the line $d = 3p/2$, we have

$$\mathbf{B} = \begin{pmatrix} 1 - \frac{p}{2} & 2 - \frac{3}{4}p \\ -p & 1 - \frac{3}{2}p \end{pmatrix} \tag{7.28}$$

while the eigenvalues become $\mu_{1,2} = 1 - p \pm \sqrt{p(p-2)}$. So, for $0 < p < 2$, $\mu_1 = \bar{\mu}_2$ and $|\mu_{1,2}| = 1$. As we already explained, in these circumstances the system undergoes a NS bifurcation. Operating similarly to the previous case, we transform the system into its Jordan normal form, i.e.

$$\begin{pmatrix} y_1 \\ y_2 \end{pmatrix} \mapsto \begin{pmatrix} 1-p & \sqrt{p(2-p)} \\ -\sqrt{p(2-p)} & 1-p \end{pmatrix} \begin{pmatrix} y_1 \\ y_2 \end{pmatrix} + \begin{pmatrix} \sum_{h+k=2,3} a_{hk} y_1^h y_2^k \\ \sum_{h+k=2,3} b_{hk} y_1^h y_2^k \end{pmatrix} \tag{7.29}$$

where the coefficients a_{hk} and b_{hk} are different from the one related to the flip bifurcation. They can be found in Appendix F. Since the NS bifurcation is related to two variables, there is no need for the center manifold reduction. Calling $z = y_1 + iy_2$, where $z \in \mathbb{C}$, we transform the system to complex variables and we obtain the map

$$z \mapsto \mu_2 z + \sum_{h+k=2,3} \alpha_{hk} z^h \bar{z}^k. \tag{7.30}$$

The coefficients α_{hk} are reported in Appendix F.

Applying the near identity transformation $z = v + \sum_{h+k=2,3} c_{hk} v^h \bar{v}^k$, choosing properly the coefficients c_{hk}, as explained in detail in Ch. 3, it is possible to transform out all the second order terms and most of the third order terms, obtaining the map

$$v \mapsto \mu_2 v + \beta_{21} v^2 \bar{v} + \text{h.o.t.}, \tag{7.31}$$

where

$$\begin{aligned} \beta_{21} &= \alpha_{21} + \frac{\alpha_{20}\alpha_{11}(1-2\mu_2)}{\mu_2^2 - \mu_2} + \frac{\alpha_{11}\bar{\alpha}_{11}}{1-\bar{\mu}_2} + \frac{2\alpha_{02}\bar{\alpha}_{02}}{\mu_2^2 - \bar{\mu}_2} \\ &= \frac{1}{2}\Bigg(- \frac{2u_0^2 p^2 \sqrt{(2-p)p}\left(8 - 32p + (30+2i)p^2 - (8+29i)p^3 + 58ip^4 - 38ip^5 + 8ip^6\right)}{(p-2)^2\left(-2ip^2 - \sqrt{(2-p)p} + p\left(3i + 2\sqrt{(2-p)p}\right)\right) Q_0^2 \tau^4} \\ &\quad - \frac{p\left(p^2 - i\sqrt{(2-p)p} + ip\left(2i + \sqrt{(2-p)p}\right)\right)\left(-1 + 3u_0^2\right)}{(-2+p) Q_0^2 \tau^4} \\ &\quad + \frac{p\left(7i\sqrt{(2-p)p} + p\left(5 - 4i\sqrt{(2-p)p}\right) - 4p^2\right) u_0^2}{\left(6 - 7p + 2p^2\right) Q_0^2 \tau^4}\Bigg). \end{aligned} \tag{7.32}$$

Substituting $z = re^{i\psi}$ and calling

$$k = |\mu_2| - 1 \approx \left.\frac{\mathrm{d}|\mu_2|}{\mathrm{d}p}\right|_{d=3p_{cr}/2, p=p_{cr}} (p - p_{cr}) = \frac{3}{4}(p - p_{cr}), \tag{7.33}$$

where $p_{cr} \in (0, 2)$, we can rewrite the map as

$$re^{i\psi} \mapsto r(1+k)e^{i(\psi+\phi)} + \beta_{21}|_{p=p_{cr}} r^3 e^{i\psi} \tag{7.34}$$

where $e^{i\phi} = \mu_2$. Selecting the absolute value of Eq. (7.34) and expanding it in its Taylor series (see again Ch. 3), we obtain the amplitude map

$$r \mapsto (1+k)r + \rho r^3 + \text{h.o.t.} \tag{7.35}$$

where $\rho = \Re(\beta_{21}|_{p=p_{cr}} e^{-i\phi})$. Fixed points of the map in Eq. (7.35) correspond to 2-torus quasiperiodic solutions of the map in Eq. (7.11). Besides the trivial solution, the map has the solution $r^* = \sqrt{-k/\rho}$, which exists for $k > 0$ if $\rho < 0$ (supercritical bifurcation with stable solutions) and for $k < 0$ if $\rho > 0$ (subcritical bifurcation with unstable solutions). Considering the specific case under study, we found the singular result of $\rho = 0$, independently of the values of p_{cr} (within the considered interval) and the asymmetry of the saturation u_0.

This means that, limiting the analysis to third order terms, the branch of quasiperiodic solution, arising at the bifurcation point, goes vertically, without generating any finite orbit.

In order to verify if the branch is actually vertical, we repeated the procedure just shown considering up to fifth order terms (but with a symmetric saturation, in order to simplify the calculation). Without going into detail of the long procedure, following all the steps we find the amplitude map

$$r \mapsto (1+k)r + \rho r^3 + \frac{I_{21}^2 + 2R_{32}(1+k)}{2(1+k)} r^5, \tag{7.36}$$

where $I_{21} = \Im(\beta_{21} e^{-i\phi})$ and $R_{32} = \Re(\beta_{32} e^{-i\phi})$ (β_{32} is the coefficient of the term $v^3 \bar{v}^2$ in a fifth order expression analogous to Eq. (7.31) not shown here). Since $\rho = 0$, the map has the fixed point

$$r^* = \sqrt[4]{\frac{-2k(1+k)}{I_{21}^2 + 2R_{32}(1+k)}} \tag{7.37}$$

which exists only if the radicand is not negative. The numerator is positive if and only if $k < 0$, while the denominator is positive if and only if $k > (-I_{21}^2 - 2R_{32})/(2R_{32})$. Considering the system under study, we have that $I_{21}^2 = -2R_{32}$, so, beside the trivial solution, the system has real solutions only for $k = 0$. This result confirms the singular result of the third order analysis.

Confirming the degeneracy of the bifurcation under study, numerical simulations of the map in Eq. (7.11) show that the system grows unboundedly for $d < 3p/2$, which is still in agreement with the result obtained analytically. It is remarkable that the line $d = 3/2p$ corresponds to the line delimiting the region of bounded motion in Fig. 4.5, regarding the system without act-and-wait controller. In order to improve the analysis and clarify the nature of the bifurcation, it would be necessary to introduce a source of damping in the system, besides the artificial damping of the differential gain of the control force. Such analysis is shown in the following section.

7.4 Damped system

We now consider the same system shown in Fig. 7.1, adding a term related to a linear damping into the equation of motion, that becomes

$$m\ddot{x} = Q - c\dot{x}. \tag{7.38}$$

We introduce the dimensionless time $T = t/\tau$ and call $\hat{Q} = Q\tau^2/m$ and $\delta = \tau c/m$. Since the system is still piecewise linear, it can be solved in closed form within each time step and transformed to a map. Defining the control force as in Eq. (7.1), the result in matrix form is

$$\mathbf{x}_{j+2} = \mathbf{D}\mathbf{x}_j \tag{7.39}$$

where

$$\mathbf{D} = \begin{pmatrix} 1 - \frac{1}{\delta^2}\left(\delta - 1 + e^{-\delta}\right) p & \frac{1}{\delta}\left(1 - e^{-\delta}\right) + \frac{e^{-\delta}}{\delta}\left(1 - e^{-\delta}\right) - \frac{1}{\delta^2}\left(\delta - 1 + e^{-\delta}\right) d \\ -\frac{1}{\delta}\left(1 - e^{-\delta}\right) p & e^{-2\delta} - \frac{1}{\delta}\left(1 - e^{-\delta}\right) d \end{pmatrix}, \tag{7.40}$$

$\mathbf{x}_j = \begin{pmatrix} x_j & x'_j \end{pmatrix}^{\mathrm{T}}$, $p = P\tau^2/m$ and $d = D\tau/m$. It can be verified that $\lim_{\delta \to 0} \mathbf{D} = \mathbf{A}$, as it is in Eq. (7.6). Considering the eigenvalues of $\mathbf{D}$, we can find that the stable region in the p, d space is delimited by the lines

$$\begin{aligned} &p = 0 \\ &d = \tfrac{1+\delta e^{-\delta} - e^{\delta}}{\delta(1-e^{-\delta})} p + \tfrac{\delta\left(e^{\delta} - e^{-\delta}\right)}{1 - e^{\delta}} \quad &\Longleftrightarrow \quad d = \left(\tfrac{3}{2} - \tfrac{13}{12}\delta + O(\delta^2)\right) p - 2\delta + O(\delta^2) \\ &d = \tfrac{e^{-\delta}\left(2e^{2\delta} - \delta e^{2\delta} - \delta - 2e^{\delta}\right)}{2\delta(e^{\delta} - 1)} p + \tfrac{\delta e^{-\delta}\left(1 + e^{2\delta}\right)}{e^{\delta} - 1} \quad &\Longleftrightarrow \quad d = \left(\tfrac{1}{2} - \tfrac{7}{12}\delta + O(\delta^2)\right) p + 2 - \delta + O(\delta^2). \end{aligned} \tag{7.41}$$

Considering Eqs. (7.41) and (7.9), the effect of δ on the stability can be appreciated. Furthermore, it is clear that for $\delta \to 0$ the stable region is the same we found in the previous section. Fig. 7.4 show the stability chart in the p, d space for different values of δ.

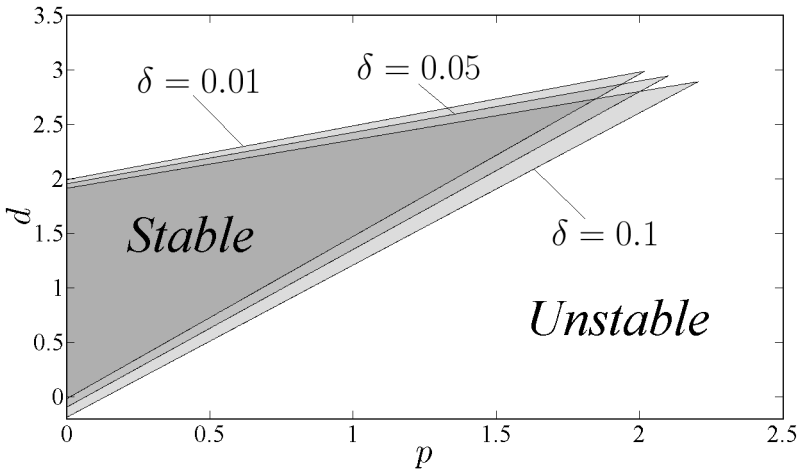

Figure 7.4: Stability chart in the p, d space, for different values of δ.

7.4.1 Bifurcation analysis

Beside the stability, it is interesting to analyze the effect of the damping on the NS bifurcation, which is singular in the case of no damping. We consider the saturation of the control force as it is in Eq. (7.10). Performing the same procedure as we did regarding the undamped system, we obtain the map

$$r \mapsto (1+k)r + \rho r^3 \tag{7.42}$$

where

$$k = f(\delta)(p - p_{cr}) = \left(\frac{3}{4} - \frac{11}{12}\delta + \frac{31}{48}\delta^2 + O(\delta^3)\right)(p - p_{cr}) \tag{7.43}$$

and $\rho = \rho(\delta, p_{cr}, u_0)/(Q_0^2\tau^4)$. The dependence of ρ on δ, p_{cr} and u_0 is very complicated to be studied analytically; however, its long expression is explicitly shown in Appendix F. Plots of its variation are shown in Fig. 7.5. In the figure it is visible that for a symmetric saturation ($u_0 = 0$) $\rho < 0$, so the bifurcation is supercritical, while for an asymmetric saturation (see Figs. 7.5(e) and (f)) ρ becomes positive and the bifurcation is subcritical. Variations of p_{cr} from 0 to 2 increase ρ almost linearly, without changing its sign, anyway for $p_{cr} \to 0$ also $\rho = 0$. For a slightly damped system, the bifurcation is supercritical for $u_0 < 1$, while it becomes subcritical for higher values of u_0. Increasing the damping, the limit for having a supercritical saturation in terms of asymmetry, slightly increases.

Figure 7.6 shows the bifurcation diagram with respect to the bifurcation parameter p, in the case of a symmetric saturation. In the figure it is visible how the branch of stable quasiperiodic solutions tends to be vertical for decreasing values of δ, both regarding the numerical and the analytical solutions, so in good agreement with the previous results regarding the undamped system. The horizontal plateaus correspond to phase locking of the quasiperiodic solutions. It is remarkable that, although the amplitude of the quasiperiodic solutions strongly depends on the damping, the amplitude of the solutions related to the phase locking does not appear to be affected by the damping. The bifurcation diagrams in Fig. 7.6 are obtained with a simple sweep up of the parameter p, in order to have a more readable figure.

Figures 7.7 (a)-(c) show the bifurcation diagrams obtained through a sweep down of the bifurcation parameter p, for different values of δ. In the figures it is visible how the horizontal plateaus exists also in large parts of the stable region. Especially for $\delta = 0$ (Fig. 7.7(a)), we could find periodic solutions even for $p < 0.45$, so very deep in the linear stable region. Increasing the damping, the region of existence of the plateaus sensibly reduces and we could not find any of them in the stable region for $\delta = 0.05$.

From Figs. 7.7(a) and (b), it is also visible that a lot of different periodic solutions coexist. The bifurcation diagrams have been obtained using random initial conditions in a selected range of values. However, especially

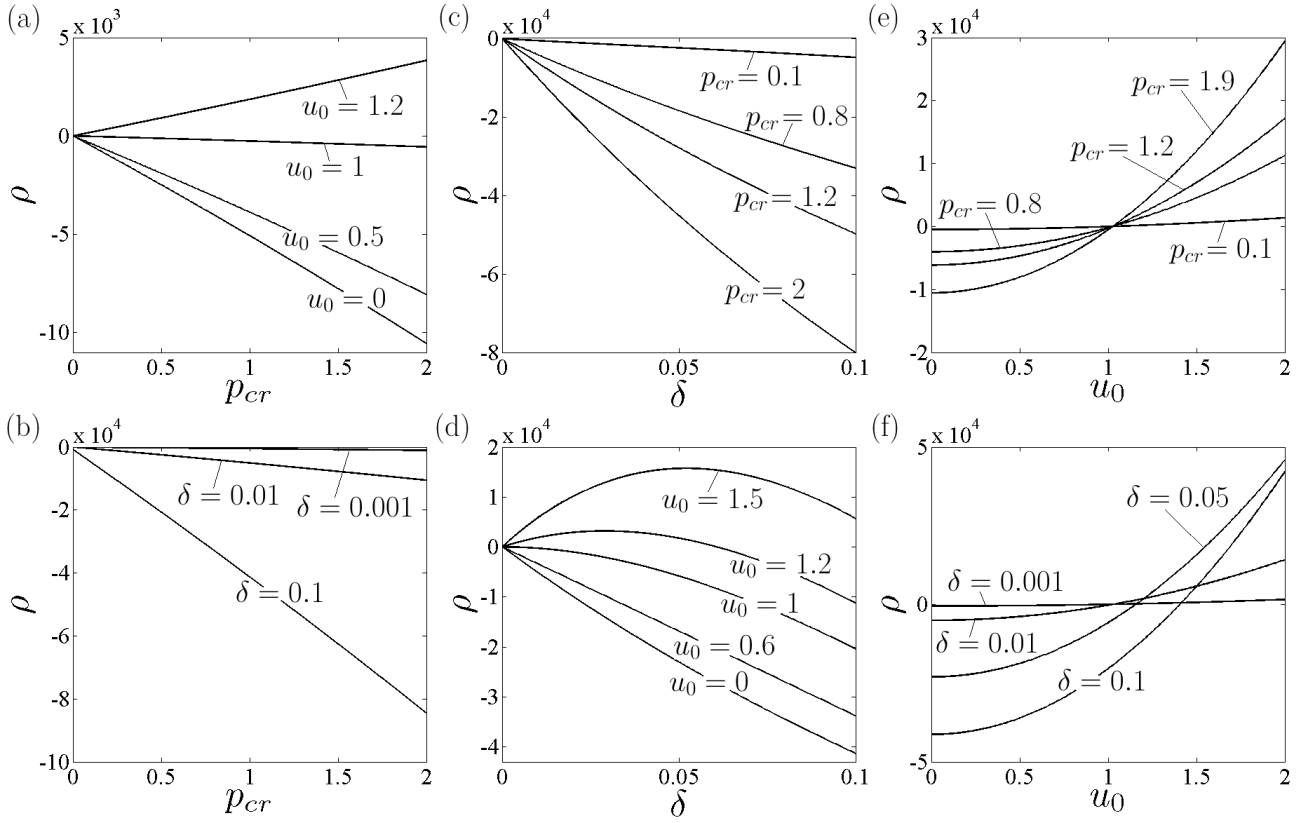

Figure 7.5: Plots of ρ as a function of p_{cr}, δ and u_0. In all the figures $Q_0 = 10$ m/s^2 and $\tau = 0.01$ s. (a): $\delta = 0.01$, (b): $u_0 = 0$, (c): $u_0 = 0$, (d): $p_{cr} = 1$, (e): $\delta = 0.01$, (f): $p_{cr} = 1$.

for $\delta = 0$, trials with very large initial conditions showed periodic attractors with amplitude of the same order of magnitude. Although we have no evidences, this suggests us that an infinite number of periodic solutions exists in the proximity of the stability border (inside the stable region). Fig, 7.7 (d) shows three different periodic attractors as an example of them.

Figure 7.8 shows basins of attraction of the trivial solution inside the stable region, for different values of p and δ. In Figs. 7.8(a), (b) and (c) $p = 0.68$ ($p_{\rm cr} = 0.7$), while δ is respectively equal to 0, 0.01 and 0.025. The figures clearly show that for increasing values of δ the region of attraction of the trivial solution enlarges, until covering the entire area of initial conditions for δ large enough (not shown in the figure). In Figs. 7.8(d) and (e) $\delta = 0$, while p is respectively 0.6 and 0.5. Comparing Figs. 7.8(a), (d) and (e) we can see how the region of attraction of the trivial solution enlarges for decreasing values of p, i.e. moving in the direction of the inner part of the stable region (it should be noted that the scale of the axes in Fig. 7.8(e) is different). Finally, Fig. 7.8(f) shows an enlargement of Fig. 7.8(a). This figure clarify the fractal nature of the basin of attraction, that could be already guessed from the other figures.

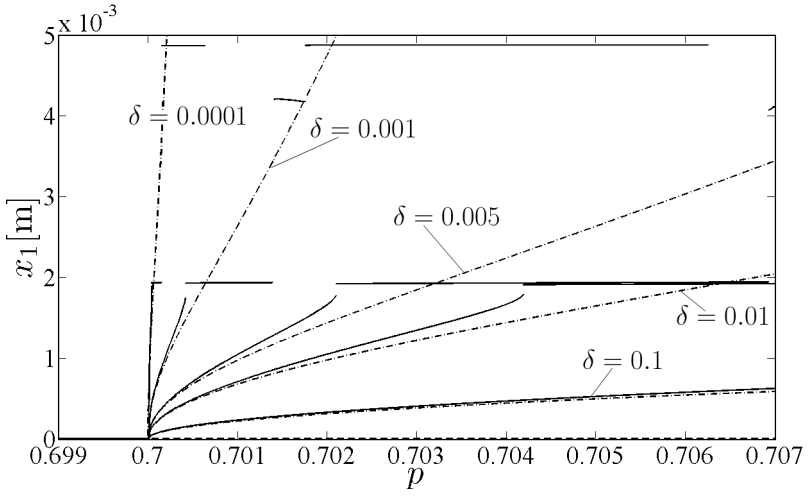

Figure 7.6: Bifurcation diagram with respect to the bifurcation parameter p, for different values of δ. Solid lines: numerical results, dash-dot lines: analytical results. In the figure $p_{cr} = 0.7$, $d = (3/2 - 13\delta/12)p_{cr} - 2\delta$, $u_0 = 0$, $Q_0 = 10$ m/s^2 and $\tau = 0.01$ s

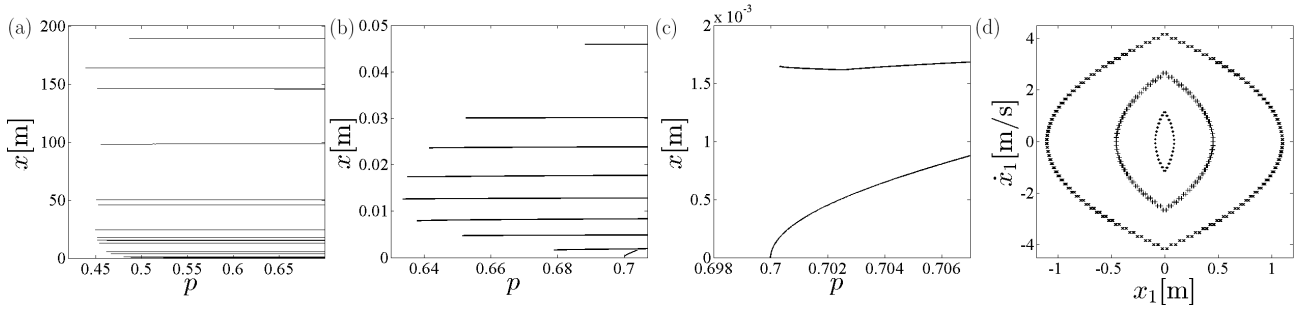

Figure 7.7: (a)-(c) numerical bifurcation diagrams with respect to the bifurcation parameter p, for different values of δ, through a sweep down and random initial conditions. Each diagram shows the results of several different initial conditions. (a) $\delta = 0$, (b) $\delta = 0.01$, (c) $\delta = 0.05$. (d) three different periodic attractors for $p = 0.6$ and $\delta = 0$. In all the figures $p_{\rm cr} = 0.7$, $d = (3/2 - 13\delta/12)p_{\rm cr} - 2\delta$, $u_0 = 0$, $Q_0 = 10$m/s^2 and $\tau = 0.01$s

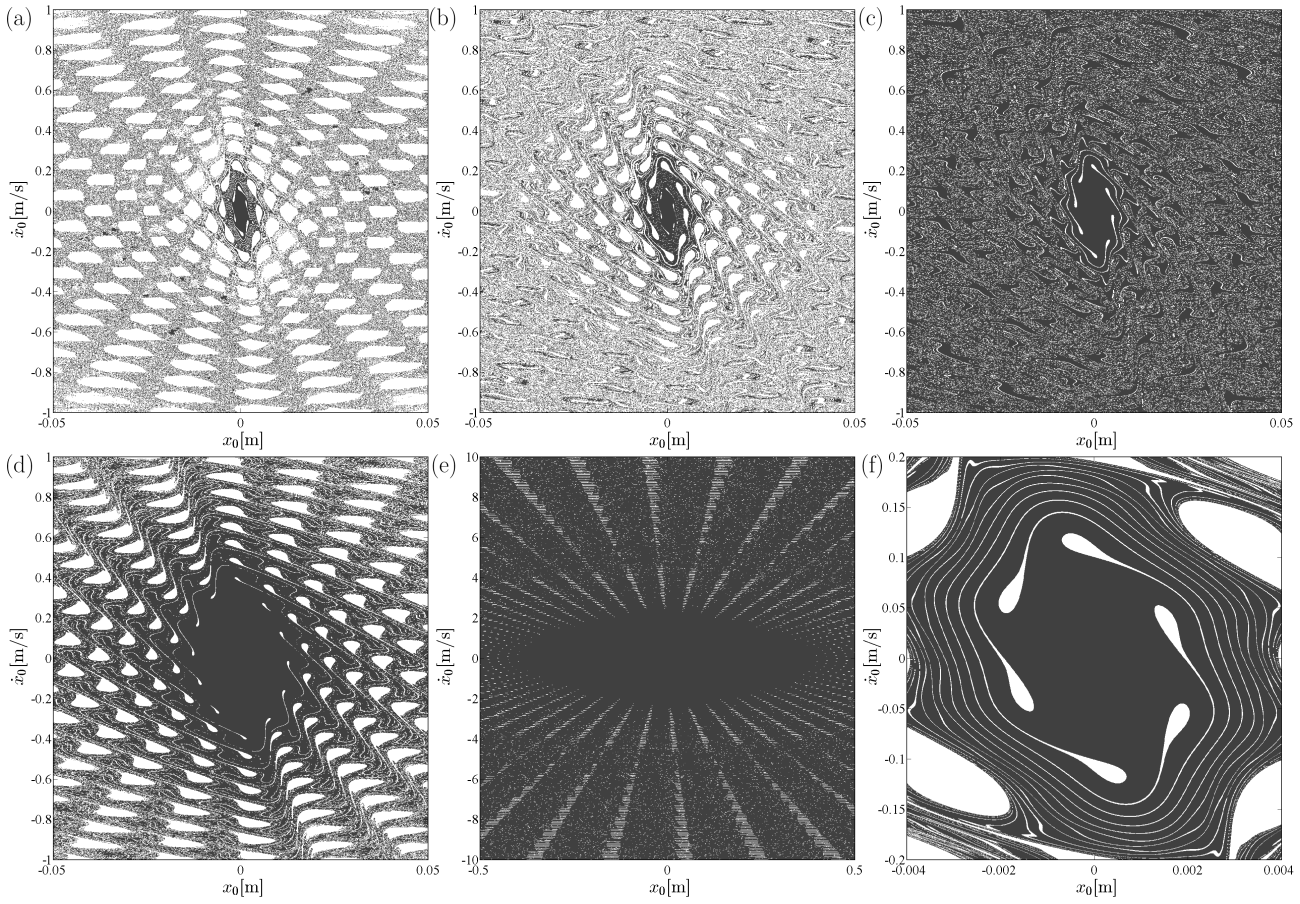

Figure 7.8: Basins of attraction of the trivial solution in its stable region for different values of δ and p. In all the figures $p_{\rm cr} = 0.7$, $d = (3/2 - 13\delta/12)p_{\rm cr} - 2\delta$, $u_0 = 0$, $Q_0 = 10\text{m/s}^2$ and $\tau = 0.01$s. (a) $p = 0.68$ and $\delta = 0$, (b) $p = 0.68$ and $\delta = 0.01$, (c) $p = 0.68$ and $\delta = 0.025$, (d) $p = 0.6$ and $\delta = 0$, (e) $p = 0.5$ and $\delta = 0$, (f) $p = 0.68$ and $\delta = 0$. Shaded area: region of attraction of the trivial solution, clear area: other solutions.

Chapter 8

Experimental investigation: aeropendulum

The so-called Aeropendulum [15] is a simple one-DoF pendulum equipped with a propeller at its end, capable of giving a control force to the pendulum itself, which allows to stabilize the pendulum virtually at any desired position. In this chapter, we will present experimental results, obtained with the Aeropendulum, which validate some of the numerical and analytical results obtained in the previous chapters. As we will show, the mechanical model of the experimental apparatus is qualitatively somewhat different from all the models studied in this work. Still, our results will show the importance of taking into account the digitization of the controller with respect to stability. Furthermore, this work is a typical example of nonlinear estimation of parameters through experimental investigation, which is an open topic in many fields of nonlinear studies.

8.1 Experimental setup

The system under study consists of a light carbon rod, connected perpendicularly to the shaft of a low-friction potentiometer (Fig. 8.1). At one of its edge, the rod is rigidly connected to a small DC electric motor, driven by a 5-V pulse-width modulated (PWM) signal. The potentiometer is fixed to a plastic frame, such that the rod and the motor form a rigid planar pendulum, freely rotating around the axis of the potentiometer. The motor drives a propeller, able to give a control force to the pendulum, linearly proportional to the PWM signal within a certain range.

The system is equipped with a custom-designed circuit board, which controls the voltage supplied to the motor with a resolution of 0.05 V and reads the voltage of the potentiometer, which is proportional to the angular position of the pendulum, allowing a precise identification and setting of the sampling frequency. More detailed information about the system and in particular the circuit board can be found in [15]. The control of the system is provided by a computer interface programmed in `MATLAB` environment.

8.2 Model

The system can be modeled as a 1.5 DoF system, one related to the rigid pendulum and half related to the propeller. Regarding the propeller, it counts as half DoF since we consider only its speed of rotation (proportional to the control force) and not its angular position.

The main forces acting on the pendulum are the gravity, the dry friction in the potentiometer, the air drag, the reaction force of the rod and the force given by the propeller, which depends on its speed of rotation. Instead, the dynamics of the propeller can be considered to be controlled by a first order equation. The equations of

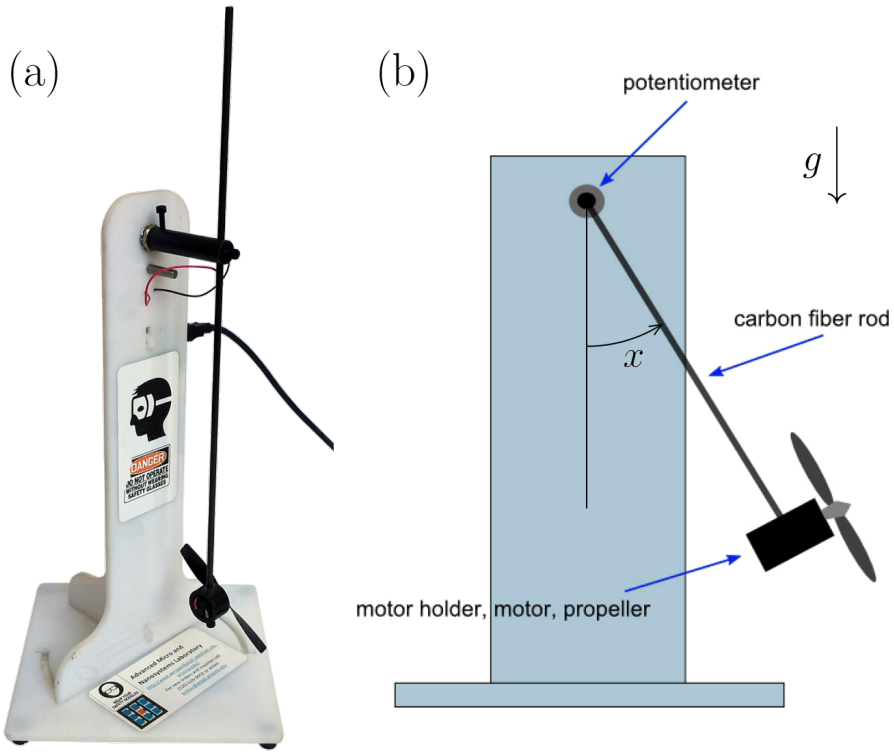

Figure 8.1: (a): Aeropendulum (photo); (b): schematic physical model

motion can be written as

$$\begin{cases} \ddot{\varphi} + 2\delta\omega_n\dot{\varphi} + \delta_2\dot{\varphi}|\dot{\varphi}| + C(\dot{\varphi})\frac{\dot{\varphi}}{|\dot{\varphi}|} + \omega_n^2\sin(\varphi) = F(\Omega) \\ \dot{\Omega} = -\frac{\Omega}{\lambda} + \frac{Q(\text{PWM})}{\lambda} \end{cases} \tag{8.1}$$

where φ is the angle of rotation of the pendulum, ω_n is its natural frequency, δ is the linear damping ratio, δ_2 is the coefficient of the quadratic damping (related to air drag), $C(\dot{\varphi})$ is the dimensionless dry friction, which depends on the angular velocity of the pendulum, and $F(\Omega)$ is the dimensionless force given by the propeller, which depends on the speed of rotation of the propeller. Regarding the second equation of (8.1), Ω represents the speed of rotation of the propeller, λ is the characteristic time of the system and the control force Q is linearly proportional to the PWM signal received in input by the motor.

As it will be shown later, we have no direct information about the speed of rotation of the propeller, thus the variable Ω is not the actual velocity of rotation of the propeller, but only a mathematical auxiliary variable. This allows us to take into account that the system has an extra half DoF, affecting the dynamics of the pendulum, without need of calculating the exact value of the speed of rotation.

In the proposed model, we did not take into account the dependence of the speed of rotation of the propeller on the angular velocity of the pendulum. Which exists, but it cannot be easily defined and can be neglected for the purpose of this work. Thus, considering the system in Eq. (8.1), the motion of the propeller is an independent differential equation, that can be analytically solved if Q is constant. However, whatever are the definitions of $C(\dot{\varphi})$ and $F(\Omega)$, the first equation has several nonlinearities.

8.3 Estimation of coefficients

The system under study has a rather simple geometry, however, we have no specifications about the geometry and material properties of the single components. Thus, it is necessary to perform experiments in order to

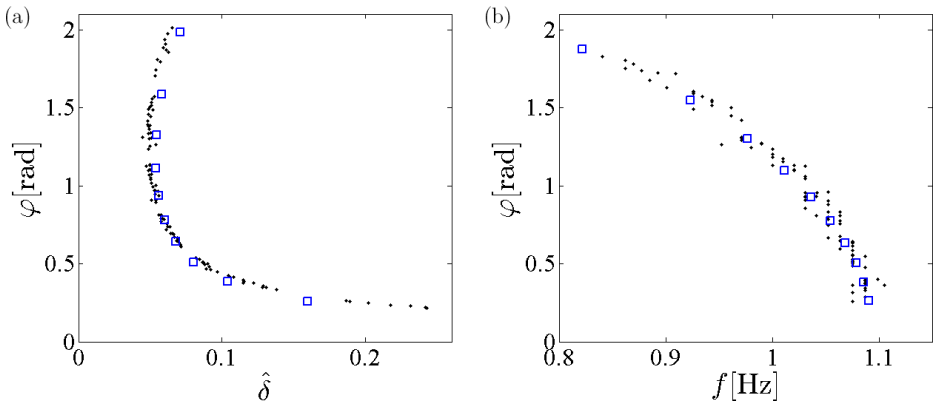

Figure 8.2: Experimental (black dots) and numerical (blue squares) damping backbone (a) and frequency backbone (b) curves. The experimental results are obtained from a superposition of ten different free vibration decays. For the numerical simulation: $\omega_n = 6.9$ rad/s, $\delta = 0$, $\delta_2 = 0.028$ rad^{-1}, $\beta = 2$, $\mu_0 = 2.6$ rad/s^2 and $\alpha = 0.77$ ($\mu_0(1+\alpha) = 4.6$ rad/s^2).

define the coefficients of Eq. (8.1) and the function $C(\dot{\varphi})$ and $F(\Omega)$.

8.3.1 Pendulum coefficients

First, we let the pendulum oscillate with free vibrations. This allows us to eliminate the variable Ω and the force F, letting the simpler system

$$\ddot{\varphi} + 2\delta\omega_n\dot{\varphi} + \delta_2\dot{\varphi}|\dot{\varphi}| + C(\dot{\varphi})\frac{\dot{\varphi}}{|\dot{\varphi}|} + \omega_n^2\sin(\varphi) = 0 \tag{8.2}$$

Few simulations immediately show that the kinetic dry friction is smaller than the static friction, so we decided to use an exponential function for $C(\dot{\varphi})$, i.e.

$$C_{\max}(\dot{\varphi}) = \mu_0\left(1 + \alpha e^{-\beta|\dot{\varphi}|}\right) \tag{8.3}$$

The value of $\mu_0(1+\alpha)$ can be directly estimated. Slowly moving the pendulum from the zero position and verifying which is the maximal angle different from zero that still gives an equilibrium position, we have the equation

$$\mu_0(1+\alpha) + \omega_n^2\sin(\varphi_{\max}) = 0. \tag{8.4}$$

Experiments show that this value can substantially change depending on weather conditions as temperature and humidity. At different time of the day we found for $\varphi_{\max}$ values varying from 0.085 to 0.105, so variations of about 20 %. Thus, we can estimate $\mu_0(1+\alpha) \approx (0.0949 \pm 0.01)\,\omega_n^2$.

Since the system is subject to softening, it is not trivial to estimate the value of ω_n. Similarly, all other coefficients cannot be directly estimated from the free vibration decay. In order to find them, we plotted several experimental free vibration decays and for all of them we plotted the damping and the frequency backbone curves (in Fig. 8.2 the superposition of several free vibration decays).

The frequency backbone curve has been obtained calculating the instantaneous periods, i.e. the distance between two subsequent peaks, and then calculating the frequency as its inverse. The curve clearly shows the expected softening behavior. Furthermore, it seems to converge to the value $f = 1.1$ Hz, which should be the value of the linear natural frequency.

The damping backbone curve has been obtained calculating, for each couple of subsequent peaks, the logarithmic decrement. Then, from the logarithmic decrement, the equivalent linear damping is calculated according

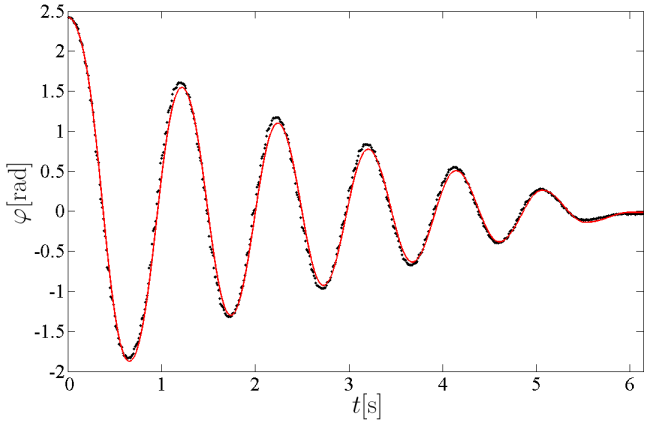

Figure 8.3: Experimental (black dots) and numerical (red solid line) free vibration decay. For the numerical simulation: $\omega_n = 6.9$ rad/s, $\delta = 0$, $\delta_2 = 0.028$ rad^{-1}, $\beta = 2$, $\mu_0 = 2.6$ rad/s^2 and $\alpha = 0.77$ ($\mu_0(1+\alpha) = 4.6$ rad/s^2).

to the formula

$$\hat{\delta} = \frac{1}{\sqrt{1 + \left(\frac{2\pi}{d}\right)}}, \tag{8.5}$$

where d is the logarithmic decrement. Although different from other definitions of damping backbone given in the literature [22,23,55], this procedure gives an estimate of the linear damping that would be necessary to obtain an equivalent decrement, given by all the damping components (so not only the linear one), as a function of the amplitude. Considering that the damping is mainly given by dry friction and (quadratic) air drag, the result shown in Fig. 8.2(a) is not surprising. The quadratic damping is dominant over the linear one for large amplitudes, while the dry friction is dominant over the linear damping for small amplitudes of oscillation. Accordingly, the diagram in the figure shows that for small amplitude a very large linear damping would be required to have the same effect of the dry friction. The value of $\hat{\delta}$ reduces increasing the amplitude of oscillation, until the curve bends forward again due to the increasing relevance of the air drag.

A comparison of the damping and frequency backbone curves and of the free vibration decay obtained by several experiments with those obtained by numerical simulations, allows us to find an optimal set of parameter values. The chosen set of parameters is $\omega_n = 6.9$ rad/s, $\delta = 0$, $\delta_2 = 0.028$ rad^{-1}, $\beta = 2$, $\mu_0 = 2.6$ rad/s^2 and $\alpha = 0.77$. A comparison of the free vibration decays obtained experimentally and numerically with these values is given in Fig. 8.3 (red line numerical result), while the blue squares in Fig. 8.2 show the numerical backbone curves.

The value of ω_n has been obtained directly from the estimated linear natural frequency of the frequency backbone curve. The value of δ_2 has been obtained with a simple trial and error procedure. It affects only large amplitudes, so basically only the first complete oscillation of the pendulum. Also in the damping backbone its influence is limited to the upper, right bending, branch of the curve. The value of μ_0 has been estimated with a trial and error approach as well. However, as already mentioned, its value can significantly change depending on the temperature, thus it is only indicative and accurate for the single experimental campaign. Larger values of β would not sensibly affect the result, so the value of 2 is purely indicative. α has been calculated from the value of the kinematic and static dry friction.

The performed procedure shows that the linear damping can be neglected: non-null values of δ do not improve the matching between experimental and numerical results. For higher amplitudes the quadratic damping is the most relevant source of damping while for smaller amplitudes the dry friction is, of course, more relevant than the quadratic damping. Although Fig. 8.2 shows results of several free vibration decays, they were all sampled subsequently, thus they do not represent all the possible behaviors of the system, rather than the behavior of the system with certain conditions of temperature and air humidity.

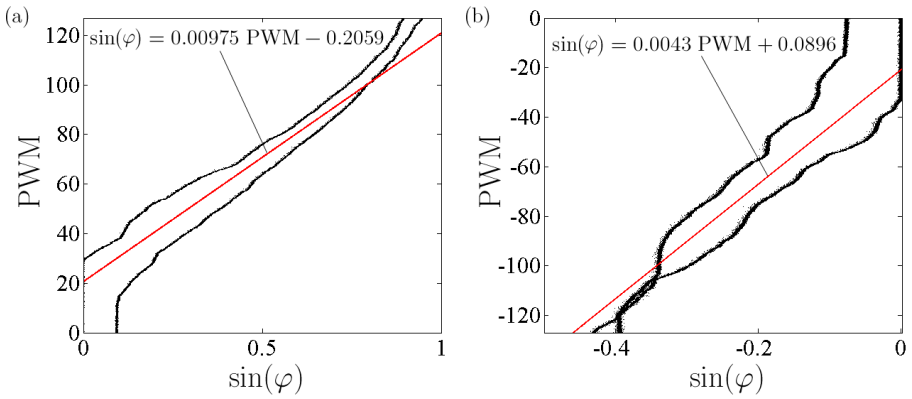

Figure 8.4: PWM vs. $\sin(\varphi)$ signal for increasing and decreasing values of PWM. Straight red line: linear interpolation of mean values in the linear range. (a): positive values of PWM; (b): negative values of PWM.

8.3.2 Propeller force

The control system of the pendulum allows to give a constant PWM signal to drive the motor. The PWM can be considered linearly proportional to Q and it can be easily verified that for constant values of Q, Ω will tend asymptotically to Q.

Giving constant (or slowly varying) input signals to the motor, it is possible to define the function $F(\text{PWM})$. Neglecting for the moment the dry friction, the equilibrium position is given by

$$\omega_n^2 \sin(\varphi) = F(\Omega) = F(Q(\text{PWM})), \tag{8.6}$$

of course, due to the dry friction, the system has infinitely many equilibrium position around this one.

PWM signal values, acceptable by the circuit board, must be included between -127 and +127. In order to define $F(\text{PWM})$, we first give a slowly increasing PWM signal, from 0 to +127, to the system, starting from the zero position of the pendulum. Than we repeated the procedure for slowly decreasing values of PWM, from +127 to 0, imposing an initial large displacement. After that we repeated the procedure for negative values of PWM. The result is shown in Fig. 8.4. An ideal system without friction and with a linear relation between F and PWM, should give a straight line in the PWM, $\sin(\varphi)$ space.

Figure 8.4 clearly show that increasing and decreasing values of PWM gives different results, this can be attributed to the dry friction. Furthermore, it appears that for large values of PWM the force saturates. Than, a dead-band can be recognized: for too small values of PWM the pendulum does not move (and neither the propeller). Finally, a comparison between Figs. 8.4(a) and (b) shows that the force provided by the propeller is strongly asymmetric. The force provided for negative values of PWM is almost the half than the one estimated for positive values of PWM.

The saturation of the force of the propeller is probably due the nonlinear relation between the speed of rotation of the fan and the provided force. However, since we are not able to measure the speed of rotation, it could be even due to the saturation of the electric motor. The dead-band is probably due to internal friction inside the motor. According to our observation, the propeller starts to rotate for $|\text{PWM}| > 20.5$, regardless of its sign. The asymmetry of the force is an obvious consequence of the asymmetric geometry of the system.

In spite of all these nonlinearities, the curves still show a linear range. For positive values of PWM it is approximately for $30 < \text{PWM} < 90$, while for negative values of PWM it is approximately for $-30 < \text{PWM} < -90$. The straight red lines in the figure are obtained through a linear approximation of the mean value, between the sweep up and the sweep down curves, considering only the linear range. As shown in the figure, the equations of these trend lines are $\sin(\varphi) = 0.0975\text{PWM} - 0.2059$ and $\sin(\varphi) = 0.0043\text{PWM} + 0.0896$.

8.3.3 Propeller time constant

The time constant λ of the propeller is the most problematic coefficient to be estimated, since the system does not provide any information regarding the speed of rotation of the fan. Furthermore, since we want to estimate a time constant, it would be required to know the speed of rotation in real time, with respect to a non-constant input signal. The only information available regards the input signal sent to the propeller and the position of the pendulum.

In order to find λ, we consider the second equation of (8.1) in the case of a time varying input signal. If Q is harmonic, i.e. $Q(t) = Q_0 \sin(\omega t)$, we have the differential equation

$$\frac{\mathrm{d}\Omega}{\mathrm{d}t} = -\frac{\Omega}{\lambda} + \frac{Q_0 \sin(\omega t)}{\lambda}, \tag{8.7}$$

given the generic initial condition $\Omega(0) = \Omega_0$, Eq. (8.7) has solution

$$\Omega(t) = \frac{\left(\Omega_0 + Q_0\lambda\omega + \Omega_0\lambda^2\omega^2\right) e^{-\frac{t}{\lambda}} + Q_0 \sin(\omega t) - Q_0\lambda\omega\cos(\omega t)}{1 + \lambda^2\omega^2} \tag{8.8}$$

that, after the transient fades away, will be

$$\Omega(t) = \frac{Q_0 \sin(\omega t) - Q_0\lambda\omega\cos(\omega t)}{1 + \lambda^2\omega^2}. \tag{8.9}$$

Eq. (8.9) is a harmonic function that can be written also as

$$\Omega(t) = \frac{Q_0}{\sqrt{1 + \lambda^2\omega^2}} \sin(\omega t + \phi), \tag{8.10}$$

where the phase shift ϕ can be neglected for our purposes.

Now, considering the full system, in the case of a harmonic excitation through the control force Q with amplitude Q_0, due to λ the pendulum will be excited with an amplitude reduced by the factor $1/\sqrt{1 + \lambda^2\omega^2}$. Since all the other parameters of the system have been already estimated, including the function $F(Q(\mathrm{PWM}))$, a comparison of numerical and experimental results of the forced system allows us to estimate the value of λ. To simplify the simulation and improve the accuracy of the result, we add a constant value to the motor input signal, in order to avoid the dead-band and stay in the linear range of F.

Figure 8.5 shows the result of the calibration for $\mathrm{PWM} = 60 + 30\sin(8t)$ with $\lambda = 0.28$ s. The red line is the numerical result while the black dots are the experimental one. The matching, once the system is at regime, is excellent. Furthermore, the numerical result is very sensitive to variation of λ, which gives more reliability to the estimation. On the other side, increments in the dry friction have a similar effect than increments in λ: they both reduce the amplitude of oscillation. It is possible to obtain a matching as good as the one shown in Fig. 8.5 reducing lambda and increasing μ_0. Thus, the uncertainty on the dry friction gives an uncertainty on λ. However, the sensibility of the amplitude of vibration on variations of λ is much larger than the sensibility on variations of the dry friction.

The procedures shown in this sections allowed us to identify all the coefficients in Eq. (8.1). The only missing relation is the function $Q(\mathrm{PWM})$. In order to estimate this function, it would be necessary to measure the speed of rotation of the propeller, which can be hardly done without any external hardware device. However, since we are not specifically interested in the rotation of the fun, we can simply substitute Q with PWM, which, excluding the dead-band, allows us describing correctly the dynamics of the pendulum. Of course, in this way, Ω loses its physical meaning.

8.4 Design of the controller

We consider the stabilization of a general position φ_0 of the pendulum. In order to make that position being of equilibrium, it is necessary that the propeller gives a corresponding constant force, according to the diagram

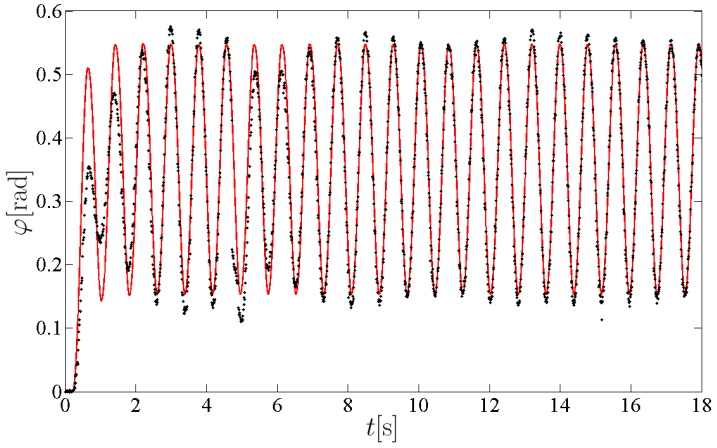

Figure 8.5: Experimental (black dots) and numerical (red solid line) force vibration response for PWM $= 60 + 30\sin(8t)$. For the numerical simulation: $\lambda = 0.28$ s, $\omega_n = 6.9$ rad/s, $\delta = 0$, $\delta_2 = 0.028$ rad^{-1}, $\beta = 2$, $\mu_0 = 2.6$ rad/s^2 and $\mu_0(1+\alpha) = 4.6$ rad/s^2.

in Fig. 8.4. For example, giving a constant PWM signal of 80, the pendulum will stabilize around $\varphi = 0.61$ ($\sin(\varphi) = 0.00975\text{PWM} - 0.2059$). Because of the dry friction and uncertainties of the estimated coefficients, the pendulum will stabilize in a position close to the desired one, but not exactly there. An active control can improve both the correct positioning and the speed of convergence to the desired position.

Similarly to the system analyzed in the previous chapters, we use a PD controller, defined as

$$F = -k_P(\varphi - \varphi_0) - k_D\dot{\varphi}, \tag{8.11}$$

where F is the control force and k_P and k_D are respectively the proportional and the differential gain. In the system under study, the control scheme needs some corrections, since it does not give a direct force to the pendulum, but it can only send modulated PWM signals to the motor driving the propeller.

First of all, it is necessary to compensate the dead-band, thus, we should add 20.5 (-20.5) to the PWM signal if it is positive (negative). Besides the dead-band, $F(\text{PWM})$ is linear with a good approximation, until saturation occurs for PWM > 90 or PWM < -100. Then, we should consider the slope of the curve in Fig. 8.4, in order to associate a value of PWM to a force. For positive values of PWM, besides the dead-band, we have that the force provided by the propeller is $F = 0.00975\omega_n^2\text{PWM}$ rad/s^2, while for negative values of PWM $F = 0.0043\omega_n^2\text{PWM}$ rad/s^2, within the linear range.

Furthermore, we should consider that the controller works at discrete time intervals. Thus, it samples the PWM signal at the time instants $t_j = j\tau$, $j = 0, 1, 2, ...$, where τ stands for the sampling time and $f_s = 1/\tau$ is the sampling frequency. PWM is then piecewise constant in the sampling interval and it is calculated from the position sampled at the beginning of the previous sampling interval. Moreover, the velocity should be calculated numerically. Calling $\varphi_j = \varphi(t_j)$ and $\text{PWM}_j = \text{PWM}(t_j)$, we can define the control scheme as

$$\text{PWM}_{j+1} = -k_P\left(\varphi_j - \varphi_0\right) - k_D\frac{\varphi_j - \varphi_{j-1}}{\tau} + \text{PWM}_0 + 20.5 \times \text{sign}\left(-k_P\left(\varphi_j - \varphi_0\right) - k_D\frac{\varphi_j - \varphi_{j-1}}{\tau} + \text{PWM}_0\right), \tag{8.12}$$

where $\text{PWM}_0 = \sin(\varphi_0)/a$ is related to the constant part of the control force. This gives the following system of equations

$$\begin{cases} \ddot{\varphi} + \delta_2\dot{\varphi}|\dot{\varphi}| + C(\dot{\varphi})\frac{\dot{\varphi}}{|\dot{\varphi}|} + \omega_n^2\sin(\varphi) = a\omega_n^2\Omega \\ \dot{\Omega} = -\frac{\Omega}{\lambda} + \frac{\text{PWM}_j}{\lambda} \\ a = \begin{cases} 0.00975 \text{ s/rad} & \text{if} \quad \text{PWM}_j > 0 \\ 0.0043 \text{ s/rad} & \text{if} \quad \text{PWM}_j < 0 \end{cases} \end{cases} \qquad t \in [t_j, t_{j+1}) \tag{8.13}$$

with PWM given by Eq. (8.12). As already mentioned, in this formulation Ω has no physical meaning, but it is still expressed in rad/s. It should also be noted that the circuit board of the pendulum allows only integer PWM signals in input. This mathematical model could be improved considering the saturation of the propeller force, easily obtainable from Fig. 8.4.

8.5 Estimation of stability

As already mentioned, because of the non-negligible dry friction, given a constant PWM input signal, the pendulum has a full range of equilibrium positions. Considering the system in Eq. (8.13) in steady state conditions, where φ_0 is the desired position and PWM_0 is the signal calculated to make φ_0 being of equilibrium, we have

$$C(\dot{\varphi}) + \omega_n^2 \sin(\varphi) = a\omega_n^2 \left(\mathrm{PWM}_0 - k_P \left(\varphi - \varphi_0\right)\right), \tag{8.14}$$

where $a\mathrm{PWM}_0 = \sin(\varphi_0)$. In the case of no active control ($k_P = 0$) the maximal positioning error is

$$\epsilon \approx \left| \frac{\mu_0(1+\alpha)}{\omega_n^2 \cos(\varphi_0)} \right|. \tag{8.15}$$

While, the proportional control gain reduces the maximal positioning error according to the formula

$$\epsilon_P \approx \left| \frac{\mu_0(1+\alpha)}{\omega_n^2 \left[\cos(\varphi_0) + ak_P\right]} \right|, \tag{8.16}$$

thus, it is clear that high proportional gains sensibly improve the positioning of the system. On the other side, as shown throughout this work, too large values of k_P could destabilize the system.

The estimation of stability of an equilibrium position of a system with the dry friction is controversial. Considering the equilibrium position φ_0, there will always exist an φ_e, with $|\varphi_e - \varphi_0|$ arbitrarily small, such that φ_e is also an equilibrium position. Thus, it can be proven that the system, as expressed in Eq. (8.13), is always stable (but never asymptotically stable) in the sense of Lyapunov. Of course, this is not true for the real system, because the potentiometer has a finite resolution ($\approx 3 \times 10^{-4}$ rad), which does not allow to exactly reach (according to the potentiometer measurement) the desired position. The consequent minimal error could be large enough to make the system diverge from φ_0, if k_P is large enough.

A linear system has a unique solution, whose asymptotic stability can be investigated in a rather simple way. A general nonlinear system has usually several solutions, but still the (linear) stability of one of its equilibrium points can be easily investigated through a linearization around that point. The linearization would locally eliminate all the nonlinear contributes, which generally have orders higher than the first, so they do not affect the local dynamics. In the case of a system with dry friction, the related nonlinear terms have order zero, so in a local analysis they are dominant over the linear terms and cannot be neglected. Thus, in this case, it has not so much practical sense in talking about Lyapunov stability of a specific position.

In a local analysis lower order terms are dominating over larger order terms. Considering larger amplitudes, higher order terms come into play and finally they prevail over lower order terms. Standard techniques to estimate stability take into account only linear terms, while in this system we have only order zero and quadratic damping. However, there is an amplitude of oscillation in which there is a balance between the effect of dry friction and quadratic damping.

A possible alternative to the estimation of stability, consists in considering the stability of the full range of possible solutions of the system ($\varphi \in [\varphi_0 - \epsilon_P, \varphi_0 + \epsilon_P]$), i.e. analyze if the system, given an initial position near this range of values, will stabilize to a value included in the considered interval. Of course, this analysis cannot be performed with standard techniques for estimating stability, furthermore it probably depends significantly on initial conditions. Thus, we should speak about basin of attraction and robustness of the stability, rather than of simple stability.

Another approach, in order to estimate the qualitative stability of the system with a significant engineering parameter, consists in analyzing a linear system equivalent to the one under study for certain range of amplitudes

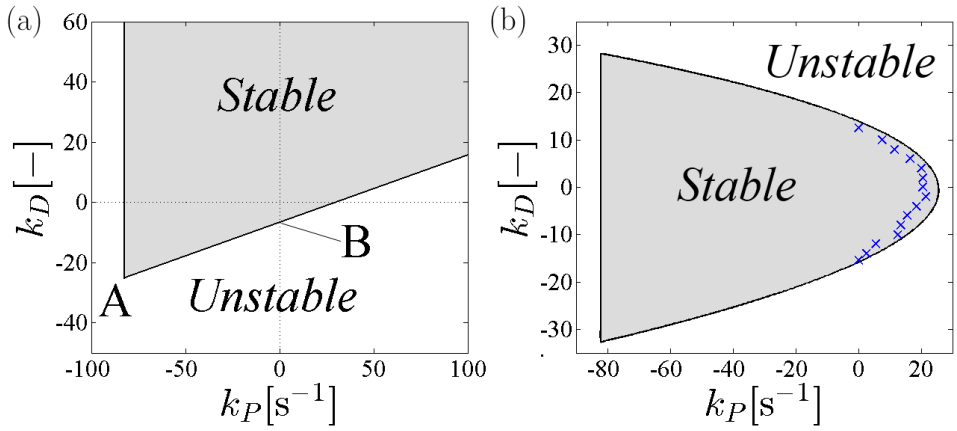

Figure 8.6: (a): Stability chart of the system in Eq. (8.17) around the point $\varphi_0 = 0.64$ rad. (a): continuous time approach (or $\tau \to 0$); (b): discrete time, $\tau = 0.05$ s. Blue $\times$-s refer to the experimental border of stability.

of oscillations. In other words, we define a linear damping which is equivalent to the total damping forces experienced by the pendulum for a specific amplitude of oscillation. A suitable value can be found considering Fig. 8.2(a); for the following investigation we chose $\hat{\delta} = 0.065$. Linearizing $\sin(\varphi)$ as well around a general position φ_0, we obtain the equation

$$\begin{cases} \ddot{\varphi} + \hat{\delta}\dot{\varphi} + \omega_n^2 \left(\sin(\varphi_0) + \cos(\varphi_0)(\varphi - \varphi_0)\right) = a\omega_n^2\Omega \\ \dot{\Omega} = -\frac{\Omega}{\lambda} + \frac{\mathrm{PWM}_j}{\lambda} \qquad\qquad t \in [t_j, t_{j+1}) \\ \mathrm{PWM}_{j+1} = -k_P\left(\varphi_j - \varphi_0\right) - k_D\frac{\varphi_j - \varphi_{j-1}}{\tau} + \mathrm{PWM}_0 + 20.5 \end{cases} \tag{8.17}$$

where $a = 0.00975$ and $\mathrm{PWM}_0 = \sin(\varphi_0)/a$. The linear asymmetry of the system is eliminated if φ_0 is chosen such that the control force is always positive or always negative around φ_0, which simplifies the stability analysis of the system. Of course, this does not eliminate the nonlinear asymmetry, in fact if $\varphi_0 \neq 0$ second order terms are introduced by the restoring force of the pendulum.

The system in Eq. (8.17) is piecewise linear and can be analyzed with a technique analogous to the one used in Ch. 2, i.e. solving it in closed form for each time step and reducing it to a map. This lengthy operation can be easily performed with computer algebra. The resulting formulas are however not interesting in this context, thus are omitted here and only some significant stability charts are represented.

Fig. 8.6(b) shows the stability chart in the k_P, k_D space obtained for $\tau = 0.05$ s around the position $\varphi_0 = 0.64$. The system admits stable solutions in a large area of negative values of k_P. This is due to the restoring force that compensate negative values of the proportional control gain. However, the whole region with $k_P < 0$ is not of practical interest, since in that case the control force is worsening the accuracy of the positioning.

The blue $\times$-s in the figure indicate the border of the experimental stability chart, for positive values of k_P. As we already mentioned, the real system is strongly nonlinear and solutions depend on their initial conditions. Thus, in order to have a significant result, the trial to verify the stability of the system for each pair of control gains was performed using approximately the same initial conditions $\varphi = 0$ and $\dot{\varphi} = 0$.

In spite of the numerous simplifications performed to linearize the system, the matching between the analytical/numerical and experimental results is satisfactory, both from a qualitative and from a quantitative point of view. The good matching confirms the practical significance of the investigated stability.

Fig. 8.6(a) shows the stability chart obtained in the theoretical case of a continuous time approach, which corresponds to the digital system where $\tau \to 0$. The stability chart is unbounded and it can be obtained

analytically. Points A and B have coordinates in the k_P, k_D space

$$\mathrm{A} = \left(-\frac{\cos(\varphi_0)}{a}, -\frac{\lambda\cos(\varphi_0)}{a} - \frac{2\hat{\delta}}{a\omega_n} \right), \qquad \mathrm{B} = \left(0, -\frac{2\hat{\delta}\left(1 + 2\hat{\delta}\lambda\omega_n + \lambda^2\omega_n^2\cos(\varphi_0)\right)}{a\omega_n\left(1 + 2\hat{\delta}\lambda\omega_n\right)} \right). \tag{8.18}$$

It should be noted that the minimal allowed value of k_P in order to have stability is the same in the continuous and in the discrete time approach. This occurs because values of k_P below the stability boundary make a statical loss of stability occur, and not a dynamical one, as when crossing any other stability boundary. Furthermore, this border is independent of the value of λ. On the other hand, the stability chart for positive values of k_P is totally different in the two cases. The good agreement between the numerical and the experimental results highlights the importance of considering the digitization of the controller.

Chapter 9

Conclusions

In this work, the stability and the bifurcation behavior of one and two-DoF systems, subject to digital position control, have been analyzed. The stability analysis compared the continuous and the discrete time approach, highlighting the differences in terms of stability and speed of convergence of the two cases.

Regarding the stability of the single DoF system analyzed in Ch. 2, our investigation showed how the digitization of the control force limits the stable region, otherwise unbounded.

The stability analysis of the two-DoF system was performed for a collocated and a non-collocated configuration, with both a continuous time and a discrete time approach. The collocated configuration (Fig. 2.6(a)) showed strong analogies with the single DoF system and a very similar stability chart, both in the continuous and in the discrete time approach. Varying the parameter related to the mass ratio of the system, it was possible to go with continuity from the two-DoF system to the single DoF system, again both with the continuous and the discrete time approach. The results showed that with a continuous time approach the collocated two-DoF system has a wider stable region than the single DoF system, however, the introduction of the discretization in time reduces the stable region more in the case of the two-DoF system. This effect is more visible if the sensed mass is smaller than the other one (high values of r, see Fig. 2.12(d)).

Regarding the non-collocated two-DoF system, our analysis showed that the stable region is bounded also using a continuous time approach. Furthermore, it showed how the stable region is gradually modifying while introducing the digitization and lowering the sampling frequency. According to our results, the digitization can also stabilize the system, e.g. in the case of no damping ($\delta = 0$) using a continuous time approach the non-collocated configuration has no stable region at all, while considering the discretization the system has almost always a stable region (see Fig. 2.16). Evidences of the accuracy of the analysis are given by the good agreement between the results obtained with the continuous time approach and those obtained with the discrete time approach with a very high sampling frequency (Fig. 2.17).

Other important results were obtained with a comparison of the two configurations, collocated and non-collocated, of the two-DoF system. With a continuous time approach the collocated configuration is definitely more stable than the non-collocated one, by virtue of its unbounded stable region. Considering the discretization in time of the control force, in the collocated case a decrease of the sampling frequency sensibly reduces the stable region, while it only modifies the stable region, without reducing its area, in the non-collocated case (see Fig. 2.17). Furthermore, both the configurations showed a strong dependence, in terms of stability, with respect to the ratio between the sampling and the natural frequency of the system, creating an interesting complementary pattern (see Figs. 2.13 and 2.15). Thus, the choice between a collocated and a non-collocated configuration should be done taking accurately into account the sampling frequency of the control system and the natural frequency of the system itself.

Large part of this work was devoted to bifurcation analysis. Besides illustrating a general procedure for analytically solving single and double NS bifurcations and flip bifurcations, we first investigated the single NS bifurcation occurring in the digital position control of a single DoF system and then the double NS bifurcation occurring in the digital position control of a two-DoF system. The analogies between the two cases are remarkable, although the double NS bifurcation has a much more involved dynamics, by virtue of the increased

dimension of the system.

The analysis evidenced that the single NS bifurcation is supercritical for a symmetric saturation of the control force, while it becomes subcritical for a sufficiently asymmetric saturation. The existence of subcritical bifurcations has important practical consequences, since it limits the robustness of the stable solution. In other words, in the stable region of the trivial solution of the system, the trivial solution will not be the only admissible solution, but there will exist an unstable quasiperiodic solution, so if the initial conditions are too far from the trivial solution, i.e. out of its basin of attraction, the system will be repelled by this unstable solution and converge to another attractor, probably large, and not to the trivial solution, resulting in an unexpected instability (see Fig. 5.5).

The double NS bifurcation consists in the interaction of two branches of single NS bifurcations, thus it is associated to two different 2-torus quasiperiodic motions. The analysis showed regions in the space of the control gains where one of the two bifurcations is dominant over the other one, in terms of stability of its associated quasiperiodic solution. It also showed a region of closer interaction of the two bifurcations, with the existence of an unstable 3-torus quasiperiodic solution dividing the two stable 2-torus quasiperiodic attractors.

The analogies between the single and the double NS bifurcations are mainly related to the effects caused by the asymmetry of the control force. With a symmetric system both the bifurcations are supercritical, while introducing an asymmetry, also in the case of the double NS bifurcation, subcriticality appears, similarly to the case of a single NS bifurcation. Also in this case, the robustness of the stable trivial solution is compromised. As already explained, this can be dangerous from an engineering point of view.

Another analogy between the two bifurcations under study is related to the transition of the systems to chaos, which is again related to the increased asymmetry of the saturation of the control force. Both the systems, undergoing a single and a double NS bifurcations, show a transition to chaos for increasing values of asymmetry. In spite of the different dimension of the systems, in some cases they show a similar chaotic attractor (compare Figs. 6.3(a) with 6.9(e) and (f)). Furthermore, in both the cases, stable chaotic motions exist also in the stable region of the trivial solution.

Regarding the double NS bifurcation, the transition to chaos is related to the breakdown of a stable three dimensional torus (of the underlying continuous time system, as explained in Ch. 6). The prove of existence of multi-frequency motions gives light on self-excited vibrations in digitally controlled mechanical system, where three or more frequencies are involved, often experienced in practice.

In Ch. 7, the act-and-wait control concept was introduced and applied to the previously investigated single DoF system. The results show how this approach allows to achieve deadbeat control and sensibly enlarges the stable region. On the other side, the bifurcation analysis showed that a loss of stability can make the system oscillate unboundedly (in spite of the saturation of the control force) and this can be very dangerous in a real application, where is preferable not to have sudden changes in the dynamics especially in cases of instability. Furthermore, it was shown that nontrivial solutions exist also in the region of stability of the trivial solution, compromising its robustness. These nontrivial attractors exist also in the case of supercriticality of the bifurcation at the loss of stability, thus they cannot be identified with standard analytical techniques of bifurcation analysis. It is remarkable and deserves further investigation the fact that the line limiting the stable region using the act-and-wait controller overlaps the line limiting the bounded motion using a regular PD controller (see Figs. 4.5 and 7.2).

The experimental investigation of the digitally controlled Aeropendulum, highlighted the importance of taking into account the digitization in the case of low sampling frequencies. Furthermore, the good matching between the analytical/numerical and experimental results gives reliability to the applied mechanical model.

Although all the analyses shown in this work regard very simple models of mechanical systems, that can be hardly led back to real engineering system, most of the obtained results summarized in this chapter can explain many behaviors experienced in more complicated real systems.

Appendix A

Conditions for stability for the two-DoF systems

Conditions for stability: discrete time approach configuration A

$$
\begin{aligned}
a_0 &= \frac{1}{\Omega^2}2e^{-2\delta\Omega}\left[2p_A r(e^{2\delta\Omega}-1)+\Omega^2(2+d_A)(1+e^{2\delta\Omega}+2e^{\delta\Omega}c_\Omega)+4e^{\delta\Omega}r\left(-\delta p_A+d\Omega+d_A\delta^2\Omega\right)s_\Omega\right]\\
a_1 &= e^{-2\delta\Omega}\frac{4p_A r(3-e^{2\delta\Omega})+e^{\delta\Omega}\left[2c_\Omega(\Omega^2(p_A-4d_A+4)-4p_A r)-16rs_\Omega(d_A\Omega(1+\delta^2)-\delta p_A)\right]}{\Omega^2}\\
&\quad +e^{-2\delta\Omega}(p_A-4-8d_A)+12+p_A\\
a_2 &= -4e^{-2\delta\Omega}\frac{p_A r(3+e^{2\delta\Omega})+\Omega^2(1-3d_A+p_A)+e^{\delta\Omega}\left[c_\Omega(\Omega^2(2+p_A)-4p_A r)-2rs_\Omega(d_A\Omega(1+\delta^2)-\delta p_A)\right]}{\Omega^2}\\
&\quad +12-4d_A\\
a_3 &= e^{-2\delta\Omega}\frac{(4-8d_A+6p_A)\,\Omega^2+4p_A r\left(1+e^{2\delta\Omega}\right)+8e^{\delta\Omega}\left((d_A-1)\Omega^2-p_A r\right)c_\Omega}{\Omega^2}+4-2p_A\\
a_4 &= 2e^{-2\delta\Omega}\left(d_A-2p_A-2e^{\delta\Omega}(d_A-p_A)c_\Omega\right)+2d_A\\
a_5 &= p_A\left(1+e^{-2\delta\Omega}-2e^{-\delta\Omega}c_\Omega\right)
\end{aligned}
$$

Conditions for stability: discrete time approach configuration B

$$
\begin{aligned}
a_0 &= \frac{1}{\Omega^2}2e^{-2\delta\Omega}\left(2p_B(1-e^{2\delta\Omega})+\Omega^2(2+d_B)(1+e^{2\delta\Omega}+2e^{\delta\Omega}c_\Omega)-4e^{\delta\Omega}\left(-\delta p_B+d_B\Omega+d_B\delta^2\Omega\right)s_\Omega\right)\\
a_1 &= e^{-2\delta\Omega}\frac{(4p_B(e^{2\delta\Omega}-3)+e^{\delta\Omega}\left[2c_\Omega(\Omega^2(p_B-4d_B+4)+4p_B)+16s_\Omega(d_B\Omega(1+\delta^2)-\delta p_B)\right]}{\Omega^2}\\
&\quad +e^{-2\delta\Omega}(p_B-4-8d_B)+12+p_B\\
a_2 &= -4e^{-2\delta\Omega}\frac{-p_B(3+e^{2\delta\Omega})+\Omega^2(1-3d_B+p_B)+e^{\delta\Omega}\left[c_\Omega(\Omega^2(2+p_B)+4p_B)+2s_\Omega(d_B\Omega(1+\delta^2)-\delta p_B)\right]}{\Omega^2}\\
&\quad +12-4d_B\\
a_3 &= e^{-2\delta\Omega}\frac{(4-8d_B+6p_B)\,\Omega^2-4p_B\left(1+e^{2\delta\Omega}\right)+8e^{\delta\Omega}\left((d_B-1)\Omega^2+p_B\right)c_\Omega}{\Omega^2}+4-2p_B\\
a_3 &= \frac{e^{-2\delta\Omega}\left(4\left(1-2d_B+e^{2\delta\Omega}\right)\Omega^2-2p_B\left(2-3\Omega^2+e^{2\delta\Omega}\left(2+\Omega^2\right)\right)+8e^{\delta\Omega}\left(p_B+(d_B-1)\Omega^2\right)c_\Omega\right)}{\Omega^2}\\
a_4 &= 2e^{-2\delta\Omega}\left(d_B-2p_B-2e^{\delta\Omega}(d_B-p_B)c_\Omega\right)+2d_B\\
a_5 &= p_B\left(1+e^{-2\delta\Omega}-2e^{-\delta\Omega}c_\Omega\right)
\end{aligned}
$$

The coefficient relative to the configuration B, can be obtained substituting r with -1. The other coefficients

that must be positive in order to have stability are

$$\begin{aligned} c_4 &= \frac{a_4 a_3 - a_5 a_2}{a_4} \\ c_3 &= \frac{a_4 a_1 - a_5 a_0}{a_4} \\ d_3 &= \frac{c_4 a_2 - a_4 c_3}{c_4} \\ e_2 &= d_3 c_3 - c_4 a_0. \end{aligned}$$

Appendix B

NS bifurcations: coefficients for general cases

Coefficients α_{hk} for the transformation in complex form in the analysis of a single NS bifurcation

$$\alpha_{20} = \frac{1}{4}(a_{20} - a_{02} + b_{11}) + i\frac{1}{4}(-a_{11} + b_{20} - b_{02}) \tag{B.1}$$

$$\alpha_{11} = \frac{1}{2}(a_{20} + a_{02}) + i\frac{1}{2}(b_{20} + b_{02}) \tag{B.2}$$

$$\alpha_{02} = \frac{1}{4}(a_{20} - a_{02} - b_{11}) + i\frac{1}{4}(a_{11} + b_{20} - b_{02}) \tag{B.3}$$

$$\alpha_{30} = \frac{1}{8}(a_{30} - a_{12} + b_{21} - b_{03}) + i\frac{1}{8}(-a_{21} + a_{03} + b_{30} - b_{12}) \tag{B.4}$$

$$\alpha_{21} = \frac{1}{8}(3a_{30} + a_{12} + b_{21} + 3b_{03}) + i\frac{1}{8}(-a_{21} - 3a_{03} + 3b_{30} + b_{12}) \tag{B.5}$$

$$\alpha_{12} = \frac{1}{8}(3a_{30} + a_{12} - b_{21} - 3b_{03}) + i\frac{1}{8}(a_{21} + 3a_{03} + 3b_{30} + b_{12}) \tag{B.6}$$

$$\alpha_{03} = \frac{1}{8}(a_{30} - a_{12} - b_{21} + b_{03}) + i\frac{1}{8}(a_{21} - a_{03} + b_{30} - b_{12}) \tag{B.7}$$

Coefficients α_{hklm} and β_{hklm} for the transformation in complex form in the analysis of a double NS bifurcation

Second order terms:

$$\alpha_{2000} = \frac{1}{4}(-a_{0200} + ia_{1100} + a_{2000} - ib_{0200} - b_{1100} + ib_{2000}) \tag{B.8}$$

$$\alpha_{0200} = \frac{1}{4}(-a_{0200} - ia_{1100} + a_{2000} - ib_{0200} + b_{1100} + ib_{2000}) \tag{B.9}$$

$$\alpha_{0020} = \frac{1}{4}(-a_{0002} + ia_{0011} + a_{0020} - ib_{0002} - b_{0011} + ib_{0020}) \tag{B.10}$$

$$\alpha_{0002} = \frac{1}{4}(-a_{0002} - ia_{0011} + a_{0020} - ib_{0002} + b_{0011} + ib_{0020}) \tag{B.11}$$

$$\alpha_{1100} = \frac{1}{2}(a_{0200} + a_{2000} + i(b_{0200} + b_{2000})) \tag{B.12}$$

$$\alpha_{1010} = \frac{1}{4}(-a_{0101} + ia_{0110} + ia_{1001} - a_{1010} - ib_{0101} + b_{0110} + b_{1001} + ib_{1010}) \tag{B.13}$$

$$\alpha_{1001} = \frac{1}{4}(a_{0101} + ia_{0110} - ia_{1001} + a_{1010} + ib_{0101} - b_{0110} + b_{1001} + ib_{1010}) \tag{B.14}$$

$$\alpha_{0110} = \frac{1}{4}(a_{0101} - ia_{0110} + ia_{1001} + a_{1010} + ib_{0101} + b_{0110} - b_{1001} + ib_{1010}) \quad \text{(B.15)}$$

$$\alpha_{0101} = \frac{1}{4}(-a_{0101} - ia_{0110} - ia_{1001} + a_{1010} - ib_{0101} + b_{0110} + b_{1001} + ib_{1010}) \quad \text{(B.16)}$$

$$\alpha_{0011} = \frac{1}{2}(a_{0002} + a_{0020} + i(b_{0002} + b_{0020})) \quad \text{(B.17)}$$

$$\beta_{2000} = \frac{1}{4}(-c_{0200} + ic_{1100} + c_{2000} - id_{0200} - d_{1100} + id_{2000}) \quad \text{(B.18)}$$

$$\beta_{0200} = \frac{1}{4}(-c_{0200} - ic_{1100} + c_{2000} - id_{0200} + d_{1100} + id_{2000}) \quad \text{(B.19)}$$

$$\beta_{0020} = \frac{1}{4}(-c_{0002} + ic_{0011} + c_{0020} - id_{0002} - d_{0011} + id_{0020}) \quad \text{(B.20)}$$

$$\beta_{0002} = \frac{1}{4}(-c_{0002} - ic_{0011} + c_{0020} - id_{0002} + d_{0011} + id_{0020}) \quad \text{(B.21)}$$

$$\beta_{1100} = \frac{1}{2}(c_{0200} + c_{2000} + i(d_{0200} + d_{2000})) \quad \text{(B.22)}$$

$$\beta_{1010} = \frac{1}{4}(-c_{0101} + ic_{0110} + ic_{1001} - c_{1010} - id_{0101} + d_{0110} + d_{1001} + id_{1010}) \quad \text{(B.23)}$$

$$\beta_{1001} = \frac{1}{4}(c_{0101} + ic_{0110} - ic_{1001} + c_{1010} + id_{0101} - d_{0110} + d_{1001} + id_{1010}) \quad \text{(B.24)}$$

$$\beta_{0110} = \frac{1}{4}(c_{0101} - ic_{0110} + ic_{1001} + c_{1010} + id_{0101} + d_{0110} - d_{1001} + id_{1010}) \quad \text{(B.25)}$$

$$\beta_{0101} = \frac{1}{4}(-c_{0101} - ic_{0110} - ic_{1001} + c_{1010} - id_{0101} + d_{0110} + d_{1001} + id_{1010}) \quad \text{(B.26)}$$

$$\beta_{0011} = \frac{1}{2}(c_{0002} + c_{0020} + i(d_{0002} + d_{0020})) \quad \text{(B.27)}$$

Third order terms:

$$\alpha_{3000} = -\frac{1}{8}i(a_{0300} - ia_{1200} - a_{2100} + ia_{3000} + ib_{0300} + b_{1200} - ib_{2100} - b_{3000}) \quad \text{(B.28)}$$

$$\alpha_{0300} = \frac{1}{8}(ia_{0300} - a_{1200} - ia_{2100} + a_{3000} - b_{0300} - ib_{1200} + b_{2100} + ib_{3000}) \quad \text{(B.29)}$$

$$\alpha_{0030} = -\frac{1}{8}i(a_{0003} - ia_{0012} - a_{0021} + ia_{0030} + ib_{0003} + b_{0012} - ib_{0021} - b_{0030}) \quad \text{(B.30)}$$

$$\alpha_{0003} = \frac{1}{8}(ia_{0003} - a_{0012} - ia_{0021} + a_{0030} - b_{0003} - ib_{0012} + b_{0021} + ib_{0030}) \quad \text{(B.31)}$$

$$\alpha_{2100} = \frac{1}{8}i(3a_{0300} - ia_{1200} + a_{2100} - 3ia_{3000} + 3ib_{0300} + b_{1200} + ib_{2100} + 3b_{3000}) \quad \text{(B.32)}$$

$$\alpha_{2010} = -\frac{1}{8}i(a_{0201} - i(a_{0210} + a_{1101} - ia_{1110} - ia_{2001} - a_{2010} - b_{0201} + ib_{0210} + ib_{1101} + b_{1110} + b_{2001} - ib_{2010})) \quad \text{(B.33)}$$

$$\alpha_{2001} = \frac{1}{8}i(a_{0201} + ia_{0210} - ia_{1101} + a_{1110} - a_{2001} - ia_{2010} + ib_{0201} - b_{0210} + b_{1101} + ib_{1110} - ib_{2001} + b_{2010}) \quad \text{(B.34)}$$

$$\alpha_{1200} = \frac{1}{8}(-3ia_{0300} + a_{1200} - ia_{2100} + 3a_{3000} + 3b_{0300} + ib_{1200} + b_{2100} + 3ib_{3000}) \quad \text{(B.35)}$$

$$\begin{aligned}
\alpha_{0210} &= \frac{1}{8}(-ia_{0201} - a_{0210} + a_{1101} - ia_{1110} + ia_{2001} + a_{2010} \\
&\quad +b_{0201} - ib_{0210} + ib_{1101} + b_{1110} - b_{2001} + ib_{2010}) && \text{(B.36)} \\
\alpha_{0201} &= \frac{1}{8}i(a_{0201} + i(a_{0210} + a_{1101} + i(a_{1110} + a_{2001} + ia_{2010} \\
&\quad -ib_{0201} + b_{0210} + b_{1101} + ib_{1110} + ib_{2001} - b_{2010}))) && \text{(B.37)} \\
\alpha_{1020} &= -\frac{1}{8}i(a_{0102} - ia_{0111} - ia_{1002} - a_{1011} + ia_{1020} + ib_{0102} + b_{0111} + b_{1002} - ib_{1011} - b_{1020}) && \text{(B.38)} \\
\alpha_{0120} &= \frac{1}{8}i(a_{0102} - ia_{0111} + ia_{1002} + a_{1011} - ia_{1020} + ib_{0102} + b_{0111} - b_{1002} + ib_{1011} + b_{1020}) && \text{(B.39)}
\end{aligned}$$

$$\begin{aligned}
\alpha_{0021} &= \frac{1}{8}i(3a_{0003} - ia_{0012} + a_{0021} - 3ia_{0030} + 3ib_{0003} + b_{0012} + ib_{0021} + 3b_{0030}) && \text{(B.40)} \\
\alpha_{1002} &= \frac{1}{8}(-ia_{0102} + a_{0111} - a_{1002} - ia_{1011} + a_{1020} + b_{0102} + ib_{0111} - ib_{1002} + b_{1011} + ib_{1020}) && \text{(B.41)} \\
\alpha_{0102} &= \frac{1}{8}i(a_{0102} + i(a_{0111} + a_{1002} + i(a_{1011} + ia_{1020} - ib_{0102} + b_{0111} + b_{1002} + ib_{1011} - b_{1020}))) && \text{(B.42)} \\
\alpha_{0012} &= \frac{1}{8}(-3ia_{0003} + a_{0012} - ia_{0021} + 3a_{0030} + 3b_{0003} + ib_{0012} + b_{0021} + 3ib_{0030}) && \text{(B.43)}
\end{aligned}$$

$$\begin{aligned}
\alpha_{1110} &= \frac{1}{4}i(a_{0201} - ia_{0210} + a_{2001} - ia_{2010} + ib_{0201} + b_{0210} + ib_{2001} + b_{2010}) && \text{(B.44)} \\
\alpha_{1011} &= \frac{1}{4}i(a_{0102} - ia_{1002} - ia_{1020} + ib_{0102} + b_{1002} + b_{1020}) && \text{(B.45)} \\
\alpha_{1101} &= \frac{1}{4}(-ia_{0201} + a_{0210} - ia_{2001} + a_{2010} + b_{0201} + ib_{0210} + b_{2001} + ib_{2010}) && \text{(B.46)} \\
\alpha_{0111} &= \frac{1}{4}(-ia_{0102} + a_{1002} + a_{1020} + b_{0102} + ib_{1002} + ib_{1020}) && \text{(B.47)}
\end{aligned}$$

$$\begin{aligned}
\beta_{3000} &= -\frac{1}{8}i(c_{0300} - ic_{1200} - c_{2100} + ic_{3000} + id_{0300} + d_{1200} - id_{2100} - d_{3000}) && \text{(B.48)} \\
\beta_{0300} &= \frac{1}{8}(ic_{0300} - c_{1200} - ic_{2100} + c_{3000} - d_{0300} - id_{1200} + d_{2100} + id_{3000}) && \text{(B.49)} \\
\beta_{0030} &= -\frac{1}{8}i(c_{0003} - ic_{0012} - c_{0021} + ic_{0030} + id_{0003} + d_{0012} - id_{0021} - d_{0030}) && \text{(B.50)} \\
\beta_{0003} &= \frac{1}{8}(ic_{0003} - c_{0012} - ic_{0021} + c_{0030} - d_{0003} - id_{0012} + d_{0021} + id_{0030}) && \text{(B.51)}
\end{aligned}$$

$$\begin{aligned}
\beta_{2100} &= \frac{1}{8}i(3c_{0300} - ic_{1200} + c_{2100} - 3ic_{3000} + 3id_{0300} + d_{1200} + id_{2100} + 3d_{3000}) && \text{(B.52)} \\
\beta_{2010} &= -\frac{1}{8}i(c_{0201} - i(c_{0210} + c_{1101} - ic_{1110} - ic_{2001} - c_{2010} \\
&\quad -d_{0201} + id_{0210} + id_{1101} + d_{1110} + d_{2001} - id_{2010})) && \text{(B.53)} \\
\beta_{2001} &= \frac{1}{8}i(c_{0201} + ic_{0210} - ic_{1101} + c_{1110} - c_{2001} - ic_{2010} \\
&\quad +id_{0201} - d_{0210} + d_{1101} + id_{1110} - id_{2001} + d_{2010}) && \text{(B.54)} \\
\beta_{1200} &= \frac{1}{8}(-3ic_{0300} + c_{1200} - ic_{2100} + 3c_{3000} + 3d_{0300} + id_{1200} + d_{2100} + 3id_{3000}) && \text{(B.55)}
\end{aligned}$$

$$\begin{aligned}
\beta_{0210} &= \frac{1}{8}(-ic_{0201} - c_{0210} + c_{1101} - ic_{1110} + ic_{2001} + c_{2010} \\
&\quad +d_{0201} - id_{0210} + id_{1101} + d_{1110} - d_{2001} + id_{2010}) && \text{(B.56)} \\
\beta_{0201} &= \frac{1}{8}i(c_{0201} + i(c_{0210} + c_{1101} + i(c_{1110} + c_{2001} + ic_{2010} \\
&\quad -id_{0201} + d_{0210} + d_{1101} + id_{1110} + id_{2001} - d_{2010}))) && \text{(B.57)} \\
\beta_{1020} &= -\frac{1}{8}i(c_{0102} - ic_{0111} - ic_{1002} - c_{1011} + ic_{1020} + id_{0102} + d_{0111} + d_{1002} - id_{1011} - d_{1020}) && \text{(B.58)} \\
\beta_{0120} &= \frac{1}{8}i(c_{0102} - ic_{0111} + ic_{1002} + c_{1011} - ic_{1020} + id_{0102} + d_{0111} - d_{1002} + id_{1011} + d_{1020}) && \text{(B.59)}
\end{aligned}$$

$$\begin{aligned}
\beta_{0021} &= \frac{1}{8}i(3c_{0003} - ic_{0012} + c_{0021} - 3ic_{0030} + 3id_{0003} + d_{0012} + id_{0021} + 3d_{0030}) && \text{(B.60)} \\
\beta_{1002} &= \frac{1}{8}(-ic_{0102} + c_{0111} - c_{1002} - ic_{1011} + c_{1020} + d_{0102} + id_{0111} - id_{1002} + d_{1011} + id_{1020}) && \text{(B.61)} \\
\beta_{0102} &= \frac{1}{8}i(c_{0102} + i(c_{0111} + c_{1002} + i(c_{1011} + ic_{1020} - id_{0102} + d_{0111} + d_{1002} + id_{1011} - d_{1020}))) && \text{(B.62)} \\
\beta_{0012} &= \frac{1}{8}(-3ic_{0003} + c_{0012} - ic_{0021} + 3c_{0030} + 3d_{0003} + id_{0012} + d_{0021} + 3id_{0030}) && \text{(B.63)}
\end{aligned}$$

$$\begin{aligned}
\beta_{1110} &= \frac{1}{4}i(c_{0201} - ic_{0210} + c_{2001} - ic_{2010} + id_{0201} + d_{0210} + id_{2001} + d_{2010}) && \text{(B.64)} \\
\beta_{1011} &= \frac{1}{4}i(c_{0102} - ic_{1002} - ic_{1020} + id_{0102} + d_{1002} + d_{1020}) && \text{(B.65)} \\
\beta_{1101} &= \frac{1}{4}(-ic_{0201} + c_{0210} - ic_{2001} + c_{2010} + d_{0201} + id_{0210} + d_{2001} + id_{2010}) && \text{(B.66)} \\
\beta_{0111} &= \frac{1}{4}(-ic_{0102} + c_{1002} + c_{1020} + d_{0102} + id_{1002} + id_{1020}) && \text{(B.67)}
\end{aligned}$$

The coefficients β_{hklm} can be simply obtained from the α_{hklm} substituting a with c and b with d.

Coefficients $\hat{\alpha}_{hklm}$ and $\hat{\beta}_{hklm}$ as a function of α_{hklm} and β_{hklm}, after the transformation in Eq. (3.46)

$$\begin{aligned}
\hat{\alpha}_{3000} &= \alpha_{3000} - \frac{\bar{\alpha}_{0200}\alpha_{1100}}{\bar{\mu}_{2,d} - \mu_{2,d}^2} - \frac{2\alpha_{2000}^2}{\mu_{2,d} - \mu_{2,d}^2} - \frac{\alpha_{1001}\bar{\beta}_{0200}}{-\mu_{2,d}^2 + \bar{\mu}_{4,d}} - \frac{\alpha_{1010}\beta_{2000}}{-\mu_{2,d}^2 + \mu_{4,d}} && \text{(B.68)} \\
\hat{\alpha}_{0300} &= \alpha_{0300} - \frac{2\alpha_{0200}\bar{\alpha}_{2000}}{\bar{\mu}_{2,d} - \bar{\mu}_{2,d}^2} - \frac{\alpha_{0200}\alpha_{1100}}{-\bar{\mu}_{2,d}^2 + \mu_{2,d}} - \frac{\alpha_{0101}\bar{\beta}_{2000}}{-\bar{\mu}_{2,d}^2 + \bar{\mu}_{4,d}} - \frac{\alpha_{0110}\beta_{0200}}{-\bar{\mu}_{2,d}^2 + \mu_{4,d}} && \text{(B.69)} \\
\hat{\alpha}_{0030} &= \alpha_{0030} - \frac{\bar{\alpha}_{0002}\alpha_{0110}}{\bar{\mu}_{2,d} - \mu_{4,d}^2} - \frac{\alpha_{0020}\alpha_{1010}}{\mu_{2,d} - \mu_{4,d}^2} - \frac{\alpha_{0011}\bar{\beta}_{0002}}{\bar{\mu}_{4,d} - \mu_{4,d}^2} - \frac{2\alpha_{0020}\beta_{0020}}{\mu_{4,d} - \mu_{4,d}^2} && \text{(B.70)} \\
\hat{\alpha}_{0003} &= \alpha_{0003} - \frac{\bar{\alpha}_{0020}\alpha_{0101}}{\bar{\mu}_{2,d} - \bar{\mu}_{4,d}^2} - \frac{\alpha_{0002}\alpha_{1001}}{\mu_{2,d} - \bar{\mu}_{4,d}^2} - \frac{2\alpha_{0002}\bar{\beta}_{0020}}{\bar{\mu}_{4,d} - \bar{\mu}_{4,d}^2} - \frac{\alpha_{0011}\beta_{0002}}{-\bar{\mu}_{4,d}^2 + \mu_{4,d}} && \text{(B.71)}
\end{aligned}$$

$$\begin{aligned}\hat{\alpha}_{2100} &= \alpha_{2100} - \frac{\alpha_{1100}\bar{\alpha}_{1100}}{-1+\bar{\mu}_{2,d}} - \frac{2\alpha_{1100}\alpha_{2000}}{-1+\mu_{2,d}} - \frac{2\alpha_{0200}\bar{\alpha}_{0200}}{\bar{\mu}_{2,d}-\mu_{2,d}^2} - \frac{\alpha_{1100}\alpha_{2000}}{\mu_{2,d}-\mu_{2,d}^2} \\ &\quad - \frac{\alpha_{1001}\bar{\beta}_{1100}}{-1+\bar{\mu}_{4,d}} - \frac{\alpha_{0101}\bar{\beta}_{0200}}{-\mu_{2,d}^2+\bar{\mu}_{4,d}} - \frac{\alpha_{1010}\beta_{1100}}{-1+\mu_{4,d}} - \frac{\alpha_{0110}\beta_{2000}}{-\mu_{2,d}^2+\mu_{4,d}} \end{aligned} \tag{B.72}$$

$$\begin{aligned}\hat{\alpha}_{2010} &= \alpha_{2010} - \frac{\alpha_{0110}\bar{\alpha}_{0200}}{\bar{\mu}_{2,d}-\mu_{2,d}^2} - \frac{\alpha_{1010}\alpha_{2000}}{\mu_{2,d}-\mu_{2,d}^2} - \frac{\alpha_{0011}\bar{\beta}_{0200}}{-\mu_{2,d}^2+\bar{\mu}_{4,d}} - \frac{2\alpha_{0020}\beta_{2000}}{-\mu_{2,d}^2+\mu_{4,d}} \\ &\quad - \frac{\bar{\alpha}_{0101}\alpha_{1100}}{\bar{\mu}_{2,d}-\mu_{2,d}\mu_{4,d}} - \frac{2\alpha_{1010}\alpha_{2000}}{\mu_{2,d}-\mu_{2,d}\mu_{4,d}} - \frac{\alpha_{1001}\bar{\beta}_{0101}}{\bar{\mu}_{4,d}-\mu_{2,d}\mu_{4,d}} - \frac{\alpha_{1010}\beta_{1010}}{\mu_{4,d}-\mu_{2,d}\mu_{4,d}} \end{aligned} \tag{B.73}$$

$$\begin{aligned}\hat{\alpha}_{2001} &= \alpha_{2001} - \frac{\alpha_{0101}\bar{\alpha}_{0200}}{\bar{\mu}_{2,d}-\mu_{2,d}^2} - \frac{\alpha_{1001}\alpha_{2000}}{\mu_{2,d}-\mu_{2,d}^2} - \frac{2\alpha_{0002}\bar{\beta}_{0200}}{-\mu_{2,d}^2+\bar{\mu}_{4,d}} - \frac{2\alpha_{1001}\alpha_{2000}}{\mu_{2,d}-\mu_{2,d}\bar{\mu}_{4,d}} \\ &\quad - \frac{\alpha_{1001}\bar{\beta}_{0110}}{\bar{\mu}_{4,d}-\mu_{2,d}\bar{\mu}_{4,d}} - \frac{\alpha_{0011}\beta_{2000}}{-\mu_{2,d}^2+\mu_{4,d}} - \frac{\alpha_{1010}\beta_{1001}}{-\mu_{2,d}\bar{\mu}_{4,d}+\mu_{4,d}} - \frac{\alpha_{0110}\alpha_{1100}}{\mu_{2,d}-\bar{\mu}_{2,d}\mu_{4,d}} \end{aligned} \tag{B.74}$$

$$\begin{aligned}\hat{\alpha}_{1200} &= \alpha_{1200} - \frac{2\alpha_{0200}\bar{\alpha}_{1100}}{-1+\bar{\mu}_{2,d}} - \frac{\alpha_{1100}\bar{\alpha}_{2000}}{\bar{\mu}_{2,d}-\bar{\mu}_{2,d}^2} - \frac{\alpha_{1100}^2}{-1+\mu_{2,d}} - \frac{2\alpha_{0200}\alpha_{2000}}{-\bar{\mu}_{2,d}^2+\mu_{2,d}} \\ &\quad - \frac{\alpha_{0101}\bar{\beta}_{1100}}{-1+\bar{\mu}_{4,d}} - \frac{\alpha_{1001}\bar{\beta}_{2000}}{-\bar{\mu}_{2,d}^2+\bar{\mu}_{4,d}} - \frac{\alpha_{0110}\beta_{1100}}{-1+\mu_{4,d}} - \frac{\alpha_{1010}\beta_{0200}}{-\bar{\mu}_{2,d}^2+\mu_{4,d}} \end{aligned} \tag{B.75}$$

$$\begin{aligned}\hat{\alpha}_{0210} &= \alpha_{0210} - \frac{\alpha_{0110}\bar{\alpha}_{2000}}{\bar{\mu}_{2,d}-\bar{\mu}_{2,d}^2} - \frac{\alpha_{0200}\alpha_{1010}}{-\bar{\mu}_{2,d}^2+\mu_{2,d}} - \frac{\alpha_{0011}\bar{\beta}_{2000}}{-\bar{\mu}_{2,d}^2+\bar{\mu}_{4,d}} - \frac{2\alpha_{0020}\beta_{0200}}{-\bar{\mu}_{2,d}^2+\mu_{4,d}} \\ &\quad - \frac{2\alpha_{0200}\bar{\alpha}_{1001}}{\bar{\mu}_{2,d}-\bar{\mu}_{2,d}\mu_{4,d}} - \frac{\alpha_{0110}\alpha_{1100}}{\mu_{2,d}-\bar{\mu}_{2,d}\mu_{4,d}} - \frac{\alpha_{0101}\bar{\beta}_{1001}}{\bar{\mu}_{4,d}-\bar{\mu}_{2,d}\mu_{4,d}} - \frac{\alpha_{0110}\beta_{0110}}{\mu_{4,d}-\bar{\mu}_{2,d}\mu_{4,d}} \end{aligned} \tag{B.76}$$

$$\begin{aligned}\hat{\alpha}_{0201} &= \alpha_{0201} - \frac{\alpha_{0101}\bar{\alpha}_{2000}}{\bar{\mu}_{2,d}-\bar{\mu}_{2,d}^2} - \frac{\alpha_{0200}\alpha_{1001}}{-\bar{\mu}_{2,d}^2+\mu_{2,d}} - \frac{2\alpha_{0002}\bar{\beta}_{2000}}{-\bar{\mu}_{2,d}^2+\bar{\mu}_{4,d}} - \frac{2\alpha_{0200}\bar{\alpha}_{1010}}{\bar{\mu}_{2,d}-\bar{\mu}_{2,d}\bar{\mu}_{4,d}} \\ &\quad - \frac{\alpha_{0101}\alpha_{1100}}{\mu_{2,d}-\bar{\mu}_{2,d}\bar{\mu}_{4,d}} - \frac{\alpha_{0101}\bar{\beta}_{1010}}{\bar{\mu}_{4,d}-\bar{\mu}_{2,d}\bar{\mu}_{4,d}} - \frac{\alpha_{0011}\beta_{0200}}{-\bar{\mu}_{2,d}^2+\mu_{4,d}} - \frac{\alpha_{0110}\beta_{0101}}{-\bar{\mu}_{2,d}\bar{\mu}_{4,d}+\mu_{4,d}} \end{aligned} \tag{B.77}$$

$$\begin{aligned}\hat{\alpha}_{1020} &= \alpha_{1020} - \frac{\bar{\alpha}_{0101}\alpha_{0110}}{\bar{\mu}_{2,d}-\mu_{2,d}\mu_{4,d}} - \frac{\alpha_{1010}^2}{\mu_{2,d}-\mu_{2,d}\mu_{4,d}} - \frac{\alpha_{0011}\bar{\beta}_{0101}}{\bar{\mu}_{4,d}-\mu_{2,d}\mu_{4,d}} - \frac{2\alpha_{0020}\beta_{1010}}{\mu_{4,d}-\mu_{2,d}\mu_{4,d}} \\ &\quad - \frac{\bar{\alpha}_{0002}\alpha_{1100}}{\bar{\mu}_{2,d}-\mu_{4,d}^2} - \frac{2\alpha_{0020}\alpha_{2000}}{\mu_{2,d}-\mu_{4,d}^2} - \frac{\alpha_{1001}\bar{\beta}_{0002}}{\bar{\mu}_{4,d}-\mu_{4,d}^2} - \frac{\alpha_{1010}\beta_{0020}}{\mu_{4,d}-\mu_{4,d}^2} \end{aligned} \tag{B.78}$$

$$\begin{aligned}\hat{\alpha}_{0120} &= \alpha_{0120} - \frac{\alpha_{0110}\bar{\alpha}_{1001}}{\bar{\mu}_{2,d}-\bar{\mu}_{2,d}\mu_{4,d}} - \frac{\alpha_{0110}\alpha_{1010}}{\mu_{2,d}-\bar{\mu}_{2,d}\mu_{4,d}} - \frac{\alpha_{0011}\bar{\beta}_{1001}}{\bar{\mu}_{4,d}-\bar{\mu}_{2,d}\mu_{4,d}} - \frac{2\alpha_{0020}\beta_{0110}}{\mu_{4,d}-\bar{\mu}_{2,d}\mu_{4,d}} \\ &\quad - \frac{2\bar{\alpha}_{0002}\alpha_{0200}}{\bar{\mu}_{2,d}-\mu_{4,d}^2} - \frac{\alpha_{0020}\alpha_{1100}}{\mu_{2,d}-\mu_{4,d}^2} - \frac{\alpha_{0101}\bar{\beta}_{0002}}{\bar{\mu}_{4,d}-\mu_{4,d}^2} - \frac{\alpha_{0110}\beta_{0020}}{\mu_{4,d}-\mu_{4,d}^2} \end{aligned} \tag{B.79}$$

$$\begin{aligned}\hat{\alpha}_{0021} &= \alpha_{0021} - \frac{\bar{\alpha}_{0011}\alpha_{0110}}{-1+\bar{\mu}_{2,d}} - \frac{\alpha_{0011}\alpha_{1010}}{-1+\mu_{2,d}} - \frac{\alpha_{0011}\bar{\beta}_{0011}}{-1+\bar{\mu}_{4,d}} - \frac{2\alpha_{0020}\beta_{0011}}{-1+\mu_{4,d}} - \frac{\bar{\alpha}_{0002}\alpha_{0101}}{\bar{\mu}_{2,d}-\mu_{4,d}^2} \\ &\quad - \frac{\alpha_{0020}\alpha_{1001}}{\mu_{2,d}-\mu_{4,d}^2} - \frac{2\alpha_{0002}\bar{\beta}_{0002}}{\bar{\mu}_{4,d}-\mu_{4,d}^2} - \frac{\alpha_{0011}\beta_{0020}}{\mu_{4,d}-\mu_{4,d}^2} \qquad \text{(B.80)}\\ \hat{\alpha}_{1002} &= \alpha_{1002} - \frac{\alpha_{1001}^2}{\mu_{2,d}-\mu_{2,d}\bar{\mu}_{4,d}} - \frac{2\alpha_{0002}\bar{\beta}_{0110}}{\bar{\mu}_{4,d}-\mu_{2,d}\bar{\mu}_{4,d}} - \frac{\bar{\alpha}_{0020}\alpha_{1100}}{\bar{\mu}_{2,d}-\bar{\mu}_{4,d}^2} - \frac{2\alpha_{0002}\alpha_{2000}}{\mu_{2,d}-\bar{\mu}_{4,d}^2} \\ &\quad - \frac{\alpha_{1001}\bar{\beta}_{0020}}{\bar{\mu}_{4,d}-\bar{\mu}_{4,d}^2} - \frac{\alpha_{0011}\beta_{1001}}{-\mu_{2,d}\bar{\mu}_{4,d}+\mu_{4,d}} - \frac{\alpha_{1010}\beta_{0002}}{-\bar{\mu}_{4,d}^2+\mu_{4,d}} - \frac{\alpha_{0101}\alpha_{0110}}{\mu_{2,d}-\bar{\mu}_{2,d}\mu_{4,d}} \qquad \text{(B.81)}\\ \hat{\alpha}_{0102} &= \alpha_{0102} - \frac{\alpha_{0101}\bar{\alpha}_{1010}}{\bar{\mu}_{2,d}-\bar{\mu}_{2,d}\bar{\mu}_{4,d}} - \frac{\alpha_{0101}\alpha_{1001}}{\mu_{2,d}-\bar{\mu}_{2,d}\bar{\mu}_{4,d}} - \frac{2\alpha_{0002}\bar{\beta}_{1010}}{\bar{\mu}_{4,d}-\bar{\mu}_{2,d}\bar{\mu}_{4,d}} - \frac{2\bar{\alpha}_{0020}\alpha_{0200}}{\bar{\mu}_{2,d}-\bar{\mu}_{4,d}^2} \\ &\quad - \frac{\alpha_{0002}\alpha_{1100}}{\mu_{2,d}-\bar{\mu}_{4,d}^2} - \frac{\alpha_{0101}\bar{\beta}_{0020}}{\bar{\mu}_{4,d}-\bar{\mu}_{4,d}^2} - \frac{\alpha_{0011}\beta_{0101}}{-\bar{\mu}_{2,d}\bar{\mu}_{4,d}+\mu_{4,d}} - \frac{\alpha_{0110}\beta_{0002}}{-\bar{\mu}_{4,d}^2+\mu_{4,d}} \qquad \text{(B.82)}\\ \hat{\alpha}_{0012} &= \alpha_{0012} - \frac{\bar{\alpha}_{0011}\alpha_{0101}}{-1+\bar{\mu}_{2,d}} - \frac{\alpha_{0011}\alpha_{1001}}{-1+\mu_{2,d}} - \frac{2\alpha_{0002}\bar{\beta}_{0011}}{-1+\bar{\mu}_{4,d}} - \frac{\bar{\alpha}_{0020}\alpha_{0110}}{\bar{\mu}_{2,d}-\bar{\mu}_{4,d}^2} - \frac{\alpha_{0002}\alpha_{1010}}{\mu_{2,d}-\bar{\mu}_{4,d}^2} \\ &\quad - \frac{\alpha_{0011}\bar{\beta}_{0020}}{\bar{\mu}_{4,d}-\bar{\mu}_{4,d}^2} - \frac{\alpha_{0011}\beta_{0011}}{-1+\mu_{4,d}} - \frac{2\alpha_{0020}\beta_{0002}}{-\bar{\mu}_{4,d}^2+\mu_{4,d}} \qquad \text{(B.83)}\end{aligned}$$

$$\begin{aligned}\hat{\alpha}_{1110} &= \alpha_{1110} - \frac{\alpha_{0110}\bar{\alpha}_{1100}}{-1+\bar{\mu}_{2,d}} - \frac{\alpha_{1010}\alpha_{1100}}{-1+\mu_{2,d}} - \frac{\alpha_{0011}\bar{\beta}_{1100}}{-1+\bar{\mu}_{4,d}} - \frac{2\alpha_{0020}\beta_{1100}}{-1+\mu_{4,d}} - \frac{\bar{\alpha}_{1001}\alpha_{1100}}{\bar{\mu}_{2,d}-\bar{\mu}_{2,d}\mu_{4,d}} \\ &\quad - \frac{2\alpha_{0110}\alpha_{2000}}{\mu_{2,d}-\bar{\mu}_{2,d}\mu_{4,d}} - \frac{\alpha_{1001}\bar{\beta}_{1001}}{\bar{\mu}_{4,d}-\bar{\mu}_{2,d}\mu_{4,d}} - \frac{\alpha_{1010}\beta_{0110}}{\mu_{4,d}-\bar{\mu}_{2,d}\mu_{4,d}} - \frac{2\bar{\alpha}_{0101}\alpha_{0200}}{\bar{\mu}_{2,d}-\mu_{2,d}\mu_{4,d}} - \frac{\alpha_{1010}\alpha_{1100}}{\mu_{2,d}-\mu_{2,d}\mu_{4,d}} \\ &\quad - \frac{\alpha_{0101}\bar{\beta}_{0101}}{\bar{\mu}_{4,d}-\mu_{2,d}\mu_{4,d}} - \frac{\alpha_{0110}\beta_{1010}}{\mu_{4,d}-\mu_{2,d}\mu_{4,d}} \qquad \text{(B.84)}\\ \hat{\alpha}_{1101} &= \alpha_{1101} - \frac{\alpha_{0101}\bar{\alpha}_{1100}}{-1+\bar{\mu}_{2,d}} - \frac{\alpha_{1001}\alpha_{1100}}{-1+\mu_{2,d}} - \frac{2\alpha_{0002}\bar{\beta}_{1100}}{-1+\bar{\mu}_{4,d}} - \frac{\bar{\alpha}_{1010}\alpha_{1100}}{\bar{\mu}_{2,d}-\bar{\mu}_{2,d}\bar{\mu}_{4,d}} - \frac{2\alpha_{0101}\alpha_{2000}}{\mu_{2,d}-\bar{\mu}_{2,d}\bar{\mu}_{4,d}} \\ &\quad - \frac{\alpha_{1001}\bar{\beta}_{1010}}{\bar{\mu}_{4,d}-\bar{\mu}_{2,d}\bar{\mu}_{4,d}} - \frac{\alpha_{1001}\alpha_{1100}}{\mu_{2,d}-\mu_{2,d}\bar{\mu}_{4,d}} - \frac{\alpha_{0101}\bar{\beta}_{0110}}{\bar{\mu}_{4,d}-\mu_{2,d}\bar{\mu}_{4,d}} - \frac{\alpha_{0011}\beta_{1100}}{-1+\mu_{4,d}} - \frac{\alpha_{1010}\beta_{0101}}{-\bar{\mu}_{2,d}\bar{\mu}_{4,d}+\mu_{4,d}} \\ &\quad - \frac{\alpha_{0110}\beta_{1001}}{-\mu_{2,d}\bar{\mu}_{4,d}+\mu_{4,d}} - \frac{2\alpha_{0110}\alpha_{0200}}{\mu_{2,d}-\bar{\mu}_{2,d}\mu_{4,d}} \qquad \text{(B.85)}\\ \hat{\alpha}_{1011} &= \alpha_{1011} - \frac{\bar{\alpha}_{0011}\alpha_{1100}}{-1+\bar{\mu}_{2,d}} - \frac{2\alpha_{0011}\alpha_{2000}}{-1+\mu_{2,d}} - \frac{\alpha_{1001}\bar{\beta}_{0011}}{-1+\bar{\mu}_{4,d}} - \frac{\alpha_{1001}\alpha_{1010}}{\mu_{2,d}-\mu_{2,d}\bar{\mu}_{4,d}} - \frac{\alpha_{0011}\bar{\beta}_{0110}}{\bar{\mu}_{4,d}-\mu_{2,d}\bar{\mu}_{4,d}} \\ &\quad - \frac{\alpha_{1010}\beta_{0011}}{-1+\mu_{4,d}} - \frac{2\alpha_{0020}\beta_{1001}}{-\mu_{2,d}\bar{\mu}_{4,d}+\mu_{4,d}} - \frac{\alpha_{0110}^2}{\mu_{2,d}-\bar{\mu}_{2,d}\mu_{4,d}} - \frac{\alpha_{0101}\bar{\alpha}_{0101}}{\bar{\mu}_{2,d}-\mu_{2,d}\mu_{4,d}} - \frac{\alpha_{1001}\alpha_{1010}}{\mu_{2,d}-\mu_{2,d}\mu_{4,d}} \\ &\quad - \frac{2\alpha_{0002}\bar{\beta}_{0101}}{\bar{\mu}_{4,d}-\mu_{2,d}\mu_{4,d}} - \frac{\alpha_{0011}\beta_{1010}}{\mu_{4,d}-\mu_{2,d}\mu_{4,d}} \qquad \text{(B.86)}\\ \hat{\alpha}_{0111} &= \alpha_{0111} - \frac{2\bar{\alpha}_{0011}\alpha_{0200}}{-1+\bar{\mu}_{2,d}} - \frac{\alpha_{0011}\alpha_{1100}}{-1+\mu_{2,d}} - \frac{\alpha_{0101}\bar{\beta}_{0011}}{-1+\bar{\mu}_{4,d}} - \frac{\alpha_{0110}\bar{\alpha}_{1010}}{\bar{\mu}_{2,d}-\bar{\mu}_{2,d}\bar{\mu}_{4,d}} - \frac{\alpha_{0101}\alpha_{1010}}{\mu_{2,d}-\bar{\mu}_{2,d}\bar{\mu}_{4,d}} \\ &\quad - \frac{\alpha_{0011}\bar{\beta}_{1010}}{\bar{\mu}_{4,d}-\bar{\mu}_{2,d}\bar{\mu}_{4,d}} - \frac{\alpha_{0110}\beta_{0011}}{-1+\mu_{4,d}} - \frac{2\alpha_{0020}\beta_{0101}}{-\bar{\mu}_{2,d}\bar{\mu}_{4,d}+\mu_{4,d}} - \frac{\alpha_{0101}\bar{\alpha}_{1001}}{\bar{\mu}_{2,d}-\bar{\mu}_{2,d}\mu_{4,d}} - \frac{\alpha_{0110}\alpha_{1001}}{\mu_{2,d}-\bar{\mu}_{2,d}\mu_{4,d}} \\ &\quad - \frac{2\alpha_{0002}\bar{\beta}_{1001}}{\bar{\mu}_{4,d}-\bar{\mu}_{2,d}\mu_{4,d}} - \frac{\alpha_{0011}\beta_{0110}}{\mu_{4,d}-\bar{\mu}_{2,d}\mu_{4,d}} \qquad \text{(B.87)}\end{aligned}$$

$$\hat{\beta}_{3000} = \beta_{3000} - \frac{\bar{\alpha}_{0200}\beta_{1100}}{\bar{\mu}_{2,d}-\mu_{2,d}^2} - \frac{2\alpha_{2000}\beta_{2000}}{\mu_{2,d}-\mu_{2,d}^2} - \frac{\bar{\beta}_{0200}\beta_{1001}}{-\mu_{2,d}^2+\bar{\mu}_{4,d}} - \frac{\beta_{1010}\beta_{2000}}{-\mu_{2,d}^2+\mu_{4,d}} \tag{B.88}$$

$$\hat{\beta}_{0300} = \beta_{0300} - \frac{2\bar{\alpha}_{2000}\beta_{0200}}{\bar{\mu}_{2,d}-\bar{\mu}_{2,d}^2} - \frac{\alpha_{0200}\beta_{1100}}{-\bar{\mu}_{2,d}^2+\mu_{2,d}} - \frac{\beta_{0101}\bar{\beta}_{2000}}{-\bar{\mu}_{2,d}^2+\bar{\mu}_{4,d}} - \frac{\beta_{0110}\beta_{0200}}{-\bar{\mu}_{2,d}^2+\mu_{4,d}} \tag{B.89}$$

$$\hat{\beta}_{0030} = \beta_{0030} - \frac{\bar{\alpha}_{0002}\beta_{0110}}{\bar{\mu}_{2,d}-\mu_{4,d}^2} - \frac{\alpha_{0020}\beta_{1010}}{\mu_{2,d}-\mu_{4,d}^2} - \frac{\bar{\beta}_{0002}\beta_{0011}}{\bar{\mu}_{4,d}-\mu_{4,d}^2} - \frac{2\beta_{0020}^2}{\mu_{4,d}-\mu_{4,d}^2} \tag{B.90}$$

$$\hat{\beta}_{0003} = \beta_{0003} - \frac{\bar{\alpha}_{0020}\beta_{0101}}{\bar{\mu}_{2,d}-\bar{\mu}_{4,d}^2} - \frac{\alpha_{0002}\beta_{1001}}{\mu_{2,d}-\bar{\mu}_{4,d}^2} - \frac{2\beta_{0002}\bar{\beta}_{0020}}{\bar{\mu}_{4,d}-\bar{\mu}_{4,d}^2} - \frac{\beta_{0002}\beta_{0011}}{-\bar{\mu}_{4,d}^2+\mu_{4,d}} \tag{B.91}$$

$$\begin{aligned}\hat{\beta}_{2100} = \beta_{2100} &- \frac{\bar{\alpha}_{1100}\beta_{1100}}{-1+\bar{\mu}_{2,d}} - \frac{2\alpha_{1100}\beta_{2000}}{-1+\mu_{2,d}} - \frac{2\bar{\alpha}_{0200}\beta_{0200}}{\bar{\mu}_{2,d}-\mu_{2,d}^2} - \frac{\alpha_{2000}\beta_{1100}}{\mu_{2,d}-\mu_{2,d}^2} - \frac{\beta_{1001}\bar{\beta}_{1100}}{-1+\bar{\mu}_{4,d}} \\ &- \frac{\beta_{0101}\bar{\beta}_{0200}}{-\mu_{2,d}^2+\bar{\mu}_{4,d}} - \frac{\beta_{1010}\beta_{1100}}{-1+\mu_{4,d}} - \frac{\beta_{0110}\beta_{2000}}{-\mu_{2,d}^2+\mu_{4,d}}\end{aligned} \tag{B.92}$$

$$\begin{aligned}\hat{\beta}_{2010} = \beta_{2010} &- \frac{\bar{\alpha}_{0200}\beta_{0110}}{\bar{\mu}_{2,d}-\mu_{2,d}^2} - \frac{\alpha_{2000}\beta_{1010}}{\mu_{2,d}-\mu_{2,d}^2} - \frac{\beta_{0011}\bar{\beta}_{0200}}{-\mu_{2,d}^2+\bar{\mu}_{4,d}} - \frac{2\beta_{0020}\beta_{2000}}{-\mu_{2,d}^2+\mu_{4,d}} - \frac{\bar{\alpha}_{0101}\beta_{1100}}{\bar{\mu}_{2,d}-\mu_{2,d}\mu_{4,d}} \\ &- \frac{2\alpha_{1010}\beta_{2000}}{\mu_{2,d}-\mu_{2,d}\mu_{4,d}} - \frac{\bar{\beta}_{0101}\beta_{1001}}{\bar{\mu}_{4,d}-\mu_{2,d}\mu_{4,d}} - \frac{\beta_{1010}^2}{\mu_{4,d}-\mu_{2,d}\mu_{4,d}}\end{aligned} \tag{B.93}$$

$$\begin{aligned}\hat{\beta}_{2001} = \beta_{2001} &- \frac{\bar{\alpha}_{0200}\beta_{0101}}{\bar{\mu}_{2,d}-\mu_{2,d}^2} - \frac{\alpha_{2000}\beta_{1001}}{\mu_{2,d}-\mu_{2,d}^2} - \frac{2\beta_{0002}\bar{\beta}_{0200}}{-\mu_{2,d}^2+\bar{\mu}_{4,d}} - \frac{2\alpha_{1001}\beta_{2000}}{\mu_{2,d}-\mu_{2,d}\bar{\mu}_{4,d}} - \frac{\bar{\beta}_{0110}\beta_{1001}}{\bar{\mu}_{4,d}-\mu_{2,d}\bar{\mu}_{4,d}} \\ &- \frac{\beta_{0011}\beta_{2000}}{-\mu_{2,d}^2+\mu_{4,d}} - \frac{\beta_{1001}\beta_{1010}}{-\mu_{2,d}\bar{\mu}_{4,d}+\mu_{4,d}} - \frac{\alpha_{0110}\beta_{1100}}{\mu_{2,d}-\bar{\mu}_{2,d}\mu_{4,d}}\end{aligned} \tag{B.94}$$

$$\begin{aligned}\hat{\beta}_{1200} = \beta_{1200} &- \frac{2\bar{\alpha}_{1100}\beta_{0200}}{-1+\bar{\mu}_{2,d}} - \frac{\bar{\alpha}_{2000}\beta_{1100}}{\bar{\mu}_{2,d}-\bar{\mu}_{2,d}^2} - \frac{\alpha_{1100}\beta_{1100}}{-1+\mu_{2,d}} - \frac{2\alpha_{0200}\beta_{2000}}{-\bar{\mu}_{2,d}^2+\mu_{2,d}} - \frac{\beta_{0101}\bar{\beta}_{1100}}{-1+\bar{\mu}_{4,d}} \\ &- \frac{\beta_{1001}\bar{\beta}_{2000}}{-\bar{\mu}_{2,d}^2+\bar{\mu}_{4,d}} - \frac{\beta_{0110}\beta_{1100}}{-1+\mu_{4,d}} - \frac{\beta_{0200}\beta_{1010}}{-\bar{\mu}_{2,d}^2+\mu_{4,d}}\end{aligned} \tag{B.95}$$

$$\begin{aligned}\hat{\beta}_{0210} = \beta_{0210} &- \frac{\bar{\alpha}_{2000}\beta_{0110}}{\bar{\mu}_{2,d}-\bar{\mu}_{2,d}^2} - \frac{\alpha_{0200}\beta_{1010}}{-\bar{\mu}_{2,d}^2+\mu_{2,d}} - \frac{\beta_{0011}\bar{\beta}_{2000}}{-\bar{\mu}_{2,d}^2+\bar{\mu}_{4,d}} - \frac{2\beta_{0020}\beta_{0200}}{-\bar{\mu}_{2,d}^2+\mu_{4,d}} - \frac{2\bar{\alpha}_{1001}\beta_{0200}}{\bar{\mu}_{2,d}-\bar{\mu}_{2,d}\mu_{4,d}} \\ &- \frac{\alpha_{0110}\beta_{1100}}{\mu_{2,d}-\bar{\mu}_{2,d}\mu_{4,d}} - \frac{\beta_{0101}\bar{\beta}_{1001}}{\bar{\mu}_{4,d}-\bar{\mu}_{2,d}\mu_{4,d}} - \frac{\beta_{0110}^2}{\mu_{4,d}-\bar{\mu}_{2,d}\mu_{4,d}}\end{aligned} \tag{B.96}$$

$$\begin{aligned}\hat{\beta}_{0201} = \beta_{0201} &- \frac{\bar{\alpha}_{2000}\beta_{0101}}{\bar{\mu}_{2,d}-\bar{\mu}_{2,d}^2} - \frac{\alpha_{0200}\beta_{1001}}{-\bar{\mu}_{2,d}^2+\mu_{2,d}} - \frac{2\beta_{0002}\bar{\beta}_{2000}}{-\bar{\mu}_{2,d}^2+\bar{\mu}_{4,d}} - \frac{2\bar{\alpha}_{1010}\beta_{0200}}{\bar{\mu}_{2,d}-\bar{\mu}_{2,d}\bar{\mu}_{4,d}} - \frac{\alpha_{0101}\beta_{1100}}{\mu_{2,d}-\bar{\mu}_{2,d}\bar{\mu}_{4,d}} \\ &- \frac{\beta_{0101}\bar{\beta}_{1010}}{\bar{\mu}_{4,d}-\bar{\mu}_{2,d}\bar{\mu}_{4,d}} - \frac{\beta_{0011}\beta_{0200}}{-\bar{\mu}_{2,d}^2+\mu_{4,d}} - \frac{\beta_{0101}\beta_{0110}}{-\bar{\mu}_{2,d}\bar{\mu}_{4,d}+\mu_{4,d}}\end{aligned} \tag{B.97}$$

$$\begin{aligned}\hat{\beta}_{1020} = \beta_{1020} &- \frac{\bar{\alpha}_{0101}\beta_{0110}}{\bar{\mu}_{2,d}-\mu_{2,d}\mu_{4,d}} - \frac{\alpha_{1010}\beta_{1010}}{\mu_{2,d}-\mu_{2,d}\mu_{4,d}} - \frac{\beta_{0011}\bar{\beta}_{0101}}{\bar{\mu}_{4,d}-\mu_{2,d}\mu_{4,d}} - \frac{2\beta_{0020}\beta_{1010}}{\mu_{4,d}-\mu_{2,d}\mu_{4,d}} - \frac{\bar{\alpha}_{0002}\beta_{1100}}{\bar{\mu}_{2,d}-\mu_{4,d}^2} \\ &- \frac{2\alpha_{0020}\beta_{2000}}{\mu_{2,d}-\mu_{4,d}^2} - \frac{\bar{\beta}_{0002}\beta_{1001}}{\bar{\mu}_{4,d}-\mu_{4,d}^2} - \frac{\beta_{0020}\beta_{1010}}{\mu_{4,d}-\mu_{4,d}^2}\end{aligned} \tag{B.98}$$

$$\begin{aligned}\hat{\beta}_{0120} = \beta_{0120} &- \frac{\bar{\alpha}_{1001}\beta_{0110}}{\bar{\mu}_{2,d}-\bar{\mu}_{2,d}\mu_{4,d}} - \frac{\alpha_{0110}\beta_{1010}}{\mu_{2,d}-\bar{\mu}_{2,d}\mu_{4,d}} - \frac{\beta_{0011}\bar{\beta}_{1001}}{\bar{\mu}_{4,d}-\bar{\mu}_{2,d}\mu_{4,d}} - \frac{2\beta_{0020}\beta_{0110}}{\mu_{4,d}-\bar{\mu}_{2,d}\mu_{4,d}} - \frac{2\bar{\alpha}_{0002}\beta_{0200}}{\bar{\mu}_{2,d}-\mu_{4,d}^2} \\ &- \frac{\alpha_{0020}\beta_{1100}}{\mu_{2,d}-\mu_{4,d}^2} - \frac{\bar{\beta}_{0002}\beta_{0101}}{\bar{\mu}_{4,d}-\mu_{4,d}^2} - \frac{\beta_{0020}\beta_{0110}}{\mu_{4,d}-\mu_{4,d}^2}\end{aligned} \tag{B.99}$$

$$\begin{aligned}\hat{\beta}_{0021} &= \beta_{0021} - \frac{\bar{\alpha}_{0011}\beta_{0110}}{-1+\bar{\mu}_{2,d}} - \frac{\alpha_{0011}\beta_{1010}}{-1+\mu_{2,d}} - \frac{\beta_{0011}\bar{\beta}_{0011}}{-1+\bar{\mu}_{4,d}} - \frac{2\beta_{0011}\beta_{0020}}{-1+\mu_{4,d}} - \frac{\bar{\alpha}_{0002}\beta_{0101}}{\bar{\mu}_{2,d}-\mu_{4,d}^2} \\ &\quad - \frac{\alpha_{0020}\beta_{1001}}{\mu_{2,d}-\mu_{4,d}^2} - \frac{2\beta_{0002}\bar{\beta}_{0002}}{\bar{\mu}_{4,d}-\mu_{4,d}^2} - \frac{\beta_{0011}\beta_{0020}}{\mu_{4,d}-\mu_{4,d}^2} \end{aligned} \tag{B.100}$$

$$\begin{aligned}\hat{\beta}_{1002} &= \beta_{1002} - \frac{\alpha_{1001}\beta_{1001}}{\mu_{2,d}-\mu_{2,d}\bar{\mu}_{4,d}} - \frac{2\beta_{0002}\bar{\beta}_{0110}}{\bar{\mu}_{4,d}-\mu_{2,d}\bar{\mu}_{4,d}} - \frac{\bar{\alpha}_{0020}\beta_{1100}}{\bar{\mu}_{2,d}-\bar{\mu}_{4,d}^2} - \frac{2\alpha_{0002}\beta_{2000}}{\mu_{2,d}-\bar{\mu}_{4,d}^2} \\ &\quad - \frac{\bar{\beta}_{0020}\beta_{1001}}{\bar{\mu}_{4,d}-\bar{\mu}_{4,d}^2} - \frac{\beta_{0011}\beta_{1001}}{-\mu_{2,d}\bar{\mu}_{4,d}+\mu_{4,d}} - \frac{\beta_{0002}\beta_{1010}}{-\bar{\mu}_{4,d}^2+\mu_{4,d}} - \frac{\alpha_{0110}\beta_{0101}}{\mu_{2,d}-\bar{\mu}_{2,d}\mu_{4,d}} \end{aligned} \tag{B.101}$$

$$\begin{aligned}\hat{\beta}_{0102} &= \beta_{0102} - \frac{\bar{\alpha}_{1010}\beta_{0101}}{\bar{\mu}_{2,d}-\bar{\mu}_{2,d}\bar{\mu}_{4,d}} - \frac{\alpha_{0101}\beta_{1001}}{\mu_{2,d}-\bar{\mu}_{2,d}\bar{\mu}_{4,d}} - \frac{2\beta_{0002}\bar{\beta}_{1010}}{\bar{\mu}_{4,d}-\bar{\mu}_{2,d}\bar{\mu}_{4,d}} - \frac{2\bar{\alpha}_{0020}\beta_{0200}}{\bar{\mu}_{2,d}-\bar{\mu}_{4,d}^2} \\ &\quad - \frac{\alpha_{0002}\beta_{1100}}{\mu_{2,d}-\bar{\mu}_{4,d}^2} - \frac{\bar{\beta}_{0020}\beta_{0101}}{\bar{\mu}_{4,d}-\bar{\mu}_{4,d}^2} - \frac{\beta_{0011}\beta_{0101}}{-\bar{\mu}_{2,d}\bar{\mu}_{4,d}+\mu_{4,d}} - \frac{\beta_{0002}\beta_{0110}}{-\bar{\mu}_{4,d}^2+\mu_{4,d}} \end{aligned} \tag{B.102}$$

$$\begin{aligned}\hat{\beta}_{0012} &= \beta_{0012} - \frac{\bar{\alpha}_{0011}\beta_{0101}}{-1+\bar{\mu}_{2,d}} - \frac{\alpha_{0011}\beta_{1001}}{-1+\mu_{2,d}} - \frac{2\beta_{0002}\bar{\beta}_{0011}}{-1+\bar{\mu}_{4,d}} - \frac{\bar{\alpha}_{0020}\beta_{0110}}{\bar{\mu}_{2,d}-\bar{\mu}_{4,d}^2} - \frac{\alpha_{0002}\beta_{1010}}{\mu_{2,d}-\bar{\mu}_{4,d}^2} \\ &\quad - \frac{\beta_{0011}\bar{\beta}_{0020}}{\bar{\mu}_{4,d}-\bar{\mu}_{4,d}^2} - \frac{\beta_{0011}^2}{-1+\mu_{4,d}} - \frac{2\beta_{0002}\beta_{0020}}{-\bar{\mu}_{4,d}^2+\mu_{4,d}} \end{aligned} \tag{B.103}$$

$$\begin{aligned}\hat{\beta}_{1110} &= \beta_{1110} - \frac{\bar{\alpha}_{1100}\beta_{0110}}{-1+\bar{\mu}_{2,d}} - \frac{\alpha_{1100}\beta_{1010}}{-1+\mu_{2,d}} - \frac{\beta_{0011}\bar{\beta}_{1100}}{-1+\bar{\mu}_{4,d}} - \frac{2\beta_{0020}\beta_{1100}}{-1+\mu_{4,d}} - \frac{\bar{\alpha}_{1001}\beta_{1100}}{\bar{\mu}_{2,d}-\bar{\mu}_{2,d}\mu_{4,d}} \\ &\quad - \frac{2\alpha_{0110}\beta_{2000}}{\mu_{2,d}-\bar{\mu}_{2,d}\mu_{4,d}} - \frac{\beta_{1001}\bar{\beta}_{1001}}{\bar{\mu}_{4,d}-\bar{\mu}_{2,d}\mu_{4,d}} - \frac{\beta_{0110}\beta_{1010}}{\mu_{4,d}-\bar{\mu}_{2,d}\mu_{4,d}} - \frac{2\bar{\alpha}_{0101}\beta_{0200}}{\bar{\mu}_{2,d}-\mu_{2,d}\mu_{4,d}} \\ &\quad - \frac{\alpha_{1010}\beta_{1100}}{\mu_{2,d}-\mu_{2,d}\mu_{4,d}} - \frac{\beta_{0101}\bar{\beta}_{0101}}{\bar{\mu}_{4,d}-\mu_{2,d}\mu_{4,d}} - \frac{\beta_{0110}\beta_{1010}}{\mu_{4,d}-\mu_{2,d}\mu_{4,d}} \end{aligned} \tag{B.104}$$

$$\begin{aligned}\hat{\beta}_{1011} &= \beta_{1101} - \frac{\bar{\alpha}_{1100}\beta_{0101}}{-1+\bar{\mu}_{2,d}} - \frac{\alpha_{1100}\beta_{1001}}{-1+\mu_{2,d}} - \frac{2\beta_{0002}\bar{\beta}_{1100}}{-1+\bar{\mu}_{4,d}} - \frac{\bar{\alpha}_{1010}\beta_{1100}}{\bar{\mu}_{2,d}-\bar{\mu}_{2,d}\bar{\mu}_{4,d}} - \frac{2\alpha_{0101}\beta_{2000}}{\mu_{2,d}-\bar{\mu}_{2,d}\bar{\mu}_{4,d}} \\ &\quad - \frac{\beta_{1001}\bar{\beta}_{1010}}{\bar{\mu}_{4,d}-\bar{\mu}_{2,d}\bar{\mu}_{4,d}} - \frac{\alpha_{1001}\beta_{1100}}{\mu_{2,d}-\mu_{2,d}\bar{\mu}_{4,d}} - \frac{\beta_{0101}\bar{\beta}_{0110}}{\bar{\mu}_{4,d}-\mu_{2,d}\bar{\mu}_{4,d}} - \frac{\beta_{0011}\beta_{1100}}{-1+\mu_{4,d}} - \frac{\beta_{0101}\beta_{1010}}{-\bar{\mu}_{2,d}\bar{\mu}_{4,d}+\mu_{4,d}} \\ &\quad - \frac{\beta_{0110}\beta_{1001}}{-\mu_{2,d}\bar{\mu}_{4,d}+\mu_{4,d}} - \frac{2\alpha_{0110}\beta_{0200}}{\mu_{2,d}-\bar{\mu}_{2,d}\mu_{4,d}} \end{aligned} \tag{B.105}$$

$$\begin{aligned}\hat{\beta}_{1101} &= \beta_{1011} - \frac{\bar{\alpha}_{0011}\beta_{1100}}{-1+\bar{\mu}_{2,d}} - \frac{2\alpha_{0011}\beta_{2000}}{-1+\mu_{2,d}} - \frac{\bar{\beta}_{0011}\beta_{1001}}{-1+\bar{\mu}_{4,d}} - \frac{\alpha_{1001}\beta_{1010}}{\mu_{2,d}-\mu_{2,d}\bar{\mu}_{4,d}} - \frac{\beta_{0011}\bar{\beta}_{0110}}{\bar{\mu}_{4,d}-\mu_{2,d}\bar{\mu}_{4,d}} \\ &\quad - \frac{\beta_{0011}\beta_{1010}}{-1+\mu_{4,d}} - \frac{2\beta_{0020}\beta_{1001}}{-\mu_{2,d}\bar{\mu}_{4,d}+\mu_{4,d}} - \frac{\alpha_{0110}\beta_{0110}}{\mu_{2,d}-\bar{\mu}_{2,d}\mu_{4,d}} - \frac{\bar{\alpha}_{0101}\beta_{0101}}{\bar{\mu}_{2,d}-\mu_{2,d}\mu_{4,d}} - \frac{\alpha_{1010}\beta_{1001}}{\mu_{2,d}-\mu_{2,d}\mu_{4,d}} \\ &\quad - \frac{2\beta_{0002}\bar{\beta}_{0101}}{\bar{\mu}_{4,d}-\mu_{2,d}\mu_{4,d}} - \frac{\beta_{0011}\beta_{1010}}{\mu_{4,d}-\mu_{2,d}\mu_{4,d}} \end{aligned} \tag{B.106}$$

$$\begin{aligned}\hat{\beta}_{0111} &= \beta_{0111} - \frac{2\bar{\alpha}_{0011}\beta_{0200}}{-1+\bar{\mu}_{2,d}} - \frac{\alpha_{0011}\beta_{1100}}{-1+\mu_{2,d}} - \frac{\bar{\beta}_{0011}\beta_{0101}}{-1+\bar{\mu}_{4,d}} - \frac{\bar{\alpha}_{1010}\beta_{0110}}{\bar{\mu}_{2,d}-\bar{\mu}_{2,d}\bar{\mu}_{4,d}} - \frac{\alpha_{0101}\beta_{1010}}{\mu_{2,d}-\bar{\mu}_{2,d}\bar{\mu}_{4,d}} \\ &\quad - \frac{\beta_{0011}\bar{\beta}_{1010}}{\bar{\mu}_{4,d}-\bar{\mu}_{2,d}\bar{\mu}_{4,d}} - \frac{\beta_{0011}\beta_{0110}}{-1+\mu_{4,d}} - \frac{2\beta_{0020}\beta_{0101}}{-\bar{\mu}_{2,d}\bar{\mu}_{4,d}+\mu_{4,d}} - \frac{\bar{\alpha}_{1001}\beta_{0101}}{\bar{\mu}_{2,d}-\bar{\mu}_{2,d}\mu_{4,d}} - \frac{\alpha_{0110}\beta_{1001}}{\mu_{2,d}-\bar{\mu}_{2,d}\mu_{4,d}} \\ &\quad - \frac{2\beta_{0002}\bar{\beta}_{1001}}{\bar{\mu}_{4,d}-\bar{\mu}_{2,d}\mu_{4,d}} - \frac{\beta_{0011}\beta_{0110}}{\mu_{4,d}-\bar{\mu}_{2,d}\mu_{4,d}} \end{aligned} \tag{B.107}$$

Appendix C

Coefficients single NS bifurcation

Coefficients s_{ihkl} relative to the nonlinear terms of the Jordan normal form, relative to the single NS bifurcation under study in Ch. 4.

$$s_{1200} = -\frac{9u_0}{32Q_0\tau^2} \tag{C.1}$$

$$s_{1020} = -\frac{7u_0}{32Q_0\tau^2} \tag{C.2}$$

$$s_{1002} = -\frac{u_0}{8Q_0\tau^2} \tag{C.3}$$

$$s_{1110} = -\frac{3\sqrt{7}u_0}{16Q_0\tau^2} \tag{C.4}$$

$$s_{1101} = -\frac{3u_0}{8Q_0\tau^2} \tag{C.5}$$

$$s_{1011} = -\frac{\sqrt{7}u_0}{8Q_0\tau^2} \tag{C.6}$$

$$s_{1300} = \frac{9\left(3u_0^2-1\right)}{128Q_0^2\tau^4} \tag{C.7}$$

$$s_{1030} = \frac{7\sqrt{7}\left(3u_0^2-1\right)}{384Q_0^2\tau^4} \tag{C.8}$$

$$s_{1003} = \frac{3u_0^2-1}{48Q_0^2\tau^4} \tag{C.9}$$

$$s_{1210} = \frac{9\sqrt{7}\left(3u_0^2-1\right)}{128Q_0^2\tau^4} \tag{C.10}$$

$$s_{1201} = \frac{9\left(3u_0^2-1\right)}{64Q_0^2\tau^4} \tag{C.11}$$

$$s_{1120} = \frac{21\left(3u_0^2-1\right)}{128Q_0^2\tau^4} \tag{C.12}$$

$$s_{1021} = \frac{7\left(3u_0^2-1\right)}{64Q_0^2\tau^4} \tag{C.13}$$

$$s_{1102} = \frac{3\left(3u_0^2-1\right)}{32Q_0^2\tau^4} \tag{C.14}$$

$$s_{1012} = \frac{\sqrt{7}\left(3u_0^2-1\right)}{32Q_0^2\tau^4} \tag{C.15}$$

$$s_{1111} = \frac{3\sqrt{7}\left(3u_0^2-1\right)}{32Q_0^2\tau^4} \tag{C.16}$$

$$s_{2200} = \frac{45u_0}{32\sqrt{7}Q_0\tau^2} \tag{C.17}$$

$$s_{2020} = \frac{5\sqrt{7}u_0}{32Q_0\tau^2} \tag{C.18}$$

$$s_{2002} = \frac{5u_0}{8\sqrt{7}Q_0\tau^2} \tag{C.19}$$

$$s_{2110} = \frac{15u_0}{16Q_0\tau^2} \tag{C.20}$$

$$s_{2101} = \frac{15u_0}{8\sqrt{7}Q_0\tau^2} \tag{C.21}$$

$$s_{2011} = \frac{5u_0}{8Q_0\tau^2} \tag{C.22}$$

$$s_{2300} = \frac{45\left(1-3u_0^2\right)}{128\sqrt{7}Q_0^2\tau^4} \tag{C.23}$$

$$s_{2030} = \frac{35\left(1-3u_0^2\right)}{384Q_0^2\tau^4} \tag{C.24}$$

$$s_{2003} = \frac{5\left(1-3u_0^2\right)}{48\sqrt{7}Q_0^2\tau^4} \tag{C.25}$$

$$s_{2210} = \frac{45\left(1-3u_0^2\right)}{128Q_0^2\tau^4} \tag{C.26}$$

$$s_{2201} = \frac{45\left(1-3u_0^2\right)}{64\sqrt{7}Q_0^2\tau^4} \tag{C.27}$$

$$s_{2120} = \frac{15\sqrt{7}\left(1-3u_0^2\right)}{128Q_0^2\tau^4} \tag{C.28}$$

$$s_{2021} = \frac{5\sqrt{7}\left(1-3u_0^2\right)}{64Q_0^2\tau^4} \tag{C.29}$$

$$s_{2102} = \frac{15\left(1-3u_0^2\right)}{32\sqrt{7}Q_0^2\tau^4} \tag{C.30}$$

$$s_{2012} = \frac{5\left(1-3u_0^2\right)}{32Q_0^2\tau^4} \tag{C.31}$$

$$s_{2111} = \frac{15\left(1-3u_0^2\right)}{32Q_0^2\tau^4} \tag{C.32}$$

$$s_{3200} = -\frac{9u_0}{32Q_0\tau^2} \tag{C.33}$$

$$s_{3020} = -\frac{7u_0}{32Q_0\tau^2} \tag{C.34}$$

$$s_{3002} = -\frac{u_0}{8Q_0\tau^2} \tag{C.35}$$

$$s_{3110} = -\frac{3\sqrt{7}u_0}{16Q_0\tau^2} \tag{C.36}$$

$$s_{3101} = -\frac{3u_0}{8Q_0\tau^2} \tag{C.37}$$

$$s_{3011} = -\frac{\sqrt{7}u_0}{8Q_0\tau^2} \tag{C.38}$$

$$s_{3300} = \frac{9\left(3u_0^2-1\right)}{128Q_0^2\tau^4} \tag{C.39}$$

$$s_{3030} = \frac{7\sqrt{7}\left(3u_0^2-1\right)}{384Q_0^2\tau^4} \tag{C.40}$$

$$s_{3003} = \frac{3u_0^2-1}{48Q_0^2\tau^4} \tag{C.41}$$

$$s_{3210} = \frac{9\sqrt{7}\left(3u_0^2-1\right)}{128Q_0^2\tau^4} \tag{C.42}$$

$$s_{3201} = \frac{9\left(3u_0^2-1\right)}{64Q_0^2\tau^4} \tag{C.43}$$

$$s_{3120} = \frac{21\left(3u_0^2-1\right)}{128Q_0^2\tau^4} \tag{C.44}$$

$$s_{3021} = \frac{7\left(3u_0^2-1\right)}{64Q_0^2\tau^4} \tag{C.45}$$

$$s_{3102} = \frac{3\left(3u_0^2-1\right)}{32Q_0^2\tau^4} \tag{C.46}$$

$$s_{3012} = \frac{\sqrt{7}\left(3u_0^2-1\right)}{32Q_0^2\tau^4} \tag{C.47}$$

$$s_{3111} = \frac{3\sqrt{7}\left(3u_0^2-1\right)}{32Q_0^2\tau^4} \tag{C.48}$$

It can be verified that $s_{1hkl} = s_{3hkl} = -s_{2hkl}\frac{5}{\sqrt{7}}$.

Coefficients a_{hk} and b_{hk} relative to the nonlinear terms after the center manifold reduction, relative to the single NS bifurcation under study in Ch. 4.

$$a_{20} = -\frac{9u_0}{32Q_0\tau^2} \tag{C.49}$$

$$a_{11} = -\frac{3\sqrt{7}u_0}{16Q_0\tau^2} \tag{C.50}$$

$$a_{02} = -\frac{7u_0}{32Q_0\tau^2} \tag{C.51}$$

$$a_{30} = \frac{-9+61u_0^2}{128Q_0^2\tau^4} \tag{C.52}$$

$$a_{21} = \frac{\sqrt{7}\left(-27+103u_0^2\right)}{384Q_0^2\tau^4} \tag{C.53}$$

$$a_{12} = \frac{7\left(-9+29u_0^2\right)}{384Q_0^2\tau^4} \tag{C.54}$$

$$a_{03} = \frac{7\sqrt{7}\left(-1+5u_0^2\right)}{384Q_0^2\tau^4} \tag{C.55}$$

$$b_{20} = \frac{45u_0}{32\sqrt{7}Q_0\tau^2} \tag{C.56}$$

$$b_{11} = \frac{15u_0}{16Q_0\tau^2} \tag{C.57}$$

$$b_{02} = \frac{5\sqrt{7}u_0}{32Q_0\tau^2} \tag{C.58}$$

$$b_{30} = \frac{5\left(9-61u_0^2\right)}{128\sqrt{7}Q_0^2\tau^4} \tag{C.59}$$

$$b_{21} = \frac{5\left(27-103u_0^2\right)}{384Q_0^2\tau^4} \tag{C.60}$$

$$b_{12} = \frac{5\sqrt{7}\left(9-29u_0^2\right)}{384Q_0^2\tau^4} \tag{C.61}$$

$$b_{03} = \frac{35\left(1-5u_0^2\right)}{384Q_0^2\tau^4} \tag{C.62}$$

Coefficients α_{hk} relative to the nonlinear terms in complex form, relative to the single NS bifurcation under study in Ch. 4.

$$\alpha_{20} = \frac{14u_0}{64Q_0\tau^2} + i\frac{13\sqrt{7}u_0}{224Q_0\tau^2} \tag{C.63}$$

$$\alpha_{11} = -\frac{u_0}{4Q_0\tau^2} + i\frac{5u_0}{4\sqrt{7}Q_0\tau^2} \tag{C.64}$$

$$\alpha_{02} = -\frac{16u_0}{64Q_0\tau^2} - i\frac{\sqrt{7}u_0}{28Q_0\tau^2} \tag{C.65}$$

$$\alpha_{30} = \frac{3(133-15\sqrt{7})}{7168Q_0^2\tau^4} + \frac{5(183\sqrt{7}-749)u_0^2}{3072Q_0^2\tau^4} - \frac{i}{Q_0^2\tau^4}\left(\frac{5}{384\sqrt{7}} + \frac{47u_0^2}{384\sqrt{7}}\right) \tag{C.66}$$

$$\alpha_{21} = \frac{1-3u_0^2}{32Q_0^2\tau^4} + \frac{i}{Q_0^2\tau^4}\left(\frac{33-226u_0^2}{96\sqrt{7}}\right) \tag{C.67}$$

$$\alpha_{12} = \frac{-3+14u_0^2}{24Q_0^2\tau^4} + i\frac{1-6u_0^2}{8\sqrt{7}Q_0^2\tau^4} \tag{C.68}$$

$$\alpha_{03} = \frac{-1+5u_0^2}{48Q_0^2\tau^4} + i\frac{-5+9u_0^2}{48\sqrt{7}Q_0^2\tau^4} \tag{C.69}$$

Appendix D

Coefficients double NS bifurcation: part I

Coefficients s_{ihklmn} relative to the nonlinear terms of the Jordan normal form, relative to the double NS bifurcation under study in Ch. 4.

$$s_{120000} = \frac{0.0000157112u_0}{Q_0\tau^2} \tag{D.1}$$

$$s_{102000} = \frac{0.0000160459u_0}{Q_0\tau^2} \tag{D.2}$$

$$s_{100200} = \frac{0.0148359u_0}{Q_0\tau^2} \tag{D.3}$$

$$s_{100020} = \frac{0.111271u_0}{Q_0\tau^2} \tag{D.4}$$

$$s_{100002} = \frac{0.0126189u_0}{Q_0\tau^2} \tag{D.5}$$

$$s_{111000} = \frac{0.0000317553u_0}{Q_0\tau^2} \tag{D.6}$$

$$s_{110100} = -\frac{0.000965586u_0}{Q_0\tau^2} \tag{D.7}$$

$$s_{110010} = -\frac{0.00264439u_0}{Q_0\tau^2} \tag{D.8}$$

$$s_{110001} = \frac{0.000890524u_0}{Q_0\tau^2} \tag{D.9}$$

$$s_{101100} = -\frac{0.000975819u_0}{Q_0\tau^2} \tag{D.10}$$

$$s_{101010} = -\frac{0.00267241u_0}{Q_0\tau^2} \tag{D.11}$$

$$s_{101001} = \frac{0.000899961u_0}{Q_0\tau^2} \tag{D.12}$$

$$s_{100110} = \frac{0.0812603u_0}{Q_0\tau^2} \tag{D.13}$$

$$s_{100101} = -\frac{0.0273652u_0}{Q_0\tau^2} \tag{D.14}$$

$$s_{100011} = -\frac{0.0749433u_0}{Q_0\tau^2} \tag{D.15}$$

$$s_{130000} = \frac{-1.62001\times10^{-8}+9.72007\times10^{-8}u_0^4+1.29601\times10^{-7}u_0^6+4.86004\times10^{-8}u_0^8}{Q_0^2\tau^4\left(1+u_0^2\right)^3} \tag{D.16}$$

$$s_{103000} = \frac{-1.67206\times10^{-8}+1.00324\times10^{-7}u_0^4+1.33765\times10^{-7}u_0^6+5.01619\times10^{-8}u_0^8}{Q_0^2\tau^4\left(1.+u_0^2\right)^3} \tag{D.17}$$

$$s_{100300} = \frac{0.000470085-0.00282051u_0^4-0.00376068u_0^6-0.00141026u_0^8}{Q_0^2\tau^4\left(1.+u_0^2\right)^3} \tag{D.18}$$

$$s_{100030} = \frac{0.00965563-0.0579338u_0^4-0.077245u_0^6-0.0289669u_0^8}{Q_0^2\tau^4\left(1.+u_0^2\right)^3} \tag{D.19}$$

$$s_{100003} = \frac{-0.000368757+0.00221254u_0^4+0.00295006u_0^6+0.00110627u_0^8}{Q_0^2\tau^4\left(1+u_0^2\right)^3} \tag{D.20}$$

$$s_{121000} = \frac{-4.91154\times10^{-8}+2.94692\times10^{-7}u_0^4+3.92923\times10^{-7}u_0^6+1.47346\times10^{-7}u_0^8}{Q_0^2\tau^4\left(1+u_0^2\right)^3} \tag{D.21}$$

$$s_{120100} = \frac{1.49346\times10^{-6}-8.96074\times10^{-6}u_0^4-0.0000119476u_0^6-4.48037\times10^{-6}u_0^8}{Q_0^2\tau^4\left(1+u_0^2\right)^3} \tag{D.22}$$

$$s_{120010} = \frac{4.09003\times10^{-6}-0.0000245402u_0^4-0.0000327203u_0^6-0.0000122701u_0^8}{Q_0^2\tau^4\left(1+u_0^2\right)^3} \tag{D.23}$$

$$s_{120001} = \frac{-1.37736\times10^{-6}+8.26415\times10^{-6}u_0^4+0.0000110189u_0^6+4.13207\times10^{-6}u_0^8}{Q_0^2\tau^4\left(1+u_0^2\right)^3} \tag{D.24}$$

$$s_{112000} = \frac{-4.96359\times10^{-8}+2.97815\times10^{-7}u_0^4+3.97087\times10^{-7}u_0^6+1.48908\times10^{-7}u_0^8}{Q_0^2\tau^4\left(1+u_0^2\right)^3} \tag{D.25}$$

$$s_{102100} = \frac{1.52528\times10^{-6}-9.15166\times10^{-6}u_0^4-0.0000122022u_0^6-4.57583\times10^{-6}u_0^8}{Q_0^2\tau^4\left(1+u_0^2\right)^3} \tag{D.26}$$

$$s_{102010} = \frac{4.17718\times10^{-6}-0.0000250631u_0^4-0.0000334174u_0^6-0.0000125315u_0^8}{Q_0^2\tau^4\left(1+u_0^2\right)^3} \tag{D.27}$$

$$s_{102001} = \frac{-1.4067\times10^{-6}+8.44023\times10^{-6}u_0^4+0.0000112536u_0^6+4.22011\times10^{-6}u_0^8}{Q_0^2\tau^4\left(1+u_0^2\right)^3} \tag{D.28}$$

$$s_{110200} = \frac{-0.0000458929+0.000275357u_0^4+0.000367143u_0^6+0.000137679u_0^8}{Q_0^2\tau^4\left(1+u_0^2\right)^3} \tag{D.29}$$

$$s_{101200} = \frac{-0.0000463792+0.000278275u_0^4+0.000371034u_0^6+0.000139138u_0^8}{Q_0^2\tau^4\left(1+u_0^2\right)^3} \tag{D.30}$$

$$s_{100210} = \frac{0.00386218 - 0.0231731u_0^4 - 0.0308974u_0^6 - 0.0115865u_0^8}{Q_0^2\tau^4\left(1+u_0^2\right)^3} \tag{D.31}$$

$$s_{100201} = \frac{-0.00130063 + 0.00780376u_0^4 + 0.010405u_0^6 + 0.00390188u_0^8}{Q_0^2\tau^4\left(1+u_0^2\right)^3} \tag{D.32}$$

$$s_{110020} = \frac{-0.000344203 + 0.00206522u_0^4 + 0.00275362u_0^6 + 0.00103261u_0^8}{Q_0^2\tau^4\left(1+u_0^2\right)^3} \tag{D.33}$$

$$s_{101020} = \frac{-0.00034785 + 0.0020871u_0^4 + 0.0027828u_0^6 + 0.00104355u_0^8}{Q_0^2\tau^4\left(1+u_0^2\right)^3} \tag{D.34}$$

$$s_{100120} = \frac{0.0105771 - 0.0634627u_0^4 - 0.0846169u_0^6 - 0.0317313u_0^8}{Q_0^2\tau^4\left(1+u_0^2\right)^3} \tag{D.35}$$

$$s_{100021} = \frac{-0.00975487 + 0.0585292u_0^4 + 0.078039u_0^6 + 0.0292646u_0^8}{Q_0^2\tau^4\left(1+u_0^2\right)^3} \tag{D.36}$$

$$s_{110002} = \frac{-0.000039035 + 0.00023421u_0^4 + 0.00031228u_0^6 + 0.000117105u_0^8}{Q_0^2\tau^4\left(1+u_0^2\right)^3} \tag{D.37}$$

$$s_{101002} = \frac{-0.0000394486 + 0.000236692u_0^4 + 0.000315589u_0^6 + 0.000118346u_0^8}{Q_0^2\tau^4\left(1+u_0^2\right)^3} \tag{D.38}$$

$$s_{100102} = \frac{0.00119952 - 0.00719711u_0^4 - 0.00959615u_0^6 - 0.00359856u_0^8}{Q_0^2\tau^4\left(1+u_0^2\right)^3} \tag{D.39}$$

$$s_{100012} = \frac{0.00328505 - 0.0197103u_0^4 - 0.0262804u_0^6 - 0.00985514u_0^8}{Q_0^2\tau^4\left(1+u_0^2\right)^3} \tag{D.40}$$

$$s_{100111} = \frac{-0.00712389 + 0.0427433u_0^4 + 0.0569911u_0^6 + 0.0213717u_0^8}{Q_0^2\tau^4\left(1+u_0^2\right)^3} \tag{D.41}$$

$$s_{101011} = \frac{0.000234284 - 0.0014057u_0^4 - 0.00187427u_0^6 - 0.000702851u_0^8}{Q_0^2\tau^4\left(1+u_0^2\right)^3} \tag{D.42}$$

$$s_{101101} = \frac{0.0000855476 - 0.000513285u_0^4 - 0.000684381u_0^6 - 0.000256643u_0^8}{Q_0^2\tau^4\left(1+u_0^2\right)^3} \tag{D.43}$$

$$s_{101110} = \frac{-0.000254032 + 0.00152419u_0^4 + 0.00203225u_0^6 + 0.000762095u_0^8}{Q_0^2\tau^4\left(1+u_0^2\right)^3} \tag{D.44}$$

$$s_{110011} = \frac{0.000231827 - 0.00139096u_0^4 - 0.00185462u_0^6 - 0.000695481u_0^8}{Q_0^2\tau^4\left(1+u_0^2\right)^3} \tag{D.45}$$

$$s_{110101} = \frac{0.0000846505 - 0.000507903u_0^4 - 0.000677204u_0^6 - 0.000253952u_0^8}{Q_0^2\tau^4\left(1+u_0^2\right)^3} \tag{D.46}$$

$$s_{110110} = \frac{-0.000251368 + 0.00150821u_0^4 + 0.00201094u_0^6 + 0.000754104u_0^8}{Q_0^2\tau^4\left(1+u_0^2\right)^3} \tag{D.47}$$

$$s_{111001} = \frac{-2.78391\times10^{-6} + 0.0000167034u_0^4 + 0.0000222713u_0^6 + 8.35172\times10^{-6}u_0^8}{Q_0^2\tau^4\left(1+u_0^2\right)^3} \tag{D.48}$$

$$s_{111010} = \frac{8.26675\times10^{-6} - 0.0000496005u_0^4 - 0.000066134u_0^6 - 0.0000248003u_0^8}{Q_0^2\tau^4\left(1+u_0^2\right)^3} \tag{D.49}$$

$$s_{111100} = \frac{3.01856\times10^{-6} - 0.0000181114u_0^4 - 0.0000241485u_0^6 - 9.05569\times10^{-6}u_0^8}{Q_0^2\tau^4\left(1+u_0^2\right)^3} \tag{D.50}$$

$$s_{220000} = -\frac{0.000015388u_0}{Q_0\tau^2} \tag{D.51}$$

$$s_{202000} = -\frac{0.000015716u_0}{Q_0\tau^2} \tag{D.52}$$

$$s_{200200} = -\frac{0.0145309u_0}{Q_0\tau^2} \tag{D.53}$$

$$s_{200020} = -\frac{0.108983u_0}{Q_0\tau^2} \tag{D.54}$$

$$s_{200002} = -\frac{0.0123595u_0}{Q_0\tau^2} \tag{D.55}$$

$$s_{211000} = -\frac{0.0000311024u_0}{Q_0\tau^2} \tag{D.56}$$

$$s_{210100} = \frac{0.000945733u_0}{Q_0\tau^2} \tag{D.57}$$

$$s_{210010} = \frac{0.00259002u_0}{Q_0\tau^2} \tag{D.58}$$

$$s_{210001} = -\frac{0.000872214u_0}{Q_0\tau^2} \tag{D.59}$$

$$s_{201100} = \frac{0.000955755u_0}{Q_0\tau^2} \tag{D.60}$$

$$s_{201010} = \frac{0.00261747u_0}{Q_0\tau^2} \tag{D.61}$$

$$s_{201001} = -\frac{0.000881457u_0}{Q_0\tau^2} \tag{D.62}$$

$$s_{200110} = -\frac{0.0795895u_0}{Q_0\tau^2} \tag{D.63}$$

$$s_{200101} = \frac{0.0268025u_0}{Q_0\tau^2} \tag{D.64}$$

$$s_{200011} = \frac{0.0734024u_0}{Q_0\tau^2} \tag{D.65}$$

$$s_{230000} = \frac{1.5867 \times 10^{-8} - 9.52022 \times 10^{-8}u_0^4 - 1.26936 \times 10^{-7}u_0^6 - 4.76011 \times 10^{-8}u_0^8}{Q_0^2\tau^4\left(1+u_0^2\right)^3} \tag{D.66}$$

$$s_{203000} = \frac{1.63768 \times 10^{-8} - 9.8261 \times 10^{-8}u_0^4 - 1.31015 \times 10^{-7}u_0^6 - 4.91305 \times 10^{-8}u_0^8}{Q_0^2\tau^4\left(1+u_0^2\right)^3} \tag{D.67}$$

$$s_{200300} = \frac{-0.00046042 + 0.00276252u_0^4 + 0.00368336u_0^6 + 0.00138126u_0^8}{Q_0^2\tau^4\left(1+u_0^2\right)^3} \tag{D.68}$$

$$s_{200030} = \frac{-0.0094571 + 0.0567426u_0^4 + 0.0756568u_0^6 + 0.0283713u_0^8}{Q_0^2\tau^4\left(1+u_0^2\right)^3} \tag{D.69}$$

$$s_{200003} = \frac{0.000361175 - 0.00216705u_0^4 - 0.0028894u_0^6 - 0.00108352u_0^8}{Q_0^2\tau^4\left(1+u_0^2\right)^3} \tag{D.70}$$

$$s_{221000} = \frac{4.81055 \times 10^{-8} - 2.88633 \times 10^{-7} u_0^4 - 3.84844 \times 10^{-7} u_0^6 - 1.44317 \times 10^{-7} u_0^8}{Q_0^2 \tau^4 \left(1 + u_0^2\right)^3} \tag{D.71}$$

$$s_{220100} = \frac{-1.46275 \times 10^{-6} + 8.7765 \times 10^{-6} u_0^4 + 0.000011702 u_0^6 + 4.38825 \times 10^{-6} u_0^8}{Q_0^2 \tau^4 \left(1 + u_0^2\right)^3} \tag{D.72}$$

$$s_{220010} = \frac{-4.00594 \times 10^{-6} + 0.0000240356 u_0^4 + 0.0000320475 u_0^6 + 0.0000120178 u_0^8}{Q_0^2 \tau^4 \left(1 + u_0^2\right)^3} \tag{D.73}$$

$$s_{220001} = \frac{1.34904 \times 10^{-6} - 8.09423 \times 10^{-6} u_0^4 - 0.0000107923 u_0^6 - 4.04712 \times 10^{-6} u_0^8}{Q_0^2 \tau^4 \left(1 + u_0^2\right)^3} \tag{D.74}$$

$$s_{212000} = \frac{4.86153 \times 10^{-8} - 2.91692 \times 10^{-7} u_0^4 - 3.88922 \times 10^{-7} u_0^6 - 1.45846 \times 10^{-7} u_0^8}{Q_0^2 \tau^4 \left(1 + u_0^2\right)^3} \tag{D.75}$$

$$s_{202100} = \frac{-1.49392 \times 10^{-6} + 8.96349 \times 10^{-6} u_0^4 + 0.0000119513 u_0^6 + 4.48175 \times 10^{-6} u_0^8}{Q_0^2 \tau^4 \left(1 + u_0^2\right)^3} \tag{D.76}$$

$$s_{202010} = \frac{-4.09129 \times 10^{-6} + 0.0000245478 u_0^4 + 0.0000327303 u_0^6 + 0.0000122739 u_0^8}{Q_0^2 \tau^4 \left(1 + u_0^2\right)^3} \tag{D.77}$$

$$s_{202001} = \frac{1.37778 \times 10^{-6} - 8.26669 \times 10^{-6} - 0.0000110223 u_0^6 - 4.13334 \times 10^{-6}}{Q_0^2 \tau^4 \left(1 + u_0^2\right)^3} \tag{D.78}$$

$$s_{210200} = \frac{0.0000449493 - 0.000269696 u_0^4 - 0.000359594 u_0^6 - 0.000134848 u_0^8}{Q_0^2 \tau^4 \left(1 + u_0^2\right)^3} \tag{D.79}$$

$$s_{201200} = \frac{0.0000454256 - 0.000272554 u_0^4 - 0.000363405 u_0^6 - 0.000136277 u_0^8}{Q_0^2 \tau^4 \left(1 + u_0^2\right)^3} \tag{D.80}$$

$$s_{200210} = \frac{0.00378277 + 0.0226966 u_0^4 + 0.0302622 u_0^6 + 0.0113483 u_0^8}{Q_0^2 \tau^4 \left(1 + u_0^2\right)^3} \tag{D.81}$$

$$s_{200201} = \frac{0.00127388 - 0.00764331 u_0^4 - 0.0101911 u_0^6 - 0.00382165 u_0^8}{Q_0^2 \tau^4 \left(1 + u_0^2\right)^3} \tag{D.82}$$

$$s_{210020} = \frac{0.000337126 - 0.00202275 u_0^4 - 0.00269701 u_0^6 - 0.00101138 u_0^8}{Q_0^2 \tau^4 \left(1 + u_0^2\right)^3} \tag{D.83}$$

$$s_{201020} = \frac{0.000340698 - 0.00204419 u_0^4 - 0.00272559 u_0^6 - 0.00102209 u_0^8}{Q_0^2 \tau^4 \left(1 + u_0^2\right)^3} \tag{D.84}$$

$$s_{200120} = \frac{-0.0103596 + 0.0621578 u_0^4 + 0.0828771 u_0^6 + 0.0310789 u_0^8}{Q_0^2 \tau^4 \left(1 + u_0^2\right)^3} \tag{D.85}$$

$$s_{200021} = \frac{0.00955431 - 0.0573258 u_0^4 - 0.0764344 u_0^6 - 0.0286629 u_0^8}{Q_0^2 \tau^4 \left(1 + u_0^2\right)^3} \tag{D.86}$$

$$s_{210002} = \frac{0.0000382324 - 0.000229394 u_0^4 - 0.000305859 u_0^6 - 0.000114697 u_0^8}{Q_0^2 \tau^4 \left(1 + u_0^2\right)^3} \tag{D.87}$$

$$s_{201002} = \frac{0.0000386376 - 0.000231825 u_0^4 - 0.0003091 u_0^6 - 0.000115913 u_0^8}{Q_0^2 \tau^4 \left(1 + u_0^2\right)^3} \tag{D.88}$$

$$s_{200102} = \frac{-0.00117486 + 0.00704913 u_0^4 + 0.00939884 u_0^6 + 0.00352457 u_0^8}{Q_0^2 \tau^4 \left(1 + u_0^2\right)^3} \tag{D.89}$$

$$s_{200012} = \frac{-0.0032175 + 0.019305 u_0^4 + 0.02574 u_0^6 + 0.00965251 u_0^8}{Q_0^2 \tau^4 \left(1 + u_0^2\right)^3} \tag{D.90}$$

$$s_{200111} = \frac{0.00697741 - 0.0418645u_0^4 - 0.0558193u_0^6 - 0.0209322u_0^8}{Q_0^2\tau^4\left(1+u_0^2\right)^3} \tag{D.91}$$

$$s_{201011} = \frac{-0.000229467 + 0.0013768u_0^4 + 0.00183573u_0^6 + 0.0006884u_0^8}{Q_0^2\tau^4\left(1+u_0^2\right)^3} \tag{D.92}$$

$$s_{201101} = \frac{-0.0000837886 + 0.000502732u_0^4 + 0.000670309u_0^6 + 0.000251366u_0^8}{Q_0^2\tau^4\left(1+u_0^2\right)^3} \tag{D.93}$$

$$s_{201110} = \frac{0.000248809 - 0.00149285u_0^4 - 0.00199047u_0^6 - 0.000746426u_0^8}{Q_0^2\tau^4\left(1+u_0^2\right)^3} \tag{D.94}$$

$$s_{210011} = \frac{-0.000227061 + 0.00136236u_0^4 + 0.00181648u_0^6 + 0.000681182u_0^8}{Q_0^2\tau^4\left(1+u_0^2\right)^3} \tag{D.95}$$

$$s_{210101} = \frac{-0.00008291 + 0.00049746u_0^4 + 0.00066328u_0^6 + 0.00024873u_0^8}{Q_0^2\tau^4\left(1+u_0^2\right)^3} \tag{D.96}$$

$$s_{210110} = \frac{0.0002462 - 0.0014772u_0^4 - 0.0019696u_0^6 - 0.000738599u_0^8}{Q_0^2\tau^4\left(1+u_0^2\right)^3} \tag{D.97}$$

$$s_{211001} = \frac{2.72667\times10^{-6} - 0.00001636u_0^4 - 0.0000218133u_0^6 - 8.18001\times10^{-6}u_0^8}{Q_0^2\tau^4\left(1+u_0^2\right)^3} \tag{D.98}$$

$$s_{211010} = \frac{-8.09678\times10^{-6} + 0.0000485807u_0^4 + 0.0000647743u_0^6 + 0.0000242903u_0^8}{Q_0^2\tau^4\left(1+u_0^2\right)^3} \tag{D.99}$$

$$s_{211100} = \frac{-2.9565\times10^{-6} + 0.000017739u_0^4 + 0.000023652u_0^6 + 8.8695\times10^{-6}u_0^8}{Q_0^2\tau^4\left(1+u_0^2\right)^3} \tag{D.100}$$

$$s_{320000} = -\frac{0.0000355095u_0}{Q_0\tau^2} \tag{D.101}$$

$$s_{302000} = -\frac{0.000036266u_0}{Q_0\tau^2} \tag{D.102}$$

$$s_{300200} = -\frac{0.0335312u_0}{Q_0\tau^2} \tag{D.103}$$

$$s_{300020} = -\frac{0.251489u_0}{Q_0\tau^2} \tag{D.104}$$

$$s_{300002} = -\frac{0.0285206u_0}{Q_0\tau^2} \tag{D.105}$$

$$s_{311000} = -\frac{0.0000717715u_0}{Q_0\tau^2} \tag{D.106}$$

$$s_{310100} = \frac{0.00218236u_0}{Q_0\tau^2} \tag{D.107}$$

$$s_{310010} = \frac{0.0059767u_0}{Q_0\tau^2} \tag{D.108}$$

$$s_{310001} = -\frac{0.00201271u_0}{Q_0\tau^2} \tag{D.109}$$

$$s_{301100} = \frac{0.00220549u_0}{Q_0\tau^2} \tag{D.110}$$

$$s_{301010} = \frac{0.00604003u_0}{Q_0\tau^2} \tag{D.111}$$

$$s_{301001} = -\frac{0.00203404u_0}{Q_0\tau^2} \tag{D.112}$$

$$s_{300110} = -\frac{0.18366u_0}{Q_0\tau^2} \tag{D.113}$$

$$s_{300101} = \frac{0.0618492u_0}{Q_0\tau^2} \tag{D.114}$$

$$s_{300011} = \frac{0.169383u_0}{Q_0\tau^2} \tag{D.115}$$

$$s_{330000} = \frac{3.66146\times10^{-8} - 2.19688\times10^{-7}u_0^4 - 2.92917\times10^{-7}u_0^6 - 1.09844\times10^{-7}u_0^8}{Q_0^2\tau^4\left(1+u_0^2\right)^3} \tag{D.116}$$

$$s_{303000} = \frac{3.7791\times10^{-8} - 2.26746\times10^{-7}u_0^4 - 3.02328\times10^{-7}u_0^6 - 1.13373\times10^{-7}u_0^8}{Q_0^2\tau^4\left(1+u_0^2\right)^3} \tag{D.117}$$

$$s_{300300} = \frac{-0.00106246 + 0.00637476u_0^4 + 0.00849968u_0^6 + 0.00318738u_0^8}{Q_0^2\tau^4\left(1+u_0^2\right)^3} \tag{D.118}$$

$$s_{300030} = \frac{-0.0218231 + 0.130939u_0^4 + 0.174585u_0^6 + 0.0654693u_0^8}{Q_0^2\tau^4\left(1+u_0^2\right)^3} \tag{D.119}$$

$$s_{300003} = \frac{0.000833443 - 0.00500066u_0^4 - 0.00666754u_0^6 - 0.00250033u_0^8}{Q_0^2\tau^4\left(1+u_0^2\right)^3} \tag{D.120}$$

$$s_{321000} = \frac{1.11008\times10^{-7} - 6.66047\times10^{-7}u_0^4 - 8.88062\times10^{-7}u_0^6 - 3.33023\times10^{-7}u_0^8}{Q_0^2\tau^4\left(1+u_0^2\right)^3} \tag{D.121}$$

$$s_{320100} = \frac{-3.37542\times10^{-6} + 0.0000202525u_0^4 + 0.0000270034u_0^6 + 0.0000101263u_0^8}{Q_0^2\tau^4\left(1+u_0^2\right)^3} \tag{D.122}$$

$$s_{320010} = \frac{-9.24406\times10^{-6} + 0.0000554644u_0^4 + 0.0000739525u_0^6 + 0.0000277322u_0^8}{Q_0^2\tau^4\left(1+u_0^2\right)^3} \tag{D.123}$$

$$s_{320001} = \frac{3.11303\times10^{-6} - 0.0000186782u_0^4 - 0.0000249042u_0^6 - 9.33908\times10^{-6}u_0^8}{Q_0^2\tau^4\left(1+u_0^2\right)^3} \tag{D.124}$$

$$s_{312000} = \frac{1.12184\times10^{-7} - 6.73105\times10^{-7}u_0^4 - 8.97473\times10^{-7}u_0^6 - 3.36552\times10^{-7}u_0^8}{Q_0^2\tau^4\left(1+u_0^2\right)^3} \tag{D.125}$$

$$s_{302100} = \frac{-3.44734\times10^{-6} + 0.000020684u_0^4 + 0.0000275787u_0^6 + 0.000010342u_0^8}{Q_0^2\tau^4\left(1+u_0^2\right)^3} \tag{D.126}$$

$$s_{302010} = \frac{-9.44102\times10^{-6} + 0.0000566461u_0^4 + 0.0000755281u_0^6 + 0.0000283231u_0^8}{Q_0^2\tau^4\left(1+u_0^2\right)^3} \tag{D.127}$$

$$s_{302001} = \frac{3.17935\times10^{-6} - 0.0000190761u_0^4 - 0.0000254348u_0^6 - 9.53806\times10^{-6}u_0^8}{Q_0^2\tau^4\left(1+u_0^2\right)^3} \tag{D.128}$$

$$s_{310200} = \frac{0.000103724 - 0.000622347u_0^4 - 0.000829795u_0^6 - 0.000311173u_0^8}{Q_0^2\tau^4\left(1+u_0^2\right)^3} \tag{D.129}$$

$$s_{301200} = \frac{0.000104824 - 0.000628942u_0^4 - 0.000838589u_0^6 - 0.000314471u_0^8}{Q_0^2\tau^4\left(1+u_0^2\right)^3} \tag{D.130}$$

$$s_{300210} = \frac{-0.00872908 + 0.0523745u_0^4 + 0.0698326u_0^6 + 0.0261872u_0^8}{Q_0^2\tau^4\left(1+u_0^2\right)^3} \tag{D.131}$$

$$s_{300201} = \frac{0.0029396 - 0.0176376u_0^4 - 0.0235168u_0^6 - 0.0088188u_0^8}{Q_0^2\tau^4\left(1+u_0^2\right)^3} \tag{D.132}$$

$$s_{310020} = \frac{0.000777947 - 0.00466768u_0^4 - 0.00622358u_0^6 - 0.00233384u_0^8}{Q_0^2\tau^4\left(1+u_0^2\right)^3} \tag{D.133}$$

$$s_{301020} = \frac{0.000786191 - 0.00471715u_0^4 - 0.00628953u_0^6 - 0.00235857u_0^8}{Q_0^2\tau^4\left(1+u_0^2\right)^3} \tag{D.134}$$

$$s_{300120} = \frac{-0.0239058 + 0.143435u_0^4 + 0.191246u_0^6 + 0.0717174u_0^8}{Q_0^2\tau^4\left(1+u_0^2\right)^3} \tag{D.135}$$

$$s_{300021} = \frac{0.0220474 - 0.132284u_0^4 - 0.176379u_0^6 - 0.0661422u_0^8}{Q_0^2\tau^4\left(1+u_0^2\right)^3} \tag{D.136}$$

$$s_{310002} = \frac{0.0000882246 - 0.000529348u_0^4 - 0.000705797u_0^6 - 0.000264674u_0^8}{Q_0^2\tau^4\left(1+u_0^2\right)^3} \tag{D.137}$$

$$s_{301002} = \frac{0.0000891596 - 0.000534957u_0^4 - 0.000713276u_0^6 - 0.000267479u_0^8}{Q_0^2\tau^4\left(1+u_0^2\right)^3} \tag{D.138}$$

$$s_{300102} = \frac{-0.00271108 + 0.0162665u_0^4 + 0.0216887u_0^6 + 0.00813325u_0^8}{Q_0^2\tau^4\left(1+u_0^2\right)^3} \tag{D.139}$$

$$s_{300012} = \frac{-0.00742467 + 0.044548u_0^4 + 0.0593974u_0^6 + 0.022274u_0^8}{Q_0^2\tau^4\left(1+u_0^2\right)^3} \tag{D.140}$$

$$s_{300111} = \frac{0.016101 - 0.096606u_0^4 - 0.128808u_0^6 - 0.048303u_0^8}{Q_0^2\tau^4\left(1+u_0^2\right)^3} \tag{D.141}$$

$$s_{301011} = \frac{-0.000529515 + 0.00317709u_0^4 + 0.00423612u_0^6 + 0.00158854u_0^8}{Q_0^2\tau^4\left(1+u_0^2\right)^3} \tag{D.142}$$

$$s_{301101} = \frac{-0.00019335 + 0.0011601u_0^4 + 0.0015468u_0^6 + 0.000580049u_0^8}{Q_0^2\tau^4\left(1+u_0^2\right)^3} \tag{D.143}$$

$$s_{301110} = \frac{0.000574148 - 0.00344489u_0^4 - 0.00459318u_0^6 - 0.00172244u_0^8}{Q_0^2\tau^4\left(1+u_0^2\right)^3} \tag{D.144}$$

$$s_{310011} = \frac{-0.000523962 + 0.00314377u_0^4 + 0.0041917u_0^6 + 0.00157189u_0^8}{Q_0^2\tau^4\left(1+u_0^2\right)^3} \tag{D.145}$$

$$s_{310101} = \frac{-0.000191322 + 0.00114793u_0^4 + 0.00153058u_0^6 + 0.000573967u_0^8}{Q_0^2\tau^4\left(1+u_0^2\right)^3} \tag{D.146}$$

$$s_{310110} = \frac{0.000568127 - 0.00340876u_0^4 - 0.00454502u_0^6 - 0.00170438u_0^8}{Q_0^2\tau^4\left(1+u_0^2\right)^3} \tag{D.147}$$

$$s_{311001} = \frac{6.29203\times10^{-6} - 0.0000377522u_0^4 - 0.0000503362u_0^6 - 0.0000188761u_0^8}{Q_0^2\tau^4\left(1+u_0^2\right)^3} \tag{D.148}$$

$$s_{311010} = \frac{-0.000018684 + 0.000112104u_0^4 + 0.000149472u_0^6 + 0.0000560521u_0^8}{Q_0^2\tau^4\left(1+u_0^2\right)^3} \tag{D.149}$$

$$s_{311100} = \frac{-6.82238\times10^{-6} + 0.0000409343u_0^4 + 0.0000545791u_0^6 + 0.0000204672u_0^8}{Q_0^2\tau^4\left(1+u_0^2\right)^3} \tag{D.150}$$

$$s_{420000} = \frac{0.0000191286u_0}{Q_0\tau^2} \tag{D.151}$$

$$s_{402000} = \frac{0.0000195362u_0}{Q_0\tau^2} \tag{D.152}$$

$$s_{400200} = \frac{0.018063u_0}{Q_0\tau^2} \tag{D.153}$$

$$s_{400020} = \frac{0.135475u_0}{Q_0\tau^2} \tag{D.154}$$

$$s_{400002} = \frac{0.0153638u_0}{Q_0\tau^2} \tag{D.155}$$

$$s_{411000} = \frac{0.0000386627u_0}{Q_0\tau^2} \tag{D.156}$$

$$s_{410100} = -\frac{0.00117562u_0}{Q_0\tau^2} \tag{D.157}$$

$$s_{410010} = -\frac{0.0032196u_0}{Q_0\tau^2} \tag{D.158}$$

$$s_{410001} = \frac{0.00108423u_0}{Q_0\tau^2} \tag{D.159}$$

$$s_{401100} = -\frac{0.00118808u_0}{Q_0\tau^2} \tag{D.160}$$

$$s_{401010} = -\frac{0.00325371u_0}{Q_0\tau^2} \tag{D.161}$$

$$s_{401001} = \frac{0.00109572u_0}{Q_0\tau^2} \tag{D.162}$$

$$s_{400110} = \frac{0.098936u_0}{Q_0\tau^2} \tag{D.163}$$

$$s_{400101} = -\frac{0.0333176u_0}{Q_0\tau^2} \tag{D.164}$$

$$s_{400011} = -\frac{0.0912449u_0}{Q_0\tau^2} \tag{D.165}$$

$$s_{430000} = \frac{-1.9724 \times 10^{-8} + 1.18344 \times 10^{-7}u_0^4 + 1.57792 \times 10^{-7}u_0^6 + 5.91719 \times 10^{-8}u_0^8}{Q_0^2\tau^4\left(1+u_0^2\right)^3} \tag{D.166}$$

$$s_{403000} = \frac{-2.03577 \times 10^{-8} + 1.22146 \times 10^{-7}u_0^4 + 1.62861 \times 10^{-7}u_0^6 + 6.1073 \times 10^{-8}u_0^8}{Q_0^2\tau^4\left(1+u_0^2\right)^3} \tag{D.167}$$

$$s_{400300} = \frac{0.000572338 - 0.00343403u_0^4 - 0.0045787u_0^6 - 0.00171701u_0^8}{Q_0^2\tau^4\left(1+u_0^2\right)^3} \tag{D.168}$$

$$s_{400030} = \frac{0.0117559 - 0.0705355u_0^4 - 0.0940473u_0^6 - 0.0352677u_0^8}{Q_0^2\tau^4\left(1+u_0^2\right)^3} \tag{D.169}$$

$$s_{400003} = \frac{-0.000448969 + 0.00269381u_0^4 + 0.00359175u_0^6 + 0.00134691u_0^8}{Q_0^2\tau^4\left(1+u_0^2\right)^3} \tag{D.170}$$

$$s_{421000} = \frac{-5.97989\times10^{-8}+3.58794\times10^{-7}u_0^4+4.78391\times10^{-7}u_0^6+1.79397\times10^{-7}u_0^8}{Q_0^2\tau^4\left(1+u_0^2\right)^3} \tag{D.171}$$

$$s_{420100} = \frac{1.81831\times10^{-6}-0.0000109099u_0^4-0.0000145465u_0^6-5.45493\times10^{-6}u_0^8}{Q_0^2\tau^4\left(1+u_0^2\right)^3} \tag{D.172}$$

$$s_{420010} = \frac{4.9797\times10^{-6}-0.0000298782u_0^4-0.0000398376u_0^6-0.0000149391u_0^8}{Q_0^2\tau^4\left(1+u_0^2\right)^3} \tag{D.173}$$

$$s_{420001} = \frac{-1.67696\times10^{-6}+0.0000100618u_0^4+0.0000134157u_0^6+5.03088\times10^{-6}u_0^8}{Q_0^2\tau^4\left(1+u_0^2\right)^3} \tag{D.174}$$

$$s_{412000} = \frac{-6.04326\times10^{-8}+3.62596\times10^{-7}u_0^4+4.83461\times10^{-7}u_0^6+1.81298\times10^{-7}u_0^8}{Q_0^2\tau^4\left(1+u_0^2\right)^3} \tag{D.175}$$

$$s_{402100} = \frac{1.85705\times10^{-6}-0.0000111423u_0^4-0.0000148564u_0^6-5.57116\times10^{-6}u_0^8}{Q_0^2\tau^4\left(1+u_0^2\right)^3} \tag{D.176}$$

$$s_{402010} = \frac{5.08579\times10^{-6}-0.0000305148u_0^4-0.0000406864u_0^6-0.0000152574u_0^8}{Q_0^2\tau^4\left(1+u_0^2\right)^3} \tag{D.177}$$

$$s_{402001} = \frac{-1.71269\times10^{-6}+0.0000102761u_0^4+0.0000137015u_0^6+5.13807\times10^{-6}u_0^8}{Q_0^2\tau^4\left(1+u_0^2\right)^3} \tag{D.178}$$

$$s_{410200} = \frac{-0.0000558754+0.000335253u_0^4+0.000447004u_0^6+0.000167626u_0^8}{Q_0^2\tau^4\left(1+u_0^2\right)^3} \tag{D.179}$$

$$s_{401200} = \frac{-0.0000564676+0.000338805u_0^4+0.00045174u_0^6+0.000169403u_0^8}{Q_0^2\tau^4\left(1+u_0^2\right)^3} \tag{D.180}$$

$$s_{400210} = \frac{0.00470228-0.0282137u_0^4-0.0376182u_0^6-0.0141068u_0^8}{Q_0^2\tau^4\left(1+u_0^2\right)^3} \tag{D.181}$$

$$s_{400201} = \frac{-0.00158354+0.00950122u_0^4+0.0126683u_0^6+0.00475061u_0^8}{Q_0^2\tau^4\left(1+u_0^2\right)^3} \tag{D.182}$$

$$s_{410020} = \frac{-0.000419073+0.00251444u_0^4+0.00335259u_0^6+0.00125722u_0^8}{Q_0^2\tau^4\left(1+u_0^2\right)^3} \tag{D.183}$$

$$s_{401020} = \frac{-0.000423514+0.00254109u_0^4+0.00338812u_0^6+0.00127054u_0^8}{Q_0^2\tau^4\left(1+u_0^2\right)^3} \tag{D.184}$$

$$s_{400120} = \frac{0.0128778-0.077267u_0^4-0.103023u_0^6-0.0386335u_0^8}{Q_0^2\tau^4\left(1+u_0^2\right)^3} \tag{D.185}$$

$$s_{400021} = \frac{-0.0118767+0.0712605u_0^4+0.095014u_0^6+0.0356302u_0^8}{Q_0^2\tau^4\left(1+u_0^2\right)^3} \tag{D.186}$$

$$s_{410002} = \frac{-0.0000475258+0.000285155u_0^4+0.000380207u_0^6+0.000142578u_0^8}{Q_0^2\tau^4\left(1+u_0^2\right)^3} \tag{D.187}$$

$$s_{401002} = \frac{-0.0000480295+0.000288177u_0^4+0.000384236u_0^6+0.000144088u_0^8}{Q_0^2\tau^4\left(1+u_0^2\right)^3} \tag{D.188}$$

$$s_{400102} = \frac{0.00146044-0.00876262u_0^4-0.0116835u_0^6-0.00438131u_0^8}{Q_0^2\tau^4\left(1+u_0^2\right)^3} \tag{D.189}$$

$$s_{400012} = \frac{0.00399961-0.0239976u_0^4-0.0319969u_0^6-0.0119988u_0^8}{Q_0^2\tau^4\left(1+u_0^2\right)^3} \tag{D.190}$$

$$s_{400111} = \frac{-0.00867347 + 0.0520408u_0^4 + 0.0693878u_0^6 + 0.0260204u_0^8}{Q_0^2\tau^4\left(1+u_0^2\right)^3} \tag{D.191}$$

$$s_{401011} = \frac{0.000285245 - 0.00171147u_0^4 - 0.00228196u_0^6 - 0.000855735u_0^8}{Q_0^2\tau^4\left(1+u_0^2\right)^3} \tag{D.192}$$

$$s_{401101} = \frac{0.000104156 - 0.000624935u_0^4 - 0.000833246u_0^6 - 0.000312467u_0^8}{Q_0^2\tau^4\left(1+u_0^2\right)^3} \tag{D.193}$$

$$s_{401110} = \frac{-0.000309288 + 0.00185573u_0^4 + 0.00247431u_0^6 + 0.000927865u_0^8}{Q_0^2\tau^4\left(1+u_0^2\right)^3} \tag{D.194}$$

$$s_{410011} = \frac{0.000282254 - 0.00169352u_0^4 - 0.00225803u_0^6 - 0.000846762u_0^8}{Q_0^2\tau^4\left(1+u_0^2\right)^3} \tag{D.195}$$

$$s_{410101} = \frac{0.000103064 - 0.000618382u_0^4 - 0.000824509u_0^6 - 0.000309191u_0^8}{Q_0^2\tau^4\left(1+u_0^2\right)^3} \tag{D.196}$$

$$s_{410110} = \frac{-0.000306045 + 0.00183627u_0^4 + 0.00244836u_0^6 + 0.000918136u_0^8}{Q_0^2\tau^4\left(1+u_0^2\right)^3} \tag{D.197}$$

$$s_{411001} = \frac{-3.38946\times10^{-6} + 0.0000203368u_0^4 + 0.0000271157u_0^6 + 0.0000101684u_0^8}{Q_0^2\tau^4\left(1+u_0^2\right)^3} \tag{D.198}$$

$$s_{411010} = \frac{0.0000100649 - 0.0000603896u_0^4 - 0.0000805194u_0^6 - 0.0000301948u_0^8}{Q_0^2\tau^4\left(1+u_0^2\right)^3} \tag{D.199}$$

$$s_{411100} = \frac{3.67516\times10^{-6} - 0.000022051u_0^4 - 0.0000294013u_0^6 - 0.0000110255u_0^8}{Q_0^2\tau^4\left(1+u_0^2\right)^3} \tag{D.200}$$

$$s_{520000} = \frac{0.0000182939u_0}{Q_0\tau^2} \tag{D.201}$$

$$s_{502000} = \frac{0.0000186836u_0}{Q_0\tau^2} \tag{D.202}$$

$$s_{500200} = \frac{0.0172747u_0}{Q_0\tau^2} \tag{D.203}$$

$$s_{500020} = \frac{0.129563u_0}{Q_0\tau^2} \tag{D.204}$$

$$s_{500002} = \frac{0.0146933u_0}{Q_0\tau^2} \tag{D.205}$$

$$s_{511000} = \frac{0.0000369755u_0}{Q_0\tau^2} \tag{D.206}$$

$$s_{510100} = -\frac{0.00112432u_0}{Q_0\tau^2} \tag{D.207}$$

$$s_{510010} = -\frac{0.00307909u_0}{Q_0\tau^2} \tag{D.208}$$

$$s_{510001} = \frac{0.00103691u_0}{Q_0\tau^2} \tag{D.209}$$

$$s_{501100} = -\frac{0.00113623u_0}{Q_0\tau^2} \tag{D.210}$$

$$s_{501010} = -\frac{0.00311172u_0}{Q_0\tau^2} \tag{D.211}$$

$$s_{501001} = \frac{0.0010479u_0}{Q_0\tau^2} \tag{D.212}$$

$$s_{500110} = \frac{0.0946184u_0}{Q_0\tau^2} \tag{D.213}$$

$$s_{500101} = -\frac{0.0318637u_0}{Q_0\tau^2} \tag{D.214}$$

$$s_{500011} = -\frac{0.087263u_0}{Q_0\tau^2} \tag{D.215}$$

$$s_{530000} = \frac{-1.88632\times10^{-8}+1.13179\times10^{-7}u_0^4+1.50906\times10^{-7}u_0^6+5.65896\times10^{-8}u_0^8}{Q_0^2\tau^4\left(1+u_0^2\right)^3} \tag{D.216}$$

$$s_{503000} = \frac{-1.94693\times10^{-8}+1.16816\times10^{-7}u_0^4+1.55754\times10^{-7}u_0^6+5.84078\times10^{-8}u_0^8}{Q_0^2\tau^4\left(1+u_0^2\right)^3} \tag{D.217}$$

$$s_{500300} = \frac{0.000547361-0.00328417u_0^4-0.00437889u_0^6-0.00164208u_0^8}{Q_0^2\tau^4\left(1+u_0^2\right)^3} \tag{D.218}$$

$$s_{500030} = \frac{0.0112429-0.0674573u_0^4-0.0899431u_0^6-0.0337287u_0^8}{Q_0^2\tau^4\left(1+u_0^2\right)^3} \tag{D.219}$$

$$s_{500003} = \frac{-0.000429376+0.00257625u_0^4+0.003435u_0^6+0.00128813u_0^8}{Q_0^2\tau^4\left(1+u_0^2\right)^3} \tag{D.220}$$

$$s_{521000} = \frac{-5.71893\times10^{-8}+3.43136\times10^{-7}u_0^4+4.57514\times10^{-7}u_0^6+1.71568\times10^{-7}u_0^8}{Q_0^2\tau^4\left(1+u_0^2\right)^3} \tag{D.221}$$

$$s_{520100} = \frac{1.73896\times10^{-6}-0.0000104338u_0^4-0.0000139117u_0^6-5.21688\times10^{-6}u_0^8}{Q_0^2\tau^4\left(1+u_0^2\right)^3} \tag{D.222}$$

$$s_{520010} = \frac{4.76238\times10^{-6}-0.0000285743u_0^4-0.0000380991u_0^6-0.0000142871u_0^8}{Q_0^2\tau^4\left(1+u_0^2\right)^3} \tag{D.223}$$

$$s_{520001} = \frac{-1.60378\times10^{-6}+9.62266\times10^{-6}u_0^4+0.0000128302u_0^6+4.81133\times10^{-6}u_0^8}{Q_0^2\tau^4\left(1+u_0^2\right)^3} \tag{D.224}$$

$$s_{512000} = \frac{-5.77953\times10^{-8}+3.46772\times10^{-7}u_0^4+4.62363\times10^{-7}u_0^6+1.73386\times10^{-7}u_0^8}{Q_0^2\tau^4\left(1+u_0^2\right)^3} \tag{D.225}$$

$$s_{502100} = \frac{1.77601\times10^{-6}-0.0000106561u_0^4-0.0000142081u_0^6-5.32803\times10^{-6}u_0^8}{Q_0^2\tau^4\left(1+u_0^2\right)^3} \tag{D.226}$$

$$s_{502010} = \frac{4.86385\times10^{-6}-0.0000291831u_0^4-0.0000389108u_0^6-0.0000145916u_0^8}{Q_0^2\tau^4\left(1+u_0^2\right)^3} \tag{D.227}$$

$$s_{502001} = \frac{-1.63795\times10^{-6}+9.82769\times10^{-6}u_0^4+0.0000131036u_0^6+4.91384\times10^{-6}u_0^8}{Q_0^2\tau^4\left(1+u_0^2\right)^3} \tag{D.228}$$

$$s_{510200} = \frac{-0.000053437+0.000320622u_0^4+0.000427496u_0^6+0.000160311u_0^8}{Q_0^2\tau^4\left(1+u_0^2\right)^3} \tag{D.229}$$

$$s_{501200} = \frac{-0.0000540033+0.00032402u_0^4+0.000432027u_0^6+0.00016201u_0^8}{Q_0^2\tau^4\left(1+u_0^2\right)^3} \tag{D.230}$$

$$s_{500210} = \frac{0.00449707 - 0.0269824u_0^4 - 0.0359766u_0^6 - 0.0134912u_0^8}{Q_0^2\tau^4\left(1+u_0^2\right)^3} \tag{D.231}$$

$$s_{500201} = \frac{-0.00151443 + 0.00908659u_0^4 + 0.0121155u_0^6 + 0.0045433u_0^8}{Q_0^2\tau^4\left(1+u_0^2\right)^3} \tag{D.232}$$

$$s_{510020} = \frac{-0.000400785 + 0.00240471u_0^4 + 0.00320628u_0^6 + 0.00120236u_0^8}{Q_0^2\tau^4\left(1+u_0^2\right)^3} \tag{D.233}$$

$$s_{501020} = \frac{-0.000405032 + 0.00243019u_0^4 + 0.00324026u_0^6 + 0.0012151u_0^8}{Q_0^2\tau^4\left(1+u_0^2\right)^3} \tag{D.234}$$

$$s_{500120} = \frac{0.0123159 - 0.0738951u_0^4 - 0.0985268u_0^6 - 0.0369476u_0^8}{Q_0^2\tau^4\left(1+u_0^2\right)^3} \tag{D.235}$$

$$s_{500021} = \frac{-0.0113584 + 0.0681507u_0^4 + 0.0908676u_0^6 + 0.0340753u_0^8}{Q_0^2\tau^4\left(1+u_0^2\right)^3} \tag{D.236}$$

$$s_{510002} = \frac{-0.0000454518 + 0.000272711u_0^4 + 0.000363615u_0^6 + 0.000136355u_0^8}{Q_0^2\tau^4\left(1+u_0^2\right)^3} \tag{D.237}$$

$$s_{501002} = \frac{-0.0000459335 + 0.000275601u_0^4 + 0.000367468u_0^6 + 0.0001378u_0^8}{Q_0^2\tau^4\left(1+u_0^2\right)^3} \tag{D.238}$$

$$s_{500102} = \frac{0.0013967 - 0.00838022u_0^4 - 0.0111736u_0^6 - 0.00419011u_0^8}{Q_0^2\tau^4\left(1+u_0^2\right)^3} \tag{D.239}$$

$$s_{500012} = \frac{0.00382506 - 0.0229504u_0^4 - 0.0306005u_0^6 - 0.0114752u_0^8}{Q_0^2\tau^4\left(1+u_0^2\right)^3} \tag{D.240}$$

$$s_{500111} = \frac{-0.00829496 + 0.0497698u_0^4 + 0.0663597u_0^6 + 0.0248849u_0^8}{Q_0^2\tau^4\left(1+u_0^2\right)^3} \tag{D.241}$$

$$s_{501011} = \frac{0.000272797 - 0.00163678u_0^4 - 0.00218238u_0^6 - 0.000818391u_0^8}{Q_0^2\tau^4\left(1+u_0^2\right)^3} \tag{D.242}$$

$$s_{501101} = \frac{0.0000996105 - 0.000597663u_0^4 - 0.000796884u_0^6 - 0.000298831u_0^8}{Q_0^2\tau^4\left(1+u_0^2\right)^3} \tag{D.243}$$

$$s_{501110} = \frac{-0.000295791 + 0.00177475u_0^4 + 0.00236633u_0^6 + 0.000887373u_0^8}{Q_0^2\tau^4\left(1+u_0^2\right)^3} \tag{D.244}$$

$$s_{510011} = \frac{0.000269936 - 0.00161962u_0^4 - 0.00215949u_0^6 - 0.000809809u_0^8}{Q_0^2\tau^4\left(1+u_0^2\right)^3} \tag{D.245}$$

$$s_{510101} = \frac{0.0000985659 - 0.000591396u_0^4 - 0.000788528u_0^6 - 0.000295698u_0^8}{Q_0^2\tau^4\left(1+u_0^2\right)^3} \tag{D.246}$$

$$s_{510110} = \frac{-0.000292689 + 0.00175614u_0^4 + 0.00234152u_0^6 + 0.000878068u_0^8}{Q_0^2\tau^4\left(1+u_0^2\right)^3} \tag{D.247}$$

$$s_{511001} = \frac{-3.24155\times10^{-6} + 0.0000194493u_0^4 + 0.0000259324u_0^6 + 9.72464\times10^{-6}u_0^8}{Q_0^2\tau^4\left(1+u_0^2\right)^3} \tag{D.248}$$

$$s_{511010} = \frac{9.6257\times10^{-6} - 0.0000577542u_0^4 - 0.0000770056u_0^6 - 0.0000288771u_0^8}{Q_0^2\tau^4\left(1+u_0^2\right)^3} \tag{D.249}$$

$$s_{511100} = \frac{3.51478\times10^{-6} - 0.0000210887u_0^4 - 0.0000281182u_0^6 - 0.0000105443u_0^8}{Q_0^2\tau^4\left(1+u_0^2\right)^3} \tag{D.250}$$

Appendix E

Coefficients double NS bifurcation: part II

Coefficients a_{hklm}, b_{hklm}, c_{hklm} and d_{hklm} relative to the nonlinear terms after the center manifold reduction, relative to the double NS bifurcation under study in Ch. 4.

All the second order terms are not written explicitly, since $a_{hklm} = s_{1hklm0}$ and similarly $b_{hklm} = s_{2hklm0}$, $c_{hklm} = s_{3hklm0}$ and $d_{hklm} = s_{4hklm0}$. This because they are not effected by the center manifold reduction.

$$\begin{aligned} a_{3000} &= \frac{-1.62001 \times 10^{-8}}{Q_0^2\tau^4\left(1+u_0^2\right)^3} + \frac{6.41313 \times 10^{-8}u_0^2 + 3.53726 \times 10^{-7}u_0^4}{Q_0^2\tau^4\left(1+u_0^2\right)^4} + \\ &\quad \frac{6.1159 \times 10^{-7}u_0^6 + 4.34727 \times 10^{-7}u_0^8 + 1.12732 \times 10^{-7}u_0^{10}}{Q_0^2\tau^4\left(1+u_0^2\right)^4} \end{aligned} \tag{E.1}$$

$$\begin{aligned} a_{0300} &= \frac{-1.67206 \times 10^{-8} + 6.67985 \times 10^{-9}u_0^2 + 1.93926 \times 10^{-7}u_0^4}{Q_0^2\tau^4\left(1+u_0^2\right)^4} \\ &\quad + \frac{3.74492 \times 10^{-7}u_0^6 + 2.77529 \times 10^{-7}u_0^8 + 7.35623 \times 10^{-8}u_0^{10}}{Q_0^2\tau^4\left(1+u_0^2\right)^4} \end{aligned} \tag{E.2}$$

$$\begin{aligned} a_{0030} &= \frac{0.000470085 - 0.00645667u_0^2 - 0.0305275u_0^4}{Q_0^2\tau^4\left(1+u_0^2\right)^4} + \\ &\quad \frac{-0.0481417u_0^6 - 0.032878u_0^8 - 0.00833701u_0^{10}}{Q_0^2\tau^4\left(1+u_0^2\right)^4} \end{aligned} \tag{E.3}$$

$$\begin{aligned} a_{0003} &= \frac{0.00965563 - 0.000544298u_0^2 - 0.0987335u_0^4}{Q_0^2\tau^4\left(1+u_0^2\right)^4} + \\ &\quad \frac{-0.196378u_0^6 - 0.147012u_0^8 - 0.0391668u_0^{10}}{Q_0^2\tau^4\left(1+u_0^2\right)^4} \end{aligned} \tag{E.4}$$

$$a_{2100} = \frac{-4.91154\times10^{-8}}{Q_0^2\tau^4\left(1+u_0^2\right)^3}+\frac{6.38795\times10^{-8}u_0^2+5.5021\times10^{-7}u_0^4}{Q_0^2\tau^4\left(1+u_0^2\right)^4}+ \frac{1.07089\times10^{-6}u_0^6+7.95787\times10^{-7}u_0^8+2.11226\times10^{-7}u_0^{10}}{Q_0^2\tau^4\left(1+u_0^2\right)^4} \tag{E.5}$$

$$a_{2010} = \frac{1.49346\times10^{-6}}{Q_0^2\tau^4\left(1+u_0^2\right)^3}+\frac{-8.11456\times10^{-6}u_0^2-0.000041419u_0^4}{Q_0^2\tau^4\left(1+u_0^2\right)^4}+ \frac{0.0000695957u_0^6-0.0000488862u_0^8-0.0000125949u_0^{10}}{Q_0^2\tau^4\left(1+u_0^2\right)^4} \tag{E.6}$$

$$a_{2001} = \frac{4.09003\times10^{-6}}{Q_0^2\tau^4\left(1+u_0^2\right)^3}+\frac{-3.90139\times10^{-6}u_0^2-0.0000401458u_0^4}{Q_0^2\tau^4\left(1+u_0^2\right)^4}+ \frac{-0.0000806688u_0^6-0.0000605959u_0^8-0.0000161715u_0^{10}}{Q_0^2\tau^4\left(1+u_0^2\right)^4} \tag{E.7}$$

$$a_{1200} = \frac{-4.96359\times10^{-8}}{Q_0^2\tau^4\left(1+u_0^2\right)^3}+\frac{2.22138\times10^{-8}u_0^2+3.8667\times10^{-7}u_0^4}{Q_0^2\tau^4\left(1+u_0^2\right)^4}+ \frac{8.28185\times10^{-7}u_0^6+6.3485\times10^{-7}u_0^8+1.71121\times10^{-7}u_0^{10}}{Q_0^2\tau^4\left(1+u_0^2\right)^4} \tag{E.8}$$

$$a_{0210} = \frac{1.52528\times10^{-6}}{Q_0^2\tau^4\left(1+u_0^2\right)^3}+\frac{-2.6449\times10^{-6}u_0^2-0.0000197313u_0^4}{Q_0^2\tau^4\left(1+u_0^2\right)^4}+ \frac{-0.0000372233u_0^6-0.0000273576u_0^8-7.22073\times10^{-6}u_0^{10}}{Q_0^2\tau^4\left(1+u_0^2\right)^4} \tag{E.9}$$

$$a_{0201} = \frac{4.17718\times10^{-6}}{Q_0^2\tau^4\left(1+u_0^2\right)^3}+\frac{-4.05064\times10^{-6}u_0^2-0.0000412656u_0^4}{Q_0^2\tau^4\left(1+u_0^2\right)^4}+ \frac{-0.0000827843u_0^6-0.0000621515u_0^8-0.0000165822u_0^{10}}{Q_0^2\tau^4\left(1+u_0^2\right)^4} \tag{E.10}$$

$$a_{1020} = \frac{-0.0000458929}{Q_0^2\tau^4\left(1+u_0^2\right)^3}+\frac{0.000414208u_0^2+0.00193219u_0^4}{Q_0^2\tau^4\left(1+u_0^2\right)^4}+ \frac{0.00312775u_0^6+0.00216165u_0^8+0.000551887u_0^{10}}{Q_0^2\tau^4\left(1+u_0^2\right)^4} \tag{E.11}$$

$$a_{0120} = \frac{-0.0000463792}{Q_0^2\tau^4\left(1+u_0^2\right)^3}+\frac{0.000286589u_0^2+0.00142463u_0^4}{Q_0^2\tau^4\left(1+u_0^2\right)^4}+ \frac{0.00236884u_0^6+0.00165653u_0^8+0.000425726u_0^{10}}{Q_0^2\tau^4\left(1+u_0^2\right)^4} \tag{E.12}$$

$$a_{0021} = \frac{0.00386218}{Q_0^2\tau^4\left(1+u_0^2\right)^3} + \frac{-0.0198608u_0^2 - 0.102616u_0^4}{Q_0^2\tau^4\left(1+u_0^2\right)^4} + \frac{-0.173235u_0^6 - 0.121927u_0^8 - 0.0314473u_0^{10}}{Q_0^2\tau^4\left(1+u_0^2\right)^4} \tag{E.13}$$

$$a_{1002} = \frac{-0.000344203}{Q_0^2\tau^4\left(1+u_0^2\right)^3} + \frac{-4.66856\times10^{-6}u_0^2 + 0.00204654u_0^4}{Q_0^2\tau^4\left(1+u_0^2\right)^4} + \frac{0.00479083u_0^6 + 0.00376756u_0^8 + 0.00102794u_0^{10}}{Q_0^2\tau^4\left(1+u_0^2\right)^4} \tag{E.14}$$

$$a_{0102} = \frac{-0.00034785}{Q_0^2\tau^4\left(1+u_0^2\right)^3} + \frac{0.000297527u_0^2 + 0.00327721u_0^4}{Q_0^2\tau^4\left(1+u_0^2\right)^4} + \frac{0.00665507u_0^6 + 0.00501646u_0^8 + 0.00134108u_0^{10}}{Q_0^2\tau^4\left(1+u_0^2\right)^4} \tag{E.15}$$

$$a_{0012} = \frac{0.0105771}{Q_0^2\tau^4\left(1+u_0^2\right)^3} + \frac{-0.00616439u_0^2 - 0.0881202u_0^4}{Q_0^2\tau^4\left(1+u_0^2\right)^4} + \frac{-0.185066u_0^6 - 0.141006u_0^8 - 0.0378957u_0^{10}}{Q_0^2\tau^4\left(1+u_0^2\right)^4} \tag{E.16}$$

$$a_{0111} = \frac{-0.000254032}{Q_0^2\tau^4\left(1+u_0^2\right)^3} + \frac{0.000254214u_0^2 + 0.00254105u_0^4}{Q_0^2\tau^4\left(1+u_0^2\right)^4} + \frac{0.00508173u_0^6 + 0.0038112u_0^8 + 0.00101631u_0^{10}}{Q_0^2\tau^4\left(1+u_0^2\right)^4} \tag{E.17}$$

$$a_{1011} = \frac{-0.000251368}{Q_0^2\tau^4\left(1+u_0^2\right)^3} + \frac{0.000500076u_0^2 + 0.00350851u_0^4}{Q_0^2\tau^4\left(1+u_0^2\right)^4} + \frac{0.00651961u_0^6 + 0.00476535u_0^8 + 0.00125418u_0^{10}}{Q_0^2\tau^4\left(1+u_0^2\right)^4} \tag{E.18}$$

$$a_{1101} = \frac{8.26675\times10^{-6}}{Q_0^2\tau^4\left(1+u_0^2\right)^3} + \frac{-4.9004\times10^{-7}u_0^2 - 0.0000515607u_0^4}{Q_0^2\tau^4\left(1+u_0^2\right)^4} + \frac{-0.000118675u_0^6 - 0.0000928944u_0^8 - 0.0000252903u_0^{10}}{Q_0^2\tau^4\left(1+u_0^2\right)^4} \tag{E.19}$$

$$a_{1110} = \frac{3.01856\times10^{-6}}{Q_0^2\tau^4\left(1+u_0^2\right)^3} + \frac{-8.09342\times10^{-6}u_0^2 - 0.0000504851u_0^4}{Q_0^2\tau^4\left(1+u_0^2\right)^4} + \frac{-0.0000908204u_0^6 - 0.0000655779u_0^8 - 0.0000171491u_0^{10}}{Q_0^2\tau^4\left(1+u_0^2\right)^4} \tag{E.20}$$

$$b_{3000} = \frac{1.5867\times10^{-8}}{Q_0^2\tau^4\left(1+u_0^2\right)^3}+\frac{-6.28127\times10^{-8}u_0^2-3.46453\times10^{-7}u_0^4}{Q_0^2\tau^4\left(1+u_0^2\right)^4}+ \frac{-5.99015\times10^{-7}u_0^6-4.25788\times10^{-7}u_0^8-1.10414\times10^{-7}u_0^{10}}{Q_0^2\tau^4\left(1+u_0^2\right)^4} \tag{E.21}$$

$$b_{0300} = \frac{1.63768\times10^{-8}-6.54251\times10^{-9}u_0^2-1.89938\times10^{-7}u_0^4}{Q_0^2\tau^4\left(1+u_0^2\right)^4} +\frac{-3.66792\times10^{-7}u_0^6-2.71822\times10^{-7}u_0^8-7.20498\times10^{-8}u_0^{10}}{Q_0^2\tau^4\left(1+u_0^2\right)^4} \tag{E.22}$$

$$b_{0030} = \frac{-0.00046042+0.00632392u_0^2+0.0298999u_0^4}{Q_0^2\tau^4\left(1+u_0^2\right)^4} +\frac{0.0471519u_0^6+0.032202u_0^8+0.0081656u_0^{10}}{Q_0^2\tau^4\left(1+u_0^2\right)^4} \tag{E.23}$$

$$b_{0003} = \frac{-0.0094571+0.000533107u_0^2+0.0967034u_0^4}{Q_0^2\tau^4\left(1+u_0^2\right)^4} +\frac{0.192341u_0^6+0.143989u_0^8+0.0383615u_0^{10}}{Q_0^2\tau^4\left(1+u_0^2\right)^4} \tag{E.24}$$

$$b_{2100} = \frac{4.81055\times10^{-8}}{Q_0^2\tau^4\left(1+u_0^2\right)^3}+\frac{-6.25661\times10^{-8}u_0^2-5.38898\times10^{-7}u_0^4}{Q_0^2\tau^4\left(1+u_0^2\right)^4}+ \frac{-1.04887\times10^{-6}u_0^6-7.79425\times10^{-7}u_0^8-2.06883\times10^{-7}u_0^{10}}{Q_0^2\tau^4\left(1+u_0^2\right)^4} \tag{E.25}$$

$$b_{2010} = \frac{-1.46275\times10^{-6}}{Q_0^2\tau^4\left(1+u_0^2\right)^3}+\frac{7.94772\times10^{-6}u_0^2+0.0000405674u_0^4}{Q_0^2\tau^4\left(1+u_0^2\right)^4}+ \frac{0.0000681648u_0^6+0.0000478811u_0^8+0.000012336u_0^{10}}{Q_0^2\tau^4\left(1+u_0^2\right)^4} \tag{E.26}$$

$$b_{2001} = \frac{-4.00594\times10^{-6}}{Q_0^2\tau^4\left(1+u_0^2\right)^3}+\frac{3.82117\times10^{-6}u_0^2+0.0000393203u_0^4}{Q_0^2\tau^4\left(1+u_0^2\right)^4}+ \frac{0.0000790102u_0^6+0.00005935u_0^8+0.000015839u_0^{10}}{Q_0^2\tau^4\left(1+u_0^2\right)^4} \tag{E.27}$$

$$b_{1200} = \frac{4.86153\times10^{-8}}{Q_0^2\tau^4\left(1+u_0^2\right)^3}+\frac{-2.17571\times10^{-8}u_0^2-3.7872\times10^{-7}u_0^4}{Q_0^2\tau^4\left(1+u_0^2\right)^4}+ \frac{-8.11157\times10^{-7}u_0^6-6.21797\times10^{-7}u_0^8-1.67603\times10^{-7}u_0^{10}}{Q_0^2\tau^4\left(1+u_0^2\right)^4} \tag{E.28}$$

$$b_{0210} = \frac{-1.49392\times10^{-6}}{Q_0^2\tau^4\left(1+u_0^2\right)^3}+\frac{2.59052\times10^{-6}u_0^2+0.0000193256u_0^4}{Q_0^2\tau^4\left(1+u_0^2\right)^4}+ \frac{0.0000364579u_0^6+0.0000267951u_0^8+7.07226\times10^{-6}u_0^{10}}{Q_0^2\tau^4\left(1+u_0^2\right)^4} \tag{E.29}$$

$$b_{0201} = \frac{-4.09129\times10^{-6}}{Q_0^2\tau^4\left(1+u_0^2\right)^3}+\frac{3.96735\times10^{-6}u_0^2+0.0000404172u_0^4}{Q_0^2\tau^4\left(1+u_0^2\right)^4}+ \frac{0.0000810822u_0^6+0.0000608736u_0^8+0.0000162412u_0^{10}}{Q_0^2\tau^4\left(1+u_0^2\right)^4} \tag{E.30}$$

$$b_{1020} = \frac{0.0000449493}{Q_0^2\tau^4\left(1+u_0^2\right)^3}+\frac{-0.000405692u_0^2-0.00189246u_0^4}{Q_0^2\tau^4\left(1+u_0^2\right)^4}+ \frac{-0.00306344u_0^6-0.00211721u_0^8-0.00054054u_0^{10}}{Q_0^2\tau^4\left(1+u_0^2\right)^4} \tag{E.31}$$

$$b_{0120} = \frac{0.0000454256}{Q_0^2\tau^4\left(1+u_0^2\right)^3}+\frac{-0.000280696u_0^2-0.00139534u_0^4}{Q_0^2\tau^4\left(1+u_0^2\right)^4}+ \frac{-0.00232013u_0^6-0.00162247u_0^8-(0.000416973u_0^{10}}{Q_0^2\tau^4\left(1+u_0^2\right)^4} \tag{E.32}$$

$$b_{0021} = \frac{-0.00378277}{Q_0^2\tau^4\left(1+u_0^2\right)^3}+\frac{0.0194524u_0^2+0.100506u_0^4}{Q_0^2\tau^4\left(1+u_0^2\right)^4}+ \frac{0.169673u_0^6+0.11942u_0^8+0.0308008u_0^{10}}{Q_0^2\tau^4\left(1+u_0^2\right)^4} \tag{E.33}$$

$$b_{1002} = \frac{0.000337126}{Q_0^2\tau^4\left(1+u_0^2\right)^3}+\frac{4.57257\times10^{-6}u_0^2-0.00200446u_0^4}{Q_0^2\tau^4\left(1+u_0^2\right)^4}+ \frac{-0.00469232u_0^6-0.00369009u_0^8-0.0010068u_0^{10}}{Q_0^2\tau^4\left(1+u_0^2\right)^4} \tag{E.34}$$

$$b_{0102} = \frac{0.000340698}{Q_0^2\tau^4\left(1+u_0^2\right)^3}+\frac{-0.00029141u_0^2-0.00320983u_0^4}{Q_0^2\tau^4\left(1+u_0^2\right)^4}+ \frac{-0.00651823u_0^6-0.00491332u_0^8-0.0013135u_0^{10}}{Q_0^2\tau^4\left(1+u_0^2\right)^4} \tag{E.35}$$

$$b_{0012} = \frac{-0.0103596}{Q_0^2\tau^4\left(1+u_0^2\right)^3}+\frac{0.00603764u_0^2+0.0863084u_0^4}{Q_0^2\tau^4\left(1+u_0^2\right)^4}+ \frac{0.181261u_0^6+0.138107u_0^8+0.0371166u_0^{10}}{Q_0^2\tau^4\left(1+u_0^2\right)^4} \tag{E.36}$$

$$b_{0111} = \frac{0.000248809}{Q_0^2\tau^4\left(1+u_0^2\right)^3} + \frac{-0.000248987u_0^2 - 0.0024888u_0^4}{Q_0^2\tau^4\left(1+u_0^2\right)^4} + \frac{-0.00497724u_0^6 - 0.00373284u_0^8 - 0.000995413u_0^{10}}{Q_0^2\tau^4\left(1+u_0^2\right)^4} \tag{E.37}$$

$$b_{1011} = \frac{0.0002462}{Q_0^2\tau^4\left(1+u_0^2\right)^3} + \frac{-0.000489794u_0^2 - 0.00343637u_0^4}{Q_0^2\tau^4\left(1+u_0^2\right)^4} + \frac{-0.00638556u_0^6 - 0.00466737u_0^8 - 0.00122839u_0^{10}}{Q_0^2\tau^4\left(1+u_0^2\right)^4} \tag{E.38}$$

$$b_{1101} = \frac{-8.09678\times10^{-6}}{Q_0^2\tau^4\left(1+u_0^2\right)^3} + \frac{4.79964\times10^{-7}u_0^2 + 0.0000505005u_0^4}{Q_0^2\tau^4\left(1+u_0^2\right)^4} + \frac{0.000116235u_0^6 + 0.0000909845u_0^8 + 0.0000247703u_0^{10}}{Q_0^2\tau^4\left(1+u_0^2\right)^4} \tag{E.39}$$

$$b_{1110} = \frac{-2.9565\times10^{-6}}{Q_0^2\tau^4\left(1+u_0^2\right)^3} + \frac{7.92701\times10^{-6}u_0^2 + 0.000049447u_0^4}{Q_0^2\tau^4\left(1+u_0^2\right)^4} + \frac{0.0000889531u_0^6 + 0.0000642295u_0^8 + 0.0000167965u_0^{10}}{Q_0^2\tau^4\left(1+u_0^2\right)^4} \tag{E.40}$$

$$c_{3000} = \frac{3.66146\times10^{-8}}{Q_0^2\tau^4\left(1+u_0^2\right)^3} + \frac{-1.44946\times10^{-7}u_0^2 - 7.99471\times10^{-7}u_0^4}{Q_0^2\tau^4\left(1+u_0^2\right)^4} + \frac{-1.38228\times10^{-6}u_0^6 - 9.82544\times10^{-7}u_0^8 - 2.5479\times10^{-7}u_0^{10}}{Q_0^2\tau^4\left(1+u_0^2\right)^4} \tag{E.41}$$

$$c_{0300} = \frac{3.7791\times10^{-8} - 1.50974\times10^{-8}u_0^2 - 4.38299\times10^{-7}u_0^4}{Q_0^2\tau^4\left(1+u_0^2\right)^4} + \frac{-8.46404\times10^{-7}u_0^6 - 6.27254\times10^{-7}u_0^8 - 1.66261\times10^{-7}u_0^{10}}{Q_0^2\tau^4\left(1+u_0^2\right)^4} \tag{E.42}$$

$$c_{0030} = \frac{-0.00106246 + 0.014593u_0^2 + 0.0689966u_0^4}{Q_0^2\tau^4\left(1+u_0^2\right)^4} + \frac{0.108807u_0^6 + 0.0743089u_0^8 + 0.0188428u_0^{10}}{Q_0^2\tau^4\left(1+u_0^2\right)^4} \tag{E.43}$$

$$c_{0003} = \frac{-0.0218231 + 0.00123019u_0^2 + 0.223152u_0^4}{Q_0^2\tau^4\left(1+u_0^2\right)^4} + \frac{0.443843u_0^6 + 0.332267u_0^8 + 0.0885226u_0^{10}}{Q_0^2\tau^4\left(1+u_0^2\right)^4} \tag{E.44}$$

$$c_{2100} = \frac{1.11008\times10^{-7}}{Q_0^2\tau^4\left(1+u_0^2\right)^3} + \frac{-1.44377\times10^{-7}u_0^2 - 1.24355\times10^{-6}u_0^4}{Q_0^2\tau^4\left(1+u_0^2\right)^4} + \frac{-2.42037\times10^{-6}u_0^6 - 1.79859\times10^{-6}u_0^8 - 4.774\times10^{-7}u_0^{10}}{Q_0^2\tau^4\left(1+u_0^2\right)^4} \tag{E.45}$$

$$c_{2010} = \frac{-3.37542\times10^{-6}}{Q_0^2\tau^4\left(1+u_0^2\right)^3} + \frac{0.0000183401u_0^2 + 0.0000936128u_0^4}{Q_0^2\tau^4\left(1+u_0^2\right)^4} + \frac{0.000157296u_0^6 + 0.00011049u_0^8 + 0.0000284663u_0^{10}}{Q_0^2\tau^4\left(1+u_0^2\right)^4} \tag{E.46}$$

$$c_{2001} = \frac{-9.24406\times10^{-6}}{Q_0^2\tau^4\left(1+u_0^2\right)^3} + \frac{8.8177\times10^{-6}u_0^2 + 0.0000907352u_0^4}{Q_0^2\tau^4\left(1+u_0^2\right)^4} + \frac{0.000182323u_0^6 + 0.000136955u_0^8 + 0.0000365499u_0^{10}}{Q_0^2\tau^4\left(1+u_0^2\right)^4} \tag{E.47}$$

$$c_{1200} = \frac{1.12184\times10^{-7}}{Q_0^2\tau^4\left(1+u_0^2\right)^3} + \frac{-5.02064\times10^{-8}u_0^2 - 8.7393\times10^{-7}u_0^4}{Q_0^2\tau^4\left(1+u_0^2\right)^4} + \frac{-1.87182\times10^{-6}u_0^6 - 1.43485\times10^{-6}u_0^8 - 3.86759\times10^{-7}u_0^{10}}{Q_0^2\tau^4\left(1+u_0^2\right)^4} \tag{E.48}$$

$$c_{0210} = \frac{-3.44734\times10^{-6}}{Q_0^2\tau^4\left(1+u_0^2\right)^3} + \frac{5.97785\times10^{-6}u_0^2 + 0.0000445955u_0^4}{Q_0^2\tau^4\left(1+u_0^2\right)^4} + \frac{0.0000841299u_0^6 + 0.0000618322u_0^8 + 0.0000163199u_0^{10}}{Q_0^2\tau^4\left(1+u_0^2\right)^4} \tag{E.49}$$

$$c_{0201} = \frac{-9.44102\times10^{-6}}{Q_0^2\tau^4\left(1+u_0^2\right)^3} + \frac{9.15502\times10^{-6}u_0^2 + 0.0000932662u_0^4}{Q_0^2\tau^4\left(1+u_0^2\right)^4} + \frac{0.000187104u_0^6 + 0.000140471u_0^8 + 0.0000374781u_0^{10}}{Q_0^2\tau^4\left(1+u_0^2\right)^4} \tag{E.50}$$

$$c_{1020} = \frac{0.000103724}{Q_0^2\tau^4\left(1+u_0^2\right)^3} + \frac{-0.000936169u_0^2 - 0.00436702u_0^4}{Q_0^2\tau^4\left(1+u_0^2\right)^4} + \frac{-0.00706916u_0^6 - 0.00488565u_0^8 - 0.00124734u_0^{10}}{Q_0^2\tau^4\left(1+u_0^2\right)^4} \tag{E.51}$$

$$c_{0120} = \frac{0.000104824}{Q_0^2\tau^4\left(1+u_0^2\right)^3} + \frac{-0.000647731u_0^2 - 0.00321987u_0^4}{Q_0^2\tau^4\left(1+u_0^2\right)^4} + \frac{-0.00535392u_0^6 - 0.00374398u_0^8 - 0.000962202u_0^{10}}{Q_0^2\tau^4\left(1+u_0^2\right)^4} \tag{E.52}$$

$$c_{0021} = \frac{-0.00872908}{Q_0^2\tau^4\left(1+u_0^2\right)^3} + \frac{0.0448882u_0^2 + 0.231927u_0^4}{Q_0^2\tau^4\left(1+u_0^2\right)^4} + \frac{0.391537u_0^6 + 0.275573u_0^8 + 0.0710755u_0^{10}}{Q_0^2\tau^4\left(1+u_0^2\right)^4} \tag{E.53}$$

$$c_{1002} = \frac{0.000777947}{Q_0^2\tau^4\left(1+u_0^2\right)^3} + \frac{0.0000105516u_0^2 - 0.00462548u_0^4}{Q_0^2\tau^4\left(1+u_0^2\right)^4} + \frac{-0.010828u_0^6 - 0.00851521u_0^8 - 0.00232329u_0^{10}}{Q_0^2\tau^4\left(1+u_0^2\right)^4} \tag{E.54}$$

$$c_{0102} = \frac{0.000786191}{Q_0^2\tau^4\left(1+u_0^2\right)^3} + \frac{-0.000672454u_0^2 - 0.00740696u_0^4}{Q_0^2\tau^4\left(1+u_0^2\right)^4} + \frac{-0.0150414u_0^6 - 0.0113379u_0^8 - 0.00303103u_0^{10}}{Q_0^2\tau^4\left(1+u_0^2\right)^4} \tag{E.55}$$

$$c_{0012} = \frac{-0.0239058}{Q_0^2\tau^4\left(1+u_0^2\right)^3} + \frac{0.0139324u_0^2 + 0.199164u_0^4}{Q_0^2\tau^4\left(1+u_0^2\right)^4} + \frac{0.418275u_0^6 + 0.318693u_0^8 + 0.0856498u_0^{10}}{Q_0^2\tau^4\left(1+u_0^2\right)^4} \tag{E.56}$$

$$c_{0111} = \frac{0.000574148}{Q_0^2\tau^4\left(1+u_0^2\right)^3} + \frac{-0.00057456u_0^2 - 0.00574313u_0^4}{Q_0^2\tau^4\left(1+u_0^2\right)^4} + \frac{-0.0114854u_0^6 - 0.00861386u_0^8 - 0.002297u_0^{10}}{Q_0^2\tau^4\left(1+u_0^2\right)^4} \tag{E.57}$$

$$c_{1011} = \frac{0.000568127}{Q_0^2\tau^4\left(1+u_0^2\right)^3} + \frac{-0.00113024u_0^2 - 0.00792974u_0^4}{Q_0^2\tau^4\left(1+u_0^2\right)^4} + \frac{-0.0147352u_0^6 - 0.0107704u_0^8 - 0.00283462u_0^{10}}{Q_0^2\tau^4\left(1+u_0^2\right)^4} \tag{E.58}$$

$$c_{1101} = \frac{-0.000018684}{Q_0^2\tau^4\left(1+u_0^2\right)^3} + \frac{1.10756\times10^{-6}u_0^2 + 0.000116534u_0^4}{Q_0^2\tau^4\left(1+u_0^2\right)^4} + \frac{0.000268222u_0^6 + 0.000209955u_0^8 + 0.0000571597u_0^{10}}{Q_0^2\tau^4\left(1+u_0^2\right)^4} \tag{E.59}$$

$$c_{1110} = \frac{-6.82238\times10^{-6}}{Q_0^2\tau^4\left(1+u_0^2\right)^3} + \frac{0.0000182923u_0^2 + 0.000114103u_0^4}{Q_0^2\tau^4\left(1+u_0^2\right)^4} + \frac{0.000205267u_0^6 + 0.000148215u_0^8 + 0.0000387594u_0^{10}}{Q_0^2\tau^4\left(1+u_0^2\right)^4} \tag{E.60}$$

$$d_{3000} = \frac{-1.9724\times10^{-8}}{Q_0^2\tau^4\left(1+u_0^2\right)^3}+\frac{7.80811\times10^{-8}u_0^2+4.30668\times10^{-7}u_0^4}{Q_0^2\tau^4\left(1+u_0^2\right)^4}+ \frac{7.44622\times10^{-7}u_0^6+5.29288\times10^{-7}u_0^8+1.37253\times10^{-7}u_0^{10}}{Q_0^2\tau^4\left(1+u_0^2\right)^4} \tag{E.61}$$

$$d_{0300} = \frac{-2.03577\times10^{-8}+8.13285\times10^{-9}u_0^2+2.36108\times10^{-7}u_0^4}{Q_0^2\tau^4\left(1+u_0^2\right)^4} +\frac{4.55951\times10^{-7}u_0^6+3.37896\times10^{-7}u_0^8+8.95635\times10^{-8}u_0^{10}}{Q_0^2\tau^4\left(1+u_0^2\right)^4} \tag{E.62}$$

$$d_{0030} = \frac{0.000572338-0.00786112u_0^2-0.0371679u_0^4}{Q_0^2\tau^4\left(1+u_0^2\right)^4} +\frac{-0.0586135u_0^6-0.0400295u_0^8-0.0101505u_0^{10}}{Q_0^2\tau^4\left(1+u_0^2\right)^4} \tag{E.63}$$

$$d_{0003} = \frac{0.0117559-0.000662694u_0^2-0.12021u_0^4}{Q_0^2\tau^4\left(1+u_0^2\right)^4} +\frac{-0.239094u_0^6-0.178989u_0^8-0.0476863u_0^{10}}{Q_0^2\tau^4\left(1+u_0^2\right)^4} \tag{E.64}$$

$$d_{2100} = \frac{-5.97989\times10^{-8}}{Q_0^2\tau^4\left(1+u_0^2\right)^3}+\frac{7.77745\times10^{-8}u_0^2+6.69892\times10^{-7}u_0^4}{Q_0^2\tau^4\left(1+u_0^2\right)^4}+ \frac{1.30383\times10^{-6}u_0^6+9.68886\times10^{-7}u_0^8+2.57171\times10^{-7}u_0^{10}}{Q_0^2\tau^4\left(1+u_0^2\right)^4} \tag{E.65}$$

$$d_{2010} = \frac{1.81831\times10^{-6}}{Q_0^2\tau^4\left(1+u_0^2\right)^3}+\frac{-9.87963\times10^{-6}u_0^2-0.0000504284u_0^4}{Q_0^2\tau^4\left(1+u_0^2\right)^4}+ \frac{-0.0000847341u_0^6-0.0000595199u_0^8-0.0000153346u_0^{10}}{Q_0^2\tau^4\left(1+u_0^2\right)^4} \tag{E.66}$$

$$d_{2001} = \frac{4.9797\times10^{-6}}{Q_0^2\tau^4\left(1+u_0^2\right)^3}+\frac{-4.75002\times10^{-6}u_0^2-0.0000488782u_0^4}{Q_0^2\tau^4\left(1+u_0^2\right)^4}+ \frac{-0.0000982158u_0^6-0.0000737767u_0^8-0.0000196891u_0^{10}}{Q_0^2\tau^4\left(1+u_0^2\right)^4} \tag{E.67}$$

$$d_{1200} = \frac{-6.04326\times10^{-8}}{Q_0^2\tau^4\left(1+u_0^2\right)^3}+\frac{2.70457\times10^{-8}u_0^2+4.70779\times10^{-7}u_0^4}{Q_0^2\tau^4\left(1+u_0^2\right)^4}+ \frac{1.00833\times10^{-6}u_0^6+7.72942\times10^{-7}u_0^8+2.08344\times10^{-7}u_0^{10}}{Q_0^2\tau^4\left(1+u_0^2\right)^4} \tag{E.68}$$

$$d_{0210} = \frac{1.85705 \times 10^{-6}}{Q_0^2\tau^4\left(1+u_0^2\right)^3} + \frac{-3.22022 \times 10^{-6}u_0^2 - 0.0000240232u_0^4}{Q_0^2\tau^4\left(1+u_0^2\right)^4} + \frac{-0.00004532u_0^6 - 0.0000333084u_0^8 - 8.79137 \times 10^{-6}u_0^{10}}{Q_0^2\tau^4\left(1+u_0^2\right)^4} \tag{E.69}$$

$$d_{0201} = \frac{5.08579 \times 10^{-6}}{Q_0^2\tau^4\left(1+u_0^2\right)^3} + \frac{-4.93173 \times 10^{-6}u_0^2 - 0.0000502417u_0^4}{Q_0^2\tau^4\left(1+u_0^2\right)^4} + \frac{-0.000100791u_0^6 - 0.0000756707u_0^8 - 0.0000201891u_0^{10}}{Q_0^2\tau^4\left(1+u_0^2\right)^4} \tag{E.70}$$

$$d_{1020} = \frac{-0.0000558754}{Q_0^2\tau^4\left(1+u_0^2\right)^3} + \frac{0.000504306u_0^2 + 0.00235248u_0^4}{Q_0^2\tau^4\left(1+u_0^2\right)^4} + \frac{0.00380809u_0^6 + 0.00263186u_0^8 + (0.000671933u_0^{10}}{Q_0^2\tau^4\left(1+u_0^2\right)^4} \tag{E.71}$$

$$d_{0120} = \frac{-0.0000564676}{Q_0^2\tau^4\left(1+u_0^2\right)^3} + \frac{0.000348927u_0^2 + 0.00173451u_0^4}{Q_0^2\tau^4\left(1+u_0^2\right)^4} + \frac{0.00288411u_0^6 + 0.00201685u_0^8 + 0.00051833u_0^{10}}{Q_0^2\tau^4\left(1+u_0^2\right)^4} \tag{E.72}$$

$$d_{0021} = \frac{0.00470228}{Q_0^2\tau^4\left(1+u_0^2\right)^3} + \frac{-0.0241809u_0^2 - 0.124937u_0^4}{Q_0^2\tau^4\left(1+u_0^2\right)^4} + \frac{-0.210917u_0^6 - 0.148449u_0^8 - 0.0382877u_0^{10}}{Q_0^2\tau^4\left(1+u_0^2\right)^4} \tag{E.73}$$

$$d_{1002} = \frac{-0.000419073}{Q_0^2\tau^4\left(1+u_0^2\right)^3} + \frac{-5.68407 \times 10^{-6}u_0^2 + 0.0024917u_0^4}{Q_0^2\tau^4\left(1+u_0^2\right)^4} + \frac{0.00583292u_0^6 + 0.00458707u_0^8 + 0.00125154u_0^{10}}{Q_0^2\tau^4\left(1+u_0^2\right)^4} \tag{E.74}$$

$$d_{0102} = \frac{-0.000423514}{Q_0^2\tau^4\left(1+u_0^2\right)^3} + \frac{0.000362245u_0^2 + 0.00399007u_0^4}{Q_0^2\tau^4\left(1+u_0^2\right)^4} + \frac{0.00810267u_0^6 + 0.00610764u_0^8 + 0.00163279u_0^{10}}{Q_0^2\tau^4\left(1+u_0^2\right)^4} \tag{E.75}$$

$$d_{0012} = \frac{0.0128778}{Q_0^2\tau^4\left(1+u_0^2\right)^3} + \frac{-0.00750526u_0^2 - 0.107288u_0^4}{Q_0^2\tau^4\left(1+u_0^2\right)^4} + \frac{-0.225321u_0^6 - 0.171677u_0^8 - 0.0461388u_0^{10}}{Q_0^2\tau^4\left(1+u_0^2\right)^4} \tag{E.76}$$

$$d_{0111} = \frac{-0.000309288}{Q_0^2\tau^4\left(1+u_0^2\right)^3} + \frac{0.00030951u_0^2 + 0.00309377u_0^4}{Q_0^2\tau^4\left(1+u_0^2\right)^4} + \frac{0.0061871u_0^6 + 0.00464021u_0^8 + 0.00123738u_0^{10}}{Q_0^2\tau^4\left(1+u_0^2\right)^4} \tag{E.77}$$

$$d_{1011} = \frac{-0.000306045}{Q_0^2\tau^4\left(1+u_0^2\right)^3} + \frac{0.000608852u_0^2 + 0.00427168u_0^4}{Q_0^2\tau^4\left(1+u_0^2\right)^4} + \frac{0.00793775u_0^6 + 0.00580191u_0^8 + 0.00152699u_0^{10}}{Q_0^2\tau^4\left(1+u_0^2\right)^4} \tag{E.78}$$

$$d_{1101} = \frac{0.0000100649}{Q_0^2\tau^4\left(1+u_0^2\right)^3} + \frac{-5.96633\times10^{-7}u_0^2 - 0.0000627761u_0^4}{Q_0^2\tau^4\left(1+u_0^2\right)^4} + \frac{-0.000144489u_0^6 - 0.000113101u_0^8 - 0.0000307914u_0^{10}}{Q_0^2\tau^4\left(1+u_0^2\right)^4} \tag{E.79}$$

$$d_{1110} = \frac{3.67516\times10^{-6}}{Q_0^2\tau^4\left(1+u_0^2\right)^3} + \frac{-9.85389\times10^{-6}u_0^2 - 0.0000614665u_0^4}{Q_0^2\tau^4\left(1+u_0^2\right)^4} + \frac{-0.000110576u_0^6 - 0.0000798423u_0^8 - 0.0000208794u_0^{10}}{Q_0^2\tau^4\left(1+u_0^2\right)^4} \tag{E.80}$$

Coefficients $\hat{\alpha}_{2100}$, $\hat{\alpha}_{1011}$, $\hat{\beta}_{0021}$ and $\hat{\beta}_{1110}$ of the system in complex form after near identity transformation, relative to the double NS bifurcation under study in Ch. 4.

$$\hat{\alpha}_{2100} = \frac{1}{Q_0^2\tau^4(1.+u_0^2)^4}\Big(\left(-1.25026\times10^{-10}+i2.44367\times10^{-8}\right)+\left(1.69258\times10^{-7}-i4.01066\times10^{-8}\right)u_0^2 + \left(6.78282\times10^{-7}-i4.04793\times10^{-7}\right)u_0^4+\left(1.01805\times10^{-6}-i7.29374\times10^{-7}\right)u_0^6 + \left(6.78907\times10^{-7}-i5.26977\times10^{-7}\right)u_0^8+\left(1.69758\times10^{-7}-i1.37853\times10^{-7}\right)u_0^{10}\Big) \tag{E.81}$$

$$\hat{\alpha}_{1011} = \frac{1}{Q_0^2\tau^4}\Big(-\frac{9.92959\times10^{-7}-i0.000194076}{\left(1+u_0^2\right)^3}+\frac{0.000467408+i0.000794087}{\left(1+u_0^2\right)^4}u_0^2 + \frac{0.00187559+i0.00201189}{\left(1+u_0^2\right)^4}u_0^4+\frac{0.00281835+i0.00204746}{\left(1+u_0^2\right)^4}u_0^6 + \frac{0.00188056+i0.00104151}{\left(1+u_0^2\right)^4}u_0^8+\frac{0.000470387+i0.000211859}{\left(1+u_0^2\right)^4}u_0^{10}\Big) \tag{E.82}$$

$$\hat{\beta}_{1110} = \frac{1}{Q_0^2\tau^4}\Big(\frac{8.10681\times10^{-7}+i5.59011\times10^{-6}}{\left(1+u_0^2\right)^3}+\frac{0.0000121356+i0.0000217654}{\left(1+u_0^2\right)^4}u_0^2 + \frac{0.0000436782+i0.000053521}{\left(1+u_0^2\right)^4}u_0^4+\frac{0.000061464+i0.0000523309}{\left(1+u_0^2\right)^4}u_0^6 + \frac{0.0000396248+i0.0000255704}{\left(1+u_0^2\right)^4}u_0^8+\frac{9.70354\times10^{-6}+i4.99508\times10^{-6}}{\left(1+u_0^2\right)^4}u_0^{10}\Big) \tag{E.83}$$

$$\hat{\beta}_{0021} = \frac{1}{Q_0^2\tau^4(1+u_0^2)^4}\Big(\left(0.00160961+i0.0110992\right)+\left(0.0214271+i0.0534341\right)u_0^2 + \left(0.0696124+i0.102745\right)u_0^4+\left(0.0963706+i0.0986214\right)u_0^6 + \left(0.0615644+i0.047249\right)u_0^8+\left(0.0149887+i0.00903746\right)u_0^{10}\Big) \tag{E.84}$$

Coefficients a_{11}, a_{12}, a_{21} and a_{22} of the amplitude map (Eq. (4.45)) related to the double NS bifurcation under study in Ch. 4.

$$\begin{aligned}
a_{11} &= \frac{1}{Q_0^2\tau^4\left(1+u_0^2\right)^6}\Big(-1.10943\times10^{-8}+1.47037\times10^{-7}u_0^2+1.11520\times10^{-6}u_0^4+2.98216\times10^{-6}u_0^6 \\
&\quad +4.10565\times10^{-6}u_0^8+3.13748\times10^{-6}u_0^{10}+1.27052\times10^{-6}u_0^{12}+2.13603\times10^{-7}u_0^{14}\Big) \qquad \text{(E.85)} \\
a_{12} &= \frac{1}{Q_0^2\tau^4\left(1+u_0^2\right)^{10}}\Big(-8.81111\times10^{-5}-5.56124\times10^{-4}u_0^2-7.15128\times10^{-4}u_0^4+0.00405109u_0^6 \\
&\quad +0.0204951u_0^8+0.0460433u_0^{10}+0.0633935u_0^{12}+0.057674u_0^{14}+0.0350335u_0^{16}+0.0137433u_0^{18} \\
&\quad +0.00316176u_0^{20}+3.24987\times10^{-4}u_0^{22}\Big) \qquad \text{(E.86)} \\
a_{21} &= \frac{1}{Q_0^2\tau^4\left(1+u_0^2\right)^{10}}\Big(-3.51185\times10^{-6}-3.20977\times10^{-5}u_0^2-1.27826\times10^{-4}u_0^4-2.85487\times10^{-4}u_0^6 \\
&\quad -3.74996\times10^{-4}u_0^8-2.50625\times10^{-4}u_0^{10}+2.37453\times10^{-5}u_0^{12}+2.12939\times10^{-4}u_0^{14} \\
&\quad +2.04459\times10^{-4}u_0^{16}+1.00816\times10^{-4}u_0^{18}+2.66958\times10^{-5}u_0^{20}+3.02077\times10^{-6}u_0^{22}\Big) \qquad \text{(E.87)} \\
a_{22} &= \frac{1}{Q_0^2\tau^4\left(1+u_0^2\right)^6}\Big(-0.00697277-0.0381324u_0^2-0.0823661u_0^4-0.0838918u_0^6-0.0305067u_0^8 \qquad \text{(E.88)} \\
&\quad +0.013727u_0^{10}+0.0152527u_0^{12}+0.00370424u_0^{14}\Big) \qquad \text{(E.89)}
\end{aligned}$$

Appendix F

Coefficients bifurcations in act-and-wait system

Coefficeints a_{hk} and b_{hk} relative to the flip bifurcation analyzed in Ch. 7.

$$a_{20} = \frac{4u_0}{(d-3)\,Q_0\tau^2} \tag{F.1}$$

$$a_{02} = \frac{4(d-2)^2u_0}{(d-3)\,Q_0\tau^2} \tag{F.2}$$

$$a_{11} = \frac{8(d-2)u_0}{(d-3)\,Q_0\tau^2} \tag{F.3}$$

$$a_{30} = \frac{8(3u_0^2-1)}{3\,(d-3)\,Q_0^2\tau^4} \tag{F.4}$$

$$a_{21} = \frac{8(d-2)(3u_0^2-1)}{(d-3)\,Q_0^2\tau^4} \tag{F.5}$$

$$a_{12} = \frac{8(d-2)^2(3u_0^2-1)}{(d-3)\,Q_0^2\tau^4} \tag{F.6}$$

$$a_{03} = \frac{8(d-2)^3(3u_0^2-1)}{3\,(d-3)\,Q_0^2\tau^4} \tag{F.7}$$

$$b_{20} = -\frac{4(d-2)u_0}{(d-3)\,Q_0\tau^2} \tag{F.8}$$

$$b_{02} = -\frac{4(d-2)^3u_0}{(d-3)\,Q_0\tau^2} \tag{F.9}$$

$$b_{11} = -\frac{8(d-2)^2u_0}{(d-3)\,Q_0\tau^2} \tag{F.10}$$

$$b_{30} = -\frac{8(d-2)(3u_0^2-1)}{3\,(d-3)\,Q_0^2\tau^4} \tag{F.11}$$

$$b_{21} = -\frac{8(d-2)^2(3u_0^2-1)}{(d-3)\,Q_0^2\tau^4} \tag{F.12}$$

$$b_{12} = -\frac{8(d-2)^3(3u_0^2-1)}{(d-3)\,Q_0^2\tau^4} \tag{F.13}$$

$$b_{03} = -\frac{8(d-2)^4(3u_0^2-1)}{3\,(d-3)\,Q_0^2\tau^4} \tag{F.14}$$

where $2 < d < 3$.

Coefficeints a_{hk} and b_{hk} relative to the NS bifurcation analyzed in Ch. 7.

$$a_{20} = -\frac{p^2u_0}{Q_0\tau^2} \tag{F.15}$$

$$a_{02} = \frac{(p-2)pu_0}{Q_0\tau^2} \tag{F.16}$$

$$a_{11} = \frac{2p\sqrt{(2-p)\,p}u_0}{Q_0\tau^2} \tag{F.17}$$

$$a_{30} = \frac{p^3\left(1-3u_0^2\right)}{3Q_0^2\tau^4} \tag{F.18}$$

$$a_{21} = \frac{p^2\sqrt{(2-p)\,p}\left(3u_0^2-1\right)}{Q_0^2\tau^4} \tag{F.19}$$

$$a_{12} = \frac{(p-2)p^2\left(3u_0^2-1\right)}{Q_0^2\tau^4} \tag{F.20}$$

$$a_{03} = \frac{((2-p)p)^{3/2}\left(3u_0^2-1\right)}{3Q_0^2\tau^4} \tag{F.21}$$

$$b_{20} = \frac{p^3u_0}{\sqrt{(2-p)\,p}Q_0\tau^2} \tag{F.22}$$

$$b_{02} = \frac{p\sqrt{(2-p)\,p}u_0}{Q_0\tau^2} \tag{F.23}$$

$$b_{11} = -\frac{2p^2u_0}{Q_0\tau^2} \tag{F.24}$$

$$b_{30} = \frac{p^4\left(3u_0^2-1\right)}{3\sqrt{(2-p)\,p}Q_0^2\tau^4} \tag{F.25}$$

$$b_{21} = \frac{p^3\left(1-3u_0^2\right)}{Q_0^2\tau^4} \tag{F.26}$$

$$b_{12} = \frac{p^2\sqrt{(2-p)\,p}\left(3u_0^2-1\right)}{Q_0^2\tau^4} \tag{F.27}$$

$$b_{03} = \frac{(p-2)p^2\left(3u_0^2-1\right)}{3Q_0^2\tau^4} \tag{F.28}$$

where $0 < p < 2$.

Coefficeints α_{hk} relative to the NS bifurcation analyzed in Ch. 7.

$$\alpha_{20} = -\frac{p\left(2+2p^2-3i\sqrt{(2-p)\,p}+p\left(-5+2i\sqrt{(2-p)\,p}\right)\right)u_0}{2(p-2)Q_0\tau^2} \tag{F.29}$$

$$\alpha_{02} = \frac{p\left(-2+p-i\sqrt{(2-p)\,p}\right)u_0}{2(p-2)Q_0\tau^2} \tag{F.30}$$

$$\alpha_{11} = -\frac{p\left(-2+p+i\sqrt{(2-p)\,p}\right)u_0}{(p-2)Q_0\tau^2} \tag{F.31}$$

$$\alpha_{30} = -\frac{p\left(4p+2p^3+i\sqrt{(2-p)\,p}-4ip\sqrt{(2-p)\,p}+2ip^2\left(3i+\sqrt{(2-p)\,p}\right)\right)\left(3u_0^2-1\right)}{6(p-2)Q_0^2\tau^4} \tag{F.32}$$

$$\alpha_{21} = -\frac{p\left(p^2-i\sqrt{(2-p)\,p}+ip\left(2i+\sqrt{(2-p)\,p}\right)\right)\left(3u_0^2-1\right)}{2(p-2)Q_0^2\tau^4} \tag{F.33}$$

$$\alpha_{12} = \frac{ip^2\left(3u_0^2-1\right)}{2\sqrt{(2-p)\,p}Q_0^2\tau^4} \tag{F.34}$$

$$\alpha_{03} = \frac{p\left(p^2+i\sqrt{(2-p)\,p}+p\left(-2-i\sqrt{(2-p)\,p}\right)\right)\left(3u_0^2-1\right)}{6(p-2)Q_0^2\tau^4} \tag{F.35}$$

Coefficient ρ relative to the NS bifurcation of the damped system analyzed in Ch. 7

$$\rho = \tfrac{1}{32\delta}e^{-3\delta}\left(2\delta + e^{-2\delta}\left(p - e^{2\delta}p + i\sqrt{\left(e^{2\delta}-1\right)p\left(4\delta e^{2\delta}+p-e^{2\delta}p\right)}\right)\right)\Bigg(\Bigg(2e^{\delta}\left(\delta\left(e^{2\delta}-1\right)+p\right)$$
$$\left(\delta e^{2\delta}+p-e^{2\delta}p-i\sqrt{\left(e^{2\delta}-1\right)p\left(4\delta e^{2\delta}+p-e^{2\delta}p\right)}\right)\Bigg(4\delta^2e^{2\delta}\left(e^{2\delta}-1\right)-2ie^{\delta}\left(e^{\delta}-1\right)$$
$$\sqrt{\left(e^{2\delta}-1\right)p\left(4\delta e^{2\delta}+p-e^{2\delta}p\right)}+\delta\left(1+e^{\delta}\right)\left(-\left(e^{\delta}-1\right)^2\left(1+e^{\delta}\right)p+i\sqrt{\left(e^{2\delta}-1\right)p\left(4\delta e^{2\delta}+p-e^{2\delta}p\right)}\right)\Bigg)$$
$$\Bigg(8\delta^4e^{2\delta}\left(e^{2\delta}-1\right)^2-2e^{\delta}\left(e^{\delta}-1\right)^2\left(1+e^{\delta}\right)p^2\left(\left(e^{2\delta}-1\right)p+i\sqrt{\left(e^{2\delta}-1\right)p\left(4\delta e^{2\delta}+p-e^{2\delta}p\right)}\right)$$
$$-2\delta^3\left(e^{2\delta}-1\right)\left(\left(1-10e^{2\delta}-4e^{3\delta}+9e^{4\delta}\right)p+i\left(-1-e^{\delta}+4e^{2\delta}\right)\sqrt{\left(e^{2\delta}-1\right)p\left(4\delta e^{2\delta}+p-e^{2\delta}p\right)}\right)$$
$$+\delta\left(e^{\delta}-1\right)p\Bigg(-e^{5\delta}(p-12)p-2p^2+2e^{2\delta}p^2+2ip\sqrt{\left(e^{2\delta}-1\right)p\left(4\delta e^{2\delta}+p-e^{2\delta}p\right)}+ie^{\delta}(3p-4)$$
$$\left(ip+\sqrt{\left(e^{2\delta}-1\right)p\left(4\delta e^{2\delta}+p-e^{2\delta}p\right)}\right)+e^{3\delta}\Bigg(4p^2+8i\sqrt{\left(e^{2\delta}-1\right)p\left(4\delta e^{2\delta}+p-e^{2\delta}p\right)}$$
$$+p\left(-16-i\sqrt{\left(e^{2\delta}-1\right)p\left(4\delta e^{2\delta}+p-e^{2\delta}p\right)}\right)\Bigg)\Bigg)+2\delta^2\left(1+e^{\delta}\right)\Bigg(4e^{5\delta}(p-2)p-2p^2-e^{4\delta}p(7p-16)$$
$$+2ip\sqrt{\left(e^{2\delta}-1\right)p\left(4\delta e^{2\delta}+p-e^{2\delta}p\right)}+e^{\delta}\Bigg(p^2-2i\sqrt{\left(e^{2\delta}-1\right)p\left(4\delta e^{2\delta}+p-e^{2\delta}p\right)}$$
$$-ip\sqrt{\left(e^{2\delta}-1\right)p\left(4\delta e^{2\delta}+p-e^{2\delta}p\right)}\Bigg)+e^{2\delta}\Bigg(9p^2+4i\sqrt{\left(e^{2\delta}-1\right)p\left(4\delta e^{2\delta}+p-e^{2\delta}p\right)}$$
$$-5ip\sqrt{\left(e^{2\delta}-1\right)p\left(4\delta e^{2\delta}+p-e^{2\delta}p\right)}\Bigg)+e^{3\delta}\Bigg(-5p^2-2i\sqrt{\left(e^{2\delta}-1\right)p\left(4\delta e^{2\delta}+p-e^{2\delta}p\right)}$$
$$+p\left(3i\sqrt{\left(e^{2\delta}-1\right)p\left(4\delta e^{2\delta}+p-e^{2\delta}p\right)}-8\right)\Bigg)\Bigg)\Bigg)u_0^2\Bigg)\Bigg/\Bigg(\left(e^{\delta}-1\right)^4\left(4\delta e^{2\delta}+p-e^{2\delta}p\right)^2\Bigg(-\left(e^{2\delta}-1\right)p$$
$$\left(\left(e^{2\delta}-1\right)p+i\sqrt{\left(e^{2\delta}-1\right)p\left(4\delta e^{2\delta}+p-e^{2\delta}p\right)}\right)+\delta e^{2\delta}\left(3\left(e^{2\delta}-1\right)p+i\sqrt{\left(e^{2\delta}-1\right)p\left(4\delta e^{2\delta}+p-e^{2\delta}p\right)}\right)\Bigg)$$
$$Q_0^2\tau^4\Bigg)+\Bigg(\left(1+e^{\delta}\right)\left(\delta\left(e^{2\delta}-1\right)+p\right)\Bigg(8\delta^3e^{2\delta}\left(e^{2\delta}-1\right)+2e^{\delta}\left(e^{\delta}-1\right)p\Bigg(\left(e^{2\delta}-1\right)p$$
$$+i\sqrt{\left(e^{2\delta}-1\right)p\left(4\delta e^{2\delta}+p-e^{2\delta}p\right)}\Bigg)+2\delta^2\Bigg(\left(-1+6e^{2\delta}+2e^{3\delta}-3e^{4\delta}\right)p-i\left(-1-e^{\delta}+2e^{2\delta}\right)$$
$$\sqrt{\left(e^{2\delta}-1\right)p\left(4\delta e^{2\delta}+p-e^{2\delta}p\right)}\Bigg)+\delta\Bigg(-e^{3\delta}(p-8)p+e^{4\delta}(p-8)p+2p^2$$
$$-2ip\sqrt{\left(e^{2\delta}-1\right)p\left(4\delta e^{2\delta}+p-e^{2\delta}p\right)}+e^{\delta}\Bigg(p^2+4i\sqrt{\left(e^{2\delta}-1\right)p\left(4\delta e^{2\delta}+p-e^{2\delta}p\right)}$$
$$-ip\sqrt{\left(e^{2\delta}-1\right)p\left(4\delta e^{2\delta}+p-e^{2\delta}p\right)}\Bigg)+ie^{2\delta}\Bigg(3ip^2-4\sqrt{\left(e^{2\delta}-1\right)p\left(4\delta e^{2\delta}+p-e^{2\delta}p\right)}$$
$$+p\sqrt{\left(e^{2\delta}-1\right)p\left(4\delta e^{2\delta}+p-e^{2\delta}p\right)}\Bigg)\Bigg)\Bigg)\left(-1+3u_0^2\right)\Bigg)\Bigg/\Bigg(\left(e^{\delta}-1\right)^2\left(4\delta e^{2\delta}+p-e^{2\delta}p\right)Q_0^2\tau^4\Bigg)$$
$$+\Bigg(8\delta e^{5\delta-4\delta}\mathrm{abs}\Bigg[\Bigg(\left(\delta\left(e^{2\delta}-1\right)+p\right)\Bigg(-4\delta^2e^{2\delta}\left(e^{2\delta}-1\right)+2ie^{\delta}\left(e^{\delta}-1\right)\sqrt{\left(e^{2\delta}-1\right)p\left(4\delta e^{2\delta}+p-e^{2\delta}p\right)}$$
$$+\delta\left(1+e^{\delta}\right)\left(\left(e^{\delta}-1\right)^2\left(1+e^{\delta}\right)p-i\sqrt{\left(e^{2\delta}-1\right)p\left(4\delta e^{2\delta}+p-e^{2\delta}p\right)}\right)\Bigg)u_0\Bigg)\Bigg/\Bigg(\left(e^{\delta}-1\right)^2$$
$$\left(4\delta e^{2\delta}+p-e^{2\delta}p\right)Q_0\tau^2\Bigg)\Bigg]^2\Bigg)\Bigg/\left(\left(e^{2\delta}-1\right)p-i\sqrt{\left(e^{2\delta}-1\right)p\left(4\delta e^{2\delta}+p-e^{2\delta}p\right)}\right)-\Bigg(\delta^2e^{7\delta-4\delta}$$
$$\mathrm{abs}\Bigg[\Bigg(\Bigg(-8\delta^4e^{2\delta}\left(e^{2\delta}-1\right)^2+2e^{\delta}\left(e^{\delta}-1\right)^2\left(1+e^{\delta}\right)p^2\left(p-e^{2\delta}p+i\sqrt{\left(e^{2\delta}-1\right)p\left(4\delta e^{2\delta}+p-e^{2\delta}p\right)}\right)$$

(continues on the next page)

(continues from the previous page)

$$
\begin{aligned}
&+2\delta^3\left(e^{2\delta}-1\right)\left(\left(1-2e^{2\delta}+4e^{3\delta}+9e^{4\delta}\right)p-i\left(1+e^{\delta}+4e^{2\delta}\right)\sqrt{\left(e^{2\delta}-1\right)p\left(4\delta e^{2\delta}+p-e^{2\delta}p\right)}\right)\\
&+\delta e^{\delta}\left(e^{\delta}-1\right)p\Bigg(\left(e^{\delta}-1\right)\left(1+e^{\delta}\right)^3p^2-4i\left(-1+2e^{2\delta}\right)\sqrt{\left(e^{2\delta}-1\right)p\left(4\delta e^{2\delta}+p-e^{2\delta}p\right)}+\left(1+e^{\delta}\right)p\\
&\left(4-12e^{2\delta}+12e^{3\delta}-i\sqrt{\left(e^{2\delta}-1\right)p\left(4\delta e^{2\delta}+p-e^{2\delta}p\right)}+e^{\delta}\left(-4-i\sqrt{\left(e^{2\delta}-1\right)p\left(4\delta e^{2\delta}+p-e^{2\delta}p\right)}\right)\right)\Bigg)\\
&-2\delta^2e^{\delta}\left(1+e^{\delta}\right)\Bigg(p^2+4e^{4\delta}p(2+p)-e^{3\delta}p(16+p)-2i\sqrt{\left(e^{2\delta}-1\right)p\left(4\delta e^{2\delta}+p-e^{2\delta}p\right)}\\
&+ip\sqrt{\left(e^{2\delta}-1\right)p\left(4\delta e^{2\delta}+p-e^{2\delta}p\right)}+e^{\delta}\Bigg(p^2+4i\sqrt{\left(e^{2\delta}-1\right)p\left(4\delta e^{2\delta}+p-e^{2\delta}p\right)}\\
&+ip\sqrt{\left(e^{2\delta}-1\right)p\left(4\delta e^{2\delta}+p-e^{2\delta}p\right)}\Bigg)+e^{2\delta}\Bigg(-5p^2-2i\sqrt{\left(e^{2\delta}-1\right)p\left(4\delta e^{2\delta}+p-e^{2\delta}p\right)}\\
&+p\left(8-3i\sqrt{\left(e^{2\delta}-1\right)p\left(4\delta e^{2\delta}+p-e^{2\delta}p\right)}\right)\Bigg)\Bigg)u_0\Bigg)\Big/\left(\delta\left(e^{\delta}-1\right)^2\left(4\delta e^{2\delta}+p-e^{2\delta}p\right)Q_0\tau^2\right)\Bigg]^2\Bigg)\Big/\\
&\left(\left(3\delta e^{2\delta}+p-e^{2\delta}p\right)\left(\left(e^{2\delta}-1\right)p+i\sqrt{\left(e^{2\delta}-1\right)p\left(4\delta e^{2\delta}+p-e^{2\delta}p\right)}\right)\right)\Bigg)
\end{aligned}
\tag{F.36}
$$

Bibliography

[1] Adams, R.J., Moreyra, M.R., Hannafors, B., (1998) Stability and performance of haptic displays: theory and experiments. In: *Proc. ASME Int. Mechanical Engineering Congress and Exhibition*, Anaheim, CA, USA, 1998, pp. 227–234.

[2] Aeyels, D., and Willems, J.L., Pole assignment for linear time-invariant system by periodic memoryless output feedback. *Automatica* **28**:6, (1992) pp. 1159–1168.

[3] Afraimovich, V.S., Shil'nikov, L.P., Invariant two-dimensional tori, their breakdown and stochasticity. *Amer. Math. Soc. Trans.* **149**:2, (1991) pp. 201–212.

[4] Alaggio, R., Rega, G., Characterizing Bifurcation and Classes of Motion in the Transition to Chaos Through 3D-tori of a Continuous Experimental System in Solid Mechanics. *Physica D.* **137**:1-2, (2000) pp. 70–93.

[5] Alazard, D. Chretien, J.P., (1993) Flexible joint control: Robustness analysis of the collocated and non-collocated feedbacks. In: *Proc. Intel. Rob. and Syst. Conf.*, Yokohama, Japan, 26–30 July 1993; 3:2102–2107

[6] Albu-Schaffer, A., Ott, Ch., Hirzinger, G., (2004) A passivity based cartesian impedance controller - part II: Full state feedback, impedance design and experiments. In: *Proc. IEEE Int. Conf. on Robotics and Automation*, New Orleans, USA, April 2004, pp. 2666–2672.

[7] Anishchenko, V.S., Savonova, M.A., Feudel, U., Kurths, J., Bifurcation and transition to chaos through three-dimensional tori. *Int. J. Bif. Chaos* **4**:3, (1994) pp. 595.

[8] Atay, F.M., Balancing the inverted pendulum using position feedback. *Applied Mathematics Letters* **12**, (1999) pp. 51–56.

[9] Bortoff, S.A., Hung, J.Y., Spong, M.W., (1989) A discrete-time observer for flexible-joint manipulators. In: *Proc. 28th IEEE CDC*, Tampa, Florida, USA, December 1989, pp. 2078–2082.

[10] Cannon, R.H., and Rosenthal, D.E., Experiments in control of flexible structure with noncollocated sensors and actuators. *J. Guidance Control and Dynamics* **7**:5, (1984) pp. 546–553.

[11] Chenciner, A.: Bifurcations de points fixes elliptiques: III - Orbites périodiques de "petites" périodes et élimination résonnante des couples de courbes invariantes. *Publications de l'I.H.E.S.* **66**, (1988) pp. 5–91.

[12] Colgate, E., Schenkel, G.G., Passivity of a Class of Sampled-Data Systems: Application to Haptic Interfaces. *J. Robot. System* **14**:1, (1997) pp. 37–47.

[13] De Luca, A., Farina, R., Lucibello, P., (2005) On the control of robots with visco-elastic joints. In: *Proc. IEEE Int. Conf. on Robotics and Automation*, Barcelona, Spain, April 2005, pp. 4297–4302.

[14] De Luca, A., Schröder, D., Thümmel, M., (2007) An acceleration based state observer for robot manipulators with elastic joints. In: *Proc. IEEE Int. Conf. on Robotics and Automation*, Rome, Italy, April 2007, pp. 3817–3823.

[15] Enikov, E.T., Campa, G. Mechatronic Aeropendulum: Demonstration of Linear and Nonlinear Feedback Control Principles With MATLAB/Simulink Real-Time Windows Target. *IEEE Transactions on Education*, **55**:4, (2012) pp. 538–545.

[16] Farmer, J.D., Ott, E., and York, J.A., The Dimension of Chaotic Attractors. *Physica D*, **7**, (1983) pp. 153–170.

[17] Fenichel, N., Persistence and smoothness of invariant manifolds for flows. *Indiana Univ. Math. J.* **21**, (1971) pp. 193–226.

[18] Gattulli, V., Di Fabio, F., Luongo, A. Simple and double Hopf bifurcations in aeroelastic oscillators with tuned mass dampers. *J. of the Franklin Institute.* **338**, (2001) pp. 187–201.

[19] Ghorbel, F., Hung, J.Y., Spong, M.W., Adaptive control of flexible joint manipulators. *IEEE Contr. Syst. Mag.* **9**, (1989) pp. 9–13.

[20] Gil, J.J., Avello, A., Rubio, A., Florez, J., Stability Analysis of a 1 DOF Haptic Interface Using the Routh–Hurwitz Criterion. *IEEE Trans. Control Syst. Technol.* **12**, (2004) pp. 583–588.

[21] Gorinevsky, D.M., Formalsky, A.M., Schneider, A.Y., *Force Control of Robotics Systems.* CRC Press LLC, Boca Raton, FL, 1997.

[22] Gottlieb, O., Feldman, M., Application of a Hilbert transform-based algorithm for parameter estimation of a nonlinear ocean system roll model. *J. of Offshore Mechanics and Arctic Engineering.* **119**, (1997) pp. 239–243.

[23] Gottlieb, O., Habib, G., Non-linear model-based estimation of quadratic and cubic damping mechanisms governing the dynamics of a chaotic spherical pendulum. *J. of Vibration and Control.* **18**:4, (2011) pp. 536-547.

[24] Grassberger, P., Procaccia, I., Characterization of Strange Attractors. *Physical Review Letters.* **50**:5, (1983) pp. 346–349.

[25] Guckenheimer, J., Holmes, P., *Nonlinear Oscillations, Dynamical Systems, and Bifurcation of Vector Fields.* Springer, NY, 1986.

[26] Hamzi, B., Barbot, J.P., Monaco, S., Normand-Cyrot, D., Nonlinear discrete-time control of systems with a Neimark-Sacker bifurcation. *Systems and Control Letters.* **44**:4, (2001) pp. 245–258.

[27] Hilborn, R.C., *Chaos and Nonlinear Dynamics: an Introduction for Scientists and Engineers.* Oxford, 2001.

[28] Ikuta, K., Ishii, H., Nokata, M., Safety evaluation method of design and control for human care robots. *Int J Robot Res.* **22**:5, (2003) pp. 281–297.

[29] Insperger, T., Concept for continuous-time control systems with feedback delay. *IET Control Sys. Tech.* **14**:5, (2006) pp. 974–977.

[30] Insperger, T., Stepan, G., Act-and-wait control concept for discrete-time systems with feedback delay. *IET Control Theory Appl.* **1**:3, (2007) pp. 553–557.

[31] Insperger, T., Stepan, G., *Semi-discretization for time-delay systems – Stability and Engineering applications*, Springer, 2011.

[32] Insperger, T., Wahi, P., Colombo, A., Stepan, G., Di Bernadro, M., Hogan, S.J., Full characterization of the act-and-wait control for first-order unstable lag processes. *J. Vibration and Control* **16**:7-8, (2010) pp. 1209–1233.

[33] Jankovic, M., (1992) Exponentially stable observer for elastic joint robots. In: *Proc. 31st ZEEE CDC*, Tucson, AZ, USA, 16–18 December 1992, pp.323–324

[34] Jankovic, M., Observer based control for elastic joint robots. *IEEE Transactions on Robotics and Automation* **11**, (1995) pp. 618–623.

[35] Khargonekar, P.P., Poolla, K., Roose, D., Robust control of linear time-invariant plants using periodic compensation. *IEEE Trans. Autom. Control* **3**:11, (1985) pp. 1088–1096.

[36] Konishi, K., Luan, Ba.Le., Hara, N., Stabilization of a steady state in oscillators coupled by a digital delayed connection. *Eur. Phys. J. B* **85**:5, (2012) 166.

[37] Kovacs, L.L., Kovecses, J., Stepan, G., Analysis of Effects of Differential Gain on Dynamic Stability of Digital Force Control. *Int. J. Nonlin. Mech.* **43**, (2008) pp. 514–520.

[38] Krutova, I.N., Studying stability of the flexible spacecraft with a discrete control system. *Automation and Remote Control* **62**:12, (2001) pp. 1964–1977.

[39] Kuo, B.C., *Digital Control Systems*. SRL Publishing Company, Champaign, IL, 1977.

[40] Kuznetsov, Yu.A., *Elements of Applied Bifurcation Theory*. Springer, NY, 1998.

[41] Kuznetsov, Yu.A., Meijer, H.G.E., Numerical normal forms for codim 2 bifurcations of fixed points with at most two critical eigenvalues. *SIAM J. Sci. Comput.* **26**:6, (2005) pp. 1932–1954.

[42] Kuznetsov, Yu.A., Meijer, H.G.E., Remarks on the interacting Neimark-Sacker bifurcations. *J. Difference Equations and Applications*. **12**:10, (2006) pp. 1009–1035.

[43] Luo, G.W., Chu, Y.D., Zhang, Y.L., Zhang, J.G., Double NeimarkSacker bifurcation and torus bifurcation of a class of vibratory systems with symmetrical rigid stops. *J. of Sound and Vibration*. **298**, (2006) pp. 154–179.

[44] Luongo, A., Paolone, A., Perturbation methods for bifurcation analysis from multiple nonresonant complex eigenvalues. *Nonlinear Dynamics*. **14**:3, (1997) pp. 193–210.

[45] Matsumoto, T., Chua, L., Tokunaga, R., Chaos via torus breakdown. *IEEE Trans. Circuits and Syst.* **34**:3, (1987) pp. 240–253.

[46] Meyer, C.D., *Matrix Analysis and Applied Linear Algebra*. SIAM, 2001.

[47] Moon, F.C., *Chaotic and Fractal Dynamics: an Introduction for Applied Scientists and Engineers*. Wiley, NY, 1992.

[48] Natale, C., *Interaction Control of Robot Manipulators*. Springer, Berlin, Heidelberg, 2003.

[49] Nayfeh, A.H., Balachandran, B., *Applied Nonlinear Dynamics*. Sringer, NY, 1995.

[50] Nejat, G, Benhabib, B. (2003) High-precision task-space sensing and guidance for autonomous robot localization. In: *Proc. 2003 IEEE Int. Conf. on Robotics and Automation*, Taipei, Taiwan, September 2003, pp. 1527–1532.

[51] Nicosia, S., Tomei, P., Tornambe, A., An approximate observer for a class of nonlinear systems. *Syst. Control Lett.* **12**, (1989) pp. 43–51.

[52] Nicosia, S., Tomei, P., Tornambe, A. (1990) Discrete time modeling of flexible robots. In: *Proc. 29th Conf. on Decision and Control*, Honolulu, Hawaii, USA, December 1990, pp.539–544.

[53] Ogata, K., *Disctrete-Time Control Systems.* Prentice Hall, 1987.

[54] Quarteroni, A., Sacco, R., Saleri, F., *Numerical Mathematics*. Springer-Verlag GmbH, 2000.

[55] Roberts, J.B., Estimation of nonlinear ship roll damping from free decay data. *J. of Ship Research* **29**, (1985) pp. 127–138.

[56] Ryvkin, S., Izosimov, D. Bayda, S. (2003) Flex mechanical digital control design. In: *Proc. IEEE Int. Conf. on Industrial Technology, IEEE ICIT'03*, Moskow, Russia, December 2003; **1** pp. 298–302.

[57] Siciliano, B., Villani, L., *Robot Force Control*. Kluwer Academic Publishers, Dordrecht, 1999.

[58] Stepan, G., Vibrations of Machines Subjected to Digital Force Control. *Int. J. Solids Structures*. **38**, (2001) pp. 2149–2159.

[59] Stepan, G., Steven, A., Maunder, L., Design principles of digitally controlled robots. *Mechanism and Machine Theory*. **25**, (1990) pp. 515–527.

[60] Stepan, G., Steven, A., Maunder, L. (1990) Dynamics of robots with digital force control. In:*Proc. CSME Mechanical engineering Forum*, Toronto, Canada, 1990, pp. 355–360.

[61] Steven, A., Hewit, J.R., Hybrid position and force control applied to robotic polishing of turbine blading. In: *Proc. 3rd Int. Conf. on Advanced Robotics (ICAR)*, Versailles, France, 1987, pp. 493–502.

[62] Sweet, L.M., Good, M.C., Redefinition of the robot motion control problem. *IEEE Contr Syst Mag.* **3**, (1985) pp. 18–24.

[63] Szalai, R., Stepan, G., Hogan, S.J., Global Dynamics of Low Immersion High-Speed Milling. *Chaos*. **14**:4, (2004) pp. 1069–1077.

[64] Tomei, P., An observer for flexible joint robots. *IEEE Trans Automat Cont.* **35**, (1990) pp. 739–743.

[65] Troger, H., Steindl, A., *Nonlinear Stability and Bifurcation Theory*. Springer, NY, 1991.

[66] Yaghoobi, H., Abed, E.H., Local feedback control of the Neimark-Sacker bifurcation". *Int. J. of Bifurcation and Chaos*. **13**:4, (2003) pp. 879–893.

[67] Yang, S.M., Lee, Y.J., Optimization of non-collocated sensor/actuator location and feedback gain in control systems. *Smart Mater. Struct.* **2**, (1993) pp. 96–102.

[68] Yoshida, K., Shimogo., T., Murano, K., Digital optimal control of elastic structure systems (Positioning control of an elastic rotating arm). *JSME Int. J.* **30**, (1987) pp. 1311–1318.

[69] Yuan, Z., Hu, D., Huang, L., Stability and bifurcation analysis on a discrete-time neural network". *J. of Computational and Applied Mathematics*. **177** (2005) pp. 89–100.

Related journal papers

[70] Habib, G., Rega, G., Stepan, G., Nonlinear bifurcation analysis of a single-DoF model of a robotic arm subject to digital position control. *J. Comput. and Nonlin. Dyn.* **8**:1, (2012) pp. 011009

[71] Habib, G., Rega, G., Stepan, G., Analytical investigation of single and double Neimark-Sacker bifurcations. *Periodica Polytechnica*. **56**:1, (2012) pp.13–22.

[72] Habib, G., Rega, G., Stepan, G., Stability analysis of a two-DoF system subject to proportional-derivative digital position control. To appear in *J. Vib. and Control*

[73] Habib, G., Rega, G., Stepan, G., Bifurcation analysis of a two-DoF mechanical system subject to digital position control. Part I: theoretical investigation. Under review at *Nonlinear Dynamics*.

[74] Habib, G., Rega, G., Stepan, G., Bifurcation analysis of a two-DoF mechanical system subject to digital position control. Part II: effects of asymmetry and transition to chaos. Under review at *Nonlinear Dynamics*.

[75] Habib, G., Rega, G., Stepan, G., Nonlinear investigation of the act-and-wait control concept applied to a single-DoF robotic arm. In preparation.

Related papers in conference proceedings

[76] Habib, G., Rega, G., Stepan, G. (2011) Stability and bifurcation analysis of robots subject to digital position control: 7th ENOC, Rome, Italy, July 2011.

[77] Habib, G., Rega, G., Stepan, G. (2011) Supercritical bifurcation of the digital position control of a single-dof robot model under symmetric nonlinear force: AIMETA 2012, Bologna, Italy, September 2011.

[78] Habib, G., Rega, G., Stepan, G. (2011) Stability analysis of an elastic robotic arm subject to digital position control: 11th Conference on Dynamical Systems – Theory and Applications, Lodz, Poland, December 2011.

[79] Habib, G., Rega, G., Stepan, G. (2012) Bifurcation analysis of a two-DoF system subject to digital position control: ASME 2012 IDETC Conference. Chicago, Illinois, USA, August 2012.

[80] Habib, G., Rega, G., Stepan, G. (2012) Improving the digital position control of a single-DoF system via the act-and-wait control concept: EUROMECH Colloquium 532 – Time-Periodic Systems Current Trends in Theory and Application, Frankfurt, Germany, August 2012.